Role and regulation of MITF in melanocytes and melanoma

Robert Siddaway
The Queen's College, Oxford, OX1 4AW
robert.siddaway@ludwig.ox.ac.uk

Disclaimer

I declare that this submission is my own written work. To the best of my knowledge, it contains no material that has been written by another or previously submitted in the same or a different form as academic work, to this or any other university.

The results presented herein derive from my own experiments, with the exception of Figure 3.1 (work performed by Alex Schepsky), Figure 5.4 (work performed by Kao-Chin Ngeow) and part of Figure 5.8 (the microarray data was supplied by Byungwoo Ryu, Boston University).

Robert Siddaway

Trinity Term 2013

Abstract

Role and regulation of MITF in melanocytes and melanoma

Robert Siddaway, The Queen's College, D.Phil. Clinical Medicine, Trinity Term 2013

One key to understanding how cells integrate and how they respond to diverse stimuli in order to direct a transcriptional response is knowing how a transcription factor may be directed to an appropriate subset of its target genes. One mechanism with which this may be achieved is by modulation of the transcription factor's post-translational modification status. The *microphthalmia*-associated transcription factor (MITF) is the master regulator of the melanocyte lineage, and it is also a lineage addiction gene in melanoma. Low or high levels of *MITF* expression induce a reversible cell cycle arrest. Invasive behaviour is characteristic of low *MITF* expression; differentiation a product of high *MITF* activity; and moderate levels of *MITF* expression promote proliferation. A major, unaddressed problem is how DNA binding by MITF may be differentially directed such that it regulates either a proliferation-associated or a differentiation-associated gene expression programme appropriate to the cellular microenvironment. This thesis explores the function and regulation of the signalling pathways controlling novel post-translational modifications of MITF. One such modification, in the DNA binding domain of MITF, defines a key switch that controls MITF's DNA binding affinity and specificity. Moreover, a novel set of MITF target genes are revealed that extend its control beyond pigmentation and cell cycle regulation to implicate MITF as an overall regulator of cell behaviour in the melanocyte lineage.

Acknowledgements

Table of Contents

List of abbreviations

A	Adenine
AMP	Adenosine monophosphate
APS	Ammonium persulfate
ATP	Adenosine triphosphate
B	Cytosine, guanine or thymine
BCL2	B-cell lymphoma 2
BER	Base excision repair
bHLH	Basic helix-loop-helix
bHLH-LZ	Basic helix-loop-helix leucine-zipper
bp	base pair
BSA	Bovine serum albumin
C	Cytosine
cAMP	Adenosine 3- 5- cyclic monophosphate
CBP	CREB-binding protein
CDK	Cyclin dependent kinase
CDKN1A	Cyclin dependent kinase inhibitor 1A
CDKN2A	Cyclin dependent kinase inhibitor 2A
cDNA	complementary DNA
C.elegans	*Caenorhabditis elegans*
ChIP	Chromatin immunoprecipitation
ChIP-Seq	ChIP coupled to deep sequencing
CIP	Calf-intestinal alkaline phosphatase
c-Myc	v-myc myelocytomatosis viral oncogene homolog
CPM	Counts per minute
CREB	cAMP response element binding protein
C-terminal	Carboxy terminal
CTP	Cytidine triphosphate
Da	Dalton
DAPI	Diaminophenyl indol
dATP	Deoxyadenosine triphosphate
dCTP	Deoxycytidine triphosphate
dGTP	Deoxyguanosine triphosphate
DIAPH1	Diaphanous-related formin 1
dIdC	Poly(deoxyinosinic-deoxycytidylic) acid
DMEM	Dulbecco's Modified Eagle Medium
DMF	Dimethylformamide
DMSO	Dimethyl sulfoxide
DNA	Deoxyribonucleic acid
dNTP	Deoxyribonucleotide
DTT	Dithiothreitol

dTTP	Deoxythymidine triphosphate
E1A	Adenovirus early region 1A
ECM	Extracellular matrix
E.coli	Escherichia coli
EDNRB	Endothelin receptor type B
EDTA	Ethylenediaminetetraacetic acid
EMSA	Electrophoretic mobility-shift assay
ER	Endoplasmic reticulum
ERK	Extracellular signal-regulated kinase
FBS	Foetal bovine serum
FITC	Fluorescein isothiocyanate
G	Guanine
G1	Gap 1
G2	Gap 2
Gbp	Giga base pair
GFP	Green fluorescent protein
GO	Gene Ontology
GSK3β	Glycogen Synthase Kinase 3β
GTP	Guanosine triphosphate
HA	Haemagglutinin
HDAC	Histone deacetylase
HEPES	4-(2-hydroxyethyl)-1-piperazineethanesulfonic acid
HIF	Hypoxia-inducible factor
HR	Homologous recombination
IgG	Immunoglobulin G
IP	Immunoprecipitation
IPTG	Isopropyl β-D-1-thiogalactopyranoside
kb	kilobase
kDa	Kilodalton
KEGG	Kyoto encyclopaedia of genes and genomes
Kit	v-kit Hardy-Zuckerman 4 feline sarcoma viral oncogene-like protein
LAMP1	Lysosomal-associated membrane protein 1
LB	Luria-Bertani broth
LEF-1	Lymphoid enhancer-binding factor 1
LZ	Leucine zipper
M	Mitosis
M	Molar
MACS	Model-based Analysis of Chip-Seq

MAPK	Mitogen-activated protein kinase
MAX	Myc-associated factor X
MC1R	Melanocortin 1 receptor
MEK	Mitogen-activated protein kinase kinase
MITF	Microphthalmia-associated transcription factor
MMR	Mismatch repair
mRNA	Messenger RNA
MSC	Melanocyte stem cell
α-MSH	Alpha melanotide stimulating hormone
MTT	3-(4,5-dimethylthiazol-2-yl)-2,5-diphenyltetrazolium bromide
MYOD	Myoblast determination protein
N	Any DNA base
NAD^+	Nicotinamide adenine dinucleotide (oxidised)
NADH	Nicotinamide adenine dinucleotide (reduced)
NER	Nucleotide excision repair
NP40	Nonylphenylpolyethylene glycol
NSCLC	Non-small-cell lung cancer
N-terminal	Amino terminal
NuRD	Nucleosome remodelling and histone deacetylase
OIS	Oncogene-induced senescence
PAS	Per-Aryl hydrocarbon receptor nuclear translocator-Sim domain
PAX3	Paired-box homeodomain transcription factor 3
PBS	Phosphate-buffered saline
PBS-T	PBS supplemented with 0.1% Tween-20
PCAF	p300/CBP-associated factor
PCG-1α	Peroxisome proliferator-activated receptor gamma coactivator 1 alpha
PCR	Polymerase chain reaction
PI	Propidium iodide
PI3K	Phosphatidylinositol 3-kinase
PIC	Protease inhibitor cocktail
PMSF	Phenylmethanesulfonylfluoride
ppERK	ERK phosphorylated on T202 and T204
PTEN	Phosphatase and tensin homologue
PVDF	Polyvinylidene difluoride
qPCR	Quantitative real-time PCR
RAF	Rapidly Accelerated Fibrosarcoma
RAS	Rat sarcoma
Rb	Retinoblastoma tumour suppressor protein
RNA	Ribonucleic acid
RNA-Seq	mRNA deep sequencing
ROS	Reactive oxygen species

RPE	Retinal pigment epithelium
RPKM	Reads per kilobase per million
RPMI	Roswell Park Memorial Institute Medium-1640
Rsk	Ribosomal protein S6 kinase
RTK	Receptor tyrosine kinase
S	Synthesis
SDS	Sodium dodecyl sulphate
SDS-PAGE	SDS-polyacrylamide gel electrophoresis
siRNA	Short interfering RNA
SIRT	Sirtuin
SUMO	Small ubiquitin-like modifier
T	Thymine
TBE	Tris/borate/EDTA
TBP	TATA box binding protein
TBS-T	Tris-buffered saline supplemented with 0.1% Tween-20
TBX2	T-box factor 2
TBX3	T-box factor 3
TE	Tris/EDTA
TEMED	Tetramethylethylenediamine
TFEB	Transcription factor EB
Tris	Tris(hydroxymethyl)aminomethane
TSS	Transcription start site
TTP	Thymidine triphosphate
TTS	Transcription termination site
UCSC	University of California at Santa Cruz
USF	Upstream stimulatory factor
UTR	Untranslated region
UV	Ultraviolet
V	Cytosine, guanine or adenine
WCE	Whole cell extract
Wnt	Wingless-type MMTV integration site family
WT	Wild-type

Chapter 1 - Introduction

1.1 Melanocytes

Melanocytes are specialised melanin synthesising cells that are responsible for pigmentation in vertebrates. Cutaneous melanocytes are found in the epidermis of the skin and in hair follicles (Figure 1A). Non-cutaneous melanocytes are found in other locations such as the iris, the choroid, and the retinal pigment epithelium (RPE) of the eye; the cochlea and the vestibular organ of the ear; the leptomeninges, which is a small, pigmented region of the brain; and in the heart (Jackson, 1994). In mice, most melanocytes are to be found in hair follicles located in the dermis, and they undergo cycles of growth and destruction throughout life (Figure 1.1B). After a period of growth (anagen), the cells forming the hair matrix lose the ability to proliferate and enter apoptosis, triggering destruction of the lower follicle (catagen), followed by a dormant period (telogen) in which the bulge and dermal papilla are in close proximity before re-entry into anagen (Alonso and Fuchs, 2006).

The bulge niche, at the top of the root, contains epithelial stem cells (Blanpain et al., 2004). The bulge also contains a reservoir of quiescent melanocyte stem cells (MSCs) which divide late in telogen (Nishimura et al., 2002). One daughter cell remains in the bulge as an MSC, ready for the end of the next hair cycle, while the second daughter exits the bulge for the new hair matrix where it proliferates and differentiates into a melanocyte (Nishimura et al., 2002).

In humans, hair follicles are sparser than in mice, and most cutaneous melanocytes are epidermal. Within the epidermis, melanocytes are found amongst the keratinocytes in the basal layer, which is separated from the dermis by the basement membrane (Figure 1.1A).
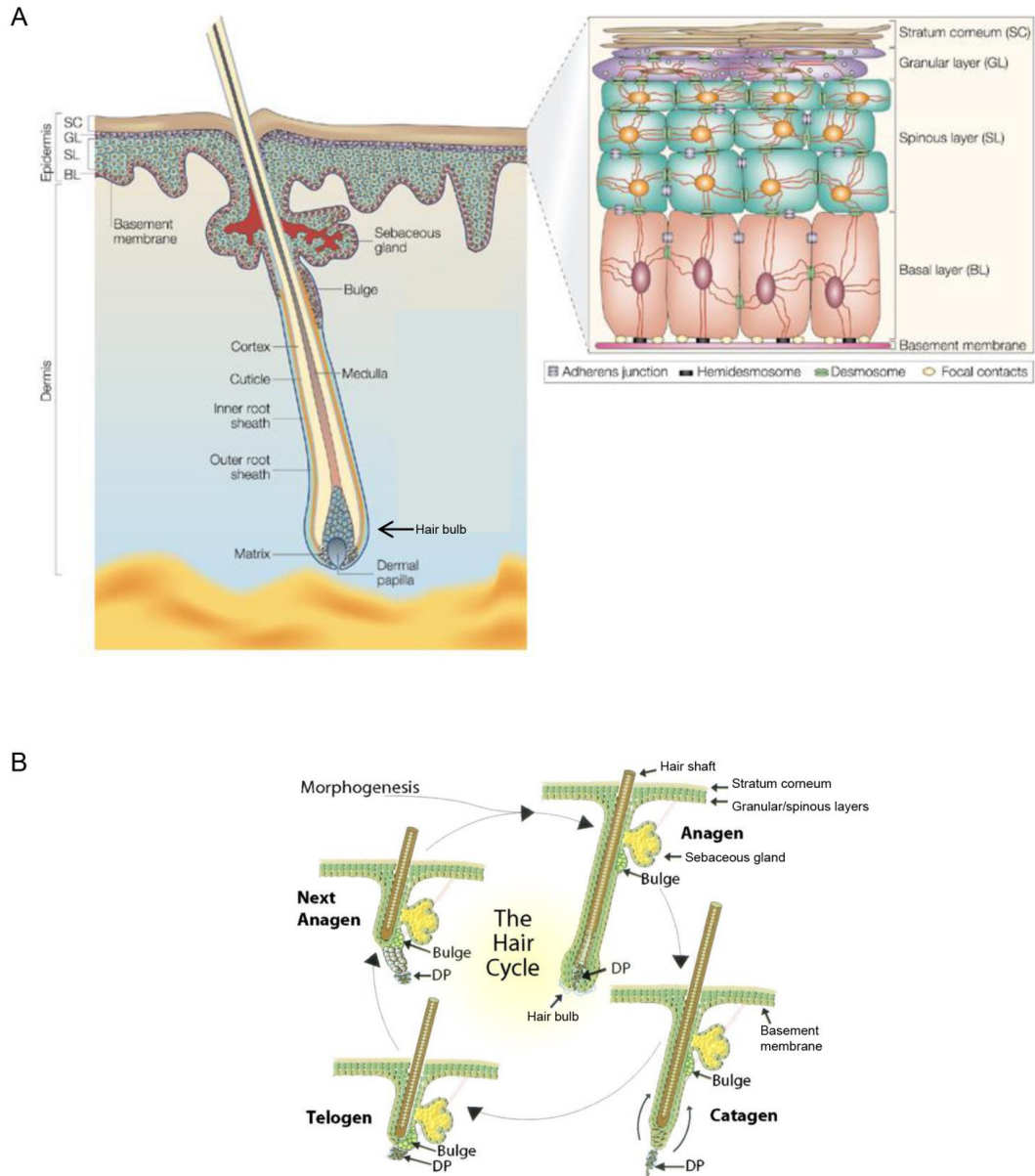
Figure 1.1. The skin and hair. (A) Structure of the dermis and epidermis, showing the location of the hair follicle within the dermis. Adapted from (Fuchs and Raghavan, 2002). (B) Stages of the hair follicle, showing the variable distance between the bulge and the dermal papilla (DP). Adapted from (Alonso and Fuchs, 2003).

1.1.1 Melanocytes in development

Cutaneous melanocytes derive from the neural crest, which forms from the dorsal part of the neural tube early in embryogenesis (Thomas and Erickson, 2008). Neural crest cells can be neurogenic, ultimately adopting a glial fate. Alternately they can be melanogenic, becoming proliferative melanoblasts before differentiating into melanocytes (Figure 1.2). Around E9.5 in mice, melanoblasts begin migrating along the dorsolateral pathway and up-regulate melanoblast markers from E10.5 (Steel et al., 1992). Melanoblasts invade the epidermis and hair follicle to differentiate and commence pigmentation at E16.5 (Serbedzija et al., 1990; Steel et al., 1992). On arrival in the hair follicle, melanoblasts are segregated between the bulge where they form MSCs, and the hair matrix where they differentiate into melanocytes (Nishimura et al., 2002).
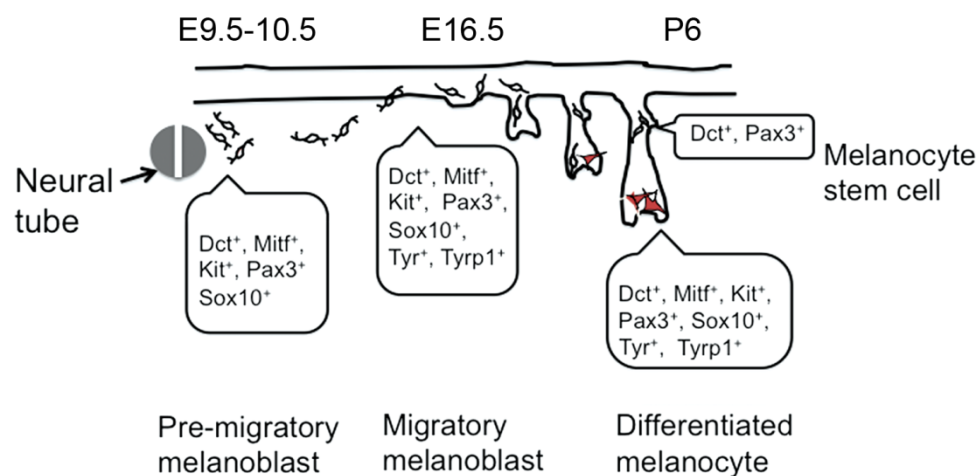
Figure 1.2. Murine melanocytes in development. At E9.5, the pre-migratory melanoblasts that have emerged from the neural tube expresses specification markers (Pax3, Sox10, Mitf), and melanocyte markers (dopachrome tautomerase [Dct], Kit). Additional melanocyte markers (Tyrosinase [Tyr] and Tyrp1) are added at E16.5 in the migrating melanoblast, on invasive of the epidermis. In the hair follicle (E16.5 onwards), differentiated melanocytes in the hair matrix continue to express these markers. MSCs in the bulge express Pax3 and Dct. Adapted from Osawa, Stem Book, (http://www.stembook.org/node/581).

Specification of melanoblasts at the expense of glial cells is induced by the actions of Wnt1 and Wnt3, which are expressed in the early neural crest (Dunn et al., 2000). Together with their effector β-catenin, these proteins positively influence the ability of the embryo to generate melanoblasts (Takada et al., 1994; Ikeya et al., 1997; Dorsky et al., 1998; Hari et al., 2002).

Two other transcription factors expressed in pre-migratory melanoblasts are critical for melanocyte specification and for neural crest development in general. The first, the paired-box homeodomain transcription factor PAX3, is expressed from the pre-migratory melanoblast stage; a heterozygous *Pax3* knockout mouse has white spots, while a homozygous knockout is embryonically lethal due to defects in muscular and neural crest development (Epstein et al., 1991; Goulding et al., 1991). In melanoblasts, Pax3 promotes the adoption of a melanocyte fate, but it paradoxically represses terminal differentiation in a manner that is relieved by β-catenin (Lang et al., 2005). Secondly, SOX10 is a member of the high mobility group family of transcription factors (Southard-Smith et al., 1998). A homozygous *Sox10* dominant negative mutant is embryonically lethal in mice due to severe defects in development of neural crest derivative cells, while the heterozygotic mouse exhibits white spotting (Potterf et al., 2001). The same has been observed in zebrafish, where SOX10 mutants fail to develop their neural crest derivatives (Dutton et al., 2001).

The actions of Wnt, PAX3, and SOX10 all converge on the activation of *microphthalmia*-associated transcription factor (MITF, *mi*; see Section 1.4)—a basic helix-loop-helix leucine zipper (bHLH-LZ) protein (Hodgkinson et al., 1993; Hughes et al., 1993). Expressed early in the neural crest in response to the combined action of these factors (Watanabe et al., 1998; Dorsky et al., 2000), Mitf is the master regulator of the melanocyte lineage, and a homozygous *mi*-null mouse lacks melanocytes

(Hodgkinson et al., 1993). Mitf plays crucial roles in promoting conversion of neural crest precursors to melanoblasts, and in influencing their subsequent survival (Opdecamp et al., 1997; Hornyak et al., 2001).

The switch between the bipotent glial/melanoblast precursors is in part controlled by the expression (or not) of FOXD3, which is expressed in the neural tube. FOXD3 represses melanoblast formation by interacting with PAX3, preventing PAX3 from binding and activating the *Mitf* promoter (Thomas and Erickson, 2009).

1.1.2 Melanocytes and pigmentation

Melanocytes play a protective role in protecting the body from ultraviolet (UV) damage. Using tyrosine and phenylalanine as starting compounds, melanocytes synthesise and package the pigment melanin in melanosomes, which are specialised lysosome-related organelles (Raposo and Marks, 2007). Melanosomes are transported to the cell surface and transferred through filopodia from epidermal melanocytes to the keratinocyte cells that form the bulk of the epidermis (Scott et al., 2002). All humans have a similar melanocyte density in their skin, and differences in skin colour arise from the balance of types of melanin synthesised (eumelanin is black-brown, and pheomelanin is red-yellow), as well as the size, number, and packaging density of melanosomes (Kadekaro et al., 2003). Black skin has an enhanced rate of melanogenesis and a greater proportion of eumelanin than white or Asian skin (Brenner and Hearing, 2008). Melanin forms a physical barrier that blocks UV-induced damage of the skin, directly absorbing UV radiation as well as quenching reactive oxygen species (ROS) that are generated intracellularly following UV irradiation (Slominski et al., 2004).

UVA (320 – 400 nm) and UVB (280 – 320 nm) are the primary ranges of UV wavelengths that damage the body, of which UVB is less prevalent in the

atmosphere. However, UVB is more mutagenic on account of its potential to be absorbed directly by DNA, in which it induces thymidine dimers (Freeman et al., 1989). UVA has a longer wavelength and thus penetrates deeper into the epidermis, where it induces ROS that can result in single-stranded DNA breaks (Kvam and Tyrrell, 1997). Melanin in the epidermis is photo-oxidised on absorption of UV, which immediately darkens the skin. A slower, longer term tanning response is triggered by the actions of UVB (Kadekaro et al., 2003; Hirobe, 2005), which promotes the release of epidermal mitogenic factors from keratinocytes. One such factor, α-melanotide stimulating hormone (α-MSH), binds the melanocortin 1 receptor (MC1R). This leads to cAMP response element-binding protein (CREB) phosphorylation; and activated CREB promotes pigmentation (Bertolotto et al., 1996b; Busca and Ballotti, 2000). At the same time, UV irradiation leads to an increase in levels of cytokines such as interleukin-1 α and tumour necrosis factor α, which activate stress signalling through the p38 and c-Jun pathways. These pathways induce a transcriptional response that promotes cell cycle arrest and apoptosis, which suggests that the UV response is finely balanced to provide maximal protection against further damage while removing irreparably damaged cells at the same time (Kadekaro et al., 2003).

2.1 Melanoma

Melanoma is a cancer arising most commonly from epidermal melanocytes, but can also occur wherever melanocytes are to be found, such as in the choroid layer in the eye. The incidence rate of melanoma in the United Kingdom is increasing, and it has climbed rapidly since 2000 to become the nation's fifth most common form of cancer in 2010 (Figure 1.3; data source: Cancer Research UK). However, although melanoma is being diagnosed more frequently, the mortality rate is not increasing

linearly with incidence (Figure 1.3), a fact attributed to earlier diagnosis. When early-stage melanoma is diagnosed, surgical excision is frequently curative but, as the disease develops, mortality rapidly increases: five-year survival tumbles from approximately 85-90% for all patients to 5-15% for those with distal metastasis (Balch et al., 2001; Tawbi and Kirkwood, 2007).

Cancer is a disease with rising incidence in an aging population. It is characterised by cellular behaviour that becomes progressively more de-regulated as its constituent cells escape and evade the controls that would normally direct their behaviour (Figure 1.4A). In this manner, tumour cells become able to sustain continual growth and proliferation while avoiding growth-inhibitory pathways, avoiding destruction by the immune system, stimulating angiogenesis and, ultimately, metastasising (Hanahan and Weinberg, 2011). To develop better treatments it will be necessary to improve our understanding of normal cellular processes and how they are de-regulated under pathological conditions.
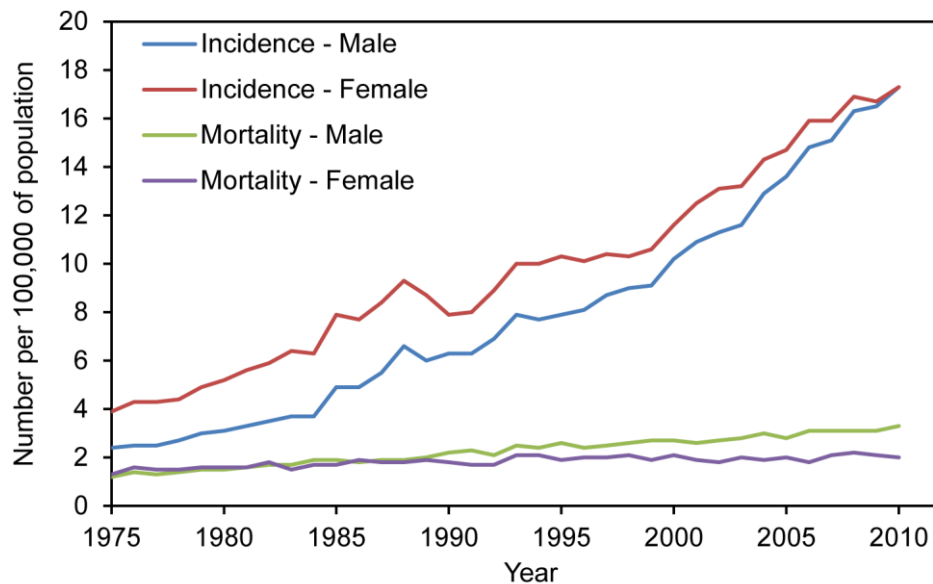
Figure 1.3. Melanoma incidence is increasing faster than mortality. Incidence of melanoma in the United Kingdom is increasing rapidly in both men and women, but mortality is lagging behind. Data collected from Cancer Research UK.
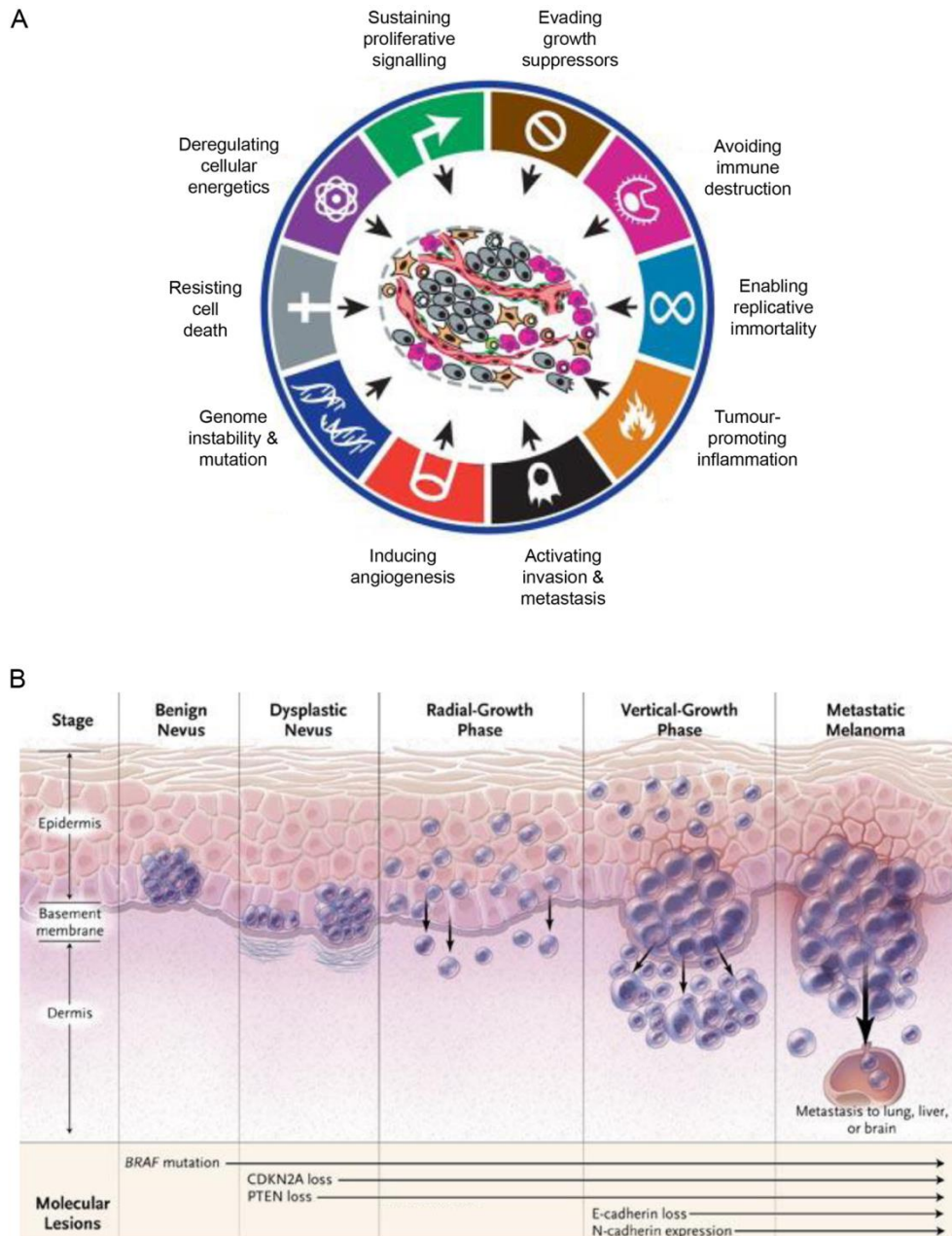
Figure 1.4. The emerging characteristics of melanoma progression. (A) In order to succeed and metastasise a tumour must subvert many physiological processes, including cell growth and survival, metabolism, angiogenesis and the immune system. Adapted from (Hanahan and Weinberg, 2011). (B) Pathphysiological stages of the Clark model of melanoma progression, indicating mutations that are commonly found in patients. Adapted from (Miller and Mihm, 2006).

2.1.1 Progression of melanoma

Melanoma progression often displays a pattern of histopathological behaviour described with the Clark model (Figure 1.4B), in which the melanocytes in a benign nevus are considered primed for melanoma development. These nevi have constant pigmentation and regular edges. Malignancy is initiated either from proliferation originating in a nevus, or *de novo* at a location that did not previously have a nevus. The dysplastic nevus tends to be larger (greater than 5 mm diameter) in size, have aberrant colouring, and irregular borders. As a melanoma develops further and becomes hyperplasic, it first has a radial growth phase where melanocytes start proliferating intraepidermally—and can also generate some dermal micro-invasions—followed by a vertical growth phase that forms nodules in the dermis. Finally, as the tumour continues to penetrate the dermis, cells begin to dissociate from the tumour, allowing metastasis to distal sites such as the lungs, liver and brain (Clark et al., 1984).

To form a nevus, a single activating mutation in a growth-stimulatory pathway is required. In the vast majority of patients, this mutation will occur in the mitogen activated protein kinase (MAPK) signalling pathway which, under normal physiological conditions, drives a growth-promoting cascade of phosphorylation events in response to extracellular growth signalling (Figure 1.5A). RAS is often mutated in cancer and, in melanoma, codon 61 of NRAS is mutated in 15% of patients (Bos, 1989; Demunter et al., 2001; Omholt et al., 2002). BRAF is mutated less frequently (7%) than RAS across all cancers, but in melanoma is mutated in 66% of patients, of whom 80% will carry a V600E mutation (Davies et al., 2002). Activating BRAF mutation drives melanoma cell growth and promotes transformation of melanocytes (Hingorani et al., 2003; Wellbrock et al., 2004a). In mouse models,
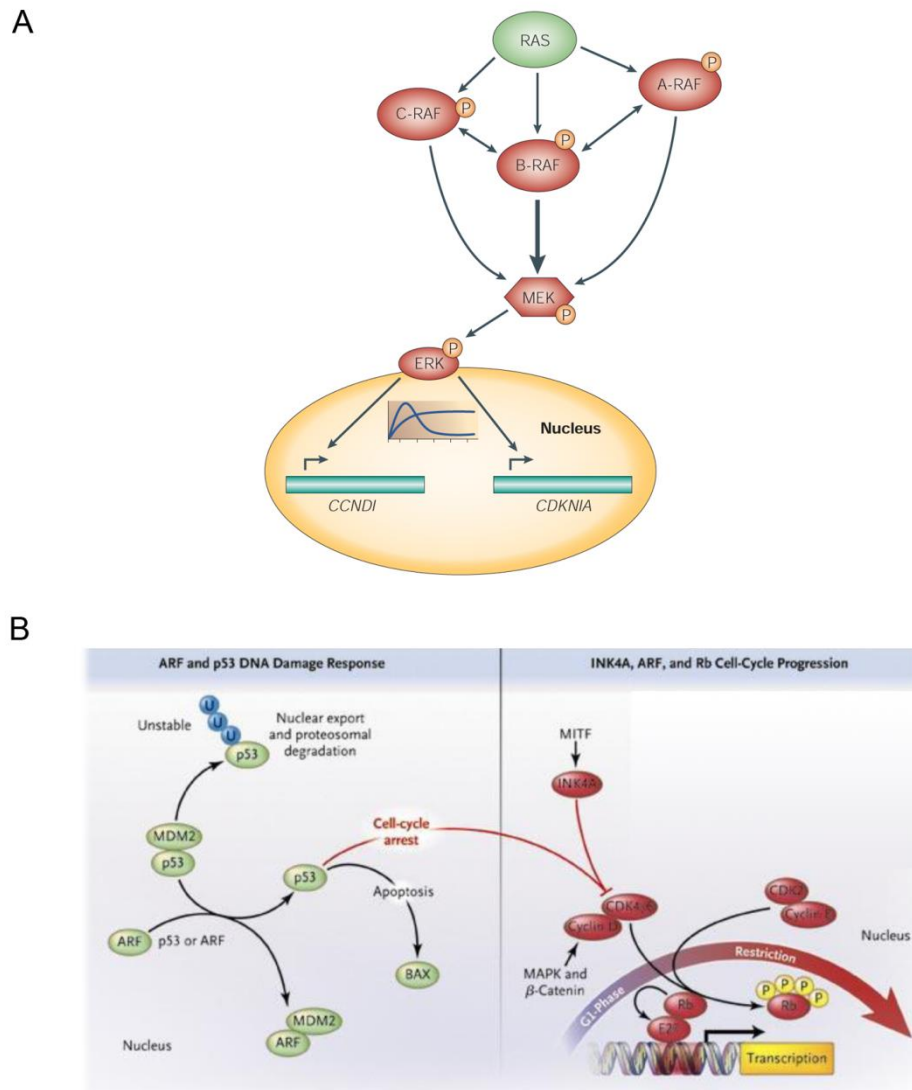
Figure 1.5. Major pathways mutated in melanoma. (A) The MAPK pathway is aberrantly activated in almost all melanomas, promoting ERK nuclear translocation and activation of its target transcription factors which drive expression of growth-promoting genes such as *CCNDI* and *CDKNIA*. Adapted from (Wellbrock et al., 2004b). (B) Left panel. p14^{ARF} stabilises p53 to induce cell cycle arrest and apoptosis by inhibiting MDM2. Right panel. p16^{INK4A} suppresses inactivation of Rb by CDK4, preventing progress through G1/S. Both are expressed from the *CDKN2A* locus which is frequently disrupted in melanoma. Adapted from (Miller and Mihm, 2006).

constitutively active BRAF promotes tumour growth and metastasis, demonstrating the major oncogenic activity of the mutated MAPK pathway (Dankort et al., 2009; Goel et al., 2009). Furthermore, in tumours where BRAF mutation drives growth, cells are absolutely dependent on MEK, which is activated by BRAF; MEK inhibitors have been shown to strongly abrogate growth of BRAF-mutant tumours (Solit et al., 2006). NRAS and BRAF mutations appear to be mutually exclusive, suggesting that double activation of the pathway is, at best, not advantageous or, at worst, harmful to the cell (Gorden et al., 2003; Omholt et al., 2003).

At least 80% of melanoma patients will have constitutively activating MAPK mutations, with around half of patients carrying BRAF^{V600E}. However, activating MAPK alone is insufficient to allow a melanoma to form: as well as promoting growth, these mutations will also promote senescence in the nevus (Tassabehji et al., 1993; Serrano et al., 1997; Bennett, 2003; Michaloglou et al., 2005; Patton et al., 2005). Indeed, approximately 75% of benign nevi have a BRAF^{V600E} mutation (Davies et al., 2002; Pollock et al., 2003). A cell may become senescent either through replicative stress associated with progressive telomere shortening, or by oncogene-induced senescence (OIS) (Shay and Roninson, 2004). OIS is a major early barrier to tumour progression, leaving cells in a static G1-like cell cycle arrest.

Further mutation is required to escape senescence. In the case of BRAF^{V600E}, OIS is triggered by induction of p16^{INK4A} (Michaloglou et al., 2005; Gray-Schopfer et al., 2006), which is expressed from the *CDKN2A* tumour-suppressor locus on chromosome 9. This locus is inactivated in around 50% of melanoma patients, and has been identified as being a driver of familial melanoma susceptibility (Hussussian et al., 1994; Kamb et al., 1994; Flores et al., 1996). In much of the remaining 50%, the locus is likely to be silenced, for example through β-catenin mediated repression

(Delmas et al., 2007). This locus also expresses another, unrelated protein, p14^{ARF} (human) or p19^{ARF} (mouse), with an alternate exon 1 and different reading frames from exon 2 onward (Quelle et al., 1995). Both of these proteins inhibit cell cycle progression, but they do so by different means (Figure 1.5B). p16^{INK4A} inhibits the cyclin-dependent kinases (CDK) CDK4 and CDK6. In turn, they phosphorylate and inactivate the retinoblastoma tumour suppressor protein (Rb), which permits passage through the G1/S cell cycle checkpoint (Serrano et al., 1993). By removing this block on cell-cycle progression, Rb is constitutively inactivated and the G1/S checkpoint is bypassed. p14^{ARF} binds and inhibits mouse double minute 2 protein (MDM2), which sequesters p53 and leads to p53 poly-ubiquitylation and degradation (Kamijo et al., 1998; Pomerantz et al., 1998; Stott et al., 1998; Zhang et al., 1998). Thus, loss of p14^{ARF} leads to p53 inactivation. Traditionally, p53 has been assumed to not be mutated at high frequency in melanoma, with its inactivation being brought about by other means, such as loss of p14^{ARF} (Chin et al., 2006). However, recent evidence has identified UV-induced p53 mutations in a group of melanomas that do not harbour p14^{ARF} mutations, suggesting that in fact direct mutation of p53 is another melanoma-controlling mutation (Hodis et al., 2012).

While *CDKN2A* inactivation in mice fails to cause a developmental phenotype, it leaves mice highly prone to spontaneous tumour formation, (Kamijo et al., 1997; Sharpless et al., 2004). In mouse melanocytes, single-copy deletion of *CDKN2A* suffices to disrupt senescence (Sharpless and Chin, 2003; Sviderskaya et al., 2003). Humans with germline *p16^{INK4A}* mutations develop large numbers of benign nevi and are highly prone to developing melanoma (Hayward, 2000; Bennett, 2003; Sviderskaya et al., 2003). Collectively, p16^{INK4A} and ARF play crucial roles in

melanoma suppression and their inactivation permits bypass of OIS induced by MAPK-activation (Chin et al., 1997).

Another tumour-suppressing protein that can be inactivated in many cancers, including approximately 10% of melanomas, is phosphatase and tensin homologue (PTEN) (Guldberg et al., 1997; Li and Sun, 1997; Li et al., 1997; Steck et al., 1997). PTEN is a negative regulator of the phosphatidylinositol 3-kinase (PI3K)-AKT pathway, which uses phosphatidylinositol phosphate as a second messenger, which is generated in response to growth factor signalling, to activate AKT. In turn, this promotes cell-cycle progression.

While combinations of mutations such as MAPK-activation and *CDKN2A* or p53 inactivation are driving mutations in melanoma (Hayward, 2000; Davies et al., 2002; Hodis et al., 2012), other proteins can also play important roles. Two such proteins, which can suppress senescence in melanoma cells, are the anti-senescence factors T-box factors TBX2 (Jacobs et al., 2000; Prince et al., 2004; Vance et al., 2005) and TBX3 (Brummelkamp et al., 2002; Rodriguez et al., 2008). TBX2 and TBX3 operate by suppressing p21^{Cip1}. Progression from the radial- to vertical-growth phase is often accompanied by loss of E-cadherin and induction of N-cadherin (Hsu et al., 1996). E-cadherin expression in melanocytes promotes association with epidermal keratinocytes, while N-cadherin-expressing melanoma cells can interact with other N-cadherin-expressing cells such as dermal fibroblasts, stimulating invasive behaviour (Hsu et al., 2000). E-cadherin is often re-expressed in metastatic melanoma (Danen et al., 1996). TBX2 and TBX3 also play a pro-invasive role in melanoma by suppressing the expression of E-cadherin, which promotes the epithelial-mesenchymal transition.

Contact with undifferentiated basal-layer keratinocytes inhibits melanocyte proliferation (Valyi-Nagy et al., 1993). Beyond permitting passage out of the

epidermis, the E-cadherin to N-cadherin switch also disrupts the Wnt/β-catenin pathway by leading to β-catenin relocalisation from the plasma membrane to the cytoplasm and nucleus, where β-catenin promotes melanoma cell survival and suppresses apoptosis and senescence (Li et al., 2001; Qi et al., 2005; Delmas et al., 2007). Beyond the effects on β-catenin that result from disrupted E-cadherin, β-catenin mutations are found in melanoma that prevent its degradation, thereby leading to constitutive nuclear localisation and activation (Rubinfeld et al., 1997; Rimm et al., 1999; Omholt et al., 2001).

2.1.2 Targeted melanoma therapy

Conventional chemotherapy works by targeting proliferating cells. Because tumour cells will typically replicate at a faster rate than healthy cells in the body, they are selectively depleted. However, unpleasant side-effects arise from this treatment because healthy cells that are dividing will be harmed too. An alternative therapeutic tactic that has seen substantial recent progress is targeted therapy, which makes use of the genetic changes in the tumour to specifically target cancer cells while not interfering with healthy cells.

One such therapy, vemurafenib, targets $BRAF^{V600E}$. V600 is in the activation loop of BRAF, which undergoes a translocation when BRAF is activated, moving towards the active site of the kinase. Mutation of this loop, particularly V600E, stimulates BRAF by locking the activation loop in the active, flipped-in conformation. Vemurafenib selectively and tightly binds $BRAF^{V600E}$, fails to bind the wild-type, inactive protein, and shows only weak binding to wild-type, active protein (Tsai et al., 2008; Bollag et al., 2010). It has shown significant anti-tumour effects in mouse models and clinical trials, leading to tumour shrinkage and increased progression-free

survival, and has been approved for use in the treatment of metastatic melanoma (Flaherty et al., 2010; Chapman et al., 2011; Sosman et al., 2012).

However, while vemurafenib has beneficial effects in the short-term, BRAF^{V600E} patients treated this way ultimately relapse because their tumours become resistant to therapy. There are a number of ways in which this has been observed to occur, including activating mutations of NRAS or the receptor tyrosine kinases that form the beginning of the MAPK cascade (Nazarian et al., 2010), BRAF amplification (Shi et al., 2012) or up-regulation of CRAF (Montagut et al., 2008). These mechanisms all overwhelm the restraint placed on the pathway by vemurafenib treatment, and they lead to the reactivation of MAPK signalling. Vemurafenib treatment can also enhance growth of BRAF wild-type or RAS-mutant tumours, and vemurafenib binding to mutant BRAF can transactivate a wild-type RAF protomer with which it has dimerised (Halaban et al., 2010; Hatzivassiliou et al., 2010; Heidorn et al., 2010; Poulikakos et al., 2010). These studies have demonstrated that, while vemurafenib can be highly effective for a period of time, it is necessary to genotype a patient before embarking on treatment. Future work will be required to counter the secondary effects of the therapy.

2.1.3 Melanoma heterogeneity

Tumours are comprised of heterogeneous populations of cells, which places an additional barrier on targeted therapy. In melanoma, it has been demonstrated that tumours contain at least two subpopulations of cells, expressing two different transcription factors, Brn-2 and MITF, in a mutually exclusive pattern (Goodall et al., 2008; Pinner et al., 2009). It is highly likely that other subpopulations could also be present. Two competing theories attempt to explain this phenomenon (Hoek and Goding, 2010). In one theory, the genetic model describes an irreversible acquisition

of mutations as the tumour develops until one cell collects all the necessary invasive advantages to permit metastasis. At this point, the cell can migrate to a new site, giving it a chance to generate a metastasis that would have a distinct genetic makeup when compared to the parental tumour (Figure 1.6A).

In the second theory, tumour cells could either adopt a proliferative phenotype or a melanoblast-like migratory one, in response to changing cues from the microenvironment (Figure 1.6B). This is the phenotype-switching model, which is gaining growing support from the field. It has been observed that the E-cadherin – N-cadherin switch that takes place on entry to the vertical growth phase can be reversed in metastasis (Danen et al., 1996), and that metastatic melanoma cells can remodel the extra-cellular matrix, reprogramming healthy melanocytes to become reversibly invasive (Seftor et al., 2005). Gene expression profiling of melanoma cell lines has
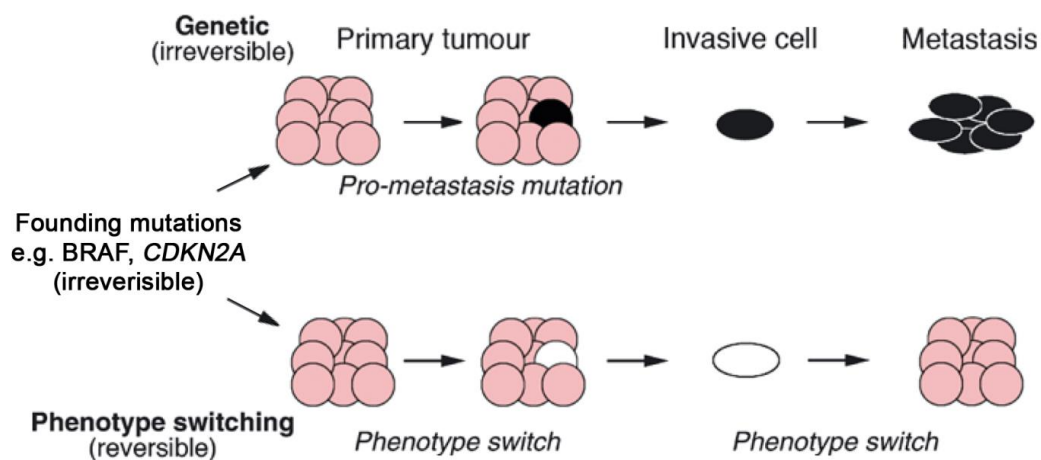
Figure 1.6. Genetic versus phenotype switching model for tumour progression. After founding mutations in the tumour to permit growth and evade senescence, there are two competing possibilities. First, invasiveness-promoting mutations are acquired in the genetic model that eventually permit migration from the parental tumour and metastasis to form a genetically distinct daughter. In the phenotype-switching model, the tumour microenvironment is key, and will promote cells to switch to advantageous phenotypes, which will encourage subsets of cells to reversibly adopt an invasive state and migrate out of the original tumour. When they reach a new site, the invading cell can revert to a proliferative phenotype to generate a metastasis. Adapted from Hoek and Goding (2010).

revealed two major expression signatures (Hoek et al., 2006). One was associated with proliferative, weakly invasive cells that are sensitive to growth inhibition by TGF-β, and the other was associated with highly migratory and invasive cells that are slow replicating and are TGF-β-insensitive. Transplantation assays with these cell lines have revealed that each class of cell line could generate heterogeneous tumours with cells matching both expression profiles, which provides strong evidence for the phenotype-switching model (Hoek et al., 2008).

1.3 Transcriptional regulation

Eukaryotes must process and respond to a wide range of extracellular stimuli to allow them to successfully function in their environment as well as to react to intracellular signals (Figure 1.7). Thus, the cell must continually receive and integrate signals simultaneously from different compartments to determine the appropriate biological response for its present situation. Once a response has been selected, it can be enacted in several ways. Protein levels, post-translational modification status, or sub-cellular localisation may be regulated. For example, Wnt signalling prevents cytoplasmic degradation of β-catenin, allowing β-catenin into the nucleus where it activates Wnt target genes, and plays crucial developmental roles (Taipale and Beachy, 2001). In the absence of Wnt signalling, β-catenin is localised in the cytoplasm and bound to E-cadherin at adherens junctions. Excess protein is targeted for proteasomal degradation in a process started by a complex comprised of axin, adenomatous polyposis coli (APC) and glycogen synthase kinase-3β (GSK-3β) (Hart et al., 1998). On stimulation of the transmembrane receptor Frizzled by Wnt molecules, Dishevelled is recruited to the membrane where it binds and inhibits the axin complex (Kishida et al., 1999; Smalley et al., 1999). β-catenin is released from the axin complex, whereupon it translocates to the nucleus and activates transcription

of Wnt target genes by interaction with the TCF/LEF family of transcription factors (Behrens et al., 1996).

Gene expression patterns are frequently modified in response to signalling pathways. This can be achieved in a number of ways. Cells can relax or compress chromatin structure, to activate or repress transcription respectively, by dynamically reconfiguring the post-translational modification status of histone tails and nucleosome deposition patterns. A large number of histone tail post-translational modifications have been identified, including phosphorylation, acetylation, methylation and SUMOylation. Histone tail lysine acetylation is generally positively associated with transcription (Figure 1.8). It neutralises the positive charge of the
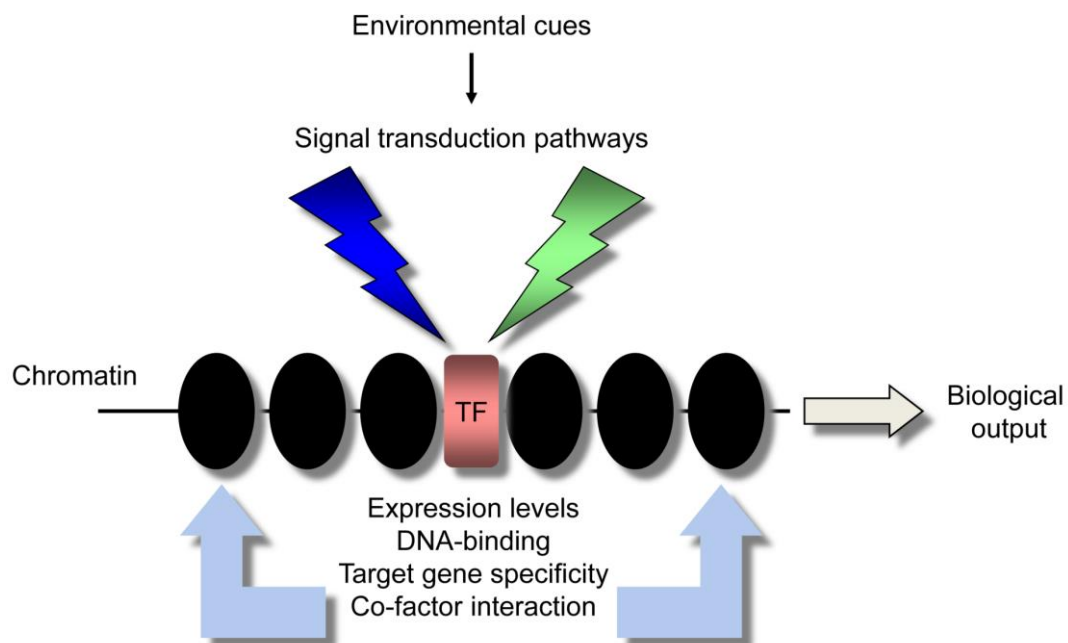
Figure 1.7. Cells are able to respond to multiple simultaneous intracellular and extracellular signals in a variety of ways. Cells integrate environmental cues via signal transduction pathways, which converge on transcription factors (TF) to induce a response. The transcription factors in turn drive a biological output by activating a gene expression programme. Transcription can be regulated at the chromatin level by altering post-translational modifications found on histone tails. Histones form nucleosomes (black), the positioning of which can also regulate transcription. Transcription factors may be regulated at the expression level, by altering their DNA binding activity or target gene specificity, or by modulating interactions with co-factors.

lysine side chain, which can interfere with charge-dependent DNA-histone interactions or interactions with other histones, with the net effect that the DNA becomes more accessible to the transcription machinery. It has been hypothesised that cumulative charge neutralisation can be important in activating transcription (Martin et al., 2004). In cancer, it has been revealed that deposition of post-translational modifications on histone tails is frequently aberrant, allowing for altered patterns of transcription (Fraga et al., 2005).

Histones are acetylated by histone acetyltransferases and deacetylated by histone deacetylases (HDACs), each of which have different substrate specificities. Turnover of histone lysine acetylation is extremely rapid, suggesting that histone acetyltransferases and the histone deacetylases (HDACs) that deacetylate histones are
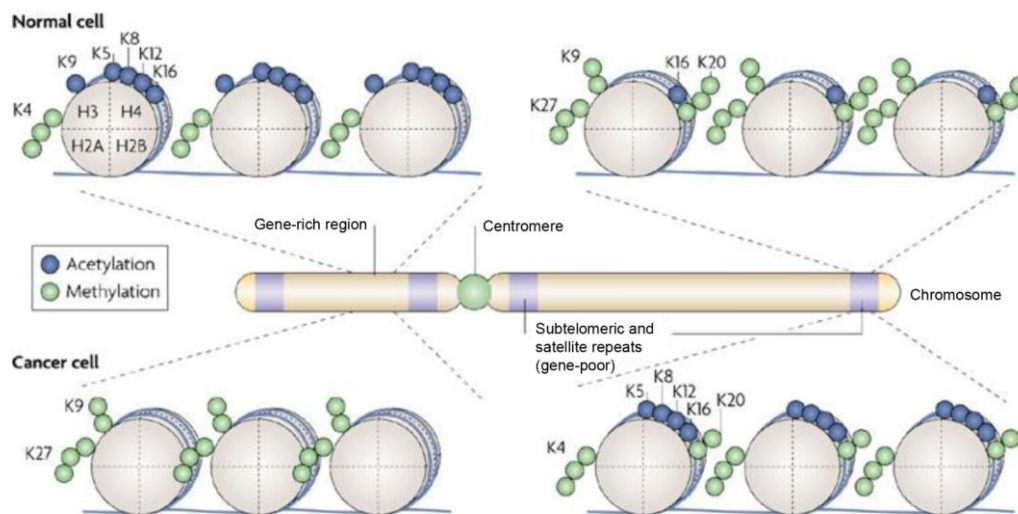
Figure 1.8. Histone modifications change in cancer. In healthy cells, actively transcribed regions are associated with post translational histone tail modifications such as H3 and H4 acetylation, and H3K4me3 while heterochromatic regions such as subtelomeres and repetitive regions are associated with modifications such as H3K9me2, H3K27me3 and H4K20me3. In cancer cells 'activating' modifications are often lost from gene-rich regions, disrupting gene expression; and repressive modifications are often lost from previously heterochromatic regions, leading to a more relaxed chromatin structure here. Adapted from (Esteller, 2007).

responsible for facilitating nucleosome mobilisation and subsequent restoration following passage of the transcription machinery (Katan-Khaykovich and Struhl, 2002; Wang et al., 2009).

Histone lysine acetylation can also provide a binding site for other proteins, and it is recognised by bromodomains (Tamkun et al., 1992). These domains are found in a range of chromatin-associated proteins and have a conserved four-helical bundle structure, with two variable loops that form the binding site for acetyl-lysine (Filippakopoulos et al., 2012). In contrast to their overall structure, bromodomains have poor sequence homology and highly variable surface electrostatic potential, which influences their substrate specificity. Further, adjacent post-translational modifications such as phosphorylation heavily influence bromodomain substrate recognition (Filippakopoulos et al., 2012).

Histones may be mono-, di-, or tri-methylated on both lysine and arginine residues with varied effects. Methylation has no effect on the lysine side-chain charge. For example, H3K4me3 has been shown to be highly associated with transcriptional start sites at actively transcribed genes (Bernstein et al., 2002; Bernstein et al., 2005). H3K36 methylation represses histone turnover at transcribed genes, which in turn represses gene expression (Venkatesh et al., 2012).

For a transcription factor to activate or repress transcription, it must be present in the nucleus, bind to promoters or enhancer regions either directly or indirectly via another DNA-bound transcription factor, and be able to influence the basal transcription machinery. Transcription factors can also be regulated by changing their sub-cellular localisation or blocking their degradation, or both, such as with the accumulation of nuclear β-catenin on activation of Wnt signalling.

1.3.1 Basic helix-loop-helix transcription factors

The basic helix-loop-helix (bHLH) family of transcription factors is a well conserved family of proteins—from yeast to multicellular organisms (Atchley and Fitch, 1997). The bHLH motif was first identified in 1989, and it plays important roles in DNA binding and dimerisation (Murre et al., 1989). The basic region binds the major groove of a consensus hexanucleotide sequence, 5'-CANNTG-3', where N is any base, termed the E-box (Voronova and Baltimore, 1990). The predicted structure of the motif was confirmed when the crystal structure of a c-Myc/Myc-associated factor X (MAX) heterodimer was solved, revealing that the bHLH protomer forms a structure of two alpha helices (α_1 contains the basic region and helix 1, and α_2 contains helix 2) connected by a loop region (Ferre-D'Amare et al., 1993). The dimer forms a parallel, left-handed, 4 helical bundle and the helices in these proteins are amphipathic; when DNA-bound, the proteins form a hydrophobic pocket that is shielded from the solvent. Protomers are DNA-bound such that they bind perpendicular to one another, on opposite sides of the E-box (Ferre-D'Amare et al., 1993). The structure of the bHLH is well conserved between different family members (Figure 1.9).

A carboxy-terminal addition to the bHLH is sometimes present, which plays roles in dimerisation and mediating extra-dimeric protein-protein interactions. Some family members, including the hypoxia-inducible factors have a Per-ARNT-Sim (PAS, ARNT, aryl hydrocarbon receptor nuclear translocator) domain (Crews et al., 1988; Nambu et al., 1991). PAS domains share poor sequence homology but are 260-300 amino acids in length, comprised of several alpha helices and 5 anti-parallel beta sheets, and play a role in mediating bHLH-PAS protein dimerization (Zelzer et al., 1997; Erbel et al., 2003).
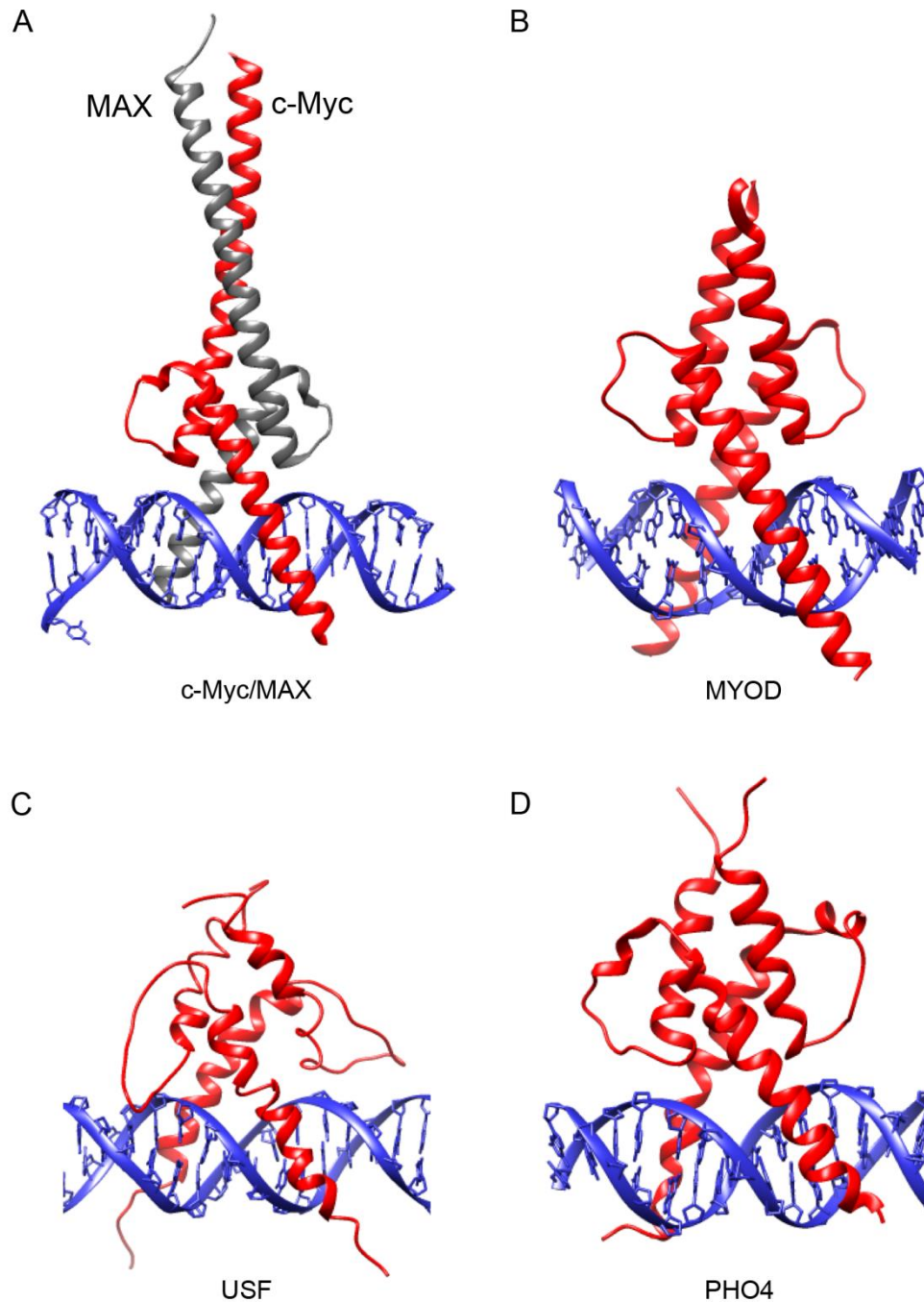
Figure 1.9. Structure of bHLH proteins. Atomic coordinates were obtained from the Protein Data Bank and visualised in Chimera v1.8. The basic region and helix 1 bind across the duplex; helix 2 (and where present, the leucine zipper) extend toward the top of the page. (A) c-Myc (red)/MAX (grey) heterodimer, 1NKP (Nair and Burley, 2003). (B) MYOD, 1MDY (Ma et al., 1994). (C) Upstream stimulatory factor (USF), a ubiquitous transcriptional activator, 1AN4 (Ferre-D'Amare et al., 1994). Note that this structure does not show the LZ of USF. (D) PHO4, a transcriptional activator from *Saccharomyces cerevisiae*, 1A0A (Shimizu et al., 1997). Note that MYOD and PHO4 are bHLH proteins, while c-Myc, MAX, and USF are bHLH-LZ proteins.

In some bHLH proteins such as c-Myc and MAX (Murre et al., 1989), the bHLH may be extended by placing leucine residues, or other hydrophobic amino acids, at approximately 7 amino acid intervals. These residues contact a leucine at the equivalent position in the second protomer, thus playing a large role in protein dimerization. α_2 may be extended into the leucine zipper (LZ), which, like the bHLH, is amphipathic; it extends the hydrophobic pocket and overall coiled coil structure of the motif.

bHLH proteins bind DNA either as homodimers or as heterodimers with other members of the family; this interaction is mediated by the HLH. When present, a PAS or LZ motif plays a role in this. Heterodimerization provides the potential for altered DNA binding specificity, either within the core E-box or in the flanking regions. For example, c-Myc is a proto-oncogene that promotes cell cycle progression and can induce apoptosis (Evan et al., 1992; Amati et al., 1993). It must be heterodimerised with MAX in order to bind DNA (Blackwood and Eisenman, 1991; Prendergast et al., 1991; Amati et al., 1992). Indeed, in cells most c-Myc is found heterodimerised with MAX (Blackwood et al., 1992; Littlewood et al., 1992). MAX can homodimerise and repress transcription (Kato et al., 1992; Kretzner et al., 1992; Prendergast et al., 1992) as well as activate it (Fisher et al., 1993). The dimerisation partner of MAX determines its DNA binding specificity. A MAX homodimer can bind to a 5'-TCACGTGA-3' motif, while the c-Myc/MAX heterodimer cannot (Fisher et al., 1993; Solomon et al., 1993). Because there are many more 5'-CANNTG-3' elements genome-wide than could possibly be bound by any one transcription factor, heterodimerisation thus represents a mechanism for redirecting molecules to a subset of these locations.

1.3.2 Lineage-specific transcription factors

Genesis of different cell types requires pluripotent stem cells to commit to lineages, which is achieved by expression of cell type-specific genes. A cell will often transit through a number of progressively differentiated steps before arriving at the final, terminally differentiated cell, which requires fine temporal and spatial control of gene expression in response to extracellular signals. This can be achieved through lineage-specific restriction of transcription. Many transcription factors can theoretically bind a particular motif in a given regulatory region, and understanding how signalling pathways bring about binding of the correct transcription factors to the correct motif, at the correct time, is a major question.

One way to lineage-restrict transcription is through interaction of lineage-specific transcription factors with ubiquitously expressed ones. For example, Glycophorin B is expressed specifically in erythroid cells and, along with Glycophorin A, is responsible for the MNS antigen system (Siebert and Fukuda, 1987). Sp1 is ubiquitously expressed and binds to an element in the *Glycophorin B* promoter, but the gene is expressed only in erythroid cells where the erythroid-specific transcription factor GATA-1 also binds to a promoter element and interacts with Sp1 to activate transcription (Rahuel et al., 1992; Gregory et al., 1996).

Alternately, lineage-specific transcription factors can directly induce transcriptional programmes themselves. Skeletal muscle development is controlled by 4 myogenic bHLH transcription factors: myoblast determination protein (MYOD), myogenic factors 5 and 6, and Myogenin, of which MYOD is the 'master regulator' (Lassar et al., 1986; Lassar et al., 1989; Braun and Gautel, 2011). In agreement with *in vitro* studies investigating MYOD DNA binding, genome-wide MYOD profiling

revealed the *in vivo* MYOD consensus E-box to be 5'-CA[C/G]CTG-3' (Blackwell and Weintraub, 1990; Blais et al., 2005; Cao et al., 2006; Cao et al., 2010).

Id is an HLH protein lacking a basic region and cannot bind DNA as homodimers. When heterodimerised with bHLH transcription factors, including MYOD, Id inhibits the transcriptional activity of the bHLH protein by preventing the heterodimers from binding DNA (Benezra et al., 1990; Sun et al., 1991; Kreider et al., 1992). However, upon commitment to myogenic differentiation, MYOD levels increase while those of Id do not, thus allowing MYOD to outcompete Id and activate skeletal muscle-specific gene expression patterns.

MYOD interacts with the histone acetyltransferase protein p300, which stimulates activation of transcription by MYOD (Yuan et al., 1996). Further, p300 recruits p300/CBP associated factor (PCAF) to MYOD, which is subsequently acetylated at K99 and K102 both *in vitro* and *in vivo* (Sartorelli et al., 1999; Polesskaya et al., 2000; Duquet et al., 2006). Acetylation of MYOD enhances its transcriptional activity and, in mice, MYOD K99/102R was sufficient to impair regeneration of skeletal muscle, demonstrating that acetylation at these sites is important for skeletal muscle differentiation (Duquet et al., 2006).

1.4 *Microphthalmia*-associated transcription factor

The *microphthalmia* (*mi*) locus was first identified in 1942, and gives rise to pigmentation and other phenotypic defects such as reduced eye size and mast cell counts (Hertwig, 1942). Twenty years ago, *microphthalmia*-associated transcription factor (Mitf) was cloned and identified as the bHLH-LZ transcription factor whose mutation was responsible for the phenotype in the *mi* mouse (Hodgkinson et al., 1993; Hughes et al., 1993). The human homologue was cloned the following year, expressed from chromosome 3p14-2 to 14-1, and was named MITF (Tachibana et al., 1994).

MITF has a complex gene structure with multiple promoters (Figure 1.10).

Exons 2 through 9 are common between the 10 isoforms that have been identified in

humans, which have short alternate sequences for exon 1. In nine isoforms, the variant

exon 1 is spliced onto a later part of exon 1b (exon 1B1b), before fusion to the shared

exons. In contrast, *MITF-M*, which is the most proximal to the joint exons, has exon

1m fused directly to exon 2 (Fuse et al., 1996). Translation is initiated at exon 1 of

MITF-A (Amae et al., 1998), *MITF-B* (Udono et al., 2000), *MITF-C* (Fuse et al.,

1999), *MITF-CM* (Shiohara et al., 2009), *MITF-H* (Steingrímsson et al., 1994), *MITF-*

J (Hershey and Fisher, 2005), *MITF-M* (Fuse et al., 1996), and *MITF-Mc* (Takemoto

et al., 2002). However, *MITF-D* and *MITF-E* lack an initiating ATG at their

respective exon 1d and 1e, and so initiate translation within exon 1B1b and encode the

same protein product as each other (Oboki et al., 2002; Takeda et al., 2002). To date,

there have been no regions found in these alternate initiating exons that play roles in
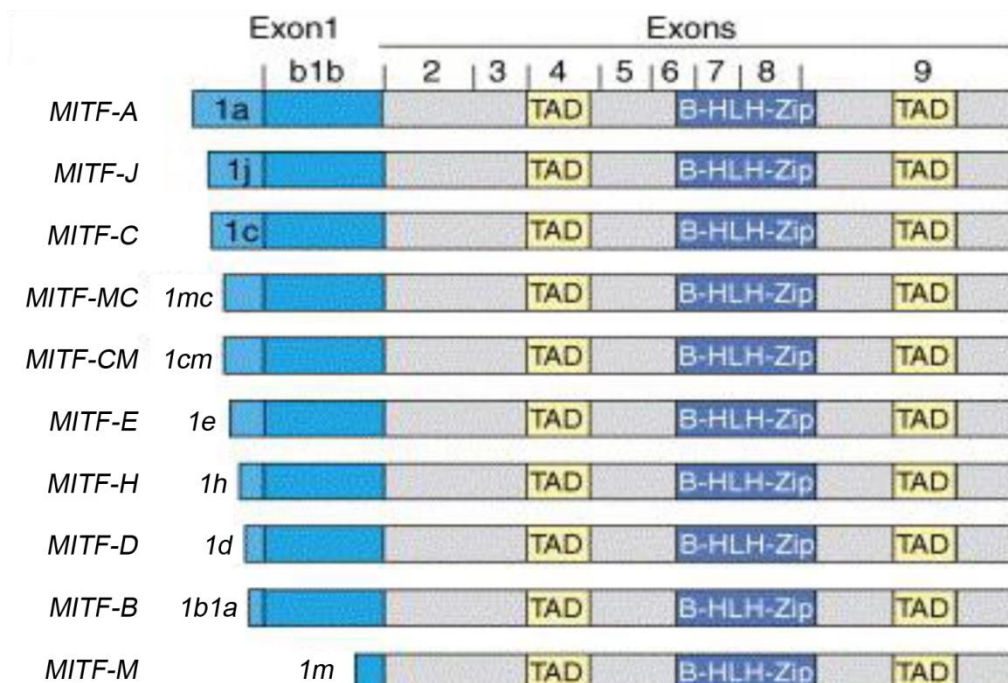
Figure 1.10. ***MITF* gene structure and mutant phenotypes.** Structure of the
characterised isoforms of human MITF, showing alternative exon 1 and common
exons 2-9. TAD: transactivation domain. Adapted from (Levy et al., 2006).

MITF function. Different isoforms of MITF display different expression patterns, with *MITF-M* restricted to melanocytes, where it is the dominantly expressed isoform.

MITF is also subject to internal splicing at exon 6a, which may or may not be included. Exon 6a inclusion encodes a 419 amino acid protein termed MITF(+), while lack of exon 6a leads to the 413 amino acid MITF(-) (Hemesath et al., 1994; Steingrimsson et al., 2002). The relative expression of these isoforms is regulated by MAPK signalling, which promotes inclusion of exon 6a (Primot et al., 2010). Unless otherwise noted, MITF refers to MITF-M(+) from this point on, which is expressed from the M-promoter and has been the main focus of study for the MITF field to date, and also to generic MITF where the authors of a paper have failed to state which isoform they worked with. Where *Mitf*/Mitf is used, it refers specifically to the mouse gene and protein, while *MITF*/MITF refers mostly to the human gene and protein, but also to MITF in general (as MITF protein structure and function is very well conserved between mouse and human).

1.4.1 MITF: master regulator of the melanocytes

MITF is essential for maintenance of the melanocyte lineage, and it acts as the master regulator. In *mi* mice, loss of an arginine in the basic region of Mitf puts the basic region out of register with helix 1, preventing the mutant protein from binding to DNA (Hodgkinson et al., 1993; Hughes et al., 1993; Hemesath et al., 1994; Steingrímsson et al., 1994). The homozygous *mi* mouse contains no melanocytes. It is completely white, with small, unpigmented eyes (Hodgkinson et al., 1993). The absence of melanocytes in the eye indicates a failure of the non-neural crest originating RPE cells to develop, showing that the phenotype is not neural-crest specific but melanocyte-specific. It was subsequently shown that Mitf is necessary for melanocyte development, playing crucial roles in promoting the conversion of

precursor cells derived from the neural crest to melanoblasts and in influencing their subsequent survival (Opdecamp et al., 1997; Hornyak et al., 2001). In the absence of Mitf, conversion to melanoblasts fails to occur.

MITF is also required to maintain the MSC population. Hair greying results from loss of MSCs, and a D222N mutation of Mitf ($Mitf^{vit}$) significantly accelerates this process (Lerner et al., 1986; Nishimura et al., 2005). Because coat colour is an easy phenotype to observe, numerous *Mitf* mutant mice have been derived, often by spontaneous mutation (Steingrimsson et al., 2004). Where the mutant alleles result in a heterozygote, they show either no pigmentation phenotype or a white belly-spot. White belly-spotted mice carry basic region Mitf mutations. Therefore, while the mutant proteins could still dimerise, they could not bind DNA, as in the case of the original *mi* mouse (Steingrímsson et al., 1994). The belly spot results from impaired migration through the neural crest of melanoblast precursor cells (Opdecamp et al., 1997).

As well as mice and man (Hodgkinson et al., 1993; Hughes et al., 1993; Tassabehji et al., 1994b), MITF has been found to be well-conserved throughout multiple animal species, including chicken, quail, hamster, rat, and dog, with mutations in these homologues all resulting in defective pigmentation phenotypes (Hodgkinson et al., 1998; Mochii et al., 1998; Opdecamp et al., 1998; Weilbaecher et al., 1998; Karlsson et al., 2007; Minvielle et al., 2010). The zebrafish *Danio rerio* contains two *MITF*-related genes, *nacre* and *mitfb*. *nacre* is expressed in both eye and neural crest melanocyte precursors, but loss-of-function mutations affect only neural crest melanophores (Lister et al., 1999). The second gene, *mitfb*, is homologous to MITF-A, and is expressed in eye precursors but not in the neural crest (Lister et al., 2001). In lower species, two isoforms of an *MITF* homologue have been identified in

Xenopus laevis (Kumasaka et al., 2005), and an *MITF* homologue has also been described in *Drosophila melanogaster*, where it plays a similar role in eye development as it does in mammals (Hallsson et al., 2004). Other invertebrates expressing an *MITF* homologue include ascidians (Yajima et al., 2003) and jellyfish (Kozmik et al., 2008). This conservation of MITF indicates that the gene must have arisen in common ancestors that existed before the division of vertebrates and invertebrates and that, with its functions in the *Drosophila* eye, its original function could have been in eye development.

Waardenburg syndrome is the collective name for a series of genetic conditions in which congenital hearing loss and changes in hair, skin and eye pigmentation occur. Not all individuals are affected in the same way and hearing can be unaffected, or deafness may occur in one or both ears and range from moderate to total. Pale blue or differently coloured eyes are common, along with prematurely greying hair or a white patch (Waardenburg, 1951; Read and Newton, 1997). There are four main types of Waardenburg syndrome, defined by their symptoms, and they correlate well with different mutations that have been identified. Type I and Type III are caused by *PAX3* mutation (Baldwin et al., 1992; Tassabehji et al., 1992; Hoth et al., 1993; Zlotogora et al., 1995); Type IIA can be caused by mutation in *MITF* (Hughes et al., 1994; Tassabehji et al., 1994a); Type IIC/D can be caused by *SNAI2* mutation (Sanchez-Martin et al., 2002); and Type IV can be caused by mutations in the *SOX10*, *EDN3*, or *EDNRB* genes (Puffenberger et al., 1994; Attie et al., 1995; Edery et al., 1996; Kuhlbrodt et al., 1998b; Pingault et al., 1998). The proteins controlling Waardenburg syndrome also regulate *MITF* expression, as will be discussed later, suggesting that MITF could be the major player in these conditions.

MITF is necessary and sufficient to induce melanocytic differentiation (Tachibana et al., 1996; Planque et al., 1999). In differentiated melanocytes, MITF is responsible for induction of the pigmentation programme (Figure 1.11), upregulating genes that play roles at each stage of the process (Cheli et al., 2010). Three of the key genes involved in synthesis of melanin, *Tyrosinase* (Lowings et al., 1992; Bentley et al., 1994; Yasumoto et al., 1994; Galibert et al., 2001), *TYRP1* (Yavuzer et al., 1995; de la Serna et al., 2006), and *DCT* (Bertolotto et al., 1998c; Lang et al., 2005), are directly regulated by MITF. In the case of *Tyrosinase* and *TYRP1*, MITF recruits the SWI/SNF ATP-dependent chromatin-remodelling complex to the promoter to activate
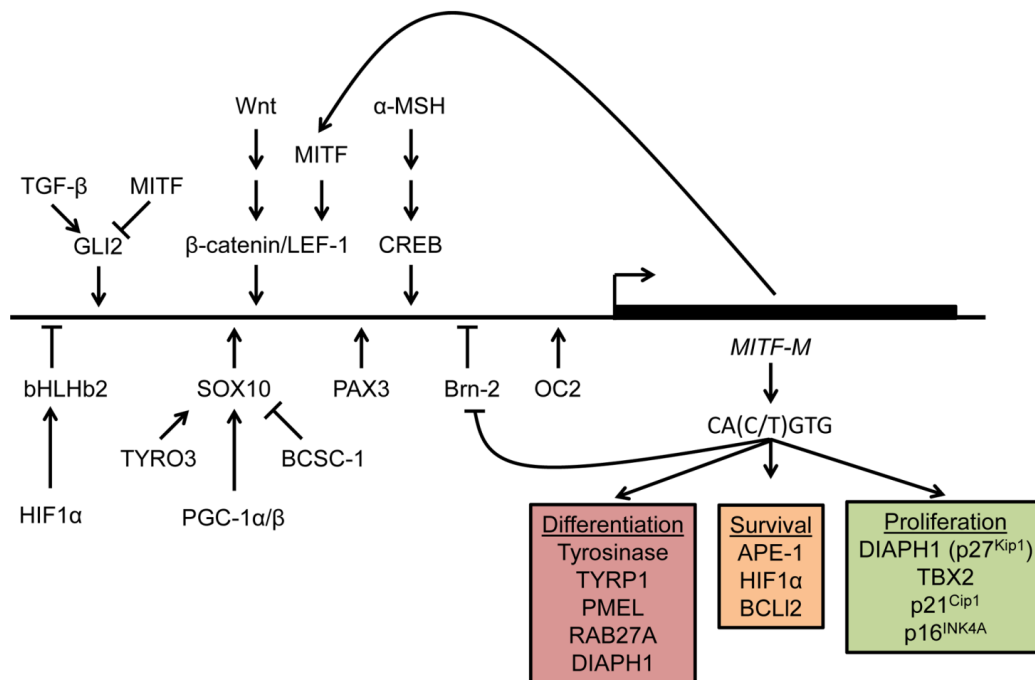
Figure 1.11. Roles and regulation of MITF-M. MITF-M is subject to complex transcriptional regulation, as outlined in the text. At the top is shown the *MITF-M* gene (thick bar) with the promoter to the left (thin bar). The transcription start site is marked by the arrow at the junction. The various transcription factors that have been shown to bind to the *MITF-M* promoter, and either stimulate or repress *MITF* expression, are illustrated. Distances to the transcription start site are not to scale. MITF-M binds to CA(C/T)GTG elements in the promoters and enhancers of its target genes (middle). MITF-M regulates a wide range of processes, including genes regulating differentiation (red box), survival (orange box), and proliferation (green box). It also represses Brn-2 expression, and can promote its own expression by binding to LEF-1 which is bound to the *MITF-M* promoter.

transcription (de la Serna et al., 2006). *DCT* expression is more complex, and the activities of CREB, SOX10 and LEF-1, which are all recruited to the *DCT* promoter by MITF, combine to activate *DCT* expression (Bertolotto et al., 1998b; Yasumoto et al., 2002; Ludwig et al., 2004), while PAX3 represses activation of *DCT* by MITF or SOX10 (Lang et al., 2005).

MITF also regulates genes that play a role in melanosome biogenesis and transport. For example, PMEL, the human Silver homologue required for melanosomal matrix formation, is up-regulated by MITF binding to an enhancer in intron 1 (Baxter and Pavan, 2003; Du et al., 2003). RAB27A is a small GTP-binding protein, embedded in the melanosome membrane, that complexes with Myosin-Va to permit the actin cytoskeleton to transport the melanosome (Bahadoran et al., 2001), and it is up-regulated by MITF (Chiaverini et al., 2008). Finally, MITF induces the *DIAPH1* gene, promoting actin polymerisation and melanocyte dendricity, and increasing the melanocyte surface area available for melanosome export (Carreira et al., 2006).

Differentiating cells frequently undergo a cell-cycle arrest, or reduce their progress through the cell cycle, and melanocytes are no exception. MITF induces G1/S arrest in melanocytes by the up-regulation of *CDKN2A* and *CDKN1A*, which encode either p16^{INK4A} and p14^{ARF} or p21^{Cip1} respectively (Carreira et al., 2005; Loercher et al., 2005). On differentiation, MITF up-regulates the DICER subunit of the RNA induced silencing complex (RISC), which processes pre-miRNAs into their mature form (Levy et al., 2010a).

Underscoring the white phenotypes of varying severity observed in *Mitf* mutant mice, MITF is capable of inducing a pattern of gene expression in melanocytes that drives the production and export of melanin. One *Mitf* mutant, *Mi^{b}*

carries Mitf^{G244E} mutation (Steingrimsson et al., 1996). G244 lies in the loop region, and mutation here was found to interfere with DNA binding and produced a mouse with a brown coat rather than the usual black found in wild-type mice (Steingrimsson et al., 1996).

1.4.2 MITF: regulation of its expression

In mice, *Mitf* expression changes throughout development. It is first detected at the 22-somite stage (approximately E9.5) throughout the optical vesicle; it is restricted to the proximal optic vesicle by the 26-somite stage; once the optic cup is present, it is expressed solely in cells that will go on to form the RPE (Nguyen and Arnheiter, 2000). *Mitf* is first expressed in neural crest-derived precursors that initially appear close to the head and express DCT and Kit, markers of melanoblasts; these cells later migrate towards the tail (Opdecamp et al., 1997; Nakayama et al., 1998). Later still *Mitf* will be found in the choroid of the eye and in whisker follicles (Nakayama et al., 1998). Newborn mice restrict *Mitf* expression to hair follicles and the RPE, while, in adult mice, melanocytes, osteoclasts mast cells, heart cells and skeletal muscle all express *Mitf* (Hodgkinson et al., 1993; Weilbaecher et al., 1998; King et al., 2002).

The *MITF-M* promoter is highly conserved between mice and humans, with 85% identity for the first 400 nucleotides upstream of the transcription start site (Potterf et al., 2000). In both species, MITF-M is melanocyte-specific, while the expression pattern of other isoforms varies by tissue (Fuse et al., 1996; Udono et al., 2000), which shows that lineage-restricted factors must play a key role in inducing *MITF-M*. *Mitf* is induced by a number of different transcription factors (Figure 1.11), many of which can subsequently cooperate with MITF to execute its role in inducing pigmentation. Wnt3a is expressed before Mitf in the developing embryo. Together

with Wnt1, Wnt3a is required for efficient generation of cells originating from neural crest precursors, in part by *Mitf* up-regulation (Takada et al., 1994; Ikeya et al., 1997; Dorsky et al., 1998; Nakayama et al., 1998). Wnt3a overexpression in melanocytes can up-regulate *MITF* through TCF/LEF, complexed with β-catenin, binding to three sites in the *MITF* promoter (Dorsky et al., 2000; Takeda et al., 2000b; Widlund et al., 2002). To date, no MITF binding site in its own promoter has been described, but MITF has been shown to positively influence its own transcription by binding LEF-1 that is bound to the *MITF* promoter (Saito et al., 2002; Yasumoto et al., 2002). Wnt signalling also plays a role in MITF function, stimulating binding of β-catenin to helix 2 of MITF (Schepsky et al., 2006). MITF recruits β-catenin to melanocyte-specific MITF target genes such as *Tyrosinase*, where it stimulates their expression (Schepsky et al., 2006).

PAX3 is also required for melanocyte specification from the neural crest (Galibert et al., 1999; Lang et al., 2005). It up-regulates *MITF* by binding to one site in the *MITF* promoter that is conserved between mice and humans (Watanabe et al., 1998; Potterf et al., 2000), and to a second site that is human-specific (Bondurand et al., 2000). SOX10 induces *MITF* expression, binding and activating the *MITF* promoter (Lee et al., 2000; Potterf et al., 2000), as well as a more distant enhancer element (Watanabe et al., 2002). In glial cells, PAX3 and SOX10 act synergistically to transactivate their targets (Kuhlbrodt et al., 1998a), and the same is true in the melanocyte lineage: they act together to drive *MITF* expression (Bondurand et al., 2000). The tyrosine-protein kinase receptor TYRO3 promotes SOX10 nuclear localisation, triggering a stronger *MITF* induction (Zhu et al., 2009). Finally, binding of breast cancer suppressor candidate-1 to SOX10 inhibited its ability to up-regulate MITF, promoting migration of melanoma cells (Anghel et al., 2012).

Early work showed that cAMP signalling in melanocytes is induced by α-MSH binding MC1R, leading to CREB activation. CREB promotes pigmentation in an MITF-dependent fashion (Bertolotto et al., 1996b; Busca and Ballotti, 2000). Taking this one step further, *MITF* is up-regulated by stimulation of cAMP signalling in both melanocytes and melanoma cells (Bertolotto et al., 1998a; Price et al., 1998b). Because CREB is ubiquitously expressed, its role in inducing *MITF* is restricted to the melanocyte lineage by the actions of SOX10, which binds 100 bp upstream from CREB (Huber et al., 2003). Both proteins are required for a robust activation of *MITF*.

In conjunction with feed-forward induction of *MITF* by α-MSH and cAMP signalling, α-MSH has recently been demonstrated to induce the mitochondrial biogenesis promoting PPAR-γ coactivator (PGC)-1α which, along with PGC-1β, up-regulates *MITF* in conjunction with SOX10 (Shoag et al., 2013). MITF, in turn, induces *PGC1α*, promoting oxidative phosphorylation in melanoma cells (Haq et al., 2013). Onecut-2, a cut-homeodomain transcription factor expressed in melanocytes, has also been reported to bind and activate the *MITF* promoter (Jacquemin et al., 2001).

The transcription factor GLI2, which mediates Hedgehog signalling (Kasper et al., 2006), promotes melanoma cell invasiveness in response to TGF-β/SMAD signalling (Dennler et al., 2007; Javelaud et al., 2008). GLI2 is able to repress *MITF* (Javelaud et al., 2011). *MITF* can also be repressed by hypoxic environments. Hypoxia inducible factor 1 (HIF1α) is up-regulated on induction of hypoxia in melanoma cells which, in turn, up-regulates a number of transcription factors including the bHLH protein bHLHb2 (Olbryt et al., 2006). Consequently, bHLHb2

has been demonstrated to bind and repress the *MITF* promoter (Feige et al., 2011; Cheli et al., 2012).

The POU domain containing transcription factor Brn-2, induced in response to β-catenin and whose activity is stimulated by MAPK signalling, promotes melanoma cell growth (Goodall et al., 2004b; Goodall et al., 2004a). Brn-2 directly binds and represses the *MITF* promoter (Goodall et al., 2008). However, Brn-2 has also been reported to activate MITF expression in certain melanoma cell lines (Wellbrock et al., 2008), reflecting a potentially complex regulatory relationship.

1.4.3 MITF: protein structure and function

MITF is a member of the Myc superfamily of bHLH-LZ transcription factors (Hodgkinson et al., 1993; Hughes et al., 1993). Like other members of this family, it binds a 5'-CANNTG-3' E-box (specifically 5'-CACGTG-3' or 5'-CATGTG-3') elements in the promoters of its target genes (Bentley et al., 1994; Hemesath et al., 1994; Yasumoto et al., 1994). In the case of a 5'-CATGTG-3' motif, a 5' flanking T residue is required for strong MITF binding, while there is no such requirement for a 5'-CACGTG-3' motif (Aksan and Goding, 1998). The 5'-TCATGTG-3' has been termed an M-box because it was conserved in all melanocyte-specific promoters. A recent review article compiled all confirmed MITF binding sites and found that among them the consensus binding site for MITF was 5'-TCA[C/G]GTG-3' (Cheli et al., 2010), in agreement with the previous studies. However, the molecular mechanism controlling how MITF is able to distinguish between 5'-CACGTG-3' and 5'-CATGTG-3' binding sites, and how the presence of different flanking sequences affects this, remains to be determined.

Like other bHLH proteins, MITF can bind to its target DNA motifs either as homodimers or as heterodimers with other members of the MiT subfamily of bHLH-

LZ transcription factors, TFE3, TFEB, and TFEC (Hemesath et al., 1994). MITF does not, however, heterodimerise with other bHLH-LZ factors such as c-Myc, MAX, and USF (Hemesath et al., 1994), even though all these proteins can bind to very similar sequences. The recent MITF-DNA co-crystal structure revealed that a three amino acid insertion, 260-262, in the first heptad of the leucine zipper introduced a break in helix α2, with the remaining heptads forming a new helix and giving the overall leucine zipper a kinked structure (Pogenberg et al., 2012). This insertion is unique to MiT proteins, and their deletion permitted MITF heterodimerisation and DNA binding with MAX, showing that the insertion is responsible for restricting MITF heterodimerisation to other MiT proteins (Pogenberg et al., 2012).

As mentioned above, MITF interacts with β-catenin and the SWI/SNF complex, which function as MITF co-activators. MITF also interacts with the histone acetyltransferases p300 and CBP, which stimulate MITF transcriptional activity (Sato et al., 1997). Two repressors of MITF transcriptional activity have been identified. Protein kinase C-interacting protein 1 binds and represses MITF in mast cells, which do not express MITF-M, and was also shown to bind MITF in melanocytes, although no functional studies were performed in the melanocytes (Razin et al., 1999). The E3 SUMO-protein ligase PIAS3 is also able to repress MITF transcriptional activity by binding to its leucine zipper and interfering with MITF DNA binding activity (Levy et al., 2002; Levy et al., 2003).

1.4.4 MITF: post-translational modifications

A number of post-translational modifications of MITF have been described. c-KIT induces ERK2-mediated phosphorylation on S73 (Hemesath et al., 1998), and subsequently ERK2 activates Rsk90 to phosphorylate MITF on S409 (Wu et al., 2000). MAPK-mediated phosphorylation of MITF is reported to increase its

transcriptional activity by association with p300/CBP (Price et al., 1998a). Phosphorylation of S73/409 is dispensable for the developmental role of MITF, as expression of *Mitf*^{S73A}, *Mitf*^{S409A}, or *Mitf*^{S73/409A} can complement an *Mitf*-null mouse, restoring a wild-type phenotype (Bauer et al., 2009). Phosphorylation at S409 also relieves repression of MITF by PIAS3 (Levy et al., 2003). Finally, stimulation of c-KIT signalling also leads to tyrosine phosphorylation at 3 sites in the N-terminus of MITF (Lars Ronnstrand, personal communication).

ERK2-mediated phosphorylation of MITF has been reported to enhance proteasomal degradation of MITF through ubiquitylation at K201 (Wu et al., 2000; Xu et al., 2000), putting a counterbalance on the activation triggered by MAPK signalling. MITF-ubiquitylation can be reversed by ubiquitin-specific protease 13 (USP13), which elevates MITF protein levels and promotes melanoma growth (Zhao et al., 2011).

MITF has been shown to be phosphorylated on S298 in response to glycogen synthase kinase 3β (GSK-3β) activity, which enhances transactivation of the *Tyrosinase* promoter in reporter assays (Takeda et al., 2000a). Finally, in osteoclasts, MITF can be phosphorylated on S307 by the MAPK p38, downstream of stimulation by receptor of NF-κB ligand (RANKL), leading to up-regulation of osteoclast-specific target genes (Mansky et al., 2002). To date, this phosphorylation event has yet to be shown to occur in the melanocyte lineage.

Two small ubiquitin-like modifier (SUMO) acceptor sites have been identified in MITF, at K182 and K316, which modulated transcription when acting in synergy with other transcription factors (Miller et al., 2005; Murakami and Arnheiter, 2005). Blocking MITF SUMOylation enhanced transactivation by MITF of promoters

carrying multiple MITF binding sites, and also MITF-SOX10 cooperation in activating the *DCT* promoter.

1.4.5 MITF: lineage survival oncogene

MITF expression is retained in many melanomas and melanoma cell lines (Vachtenheim and Novotna, 1999; Garraway et al., 2005). It is required for melanoma cell proliferation (Widlund et al., 2002; Du et al., 2004), and it has been implicated in melanoma progression. Mutations in the activation domains have been identified in melanoma patients which, *in vitro*, give rise to altered DNA binding activity (Cronin et al., 2009; Grill et al., 2013). One bHLH-LZ mutation has been identified, MITF^{G244R}, which also altered DNA binding (Cronin et al., 2009), similar to the effects of the *Mi^b*-causing Mitf^{G244E} mutation (Steingrimsson et al., 1996). Importantly, an MITF^{E318K} mutation has been identified in patients with a familial predisposition to melanoma, resulting in defective SUMOylation at K316 and increased genome-wide MITF DNA binding (Bertolotto et al., 2011; Yokoyama et al., 2011). *MITF* may be amplified in melanoma, especially metastatic disease (Garraway et al., 2005), and it is able to synergise with BRAF activation to transform melanocytes and promote melanoma cell growth (Garraway et al., 2005; Wellbrock et al., 2008). It has been proposed that MITF is a lineage survival oncogene, where the dependency on *MITF* for melanocyte lineage maintenance is carried over into the melanoma (Garraway et al., 2005).

Brn-2 has been reported to up-regulate *MITF in vitro* (Wellbrock et al., 2008), and to repress *MITF in vivo*, where MITF and Brn-2 expression patterns were mutually exclusive within the same melanoma and served to mark distinct subpopulations of cells (Goodall et al., 2008; Thurber et al., 2011). Brn-2 positive cells are more invasive with enhanced Notch signalling than MITF positive cells,

which are less invasive with reduced Notch signalling (Pinner et al., 2009; Thurber et al., 2011). These conflicting results were reconciled by the discovery that miR-211 is a repressor of Brn-2 (Boyle et al., 2011). miR-211 is expressed from the *Melastatin* (*TRPM1*) locus, which is regulated by MITF (Miller et al., 2004), presenting a positive feedback loop generating a bi-stable state where either MITF or Brn-2 can be expressed, but not both. miR-211 also functions as a tumour suppressor and represses melanoma cell invasiveness (Levy et al., 2010b; Mazar et al., 2010), which is mediated by Brn-2-suppression (Boyle et al., 2011). miR-211 can be significantly down-regulated in melanoma and melanoblasts relative to melanocytes (Jukic et al., 2010; Stark et al., 2010), allowing Brn-2 to dominate the balance between MITF and Brn-2 levels, promoting a phenotype switch to show more invasive behaviour (Hoek et al., 2008; Pinner et al., 2009).

MITF plays important roles in melanoma cell growth and survival. It induces the apurinic/apyrimidinic endonuclease 1 (APE-1) (Liu et al., 2009), which relieves the oxidative stress caused by ROS that are elevated in melanoma (Meyskens et al., 1997). MITF also up-regulates the *MET* proto-oncogene, encoding the hepatocyte growth factor receptor, which promotes invasiveness and protectes melanocytes and melanoma cells from apoptosis (McGill et al., 2006; Beuret et al., 2007). MITF has also been reported to target the anti-apoptotic protein BCL2 (McGill et al., 2002), which is essential for the maintenance of MSCs, melanoblasts and melanocytes, as well as melanoma cells (McGill et al., 2002; Nishimura et al., 2005; Mak et al., 2006).

Furthermore, MITF, downstream of α-MSH signalling, induces *HIF1α*, conferring protection against cellular stresses (Busca et al., 2005). Conflictingly, it has also been reported that while MITF down-regulation does not induce apoptosis, it is cleaved by caspases during the apoptotic process, and that the C-terminal fragment

could activate caspase 3 and promote adoption of pro-apoptotic melanoma cell morphology (Larribere et al., 2005).

MITF plays a role in suppression of senescence by inducing the anti-senescence factor TBX2 (Carreira et al., 2000), which is up-regulated in melanoma and inhibits senescence and cell cycle arrest by repressing p21^{Cip1} and p19^{ARF} (Jacobs et al., 2000; Prince et al., 2004; Vance et al., 2005). Indeed, MITF-silencing by siRNA depletion can induce senescence (Giuliano et al., 2010). MITF activity is required for faithful passage through mitosis and DNA replication and repair which, if uncorrected, can result in senescence (Strub et al., 2011).

MITF promotes growth by inducing CDK2, allowing progression through G1/S (Widlund et al., 2002; Du et al., 2004). Low *MITF* expression induces a G1/S cell cycle arrest, accompanied by invasive behaviour, by indirectly inducing p27^{Kip1} as a result of loss of expression of the MITF target gene *DIAPH1* (Carreira et al., 2006). Loss of DIAPH1 resulted in inhibition of the F-box protein SKP2, which functions as part of a complex that targets cell cycle regulating proteins for proteasomal degradation (Mammoto et al., 2004). One of the proteins SKP2 degrades is p27^{Kip1} (Carrano et al., 1999; Tsvetkov et al., 1999), hence the G1 arrest induced by loss of *MITF* (Carreira et al., 2006).

However, in contrast to this, high *MITF* induces a cell cycle arrest. MITF physically interacts with Rb, and the two cooperate in melanocytes and melanoma cells by inducing expression of p21^{Cip1}, which causes a G1/S cell cycle arrest (Carreira et al., 2005). In melanocytes, elevated *MITF* expression can also induce a cell cycle arrest through p16^{INK4A} up-regulation (Loercher et al., 2005). However, the same is not true in melanoma cell lines, and it was hypothesised that one potential reason for the loss of p16^{INK4A} in so many melanomas could be selection pressure for

mutations that confer an escape from MITF-induced growth arrest in melanocytes (Loercher et al., 2005).

A rheostat model of MITF activity has been proposed to explain the pro- and anti-proliferative activities of MITF on melanoma and melanocyte lineage cells (Carreira et al., 2006). A range of outcomes can result from differing MITF levels: apoptosis or senescence in otherwise healthy cells lacking MITF; G1/S cell cycle arrest resulting from low MITF, which induces p27^{Kip1} (low MITF also induces an invasive, stem cell-like state); proliferation with intermediate MITF; and differentiation accompanied by a p21^{Cip1}/p16^{INK4A}-induced G1/S cell cycle arrest by very high MITF (Figure 1.12). While apoptosis is irreversible and terminal differentiation thought to be too, it was speculated that, within the range of more moderate *MITF* expression, phenotypic changes should be reversible (Carreira et al., 2006). Subsequent evidence suggests this to be the case (Hoek et al., 2008; Pinner et al., 2009; Hoek and Goding, 2010). Hypoxic regions in tumours tend to suppress
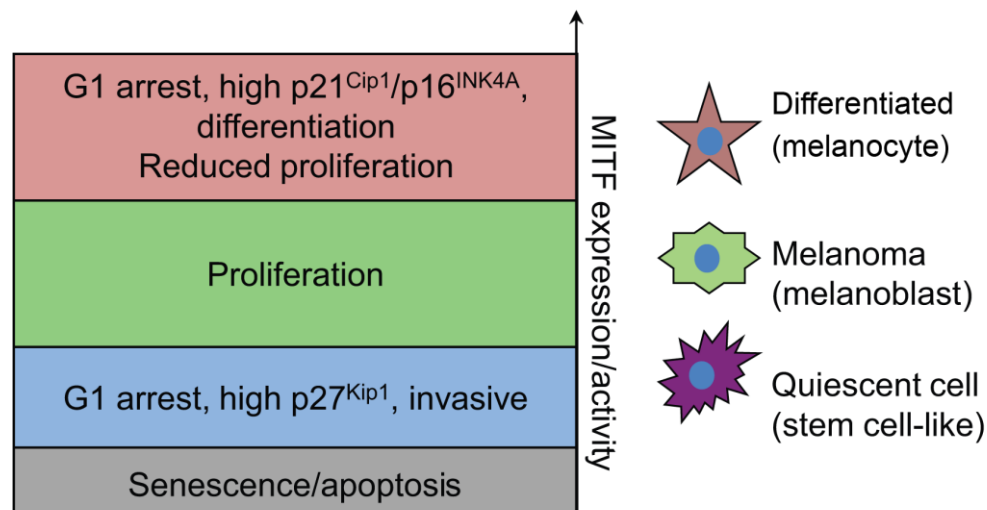
Figure 1.12. Rheostat model of MITF expression and activity. In the absence of MITF, melanocytes undergo apoptosis early in development. Very low MITF expression in melanoma cells or in melanocytes results in senescence. Low MITF expression results in invasive, stem-like cells with high p27^{Kip1}. MITF-positive cells are either proliferative or differentiate via p16^{INK4A} and p21^{Cip1}. Adapted from Carreira et al. (2006).

MITF expression, promoting a more invasive phenotype (Feige et al., 2011; Cheli et al., 2012). Additionally, TBX2 will block p21^{Cip1} activity (Prince et al., 2004; Vance et al., 2005); p16^{INK4A} is frequently silenced; and apoptosis is often disrupted, for example through inactivation of Apaf-1 (Soengas et al., 2001). Therefore, the melanoma cell could very well be trapped within the range of proliferative and invasive phenotypes, and thus be able to selectively switch back and forth based on the microenvironment.

1.4 Summary and aims

Melanocytes are pigment producing cells under the direct control of MITF, which is a lineage survival oncogene in many melanomas. Malignant melanoma provides an excellent model to study of cancer progression, as its early stages are well characterised and easily accessible. MITF plays a varied role throughout foetal and adult life, promoting growth on the one hand but growth arrest on the other, and inducing the photo-protective pigmentation pathway to protect against UV damage. It achieves this by directly binding E-box and M-box elements in the promoters and enhancers of its target genes.

There is some knowledge about how upstream signalling pathways will aid the choice of the appropriate set of target genes to be activated by MITF, but the precise molecular mechanism permitting MITF to recognise different subsets of its target genes, and what those subsets may be, still needs to be elucidated. The objective of this thesis will therefore be to investigate whether post-translational modifications of MITF control its ability to bind DNA and regulate its specificity for different subsets of binding sites. Specifically, the following aims will be addressed:

1. Determine the effect of MAPK-mediated, p300-mediated MITF-acetylation the ability of MITF to bind DNA and activate expression of its target genes,

2. Identify deacetylases that can deacetylate with and/or interact with MITF,

3. Characterise the role of site-specific acetylation of MITF within its DNA-binding domain in regulating the ability of MITF to productively bind DNA,

4. Investigate the regulation of the upstream signalling pathways regulating MITF acetylation.

Chapter 2 – Materials and Methods

2.1 Reagents

Chemicals and reagents were purchased from Sigma-Aldrich unless otherwise stated. C646 was purchased from Merck, UO126 was from Cell Signaling. PLX4720 was a gift from Richard Marais (ICR, London).

Throughout the study, autoclaved double-distilled 18 MΩ water was used for DNA and RNA solutions. Double-distilled 15 MΩ water was used to prepare all buffers and solutions.

2.2 Bacterial methods

2.2.1 Growth media

The specialised components of all media were purchased from Difco Laboratories Ltd., and media were autoclaved prior to use.

Unless otherwise stated, liquid bacterial cultures were grown with shaking at 225 rpm, at 37°C in Luria-Bertani broth (LB; 1% w/v bactotryptone, 0.5% w/v yeast extract, 1% w/v NaCl, pH 7.5), supplemented with appropriate antibiotics: ampicillin (100 µg/ml) or kanamycin (30 µg/ml).

Bacteria were streaked to obtain clonal colonies on agar plates, comprised of LB containing 1.5% agar, supplemented with appropriate antibiotics, and poured into Petri dishes (Sterilin). Plates were stored at 4°C, and air dried and warmed to 37°C before use. They were incubated upside down overnight at 37°C to allow colony formation.

2.2.2 Bacterial strains

For general cloning, *E.coli* strain DH5α (F⁻ Φ80lacZΔM15 Δ[lacZYA-argF] U169 recA1 endA1 hsdR17[r_k, m_k^+] phoA supE44 thi-1 gyrA96 relA1 λ⁻) or TOP10

(Invitrogen; F- mcrA Δ[mrr-hsdRMS-mcrBC] Φ80lacZΔM15 Δ lacX74 recA1 araD139 Δ[araleu]7697 galU galK rpsL [StrR] endA1 nupG) were used. For site-directed mutagenesis, *E.coli* strain XL1-Blue (Agilent; *recA1 endA1 gyrA96 thi-1 hsdR17 supE44 relA1 lac* [F′ *proAB lacI*^{q}*ZΔM15* Tn*10* Tet^r]) was used. For expression of recombinant protein, *E.coli* strain BL21(DE3) (F– *omp*T *hsd*SB(rB–, mB–) *gal dcm* (DE3)) was used.

2.2.3 Preparation and storage of competent bacteria

Bacterial stocks were prepared by streaking bacteria onto agar plates to give clonal colonies after incubating overnight at 37°C. 3 colonies were transferred to 5 ml LB and grown overnight. The next day a 250 ml culture was inoculated with 250 µl overnight culture, and grown at 30°C until A_{600}=0.5-0.6. Cells were transferred to ice-cold centrifuge tubes and cooled on ice for 10 minutes, before harvesting at 1,400 g, 10 minutes at 4°C. The pellet was suspended in 80 ml ice cold transformation buffer (10 mM HEPES, 55 mM $MnCl_2$, 15 mM $CaCl_2$, 250 mM KCl) and incubated on ice for 10 minutes before re-centrifuging. The pellet was suspended in 20 ml ice cold transformation buffer, and 1.5 ml DMSO added and gently mixed. 30 µl aliquots were snap-frozen in a dry ice-ethanol bath for long-term storage at -80°C.

2.2.4 Transformation of competent bacteria

For strains except XL1-Blue, 30 µl cell aliquots were thawed and gently returned to suspension on ice. Plasmid DNA was added to the cells (no more than 10% v/v) and the mix incubated on ice for 10 minutes. To permit uptake of DNA, the bacteria were subjected to heat shock at 42°C for 30 seconds (TOP10, BL21[DE3]), or 90 seconds (DH5α), and allowed to recover on ice, 2 minutes. 200 µl S.O.C. media (Invitrogen; 2% w/v tryptone, 0.5% w/v yeast extract, 10 mM NaCl, 2.5 mM KCl, 10

mM $MgCl_2$, 10 mM $MgSO_4$, 20 mM glucose) was added and the cells incubated for 1 hour at 37°C with shaking before spreading on LB-agar plates.

To transform XL1-Blue, 50 µl bacteria were transferred to ice-cold 14 ml Falcon polypropylene round-bottom tubes, and 1 µl DNA added. After a 30 minute incubation on ice, the bacteria were heat-shocked at 42°C for 45 seconds and returned to ice for 2 minutes. 250 µl S.O.C. media was added and samples shaken at 37°C for 1 hour before the bacteria were spread on LB-agar plates.

2.2.5 Expression of recombinant protein

Constructs to be expressed were transformed into BL21(DE3). 3 colonies were grown overnight in 5 ml LB. The next day this was diluted 20 times into 100 ml LB containing antibiotics but no chloramphenicol and grown until OD_{600}=0.7-0.8. Isopropyl β-D-1-thiogalactopyranoside (IPTG) was added to a final concentration of 0.5 mM to induce recombinant protein expression. The culture was grown for a further 2-6 hours and the bacteria harvested. Prior to protein purification, the pellet was frozen overnight at -20°C.

2.3 Mammalian cell methods

2.3.1 Mammalian cell maintenance

Unless otherwise stated, all monolayer cell cultures were available from long-term laboratory stocks and were grown at 37°C in humidified air containing 10% CO_2. Human melanoma cell lines (Table 2.1) and B16F10 (mouse melanoma cell line) were grown in Roswell Park Memorial Institute Medium-1640 (RPMI; Gibco), supplemented with 10% foetal bovine serum (Biosera; FBS), 100 U/ml penicillin and 100 µg/ml streptomycin (Invitrogen). Me235, T333A, and T1397A, low passage

patient-derived melanoma cell lines (Valsesia et al., 2011; Nikolaev et al., 2012), were a gift from Donata Rimoldi (Ludwig Institute for Cancer Research, Université de Lausanne). MCF7 and T47D cell lines (breast cancer) were cultured as for melanoma cell lines.

HeLa cells were cultured in Dulbecco's Modified Eagle Medium (DMEM; Lonza), supplemented as for RPMI-1640. Phoenix-Ampho cells (termed Phoenix hereafter) are derived from 293T cells—a human embryonic kidney cell line transformed with adenovirus E1a and expressing the SV40 large T antigen to be capable of producing amphotropic viruses. Here they were used as a non-melanocyte lineage cell line that is highly transfectable, and maintained as for HeLa cells.

501mel.3×HA-MITF cells, stably expressing wild-type HA-MITF, were a gift from Irwin Davidson (IGBMC, Strasbourg). These and 501mel cell lines stably expressing mutated HA-MITF (section 2.3.3) were maintained as for parental 501mel cells but with a further supplement of puromycin (3 μg/ml). When plated for experiments, puromycin was removed from cultures to avoid potential side-effects.

Table 2.1. Human melanoma cell lines, indicating mutational status, where known.

Cell line	Metastasis	NRAS	BRAF	MEK	PTEN	β-catenin	p53
501mel		WT	V600E		WT	S37F	C277W
SKmel3		Mutant	WT		Deleted		
SKmel28	Lung/liver	WT	V600E		A449G, T167A		L145R
SKmel30		Mutant	WT				
CHL		WT	WT		WT		Mutant
HBL		WT	WT			Mutant	WT
Me235		WT	K601E	E207K (MEK2)			
T333A		Q61K	WT	E203K (MEK1)			
T1397A		WT	V600E	P124S (MEK1)			
Lu1205	Lung	WT	V600E		Deletion		WT
MDA-MB-435		WT	V600E		WT	WT	G266E

Cell lines were regularly passaged at no more than 80-90% confluence, and generally used for experiments between passages 3 and 20, to allow recovery from stress associated with liquid nitrogen storage, and to prevent replication-induced senescence or other problems associated with long-term culture. To passage cells, the culture dish was washed with PBS and 0.25% Trypsin (Gibco) was added to dissociate cells. After being returned to the incubator for two minutes, trypsin was inactivated in two volumes of complete medium, and the cells centrifuged at 200 g, 4 minutes. The cell pellet was suspended in complete medium, ready for either passage or experimental use.

Cells were kept in long-term storage under liquid nitrogen by freezing cells in fresh complete media (supplemented with 10% FBS, 100 U/ml penicillin and 100 µg/ml streptomycin, but no additional antibiotics) containing 10% DMSO.

On application of drug treatments to cell cultures, DMSO- or ethanol-diluted drugs were added to cultures in fresh media with a maximum solvent concentration of 0.1% to avoid possible solvent-mediated toxicity.

2.3.2 Transient transfection of DNA into mammalian cells

Cells were plated and grown overnight to approximately 40% confluence. FuGENE 6 (Roche), a blend of lipids, was used as a transfection reagent at the manufacturer's recommended ratio of 3 µg DNA: 1 µl FuGENE 6. FuGENE 6 was mixed with Optimem (Invitrogen) for 5 minutes at room temperature to allow micelles to form. Plasmid DNA was added to this, and the mix incubated for a further 15 minutes at room temperature before being added drop-wise to cells, which were incubated for up to 72 hours prior to analysis.

2.3.3 Stable transfection of DNA into mammalian cells

Cell lines stably expressing pcDNA3×HA-Mitf(+)^{K243R} or pcDNA3×HA-Mitf(+)^{K243Q} under puromycin selection were generated by transfecting low-passage 501mel cells seeded in a 10 cm dish with 1 µg pcDNA-MITF construct and 100 ng pBABE-puro using FuGENE 6 as described above. The media was replaced the next day and the culture grown to confluence. Selection with puromycin (3 µg/ml) was applied for approximately 1 week until colonies could be observed. The colonies were gently scraped off the dish with a pipette tip, dissociated with trypsin and plated under selection in 96-well plates. Once confluent, clones were expanded into larger culture vessels and assayed for HA-MITF expression. Samples of the final clones were stored in liquid nitrogen, or grown further under selection with puromycin.

2.3.4 siRNA transfection

Short interfering RNA (siRNA) was used to transiently knock down expression of endogenous genes. Cells were grown to 50% confluence. Lipofectamine 2000 (Invitrogen) was diluted 20 times in Optimem to a final volume of 200 µl, and siRNA was diluted to a concentration of 83 nM in 200 µl Optimem in a separate tube. After standing at room temperature for 5 minutes, they were mixed and incubated for 15 minutes. The cells' media was changed for fresh media supplemented with 10% FBS but no antibiotics, before the siRNA-Lipofectamine mixture added drop-wise to the surface of the media. The siRNA sequences used were purchased from QIAGEN and were: siMITF, 5′-r(AGCAGUACCUUUCUACCAC)d(TT)-3′; and siLuciferase (siCTR), 5′-r(UUCUCC GAACGUGUCACGU)d(TT)-3′ (Carreira et al., 2006).

2.4 Nucleic acid methods

2.4.1 Plasmid purification

Clonal bacterial cultures were prepared for small- and large-scale plasmid purification. For small-scale purifications, colonies were grown overnight in 3 ml LB, processed with a QIAprep Spin Miniprep Kit (QIAGEN), and the DNA eluted in water. For large-scale purifications, colonies were picked into 2 ml LB and grown for 8 hours before being diluted into 200 ml LB containing appropriate antibiotics and grown overnight. DNA was purified from the culture using the Plasmid Maxi Kit (QIAGEN) and the DNA pellet suspended in water.

2.4.2 Quantification of nucleic acids

Nucleic acids were quantified with a NanoDrop 2000 (Thermo). For a sample of absorbance at 260 nm A_{260} and extinction coefficient ε ([µg/ml]$^{-1}$ cm^{-1}) measured at path-length l (cm), the concentration c (µg/ml) may be calculated according to the Beer-Lambert Law:

$$c = \frac{A_{260}}{\varepsilon l}$$

For double-stranded DNA, $\varepsilon = 0.02$ (µg/ml)$^{-1}$ cm^{-1} and, for single-stranded RNA, $\varepsilon = 0.025$ (µg/ml)$^{-1}$ cm^{-1}. Sample purity was assessed using the absorbance ratio at 260 nm and 280 nm.

For pure DNA, $A_{260}:A_{280} \cong 1.8$ and, for pure RNA, $A_{260}:A_{280} \cong 2$.

2.4.3 Agarose gel electrophoresis

To resolve different sized DNA fragments, agarose gels were prepared by dissolving agarose (Fisher) in 1×TBE (100 mM Tris, 90 mM boric acid, 1 mM

EDTA, pH 8.0) in a microwave. Ethidium bromide (Severn Biotech) was added to 1 µg/ml (ethidium bromide is fluorescent under UV light, and intercalates into double stranded nucleic acids which greatly enhances this fluorescence). Samples were prepared in 1× loading buffer (16% v/v formamide, 1% v/v 1×TBE) and subjected to electrophoresis at 100 V. Gels were visualised under ultraviolet light using a UVIdoc (UVItec).

Fragments were excised and purified from gels using the QIAquick Gel Extraction Kit (QIAGEN) according to the manufacturer's recommendations.

2.4.4 Polymerase chain reaction

DNA fragments were amplified from cDNA stocks by polymerase chain reaction (PCR) for downstream cloning purposes using Illustra PuReTaq Ready-To-Go PCR beads (VWR). The reaction volume was 25 µl, made up with 1 µg of each oligonucleotide primer and 100 pg of cDNA template. Reactions were carried out in a T100 Thermal Cycler (BioRad) by denaturing the samples at 95°C, 5 minutes; followed by 30 cycles of denaturation (95°C, 45 seconds), annealing (melting temperature, 45 seconds), and elongation (72°C, 2 minutes); and concluded with a final elongation phase of 72°C, 10 minutes to allow extension of all templates. The PCR product was purified with the QIAquick PCR Purification Kit (QIAGEN) and eluted in water.

2.4.5 Site-directed mutagenesis

Point mutations were introduced in existing plasmids with the QuikChange Site-Directed Mutagenesis Kit (Agilent). Primers were designed to span the mutation site by a minimum of 20 bases and, where possible, a restriction site was introduced to simplify screening for positive clones. A reaction mix containing 30 ng DNA

template, 1.25 ng each primer, 1 µl dNTP mix, 1× reaction buffer, 1 µl (2.5 U) *Pfu*Turbo DNA polymerase in a final volume of 50 µl was subjected to an initial denaturation step of 95°C, 30 seconds; followed by 18 cycles of denaturation (95°C, 30 seconds), annealing (55°C, 1 minute), and elongation (68°C, 1 minute/kb of plasmid length). Reactions were cooled on ice for 2 minutes, before addition of 1 µl DpnI (10U/µl) and incubation at 37°C for 1 hour to digest parental (non-mutated) dam-methylated DNA.

2.4.6 Restriction enzyme digestion

To prepare DNA fragments for ligation, or to screen clones for successful ligation reactions, restriction enzyme (NEB, Invitrogen, Promega) digests were carried out in an appropriate 1× reaction buffer at 37°C for 1.5 hours. For some enzymes, bovine serum albumin (BSA; 100 µg/ml) was added to maintain enzymatic stability during incubation. A minimum 5-fold enzyme excess was used, at a maximum concentration of 10% of the final volume—enzymes are supplied in 50% glycerol for storage but are inhibited at levels exceeding 5%. PCR samples were digested for 2 hours, and all preparative samples were purified with the QIAquick PCR Purification Kit. Digests were analysed by agarose gel electrophoresis.

2.4.7 Ligation

Vectors were digested with restriction enzymes at 37°C for 1.5 hours, and 20 U calf-intestinal alkaline phosphatase (CIP; NEB) added for a further hour. To prevent re-ligation of the vector, restriction enzymes leaving non-complementary ends were used where possible. CIP treatment removes 5'-phosphate groups, again to help prevent re-ligation of the vector.

Vector and insert samples were quantified on a single agarose gel and approximately 100 ng vector was ligated with a 5- to 10-fold excess of insert in a reaction containing 400 U T4 DNA ligase in 1× reaction buffer (NEB) for 1 hour at room temperature, or at 4°C overnight. 5 µl of the reaction was transformed into competent bacteria, and colonies screened for successful incorporation of the insert by restriction digestion or PCR.

2.4.8 Plasmids

Plasmids used in the study were either available in the laboratory, externally sourced, or constructed by the candidate as indicated (Table 2.2). All plasmids not already available in the laboratory were sequenced prior to use. Note that all MITF expression constructs encode the (+) splice variant of Mitf-M, the major isoform of the protein present in the melanocyte lineage.

cDNA was cloned into plasmids using restriction enzymes as indicated (Table 2.2). pcDNA3-3×HA-Mitf^{K243R} and pcDNA3-3×HA-Mitf^{K243Q} point mutants were cloned into pcDNA3-3×HA (Figure 2.1a) by amplification of Mitf cDNA from existing pcDNA14-3×FLAG-Mitf constructs. The PCR products were digested with BglII at sites incorporated at the 5' and 3' ends of the coding sequence and ligated into pcDNA3-3×HA that been digested with BamHI.

The pUCET-Mitf plasmid for expressing Mitf fragments in bacteria was created by digesting pUC19 and pETM-11-Mitf 180-296 with KpnI and SapI, and ligating the products, which had the effect of exchanging the kanamycin resistance cassette in pETM-11-Mitf with the ampicillin resistance cassette of pUC19 (Figure 2.1b). The cassette expressing the recombinant protein was unchanged. K243R and K243Q point mutations were introduced by site-directed mutagenesis.

Table 2.2. Plasmids used in the study.

Construct	Source and notes
pCMV14-3×FLAG	Sigma, available in the laboratory
pCMV14-3×FLAG-Mitf	Wild-type and all mutant constructs were available in the laboratory
pcDNA3-3×HA	Invitrogen, available in the laboratory
pcDNA3-3×HA-Mitf	Available in the laboratory
pcDNA3-3×HA-Mitf^{K243R}	Prepared by the candidate
pcDNA3-3×HA- Mitf^{K243Q}	Prepared by the candidate
pEGFP-C1	Novagen, available in the laboratory
pEGFP-C1-Mitf	Available in the laboratory
pEF-Myc-BRAF^{V600E}	Available in the laboratory
pcDNA3-3×HA-p300	Available in the laboratory
pcDNA3-3×HA-CBP	Available in the laboratory
pCMV-FLAG-PCAF	Available in the laboratory
pCMV-3×FLAG-HDAC	Constructs expressing HDAC1, HDAC2, HDAC3 HDAC4, HDAC5 were from Heinz Arnheiter (NIH)
pcDNA3.1-Myc-His-SIRT1	Tony Kouzarides (Cambridge University)
pcDNA3.1-FLAG-SIRT6	Purchased from Addgene (entry 13817)
pGL3-basic	Firefly luciferase expression construct lacking any promoter region; Promega, available in the laboratory
pGL3-hTyr WT	-300/+80 bp of human *Tyrosinase* promoter; available in the laboratory. Contains two CATGTG M-box sequences,
pGL3-hTYR TA	pGL3-hTyr with flanking sequences of M-boxes mutated to T—A; available in the laboratory
pGL3-hTYR NN	pGL3-hTyr with flanking sequences of M-boxes mutated to C—C; available in the laboratory
pETM-11-Mitf.180-296	Matthias Wilmans (EMBL, Hamburg)
pUC19	Invitrogen
pUCET-Mitf.180-296	Prepared by the candidate
pUCET-Mitf.180-296^{K243R}	Prepared by the candidate
pUCET-Mitf.180-296^{K243Q}	Prepared by the candidate
pUCET-Mitf.180-296^{G244R}	Prepared by the candidate

2.4.9 mRNA purification

Cells were grown to 80% confluence and harvested at room-temperature using the RNeasy mini kit (QIAGEN). Cells were scraped in PBS and lysed in Buffer RLT supplemented with 143 mM β-mercaptoethanol. The lysate was homogenised by being passed 10 times through a 0.9 mm needle and RNA purified on RNeasy spin columns before being eluted in nuclease free water.

2.4.10 Quantifying gene expression levels

1 µg RNA was used processed with the QuantiTect Reverse Transcriptase Kit (QIAGEN), which removes genomic DNA before catalysing first-strand cDNA synthesis and, finally, removal of any remaining RNA. Quantitative PCR (qPCR) was used to analyse gene expression levels. Primers used to measure gene expression were designed, wherever possible, to be intron spanning so as to avoid amplification of any contaminating genomic DNA. qPCR was performed in technical duplicate in a 15 µl
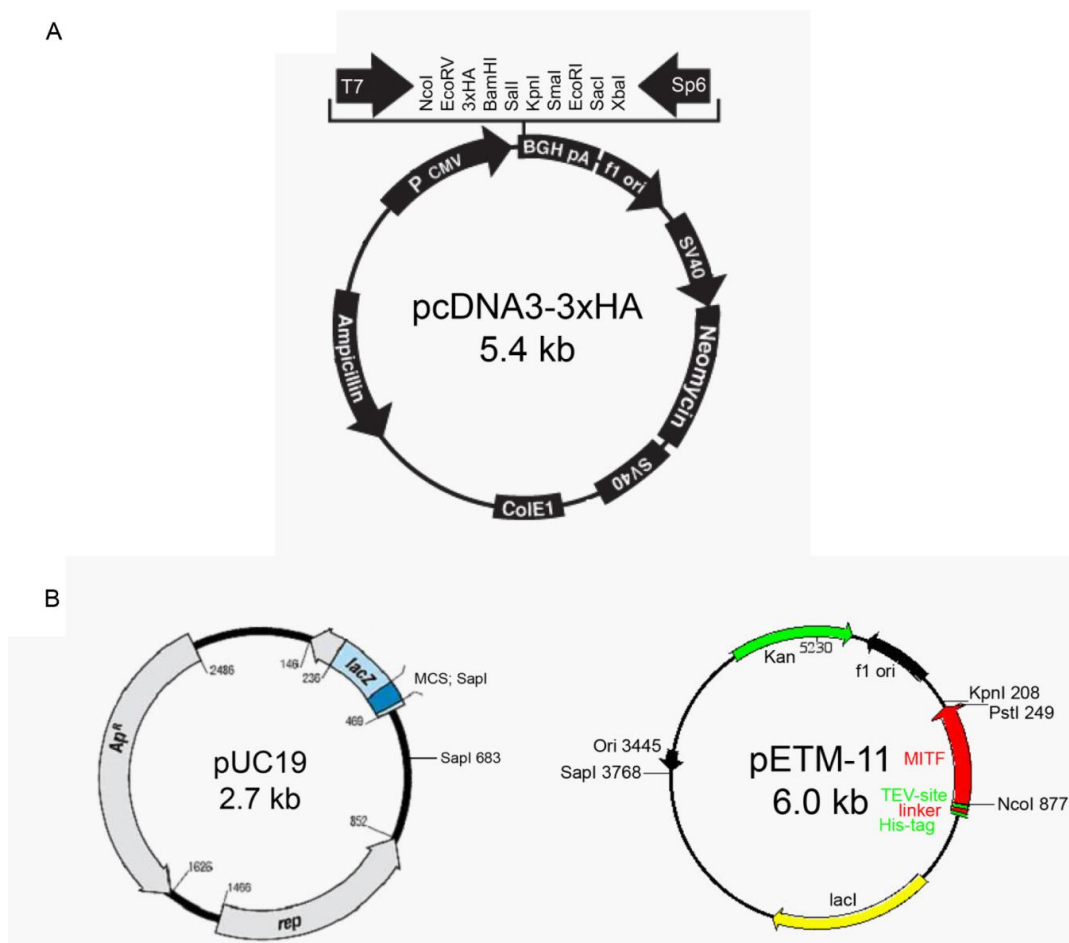
Figure 2.1. Plasmids used for subcloning in the study. Relevant unique restriction sites are indicated. (A) pcDNA3-3×HA (modified in-house from Invitrogen pcDNA3) was used to clone full-length MITF constructs. (B) pUCET was created from the SapI-KpnI fragments of pUC19 (Invitrogen) and pETM-11-Mitf.180-296 (Matthias Wilmans). Images adapted from materials supplied from the original source of the plasmid.

reaction volume containing 1X SensiMix SYBR kit (Bioline), forward and reverse primers (each 0.3 µM), and an appropriate amount of first-strand cDNA as a template.

PCR reactions were performed in a Corbett Rotor-Gene 6000 (QIAGEN). Reactions were held at 95°C for 10 minutes before 55 cycles of 96°C, 5 seconds; 61°C, 10 seconds; 72°C, 5 seconds in a Corbett Rotor-Gene 6000 (QIAGEN). Finally the temperature was raised from 72°C to 96°C in steps of 1°C every 5 seconds to generate melt-curves. Reactions that passed an empirically determined amplification threshold and where the melt-curve indicated a faithful amplification rather than one started by primer dimerization.

Results are expressed using the 2(-Delta Delta C(T)) method, relative to a housekeeping gene as indicated below (Livak and Schmittgen, 2001):

$$Amount\ of\ target = 2^{-\Delta\Delta C_T}$$

$$-\Delta\Delta C_T = -\left(\Delta C_{T[sample]} - \Delta C_{T[reference]}\right)$$

where $\Delta C_{T[sample]}$ is the threshold value of the sample gene, and $\Delta C_{T[reference]}$ is the threshold value of the reference housekeeping gene.

2.4.11 Gene expression arrays

30 ng of RNA extracted as described above was hybridised in triplicate to a Human HT-12 v4.0 Expression BeadChip (Illumina) and scanned on an IScan (Illumina). Array measurements, along with initial analysis in Genome Studio (Illumina) to extract average probe intensities, were conducted by Dilair Baban (High Throughput Genomics, Wellcome Trust Centre for Human Genetics, University of Oxford). See section 2.7.1 for details of the subsequent analysis.

2.4.12 RNA-Sequencing

Total RNA was extracted from cells essentially as described as in Section 2.4.9. An additional step of on-column DNase digestion, performed at room temperature for 15 minutes, was added between adding lysate to the column and the washing steps. Library preparation and paired-end sequencing (RNA-Seq) was performed by Lorna Gregory (High Throughput Genomics, Wellcome Trust Centre for Human Genetics, University of Oxford). See section 2.8.2 for details of the analysis.

2.5 Protein methods

2.5.1 Cell extracts

2.5.1.1 Whole cell extracts

Whole cell extracts were prepared by washing cells in ice-cold PBS followed by lysis in hot 2× SDS-PAGE loading buffer (78.0 mM Tris [pH 6.8], 4% SDS, 20% glycerol, 0.2% bromophenol blue, supplemented with 100 mM DTT). Extracts were boiled at 95°C for 5 minutes and stored at -80°C.

2.5.1.2 Nuclear extracts

Nuclear extracts were prepared on ice or at 4°C (Dignam et al., 1983). Cells were washed and scraped in ice-cold PBS, pelleted at 200 g, 5 minutes, and suspended in nuclear-isolation buffer (10 mM HEPES [pH 7.9], 1.5 mM $MgCl_2$, 10 mM KCl, 0.5 mM DTT, 1× protease inhibitor cocktail [PIC; Roche], 10 mM sodium butyrate), 10 minutes. NP-40 was added to 0.2% for 5 minutes to remove the cell membrane (it is not a sufficiently powerful detergent to disrupt the nuclear envelope), and nuclear

exposure monitored under the microscope. Nuclei were collected at 600 g, 5 minutes, lysed in nuclear-extraction buffer (20 mM HEPES [pH 7.9], 420 mM NaCl, 1.5 mM MgCl$_2$, 0.2 mM EDTA, 0.5 mM DTT, 25% glycerol, 1× PIC, 10 mM sodium butyrate), 10 minutes, and centrifuged at 10,000 g, 10 minutes. Extracts were frozen on dry ice and stored at -80°C until use.

2.5.2 Protein purification

2.5.2.1 Immunoprecipitation

All steps were carried out with ice-cold buffers, on ice or at 4°C. Cells were scraped and washed in PBS. Cell pellets were lysed for 5 minutes in 1 ml lysis buffer (50 mM Tris [pH 8.0], 150 mM NaCl, 1 mM EDTA, 1% Triton X-100, supplemented with 1× PIC, 1× phosphatase inhibitor cocktails [Roche], 10mM sodium butyrate, 10 mM nicotinamide) and clarified by centrifugation (10,000 g, 10 minutes). 50 µl of the supernatant was retained as an input, and the remainder rotated overnight with 1 µg antibody (Myc-9E10 [Santa Cruz], HA [Sigma]). 50 µl of a 50% protein G-agarose bead slurry (Roche), previously equilibrated in lysis buffer, was added and the samples rotated for 2 hours. For FLAG IPs, 20 µl of a 50% slurry of anti-FLAG conjugated protein G-agarose beads, previously equilibrated in lysis buffer, was directly added to the clarified lysate for 2 hours, eliminating the need for overnight incubation. The beads were washed three times for 10 minutes in lysis buffer, and boiled in 2× SDS-PAGE loading buffer.

2.5.2.2 His-tagged protein purification

All steps were carried out on ice at 4°C with ice-cold buffers. Frozen pellets of 100 ml bacterial cultures were thawed and suspended in 10 ml native lysis buffer

(50 mM NaH_2PO_4, 300 mM NaCl, 10 mM imidazole, 10% v/v glycerol, pH 7.4 [NaOH], supplemented with $1\times$ protease inhibitor cocktail; inclusion of a small amount of imidazole in the lysis buffer helps prevent non-specific binding to nickel beads) for 10 minutes. Lysozyme was added to 0.2 mg/ml to digest bacterial cell walls for 20 minutes before sonication on ice with 6 bursts at full-power, 12 seconds, with 18 seconds recovery between pulses, and clarification by centrifugation at 10,000 g, 30 minutes. The clarified lysate was mixed by rotation for two hours with 150 µl of a 50% Ni-NTA slurry previously equilibrated in lysis buffer. The mix was loaded into a polypropylene chromatography column (Bio-Rad) that had been washed in lysis buffer and the beads settled by gravity flow. After passing the flow-through back over the column, it was washed twice in wash buffer (50 mM NaH_2PO_4, 300 mM NaCl, 20 mM imidazole, 10% v/v glycerol, pH 7.4 [NaOH]) and bound material eluted in five 500 µl fractions of elution buffer (50 mM NaH_2PO_4, 300 mM NaCl, 250 mM imidazole, 10% v/v glycerol, pH 7.4 [NaOH]). Aliquots of input and unbound lysate and wash fractions were collected to confirm that the recombinant protein was specifically purified in the eluate fractions. Fractions containing near-pure recombinant protein were pooled and glycerol added to a final concentration of 30% to act as a preservative. Proteins were aliquoted and stored at -20°C.

2.5.3 SDS-PAGE

Extracts were resolved by SDS-polyacrylamide gel electrophoresis (SDS-PAGE) containing an appropriate acrylamide concentration, 375 mM Tris (pH 8.9), 0.1% (v/v) SDS, and polymerised with 0.1% ammonium persulfate (APS) and Tetramethylethylenediamine (TEMED). Gels were poured with 45% stock acrylamide (200:1 acrylamide:bis-acrylamide; Severn Biotech). Resolving gels were overlain with a stacking gel comprising 6% acrylamide (30%, 37.5:1 acrylamide:bis-

acrylamide; Severn Biotech), 146 mM Tris (pH 6.8), 0.05% (v/v) SDS, and polymerised with 0.1% APS and TEMED. Gels were run at 175 V in running buffer (52 mM Tris, 53 mM glycine, 1% SDS) for approximately 50 minutes until the loading dye front had just run off the gel.

2.5.4 Coomassie staining

To visualise proteins directly, SDS-PAGE gels were stained with Coomassie Brilliant Blue R250, which tightly binds to proteins. Gels were fixed in fixing solution (10% glacial acetic acid [Fisher], 20% ethanol [Fisher]) to dehydrate them prior to staining. Fixing solution was removed, the gel covered with Coomassie solution (0.1% w/v Coomassie Brilliant Blue R250, 10% glacial acetic acid, 40% methanol, filtered to remove particulates), and microwaved for 20 seconds to boil the solution. The gel was rocked for 10 minutes at room temperature to allow incorporation of the stain, before being rinsed in water and rocked with destaining solution (10% glacial acetic acid, 40% methanol) for 1 hour at room temperature to overnight at 4°C to remove excess Coomassie. Gels were photographed using a Gel Doc (Bio-Rad).

2.5.5 Western blotting

Proteins were electro-transferred (150 mA, 90 minutes) in transfer buffer (31 mM Tris, 192 mM glycine, 20% methanol) from SDS-PAGE gels to methanol-soaked polyvinylidene difluoride (PVDF; GE Healthcare) membranes. The membranes were subsequently blocked for 1 hour at room-temperature in 5% nonfat milk in PBS supplemented with 0.1% Tween-20 (PBS-T), before being incubated with primary antibody diluted as indicated (Table 2.4) in 5% nonfat milk in PBS-T for 1 hour at room-temperature, or overnight at 4°C. After three PBS-T washes, membranes were incubated with horseradish peroxidase-conjugated secondary antibodies for 1 hour at

room-temperature, washed and visualised with enhanced chemiluminescence reagents (Amersham). For phospho-specific and anti-acetyl-lysine antibodies, membranes were blocked and incubated with primary antibody in 5% BSA diluted in Tris-buffered saline (TBS; 25 mM Tris base, 150 mM NaCl, 2 mM KCl, pH 7.4) supplemented with 0.1% Tween-20 (TBS-T). Washes were in TBS-T, and secondary antibodies used as above.

2.5.6 Electrophoretic mobility-shift assay

Protein-DNA interactions can be investigated *in vitro* through an electrophoretic mobility-shift assay (EMSA). An end-labelled double-stranded oligonucleotide probe is mixed with a protein of interest. If the protein binds to the probe, then the probe's mobility in a native gel will be retarded.

2.5.6.1 Probe preparation

20 µg of each strand of an oligonucleotide probe sequence, with a 5' overhang, were annealed in the presence of 1× React 3 buffer (Invitrogen) in a programme comprised of 2 minutes, 94°C; 10 minutes, 65°C; 10 minutes, 37°C; 10 minutes, 25°C. 200 ng annealed probe was labelled in a 50 µl reaction containing 1× React 2 buffer (Invitrogen); 200 µg/ml BSA; 2 µM DTT; 200 µM each dATP, dGTP, dTTP (Invitrogen); 1 µl Klenow Polymerase (Invitrogen); 1.5 µl $^{\alpha}$32-P-dCTP (15 µCi). The reaction was incubated for 1 hour at room temperature before addition of 20 µg glycogen to act as a carrier for the labelled probe and 50 µl water. The mix was extracted twice through an equal volume of phenol-chloroform and precipitated overnight in 20 µg glycogen, 1 volume ammonium acetate (5 M), and 6 volumes ethanol at -20°C. The next day the probe was recovered by centrifugation (16,000 g, 30 minutes) and suspended in water. It was usable for at least two weeks.

2.5.6.2 EMSA 1: pure protein

To carry out EMSA with pure protein, a 20 µl reaction mix was prepared on ice containing 14 µl bandshift buffer (25 mM HEPES [pH 7.4], 150 mM KCl, 10% glycerol), 200 µg/ml BSA, 5 µM DTT and 1 µl protein. This was incubated for 15 minutes at room temperature with 1 µl labelled probe which had been diluted to approximately 50 counts-per-minute before loading on a native gel containing 6% acrylamide (44% stock solution, 29:1 acrylamide:bis-acrylamide; Severn Biotech) and 0.5X TBE (Gibco), polymerised with addition of 0.09% APS and TEMED. Gels were run at 180V, 100 minutes, before drying under vacuum for 40 minutes, 80°C. Dried gels were exposed to autoradiography film for an appropriate length of time.

2.5.6.3 EMSA 2: crude lysate

Numerous factors (for example: c-Myc, USF) can also bind to MITF binding sites *in vitro*. This could either lead to their outcompeting MITF for binding to the probe, or their obscuring MITF-specific bands. Therefore a more stringent binding assay was employed when cell lysates were used (Bertolotto et al., 1996a). A 20 µl reaction mix was prepared on ice by diluting 1 µl of a nuclear extract diluted in 16 µl MITF bandshift buffer (10 mM Tris [pH 7.5], 100 mM NaCl, 2 mM $MgCl_2$, 1mM EDTA [pH 8.0], 1 mM DTT, 4% glycerol, 10% foetal calf serum [Biosera], 80 µg/ml sonicated salmon sperm DNA [Agilent], 2 mM spermidine). 1 µl (50 counts-per-minute) labelled probe was added for 20 minutes at room temperature before the gel was loaded and run as before.

2.5.6.4 Antibody supershift

To confirm that bands observed in an EMSA result from the protein of interest binding to the probe, 1 µl antibody against the protein of interest can be added

to the reaction mix, on ice, for 20 minutes prior to addition of labelled probe. For MITF EMSA using cell lysates, this was necessary to identify MITF-specific binding; although a more stringent assay was employed, several shifted bands were still seen on the gel, only one of which results from MITF-binding. The antibody used was against FLAG (Sigma).

2.5.6.5 Competition EMSA

EMSA may be used to determine relative binding affinities of a protein to different target sequences. To perform these experiments, a dilution series of either unlabelled oligonucleotide probes or sonicated salmon sperm DNA were titrated into the protein-bandshift buffer for 20 minutes on ice prior to addition of labelled probe as described above. For experiments involving antibodies and competitor DNA, the antibody was incubated with the protein for 20 minutes prior to addition of competitor DNA, and the labelled probe added 20 minutes after this.

2.5.7 Chromatin immunoprecipitation (ChIP)

Cells were grown to 80% confluence in 15 cm dishes, washed in cold PBS, and fixed for 10 minutes at room temperature on a plate rocker in cold PBS containing 0.4% paraformaldehyde (Electron Microscopy Science), which cross-links primary amino groups in proteins with nearby nitrogen atoms in protein or DNA via a $-CH_2-$ linkage. Glycine was added to a final concentration of 0.2 M to quench the cross-linking reaction and the plates rocked for a further 10 minutes. Cells were washed and scraped in cold PBS, pooled in groups of 3 plates and centrifuged at 1500 g, 5 minutes. The pellet was suspended on ice for 10 minutes in 1 ml ChIP lysis buffer (50 mM Tris-HCl [pH 8.0], 10 mM EDTA [pH 8.0], 1% SDS, supplemented with 1× protease inhibitor cocktail [Roche] and 0.5 mM phenylmethanesulfonylfluoride

[PMSF]) and sonicated for 16 minutes in a Covaris S220 at 140 W Peak Incident Power, 5% Duty Cycle and 200 Cycles per Burst. The water bath was continually degassed and maintained at 4°C throughout the sonication process. An aliquot of chromatin was taken to reverse the cross-linking (see below) to confirm that sonication resulted in fragmentation to approximately 300 bp, and to quantify the chromatin concentration. It was retained as an input fraction.

70 µg chromatin was diluted 9 times in ChIP dilution buffer (16.7 mM Tris-HCl [pH 8.0], 167 mM NaCl, 1.2 mM EDTA [pH 8.0], 0.01% SDS, 1.1% Triton X-100) and pre-cleared for (2 hours at 4°C) by rotation with 50 µl of a 50% protein-G sepharose slurry (Roche), previously equilibrated in ChIP dilution buffer and blocked with 0.5 mg/ml BSA and 0.5 mg/ml sonicated salmon sperm DNA for at least 4 hours. The supernatant was rotated overnight at 4°C with 5 µg of anti-HA antibody (clone 12C5, Roche). Bound material was recovered after incubation for 1 hour with 50 µl pre-blocked protein-G sepharose slurry. The beads were washed for 10 minutes, at 4°C, two times each in low salt buffer (20 mM Tris-HCl [pH 8.0], 150 mM NaCl, 2 mM EDTA [pH 8.0], 0.1% SDS, 1% Triton X-100), high salt buffer (20 mM Tris-HCl [pH 8.0], 500 mM NaCl, 2 mM EDTA [pH 8.0], 0.1% SDS, 1% Triton X-100), lithium chloride buffer (0.25 M LiCl, 10 mM Tris-HCl [pH 8.0], 1 mM EDTA [pH 8.0], 1% NP-40, 1% sodium deoxycholate), and TE buffer (10 mM Tris-HCl, 1 mM EDTA, pH 8.0) and recovered by centrifugation at 200 g, 30 seconds. Chromatin was eluted from the beads twice at room temperature for 15 minutes in 250 µl fresh elution buffer (100 mM NaHCO$_3$, 1% SDS).

Cross-links were reversed by overnight incubation at 65°C with 0.3 M NaCl and 10 µg RNase A followed by addition of 4 mM Tris-HCl (pH 8.0), 10 mM EDTA (pH 8.0) and 20 µg Proteinase K (Fermentas) for 1 hour at 42°C. DNA was extracted

sequentially through equal volumes of phenol-chloroform followed by chloroform, and precipitated with 1 µg glycogen [Roche]) in 0.1 volumes sodium acetate (3 M) and 2 volumes 100% ethanol for 4 hours to overnight at -20°C before centrifugation for 30 minutes at 16,000 g. The pellet was washed in 70% ethanol and suspended in 50 µl water.

Analysis was by qPCR. qPCR was performed in technical duplicate in a 15 µl reaction volume containing 1X SensiMix SYBR kit (Bioline), forward and reverse primers (each 0.3 µM), and an appropriate amount of ChIP product. A standard curve using a dilution series of input DNA was prepared for each target amplicon and ChIP condition. PCR reactions were held at 95°C for 10 minutes before 55 cycles of 96°C, 5 seconds; 61°C, 10 seconds; 72°C, 5 seconds in a Corbett Rotor-Gene 6000 (QIAGEN). Finally the temperature was raised from 72°C to 96°C in steps of 1°C every 5 seconds to generate melt-curves. Reactions that passed an empirically determined amplification threshold and where the melt-curve indicated a faithful amplification rather than one started by primer dimerization were analysed by calculating the enrichment of each target in the ChIP product relative to the amount of DNA present in the input control.

2.5.7.1 ChIP-Sequencing

For ChIP-Sequencing (ChIP-Seq) experiments, 10 parallel ChIPs were pooled to a final volume of DNA of 50 µl, and an aliquot verified by qPCR. Samples were subjected to 50 bp, single-end sequencing using an Illumina HiSeq 2500 following the manufacturer's instructions and processed to align the reads to human genome build hg19 (GRCh37, February 2009) using Bowtie (Langmead et al., 2009), allowing for 2 mismatches. Sequencing and this initial analysis was carried out by the

IGBMC Microarray and Sequencing platform (IGBMC, Strasbourg). See section 2.7.3 for details of the analysis.

2.6 Cell biology methods

2.6.1 Brightfield imaging

Brightfield images to examine cell morphology were obtained by photography at 20× magnification using a Nikon microscope and Metamorph software.

2.6.2 Scratch-wound healing assay

Cells were plated in 12-well plates and grown to confluence, after which scratch-wounds were introduced with a pipette tip. The media was removed and cells washed with two changes of PBS to remove dislodged cells, and fresh media added. Photographs were taken every 15 minutes at the same stage coordinates at 10× magnification using a Nikon microscope equipped with Metamorph software to follow closure of the wound. Wound closure was analysed with custom macros from Mark Shipman (Ludwig Institute for Cancer Research, University of Oxford) to measure the remaining area of the wound at each time point.

2.6.3 Confocal microscopy

Cells were grown to 80% confluence on 16 mm thickness number 1 glass cover slips (VWR) in 12-well plates, washed 3 times in PBS and fixed at room temperature, 10 minutes, in 4% paraformaldehyde dissolved in PBS. After 3 PBS washes cells were permeabilised in PBS containing 0.2% Triton X-100 at room temperature, 10 minutes. After 3 further PBS washes, the coverslips were blocked in

5% BSA dissolved in PBS-T at room temperature for 30 minutes. Primary antibodies were diluted as indicated (Table 2.4) in 5% BSA in PBS-T and added overnight at 4°C. After 3 PBS-T washes, Alexa Fluor-conjugated secondary antibodies (Invitrogen) diluted 1:1000 in 5% BSA in PBS-T were added for 1 hour at room temperature. The coverslips were washed 3 final times in PBS-T and mounted on slides with a drop of Vectashield mounting medium containing DAPI (Vector Laboratories). Slides were imaged on a LSM710 confocal microscope using ZEN software.

2.6.4 Cell growth assays

3-(4,5-Dimethylthiazol-2-yl)-2,5-diphenyltetrazolium bromide (MTT) is a yellow tetrazole that is reduced to purple formazan by mitochondrial reductases in viable, metabolically active cells, and can thus provide a simple spectrophotometric viable cell count. Cells were cultured in 96-well plates. At appropriate times, the growth media was replaced with fresh medium containing MTT (1 mg/ml). After incubation in the dark at 37°C for 2 hours, cells were lysed in 100 µl DMSO and absorbance at 570 nm measured with a Glomax Multi-detection System (10 second integration time; Promega).

2.6.5 Flow cytometry

GFP content of cells was measured by flow cytometry. Cells were grown to 80% confluence in 6-well plates and dyes added to an appropriate concentration. After 15 minutes, cells were trypsinised and harvested by centrifugation at 200 g, 2 minutes. The pellet was suspended in 250 µl staining solution (PBS supplemented with 2 mM EDTA [pH 8.0], 5% FBS, 0.01% NaN_3) and kept on ice before reading.

Measurements were taken on a FACS Canto (BD), by scoring FITC fluorescence in live cells relative to side-scattering (which measures the inner granularity of the cell).

Cell-cycle distribution of a population of cells was also analysed by flow cytometry. Cells were grown and harvested as above. Cell pellets were fixed in PBS containing 70% ethanol by incubation on ice for 1 hour. After centrifugation at 200 g, 2 minutes, cells were suspended in propidium iodide (PI) solution (PBS supplemented with 50 μg/ml PI, 100 μg/ml RNAse A, 0.05% Triton X-100) and incubated at 37°C, 40 minutes. After centrifugation at 200 g, 2 minutes, cells were suspended in 250 μl staining solution and kept on ice before reading. Cell cycle measurements were made on a FACS Canto. Among the population of live cells, cell cycle profiles were prepared by measuring the PI fluorescence in each cell.

2.6.6 Luciferase reporter assays

Luciferase reporters, which drive expression of luciferase under the control of a promoter region of interest, were used to gain a measure of the ability of proteins to activate transcription under variable conditions. Cells were plated in 24-well plates and, 40 hours post-transfection, lysed in 100 μl Passive Lysis Buffer (Promega) for 20 minutes at room temperature with rocking. 50 μl Luciferase Assay Buffer was added to 20 μl lysate and luminescence measured with a Glomax Multi-detection System (10 second integration time; Promega).

2.7 Bioinformatics

2.7.1 Microarrays

Probe average intensities for probes describing coding genes were imported into Bioconductor (www.bioconductor.org) and analysed with the limma package

(Smyth, 2004; Shi et al., 2010). Probe intensities were background corrected against negative control probes for each array, and quantile normalisation performed. Intensities for expressed probes were averaged within each array to give a per-gene intensity, after which differential expression was assessed between each sample type. Genes were considered to be significantly upregulated where the absolute log2 fold change between two sample types exceeded 1, corresponding to a fold-change in expression of 2. Principal component analysis was performed with limma.

Clustering analysis of both genes and sample types was carried out with the Easy Microarray Analysis package, using Pearson's correlation coefficient and Ward linkage (Servant et al., 2010).

2.7.2 RNA-Seq

Files containing paired-end sequencing reads were mapped to human genome build hg19 using CLC Genomics Workbench software (CLC Bio) by Qi Zhao (Ludwig Collaborative Laboratory, Johns Hopkins University). Expression values for each gene were calculated as the number of exon-aligned reads exons, per kilobase of exon, per million total uniquely mapping reads (RPKM). The Pearson correlation coefficients and corresponding scatter plots of the RPKM between different RNA-Seq experiments were computed in R (http://www.R-project.org/).

2.7.3 ChIP-Seq

Files containing reads mapped to hg19 were filtered to remove PCR duplicates using the MarkDuplicates function of Picard Tools (version 1.96, http://picard.sourceforge.net) and samples were randomly subsampled to normalise the number of reads used for analysis. Wiggle files displaying continuous read density were compiled at 25 bp resolution using Model-based Analysis of ChIP-Seq (MACS,

version 1.42) (Zhang et al., 2008) and uploaded to the University of California at Santa Cruz (UCSC) Genome Browser for visualisation.

Peak coordinates were identified using MACS2 through a local installation of Galaxy (Giardine et al., 2005; Blankenberg et al., 2010; Goecks et al., 2010) using the default settings. Two statistical parameters are calculated by MACS2 for each peak: a p-value assessing the significance of a peak, and a q-value, adjusting the p-values of the dataset based on the false-discovery rate (Storey, 2002). After peak-calling, a q-value threshold of 10^{-10} was applied to select only the most statistically significant peaks in each sample.

Genome-wide analysis of binding distributions (Figures 3.18 and 4.14) were produced using the Cistrome server (Liu et al., 2011). Heatmaps (parts A and B) were produced using the Heatmap tool, taking as a reference the 1 kb around the summits of peaks in one ChIP-Seq sample. Within every region, read density in each sample was measured in 10 bp windows, and regions were sorted by the intensity of the reference peaks. Genome-wide Pearson correlation (part C) was performed by measuring the median read density in 100 kb windows throughout the genome, prior to calculating the Pearson correlation coefficient between the samples across these windows. To prevent bias in interpreting the results, the scatter is smoothed and coloured by pixel density at each position in the chart: the deeper the colour, the greater number of windows are lying under the pixel. Pearson correlation within peak coordinates (parts D and E) was performed as for part C of the figure, except that the median read density in the samples being compared within the boundaries of each peak of the reference sample was measured.

Peaks were assigned to genes if they lay either within the gene body or within 20 kb of the transcription end site (TES) and transcription start site (TSS) using

CisGenome (Ji et al., 2008). Categorisation of peaks as falling into introns, exons, 5'
and 3' untranslated regions, core and distal promoters, or intergenic regions was
performed with Cis-regulatory Element Annotation System (CEAS; version 1.0.2)
(Shin et al., 2009).

To find overlapping and unique peaks between two samples, the peak
coordinates were compared using Bedtools (Quinlan and Hall, 2010). Histograms of
summit density around the TSS peak height, and boxplots of different peak samples,
were produced in R.

Genome-wide locations of all 5'-CATGTG-3' and 5'-CACGTG-3' were
provided by Benjamin Schuster-Böckler (Ludwig Institute for Cancer Research,
University of Oxford). Mitf ChIP-Seq peaks were expanded 8 bp in both directions
using Bedtools, to permit detection of any motifs overlapping the edges of the peak
region. Files containing motif coordinates were intersected with these expanded peak
regions using Bedtools. Subsequent motif analysis was conducted in R. *De novo* motif
prediction was conducted by extracting the sequence from the 60 bp surrounding the
summit region of 900 peaks as specified using CisGenome, and by submitting these
sequences to the MEME-ChIP online tool (Machanick and Bailey, 2011). Default
settings were used, except that multiple occurrences of the consensus motif per
sequence were permitted.

ChIP-Seq peaks were compared with RPKM values from RNA-Seq
experiments using R.

2.7.2 Gene ontology analysis

Gene ontology (GO) and Kyoto encyclopaedia of genes and genomes
(KEGG) pathway analysis was conducted using the Database for Annotation,

Visualization and Integrated Discovery (DAVID) (Huang da et al., 2009) against a whole-genome background using default settings.

2.8 Oligonucleotides

Oligonucleotide primers were designed in the laboratory and synthesised by Integrated DNA Technologies for use as outlined (Table 2.3). Note that for EMSA, only the top strand sequence is listed. A second complementary sequence was prepared that reversed and complemented the top strand with the exception of the initiating CTAG, which was placed at the start of all EMSA oligonucleotides to leave a 5'-overhanging CTAG at both ends. Underlined bases in EMSA primers are mutated relative to the *Tyr* CAT sequence, which is based on the *Tyrosinase* enhancer M-box.

Table 2.3. Primers used in the course of the study.

Use	Sequence	Comments
EMSA	CTAGACTTGTGGAGATCATGTGATGACTTCCTGATTCCT	*Tyr* CAT
	CTAGACTTGTGGAGATCATGTGCTGACTTCCTGATTCCT	*Tyr* CAT_TC
	CTAGACTTGTGGAGATCATGTGTTGACTTCCTGATTCCT	*Tyr* CAT_TT
	CTAGACTTGTGGAGACCATGTGATGACTTCCTGATTCCT	*Tyr* CAT_CA
	CTAGACTTGTGGAGACCATGTGCTGACTTCCTGATTCCT	*Tyr* CAT_CC
	CTAGACTTGTGGAGATCACGTGATGACTTCCTGATTCCT	*Tyr* CAC
	CTAGACTTGTGGAGATCACGTGCTGACTTCCTGATTCCT	*Tyr* CAC_TC
	CTAGACTTGTGGAGATCACGTGTTGACTTCCTGATTCCT	*Tyr* CAC_TT
	CTAGACTTGTGGAGACCACGTGATGACTTCCTGATTCCT	*Tyr* CAC_CA
	CTAGACTTGTGGAGACCACGTGCTGACTTCCTGATTCCT	*Tyr* CAT_CC
	CTAGACTTGTGGAGATCACGTGATGACTTCCTGATTCCT	*Tyr* CAC M1
	CTAGACTTGTGGAGATCACTTTATGACTTCCTGATTCCT	*Tyr* CAC M2
	CTAGACTTGTGGAGATCATTTTATGACTTCCTGATTCCT	*Tyr* CAC M3
	CTAGACTTGTGGAGATCTTTTTATGACTTCCTGATTCCT	*Tyr* CAC M4
	CTAGACTTGTGGAGATTTTTTTATGACTTCCTGATTCCT	*Tyr* CAC M5

Use	Sequence	Comments
Cloning and SDM	AGAC*GAATTCAGATCT*<u>ATG</u>CTCGAAA TGCTAGAATACAGTCACTA	Forward. To clone Mitf from residue 1. EcoRI and BglII sites in italics, ATG underlined.
	AGAC*GAATTCAGATCT*<u>CTA</u>ACACGCA TGCTCCGTTTCTTC	Reverse. To clone Mitf up to residue 419 (C-terminus). EcoRI and BglII sites in italics, TAG underlined.
	GATCCAGACATGCGGTGGAACCAG GGTACCATTCTCAAGGCCTCTGTG	Mitf^{K243Q} mutagenesis forward
	CACAGAGGCCTTGAGAATGGTACCC TGGTTCCACCGCATGTCTGGATC	Mitf^{K243Q} mutagenesis reverse
	GATCCAGACATGCGGTGGAACAGA GGTACCATTCTCAAGGCCTCTGTG	Mitf^{K243R} mutagenesis forward
	CACAGAGGCCTTGAGAATGGTACCT CTGTTCCACCGCATGTCTGGATC	Mitf^{K243R} mutagenesis reverse
	GATCCAGACATGCGGTGGAACAAG AGAACCATTCTCAAGGCCTCTGTG	Mitf^{G244R} mutagenesis forward
	CACAGAGGCCTTGAGAATGGTTCTC TTGTTCCACCGCATGTCTGGATC	Mitf^{G244R} mutagenesis reverse
Gene expression	CTGATGGACGATGCCCTCTC	Mouse *Mitf* forward
	TCCGTTTCTTCTGCGCTCAT	Mouse *Mitf* reverse
	TTGGGTTTTCCAGCTAAGTTCT	Human *TBP* forward
	CCAGGAAATAACTCTGGCTCA	Human *TBP* reverse
ChIP	CGAGAACATAGAAAAGAATTATGA AA	Human *Tyrosinase* Enhancer (-1.8 kb) forward
	CTCTGGCTGGAATCAGGAAG	Human *Tyrosinase* Enhancer (-1.8 kb) reverse
	TTTCCCCTGTCTCAGGAGTT	Human *Tyrosinase* -1 kb forward
	TGCAAGTGTTATCAAGGGAGTG	Human *Tyrosinase* -1 kb reverse
	ACCGACATCTTTCTCCCGTT	Human *Protamine* forward
	AGTCATCCCACTCTTCTCTCC	Human *Protamine* reverse

2.10 Antibodies

Table 2.4. Antibodies and their dilutions used in the study.

Antibody	Reactive against	Source	Dilution used in application		
			Western blot	IF	IP/ChIP
α-MITF mouse monoclonal	C-terminus	Developed in house	1:2000		
α-MITF rabbit polyclonal	Unknown			1:500	
α-Tbx2 mouse monoclonal	Unknown		1:1000		
α-ERK2 (SC154) rabbit polyclonal	C-terminus	Santa Cruz	1:10000		
α-Lamin B (C20) goat polyclonal	C-terminus		1:1000		
α-Tbx3 (C20) goat polyclonal	Unknown		1:1000		
α-c-Myc 9E10 (SC40) mouse monoclonal	EQKLISEEDLN		1:2000		1 μg IP
α-6×His rabbit polyclonal	HHHHHH		1:1000		
α-Actin (AC-40) mouse monoclonal	C-terminus	Sigma	1:1000		
α-FLAG (M2) mouse monoclonal	DYKDDDDK		1:10000		
α-HA (HA-7) mouse monoclonal	YPYDVPDYA		1:2000	1:100	1 μg IP
α-HA (12CA5) mouse monoclonal	YPYDVPDYA	Roche			1 μg IP 5 μg ChIP
α-p66β mouse polyclonal	Unknown	Novus Biologicals	1:1000		
α-acetyl-lysine rabbit polyclonal	Acetylated lysine	Cell Signaling	1:2000*		
α-MEK1/2 rabbit polyclonal	Unknown		1:1000		
α-phospho-MEK1/2 (Ser217/221) rabbit polyclonal	Phospho-Ser217/221		1:1000*		
α-S6 ribosomal protein (S6) rabbit monoclonal	Unknown		1:1000		
α-phospho-S6 (Ser235/236) rabbit polyclonal	Phospho-Ser235/236		1:1000*		
α-phospho-ERK1/2 (Thr202/204) rabbit monoclonal	Phospho-Thr202/204		1:2000*		
α-Brn-2 rabbit polyclonal	N-terminus		1:1000		
α-γ-H2AX mouse monoclonal	Phospho-Ser139			1:500	
α-β-catenin rabbit polyclonal	Unknown	Abcam	1:1000		
α-p300 mouse monoclonal	Unknown	Pharminogen	1:1000		

* Antibodies marked with asterisk were diluted in 5% BSA in TBS-T for Western blot

Chapter 3 – Regulation of MITF acetylation and DNA binding

3.1 Introduction

The rheostat model that explains the ability of MITF to both promote and prevent proliferation relies on changing expression levels and activity of MITF throughout development and in melanoma cells (Carreira et al., 2006). In proposing this model, Carreira and colleagues did not provide a mechanism to explain how varying MITF levels could directly impact the transcriptional programme MITF induces, nor what other factors may be important in regulating MITF activity. They did however note that it was unlikely that MITF protein levels alone could explain its capacity to regulate different subsets of target genes at different developmental stages or in melanoma cells and they hypothesised that post-translational modifications could play a role in controlling MITF DNA binding (Carreira et al., 2006).

MITF can be SUMOylated on two sites, K182 and K316, and it has been shown that SUMO-MITF has an enhanced ability to transactivate a promoter containing multiple MITF binding sites (Miller et al., 2005; Murakami and Arnheiter, 2005). However, SUMOylation of MITF is insufficient to explain the varied functions of MITF at different stages of the rheostat model, because the subsets of genes controlling differentiation or proliferation will contain variable numbers of MITF binding sites that regulate them. Furthermore, a recent study has revealed that an MITF^{E318K} mutant, which has disrupted SUMOylation, has enhanced genome-wide occupancy without increased binding at specific sets of loci (Bertolotto et al., 2011).

Previous work in our laboratory has demonstrated that Mitf can be acetylated by p300/CBP on at least ten lysine residues throughout the protein, including 2 in the basic region (K205, K206) and 4 throughout the HLH-LZ (Alex Schepsky, unpublished, Figure 3.1A). It is possible that acetylation of the bHLH-LZ could regulate the ability of MITF to either interact with DNA in general or with different

specific sequences, while acetylation throughout the protein could affect the interaction between MITF and its cofactors. This chapter focusses on the effect of MITF acetylation on its ability to bind DNA and activate transcription.

Our previous work also revealed that Mitf-acetylation is MAPK-dependent. In cotransfection assays, 293 cells coexpressing HA-tagged Mitf and p300 showed robust induction of Mitf-acetylation following HA-immunoprecipitation (Alex Schepsky, unpublished, Figure 3.1B). In cells treated with the MEK inhibitor UO126, however, Mitf-acetylation was not induced, suggesting that MAPK activity was required for Mitf-acetylation. After SDS-PAGE, MITF is resolved as two bands. The upper, slower-migrating band has been determined to be MITF hyper-phosphorylated
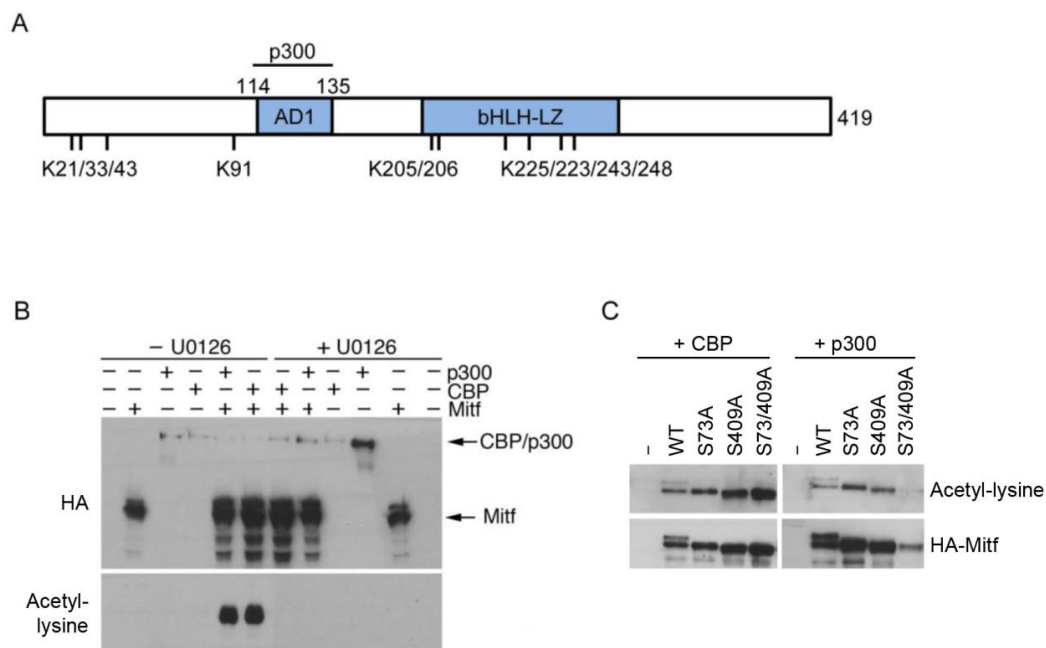
Figure 3.1. Mitf is acetylated by p300/CBP in response to MAPK signalling. Work in this figure was carried out by Alex Schepsky. (A) p300/CBP interacts with the N-terminus of MITF (AD1; Sato et al., 1997), and acetylation sites were mapped by IP of Myc-Mitf in the presence of p300/CBP followed by mass spectrometry. (B) 293 cells transfected with HA-Mitf in the presence or absence of HA-p300/CBP were treated or not with UO126 (20 μM, 8 hours). Following anti-HA IP, purified protein was analysed by Western blotting with the indicated antibodies. (C) 293 cells were transfected with the indicated HA-Mitf construct in the presence of HA-p300/CBP. After HA-IP, samples were analysed as in (B).

on S73 and S409, while the lower, faster-migrating band is MITF hypo-phosphorylated on these residues (Hemesath et al., 1998). HA-Mitf with S73A, S409A or S73/409A mutations can all be acetylated by CBP and p300 (Alex Schepsky, unpublished, Figure 3.1C); although the acetyl-lysine signal for HA-Mitf$^{S73/409A}$ in the presence of p300 was very weak, the HA-Mitf yield for this sample was substantially lower than the others. These experiments showed that Mitf-acetylation was MAPK-signalling dependent but independent of MAPK-driven phosphorylation of Mitf. It is known that ERK can phosphorylate and activate p300 (Chen et al., 2007), which could explain the requirement of MAPK activity for Mitf-acetylation. Here, the effect of modulating MAPK activity on MITF DNA binding activity is studied.

3.2 Control of MITF-acetylation and its effect on DNA binding

Previous work in our laboratory showed that Mitf can be acetylated following overexpression of p300/CBP (our unpublished data, Figure 3.1). p300 and CBP can both directly act as acetyltransferases, but are also able to recruit p300/CBP-associated factor (PCAF) to their targets, whereupon PCAF may also act as an acetyltransferase (Yang et al., 1996). The overexpressed proteins in this previous work were all HA-tagged, making it possible that the observed acetylated species could result from a degradation product of p300/CBP. To confirm that the acetylation previously observed was Mitf-specific and due to the activity of p300 and CBP, FLAG-Mitf was expressed in Phoenix cells in the presence or absence of HA-p300, HA-CBP, or FLAG-PCAF. Western blotting of the input fractions revealed that overexpression of HA-p300/CBP, but not FLAG-PCAF, significantly increased global acetylation levels relative to the ERK2 input fraction loading control (Figure 3.2A). Additionally, overexpression of HA-p300/CBP increased the FLAG-Mitf protein level

in the cells. Following anti-FLAG immunoprecipitation and equalising the amount of purified FLAG-Mitf, Western blotting with pan anti-acetyl-lysine revealed that coexpression with HA-p300 and HA-CBP, but not FLAG-PCAF, induced FLAG-Mitf acetylation (Figure 3.2A). Overnight exposure of the same membrane revealed that a small amount of FLAG-Mitf may be found acetylated in the absence of overexpressed acetyltransferases, demonstrating that this is not purely a phenomenon deriving from overexpression of acetyltransferases.
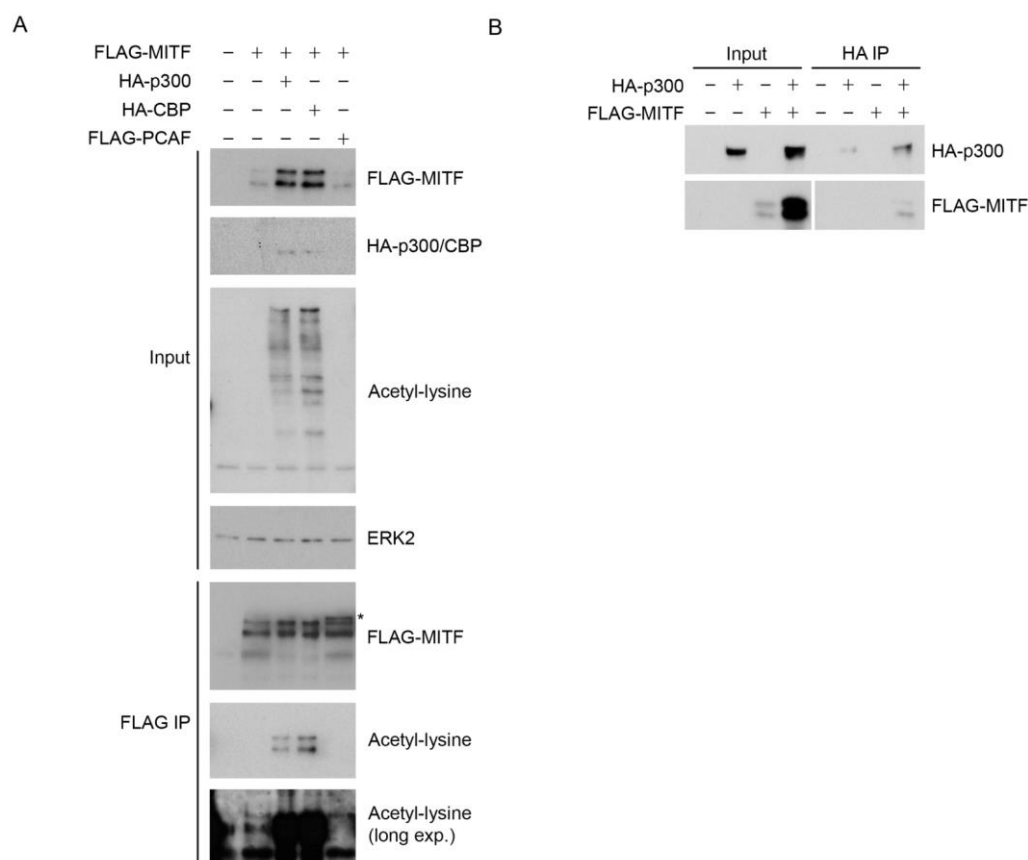
Figure 3.2. p300/CBP acetylates and interacts with Mitf. (A) Phoenix cells were transfected with the indicated constructs. After 40 hours, cell lysates were subjected to anti-FLAG IP and input/IP fractions analysed by Western blotting with the indicated antibodies. * denotes immunoprecipitated FLAG-PCAF. (B) Lysates from Phoenix cells 40 hours post-transfection with the indicated constructs were subjected to anti-HA IP and input/IP fractions analysed by Western blotting with the indicated antibodies.

Both Mitf bands were acetylated by p300/CBP (Figure 3.2A). This appeared to be consistent with a previous report showing that CBP interacted with both hyper- and hypo-phosphorylated forms of Mitf (Sato et al., 1997), but contradicted a subsequent study suggesting that p300 was preferentially recruited to the hyper-phosphorylated form of Mitf (Price et al., 1998a). To investigate this, HA-p300 was expressed in Phoenix cells in the presence or absence of FLAG-Mitf (Figure 3.2B). As before, coexpression of HA-p300 with FLAG-Mitf increased levels of FLAG-Mitf. This effect appeared to be partially reciprocal, as there was slightly more HA-p300 present in cells also transfected with FLAG-Mitf. Following anti-HA-p300 immunoprecipitation, Western blotting revealed that FLAG-Mitf was not detected in cells transfected with FLAG-Mitf alone, indicating that there were no non-specific effects from the procedure. In cells that were co-transfected with HA-p300 and FLAG-Mitf, anti-HA immunoprecipitation resulted in co-immunoprecipitation of both hyper-phosphorylated and hypo-phosphorylated forms of FLAG-Mitf, showing that, in our hands, p300 will interact with both. This is in good agreement with Sato et al. (1997) and in contrast to the study of Price et al. (1998).

Coexpression of HA-p300 with FLAG-Mitf led to elevated FLAG-Mitf protein in clarified cell lysates (Figure 3.2A). To confirm that this resulted from an increase in FLAG-Mitf protein in the entire cell and not just from an increase in soluble protein, Phoenix cells were transfected with FLAG-Mitf, HA-p300, or both, and whole cell extracts were subjected to Western blotting. As before, there was a slight increase in HA-p300 in cells also transfected with FLAG-Mitf. In addition, expression of FLAG-Mitf in the presence of HA-p300 served to dramatically increase protein levels of FLAG-Mitf relative to an ERK2 loading control (Figure 3.3A), confirming that HA-p300 activity was indeed able to increase the amount of FLAG-

Mitf in cells. This raised the possibility that p300 either increased FLAG-Mitf stability, or that it was increasing FLAG-Mitf expression. To investigate this, RNA was extracted from Phoenix cells expressing FLAG-Mitf in the presence or absence of HA-p300. qPCR analysis revealed that the presence of HA-p300 in cells resulted in a four-fold increase in expression of *FLAG-Mitf* from its plasmid as compared with levels of *TBP* (TATA binding protein), the housekeeping gene used as a loading control (Figure 3.3B). Negligible expression was detected in cells transfected with just HA-p300, or untransfected cells. Although the increase in *FLAG-Mitf* expression does not match the increase in FLAG-Mitf, this result shows that, at least in part, the increase in protein does arise from elevated expression, and that HA-p300 can activate the CMV promoter. It is possible that the remaining difference does arise from an effect on FLAG-Mitf stability, and this will be investigated in the future.
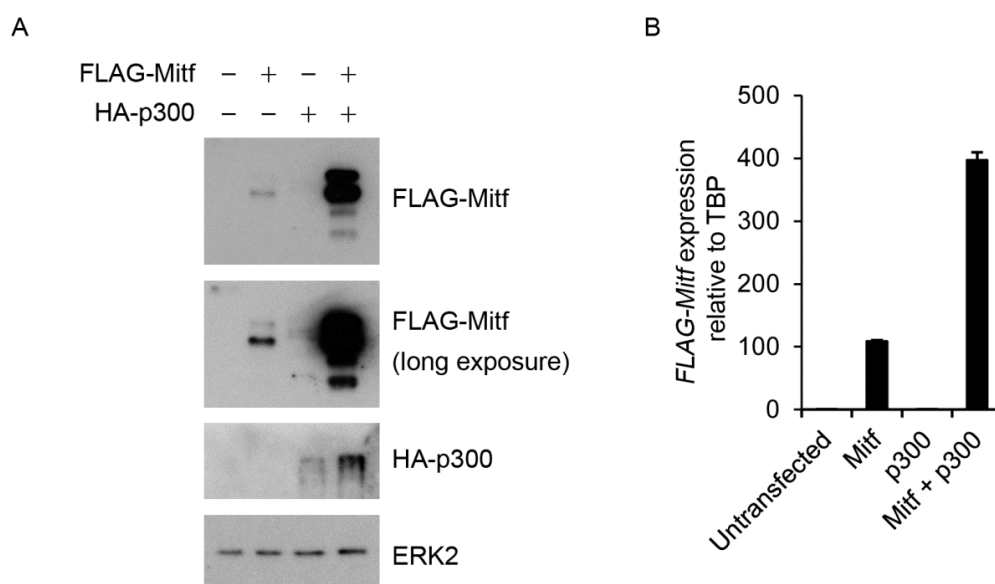
Figure 3.3. Coexpression with p300 increases Mitf protein level. (A) Whole cell extracts from Phoenix cells 40 hours post-transfection with the indicated constructs were analysed by Western blotting with the indicated antibodies. (B) Total RNA was extracted from Phoenix cells transfected with FLAG-Mitf or HA-p300 as indicated and expression of the indicated genes analysed by qPCR. Results are presented relative to *TBP* expression and indicate the mean ± standard deviation of two independent experiments performed.

To characterise the effect of MITF-acetylation on the ability of MITF to bind to DNA, nuclear extracts were prepared from Phoenix cells expressing FLAG-Mitf in the presence or absence of HA-p300. When compared with ERK2 levels, an increase in nuclear-extractable FLAG-Mitf was found in cells cotransfected with HA-p300 (Figure 3.4A). The difference in the DNA binding potential of Mitf in these nuclear extracts was assessed by EMSA using a radiolabelled probe against the *Tyrosinase* enhancer, which has a 5'-TCATGTGA-3' MITF binding site (Figure 3.4B). This probe sequence was chosen because *Tyrosinase* is one of the best characterised prototypical MITF target genes (Cheli et al., 2010), and a 5'-T is required for strong binding to 5'-CATGTG-3' (Aksan and Goding, 1998). In EMSA, the free
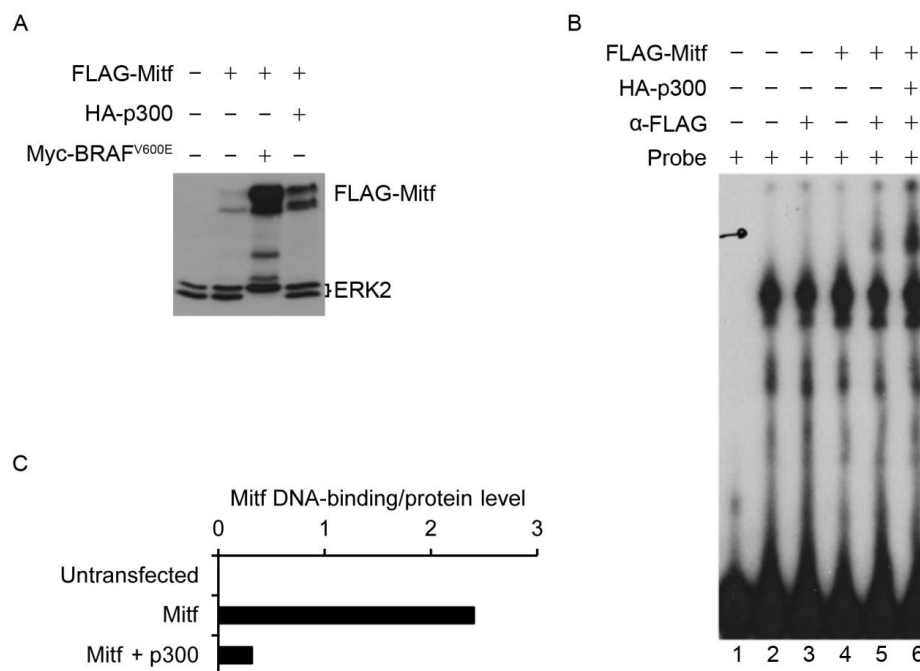
Figure 3.4. Coexpression with p300 inhibits Mitf DNA binding. (A) Nuclear extracts were prepared from Phoenix cells 40 hours post-transfection with the indicated constructs and subjected to Western blotting with the indicated antibodies. (B) EMSA using nuclear extracts from (A), in the presence or absence of FLAG antibody (α-FLAG), bound to a probe containing a 5'-TCATGTGA-3' MITF binding site. Pen-drawn arrow indicates migration of the Mitf-specific band. (C) Quantification of the ratio of the band intensity of the FLAG-Mitf protein level (relative to ERK2 bands) in (A) versus the FLAG-Mitf specific band in (B). Note that the Myc-BRAF sample in (A) is used later and is shown here to allow the full panel to be shown.

radiolabelled probe runs to the bottom of the gel, while migration of the protein-bound probe is retarded. There was residual binding to the probe in nuclear extracts from untransfected cells. This arises from the presence of other bHLH-LZ proteins such as USF in the cells, which are also able to bind to these sequences *in vitro*. In nuclear extract from FLAG-Mitf-expressing cells, there were no additional bands induced compared to untransfected cells, most likely owing to low transfection efficiency. To visualise Mitf binding, monoclonal anti-FLAG antibody was added to the binding reaction which, when mixed with untransfected nuclear extract, did not generate any further mobility shifts (Figure 3.4B, lane 3). However, addition of anti-FLAG antibody into the binding reaction led to the appearance of an Mitf-specific band in the Mitf-transfected extract (Figure 3.4B, lane 5). Although there was clearly more binding observed from the cells transfected with FLAG-Mitf and HA-p300, compared to those transfected with just FLAG-Mitf (Figure 3.4B, compare lanes 5 and 6), this could have been due to a greater FLAG-Mitf concentration in the cells. Therefore, the relevant bands in the Western blot and EMSA were quantified and the FLAG-Mitf DNA binding to protein ratio was calculated. Coexpression of p300 with (and hyper-acetylation of) Mitf led to a 7.5-fold reduced Mitf capacity to bind DNA *in vitro* (Figure 3.4C).

Having determined that the overexpression of p300 reduced *in vitro* DNA binding by Mitf, it was important to see if the same was true in cells and if there were any consequent effects on MITF target gene activation. To this end a luciferase assay was performed on a reporter derived from the *Tyrosinase* promoter (Figure 3.5A). The natural promoter contains two core M-boxes, each with one flanking 5'-T, and one enhancer element containing a flanking 5'-T on each strand, all of which may be bound by MITF. The promoter fragment used in this experiment contained both core

promoter M-box elements (WT), but not the enhancer motif used in Figure 3.4; because the enhancer element lies 1.8 kb upstream from the *Tyrosinase* transcription start site, it was felt that the intervening sequence would provide many potential confounding binding sites for other transcription factors. In Phoenix cells transfected with reporter alone, a basal level of luciferase activity was observed HA-p300, as compared with ERK2 levels. After normalising luciferase activity for FLAG-Mitf levels in the cell lysates, it was clear that coexpression of HA-p300 repressed the ability of FLAG-Mitf to transcriptionally activate a target gene by approximately two-fold (Figure 3.5D). Caution is required when interpreting the collective results of Figures 3.4 and 3.5, however, because it is possible that the higher FLAG-Mitf titre in cells co-transfected with p300 could have also resulted in altered FLAG-Mitf behaviour. To avoid having to normalise for very different FLAG-Mitf levels, an alternate approach could be to transfect cells with less FLAG-Mitf plasmid in the presence of p300 in an attempt to balance the final FLAG-Mitf expression level.

To investigate deacetylation of Mitf, Phoenix cells were transfected with FLAG-Mitf and HA-p300 in the presence or absence of various histone deacetylases for FLAG-immunoprecipitation (Figure 3.6). On Western blotting of the input fractions, a robust induction of global acetylation was revealed in HA-p300-transfected cells by using a pan-acetyl-lysine antibody, relative to the ERK2 loading control. HA-p300 coexpression served to increase FLAG-Mitf levels. When histone deacetylases were present in triply-transfected cells, different effects were seen. FLAG-HDAC1 and FLAG-HDAC3 expression resulted in unchanged levels of FLAG-MITF or HA-p300. FLAG-HDAC3 induced no change in global acetyl-lysine, while FLAG-HDAC1 reduced the intensity of some bands in the middle of the membrane, suggesting that it could be deacetylating these species. FLAG-HDAC4

and FLAG-HDAC5 both increased the level of FLAG-MITF, but, while FLAG-HDAC4 led to a slightly reduced level of HA-p300, FLAG-HDAC5 increased the level of HA-p300 in the lysates. The increased HA-p300 induced by FLAG-HDAC5 correlated with an increase in global acetyl-lysine compared to cells not expressing an HDAC. This suggested that the elevated HA-p300 content is causing the enhanced acetyl-lysine, and perhaps also the increase in FLAG-Mitf, although it is not possible to rule out a direct effect on FLAG-Mitf by FLAG-HDAC5. For FLAG-HDAC4,
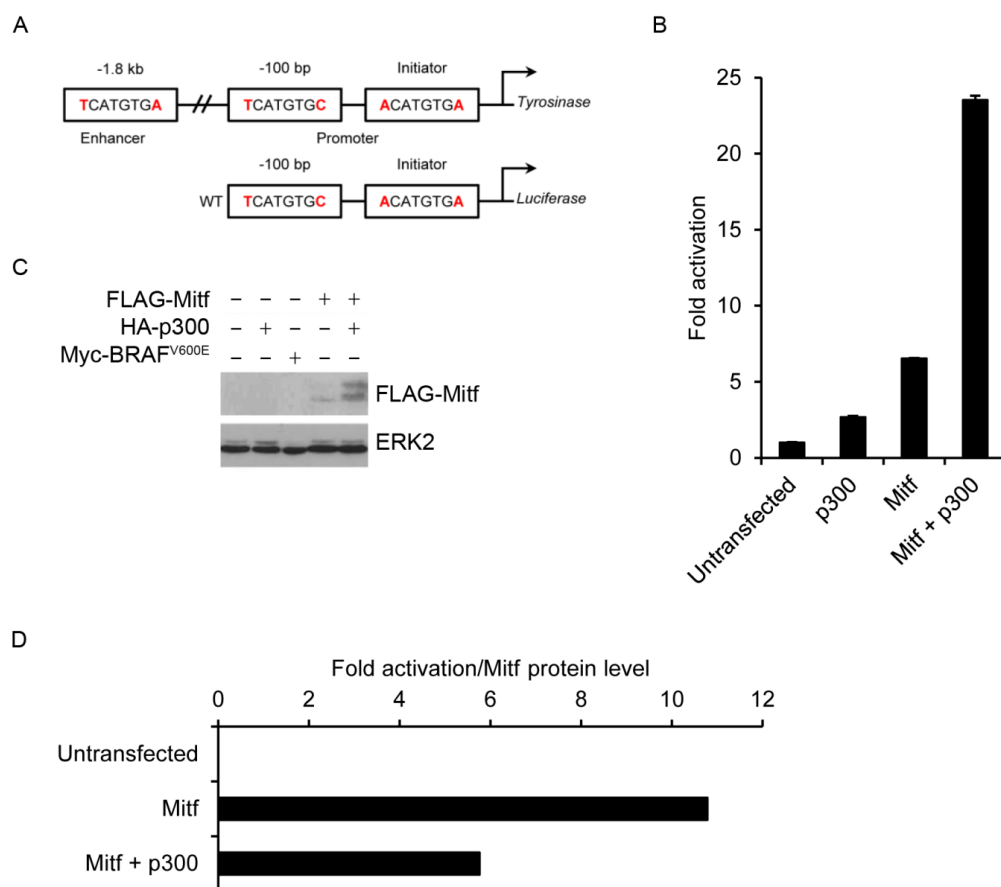
Figure 3.5. Coexpression with p300 represses the ability of Mitf to activate a *Tyrosinase* promoter luciferase reporter. (A) Scheme of the *Tyrosinase* promoter and enhancer regions (top) and *Tyrosinase* luciferase reporter (bottom). (B) 40 hours post-transfection with the indicated constructs plus the luciferase reporter, Phoenix cells were subjected to a luciferase assay. Results are presented as the mean ± standard error of the mean for 3 independent experiments. (C) Lysate from (B) was analysed by Western blotting with the indicated antibodies. (D). Quantification of the ratio of the band intensity of representative FLAG-Mitf protein level (relative to ERK2) in (B) versus mean reporter activation in (C).

global acetyl-lysine unexpectedly did not diminish relative to the level in cells not expressing an HDAC. This suggests that, although HA-p300 is reduced, it may be more active. This cannot, however, explain why there is more FLAG-Mitf, and it could be that FLAG-HDAC4 either regulates FLAG-Mitf stability or increases its
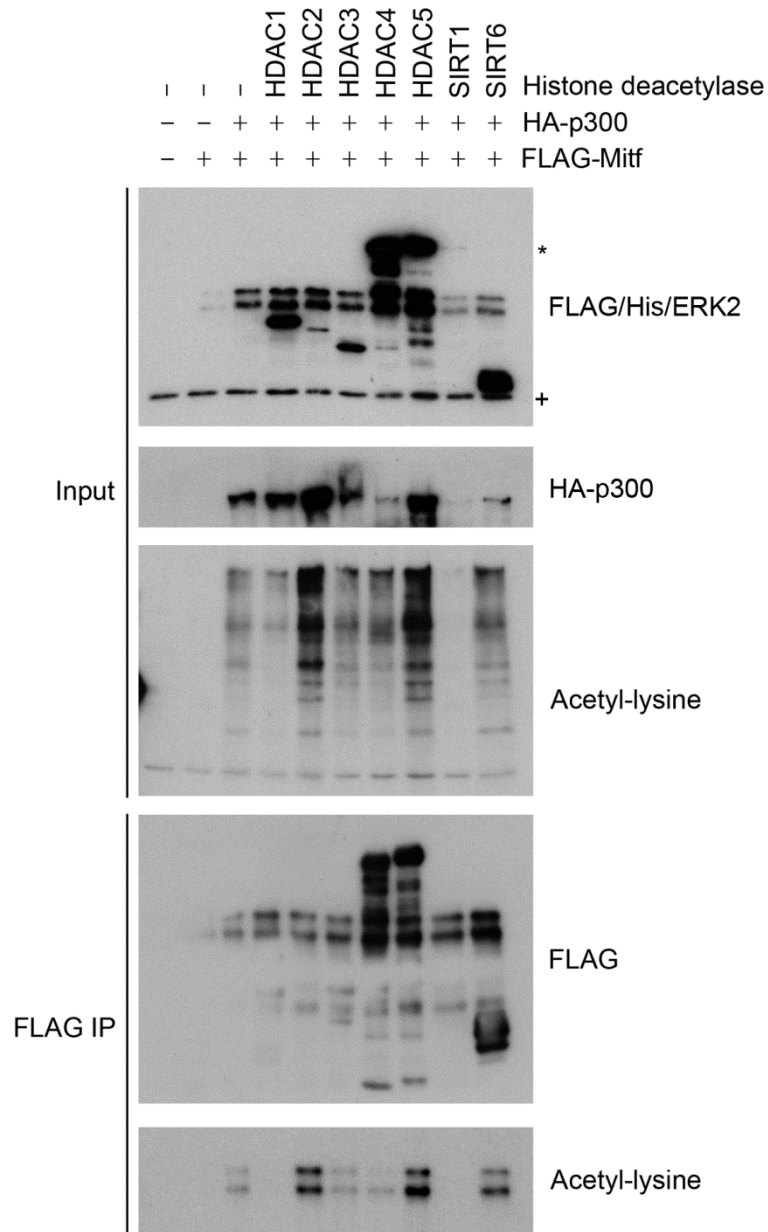
Figure 3.6. Identification of Mitf deacetylases. 40 hours post-transfection with constructs as shown (HDACs and SIRT6 are FLAG-tagged, SIRT1 is His-tagged), lysates from Phoenix cells were subjected to FLAG-IP and, along with input fractions, Western blotted with the indicated antibodies. * indicates mobility of His-SIRT1. + indicates mobility of ERK2.

expression. Like FLAG-HDAC5, FLAG-HDAC2 also increased HA-p300 by an unknown mechanism and was correlated with an increase in global acetyl-lysine levels. FLAG-Mitf was slightly elevated in these cells, but not sufficiently to correlate with the gain in HA-p300. It could be that FLAG-HDAC2 was able to slightly increase the amount of FLAG-Mitf in the cells.

His-SIRT1 coexpression reduced FLAG-Mitf in cells relative to those not expressing His-SIRT1 (Figure 3.6); triple-transfected cells had an amount of FLAG-Mitf between those expressing just FLAG-Mitf and those expressing FLAG-Mitf and HA-p300. Notably, HA-p300 was almost completely absent from cells expressing His-SIRT1, suggesting that His-SIRT1 was destabilising HA-p300 or reducing its expression. The increase in global acetylation seen on expression of HA-p300 was severely diminished. There have been no reports on SIRT1 regulating p300 stability, although it has been shown that SIRT1 deacetylates and inhibits p300 (Bouras et al., 2005). This could explain why, although there is still some HA-p300 present in the cells, none of the acetyl-lysine signal that is induced by HA-p300 expression remains. Finally, FLAG-SIRT6 also reduced FLAG-Mitf levels slightly, and it led to a similarly reduced level of HA-p300 to that observed in cells expressing FLAG-HDAC4. As with FLAG-HDAC4, there was no change in global acetyl-lysine, indicating that the same mechanism could be at play, and that FLAG-SIRT6 could be activating HA-p300.

Following anti-FLAG immunoprecipitation, a varying amount of FLAG-Mitf was recovered from the different samples (Figure 3.6). The purified proteins were probed with anti-acetyl-lysine antibodies to see whether any of these histone deacetylases blocked FLAG-Mitf acetylation. In the absence of HA-p300, at the short exposure shown here, no acetyl-Mitf was detected, while coexpression of HA-p300

induced acetylation of both bands of FLAG-Mitf. FLAG-HDAC1 completely abolished FLAG-Mitf acetylation which, given that there was only a very minor change in global acetylation, suggests that FLAG-HDAC1 is capable of deacetylating FLAG-Mitf on the acetylated sites detected by this antibody. FLAG-HDAC2 enhanced acetylation of FLAG-Mitf, indicating that it likely does not deacetylate FLAG-Mitf. The probable cause of the increase in acetylation signal is the increase in HA-p300 in these cells, which would be expected to increase the overall acetylation level of a given protein. FLAG-HDAC3 had no effect on FLAG-Mitf acetylation, as was expected given that there was no change observed in either HA-p300 or global acetyl-lysine in the input fractions. FLAG-HDAC4 led to reduced FLAG-Mitf acetylation. More FLAG-Mitf was recovered in this sample than in the IP from cells not expressing an HDAC, but the intensity of the lower band of FLAG-Mitf is the same between these two samples, suggesting that some sites on acetyl-FLAG-Mitf may be deacetylated by FLAG-HDAC4. Interestingly, although the ratio between the bands of total recovered FLAG-Mitf is approximately equal, the upper band of FLAG-Mitf was almost completely deacetylated in the presence of FLAG-HDAC4, suggesting that not only does FLAG-HDAC4 selectively deacetylate certain lysines within FLAG-Mitf, but that the distribution of acetyl-lysine in FLAG-Mitf may be different between the hyper-phosphorylated and hypo-phosphorylated forms of the protein. In the FLAG-HDAC5 sample, more FLAG-Mitf was recovered, with a comparable increase in acetyl-lysine signal. More of the lower band of FLAG-Mitf was recovered, and this is reflected in the acetyl-lysine signal.

In the presence of His-SIRT1, there was no detectable acetyl-FLAG-Mitf recovered (Figure 3.6). This was expected as His-SIRT1 also almost completely abolished detectable HA-p300 in these cells. Finally, more FLAG-Mitf was recovered

in the presence of FLAG-SIRT6 than from cells expressing just FLAG-Mitf and HA-p300. Although the acetyl-FLAG-Mitf signal was slightly elevated in the presence of FLAG-SIRT6, this is likely due to the stimulating effect on HA-p300 activity that was observed in the input fraction for this sample.

This experiment indicates that both class I (FLAG-HDAC1) and class II FLAG-HDAC4) HDACs are capable of deacetylating FLAG-Mitf. FLAG-HDAC1 was able to remove all the detectable acetyl marks deposited on FLAG-Mitf by HA-p300, suggesting that this protein could be a major Mitf deacetylase. FLAG-HDAC4 appeared able to selectively deacetylate the hyper-phosphorylated form of FLAG-Mitf, perhaps because the hyper-phosphorylated form of MITF is more active (Price et al., 1998a), and hence more likely to encounter HDAC4. This would in turn suggest that HDAC1 deacetylates MITF in a manner not dependent on MITF activation. It is also possible that FLAG-HDAC4 is only able to deacetylate certain sites within Mitf, and that these are predominantly found in the hyper-phosphorylated form of Mitf. Further work is required to distinguish between these possible explanations, and also to determine which sites are deacetylated by FLAG-HDAC1 and FLAG-HDAC4.

To date, no interactions between MITF and histone deacetylases have been reported. Having shown that HDAC1 and HDAC4 can deacetylate Mitf, we wanted to determine whether histone deacetylases could directly interact with Mitf. Phoenix cells were transfected with HA-Mitf in the presence or absence of FLAG-HDACs 1 through 5 (Figure 3.7A). Following Western blotting of the input fractions, an increase in HA-Mitf in cells also transfected with FLAG-HDACs 4 and 5 relative to ERK2 was seen, similar to the previous experiment. Although HA-Mitf appeared to diminish in the presence of FLAG-HDAC3, this may be explained by reduced total protein recovered in this sample, as evidenced by decreased ERK2. Following anti-

HA immunoprecipitation, approximately equal amounts of HA-Mitf was recovered in each sample. Probing with anti-FLAG antibody revealed that a fraction of both FLAG-HDAC1 and FLAG-HDAC5 were co-purified with HA-Mitf. There was no interaction seen with FLAG-HDAC4. This is an interesting finding given that HDAC4 and HDAC5 are class II HDACs with close to 60% sequence identity, suggesting that the interaction with HDAC5 could be highly specific.
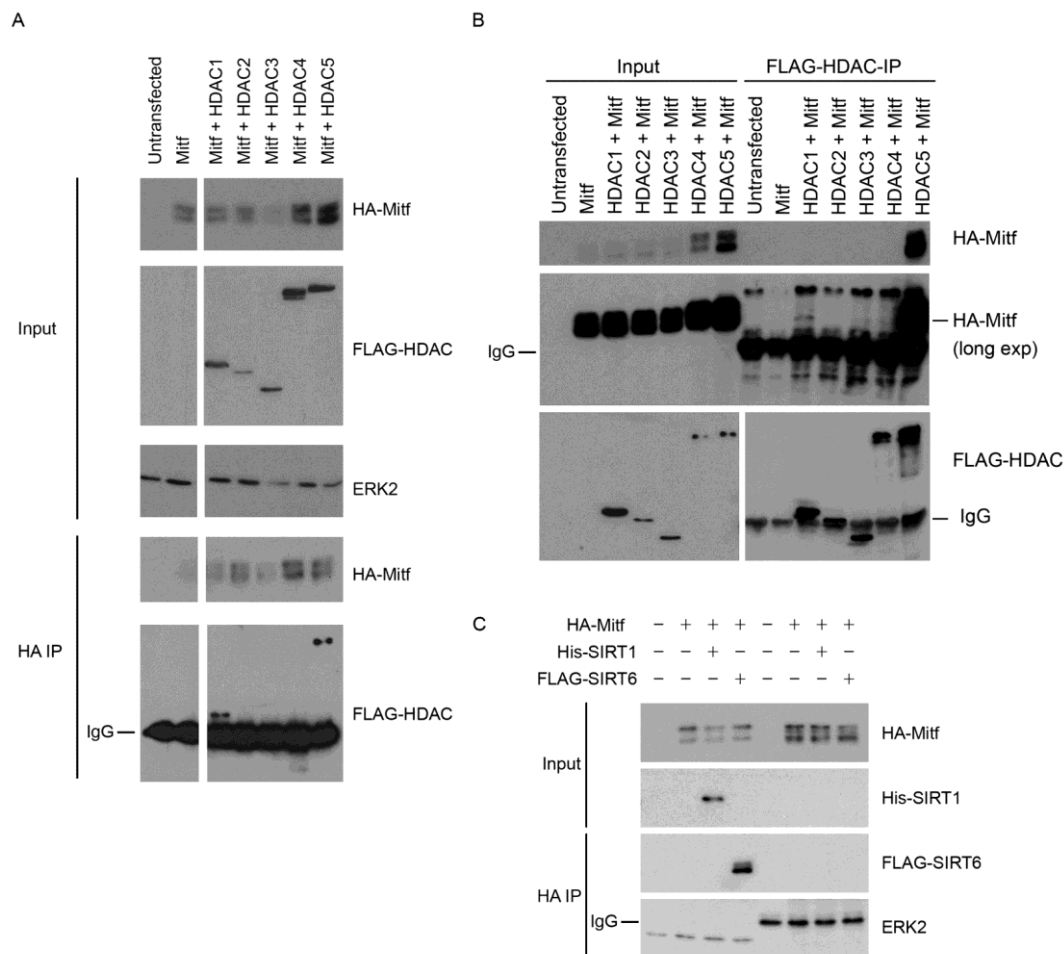
Figure 3.7. Identification of Mitf-interacting deacetylases. (A) 40 hours post-transfection, lysates from Phoenix cells transfected with the indicated constructs were subjected to HA-IP followed by Western blotting of input/IP fractions with the indicated antibodies. (B) Cells transfected as in (A) were subjected to FLAG-IP followed by Western blotting of input/IP fractions. (C) Phoenix cells transfected for 40 hours with the indicated antibodies were subjected to FLAG-IP followed by Western blotting of input/IP fractions with the indicated constructs.

It was not possible to conclude whether FLAG-HDACs 2 and 3 might interact with HA-Mitf, as they would have resolved underneath the intense IgG band visible on the membrane in this experiment. Therefore, a reciprocal experiment was performed. As Mitf resolves above IgG, an interaction with any of the HDACs should be apparent following an HDAC IP. The same transfections were performed and, again, in the input fractions there was an increase in HA-Mitf in the presence of HDACs 4 and 5 compared to cells not expressing an HDAC (Figure 3.7B). There was no change in HA-Mitf in the presence of HDACs 1, 2 or 3. Anti-FLAG immunoprecipitation was used to recover the FLAG-HDACs; they were purified in similar amounts, with HDACs 1, 2 and 3 all resolving close to, but clearly distinguishable from, the IgG band. No HA-Mitf was purified from cells not expressing a FLAG-HDAC, indicating that the purification procedure was sufficiently stringent to prevent non-specific interactions with either antibody or beads. In cells expressing FLAG-HDAC5 but not FLAG-HDAC1, a strong interaction was seen with HA-Mitf. As there was a comparable amount of each HDAC recovered in the previous experiment, this was surprising. In an overnight exposure a little HA-Mitf was seen to have been recovered from cells expressing FLAG-HDAC1. Because there were significantly different levels of HA-Mitf in the input fractions for these two samples and between the two experiments conducted here, it is not possible to conclude anything about the relative strength of the interaction between Mitf and HDAC1 and HDAC5, just that these two HDACs can interact with Mitf. It was interesting that HDAC1 was able to interact with and deacetylate Mitf in these assays, while HDAC4 did not appear to directly interact with Mitf. This suggests that an additional scaffolding factor is required to bridge the gap between HDAC4 and Mitf.

Similar experiments were performed with His-SIRT1 and FLAG-SIRT6. Phoenix cells were transfected with HA-Mitf in the presence or absence of these sirtuins. There were similar levels of expression of the SIRTs relative to the ERK2 loading control (Figure 3.7C). Unlike in the deacetylation assay, there was no change in the HA-Mitf level in the input fraction from cells expressing either SIRT. Following HA-immunoprecipitation, ERK2 was not recovered in any of the samples, including the untransfected control lane, suggesting that the IP was stringent. No interaction was observed between either His-SIRT1 or FLAG-SIRT6, suggesting that, MITF cannot interact with these proteins in Phoenix cells, although it cannot be confirmed in the absence of a positive control that the assay was not too stringent. However, this is perhaps unlikely given the identical extraction conditions compared with the previous experiments.

3.3 The role of MAPK-signalling in MITF DNA binding

Prior work has shown that MAPK signalling is required for Mitf acetylation (Alex Schepsky, unpublished, Figure 3.1B), but that Mitf does not need to be phosphorylated by ERK in order to be acetylated (Alex Schepsky, unpublished, Figure 3.1C). It has previously been shown that ERK2 can phosphorylate and activate p300 downstream from epidermal growth factor signalling (Chen et al., 2007). To investigate whether a similar mechanism could be occurring in this system, Phoenix cells were transfected with HA-p300 in the presence or absence of constitutively activated Myc-BRAF^{V600E} (Figure 3.8A). Expression of Myc-BRAF^{V600E} in cells induced ERK1/2 phosphorylation on T202 and T204 (referred to as phospho-ERK hereafter), which could also be seen in an upward mobility shift of the total ERK2 in these extracts. Expression of Myc-BRAF^{V600E} slightly increased the amount of HA-p300 in cells. Compared to an actin loading control, expression of HA-p300 caused a

large increase in acetylation of numerous species, while in cells not expressing HA-p300 there was relatively little detectable acetyl-lysine. This is perhaps because acetylation and deacetylation are very rapid, dynamically regulated processes with individual modifications being swiftly removed, which in a non-perturbed system as is found in the non-transfected cells, would serve to limit the degree of acetylation that is detected (Katan-Khaykovich and Struhl, 2002). Coexpression of Myc-BRAF^{V600E} was accompanied by a significant increase in acetyl-lysine, suggesting that BRAF and p300 cooperate to drive acetylation of p300-target proteins. This finding raises the possibility that a system exists whereby BRAF-signalling could have two interconnected effects on MITF, by inducing its phosphorylation, activation,
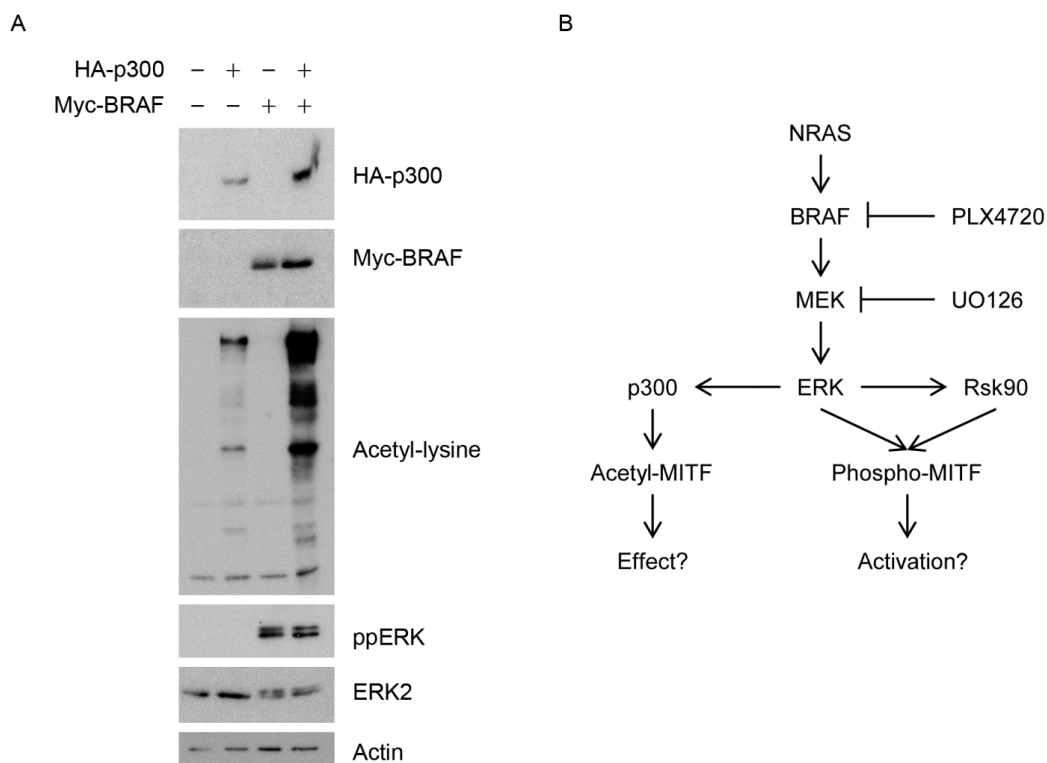
Figure 3.8. BRAF and p300 cooperate to increase acetylation. (A) Whole cells extracts from Phoenix cells transfected for 40 hours with the indicated constructs (note: BRAF is BRAF^{V600E}) were subjected to Western blotting with the indicated antibodies. (B) Scheme of the MAPK pathway leading to phosphorylation and, via activation of p300, acetylation of MITF. PLX4720 and UO126 are MAPK pathway inhibitors.

95

and ultimately degradation on the one hand, but also by promoting MITF acetylation by p300 on the other (Figure 3.8B).

In almost all melanoma patients, MAPK-signalling is constitutively activated (Brose et al., 2002; Davies et al., 2002). This raises the possibility that in melanoma MAPK will promote MITF acetylation, and that, because MITF is acetylated within the DNA binding domain, this could impact on MITF's DNA binding activity. We therefore investigated the effect of MAPK-inhibition on MITF behaviour. Before doing this, however, it was necessary to characterise the effect of MAPK inhibition on melanoma cells. The MAPK pathway was inhibited at two levels (Figure 3.8B) using UO126, a noncompetitive MEK inhibitor (Favata et al., 1998), and PLX4720, an analogue of vemurafenib, which is now used in the clinic (Tsai et al., 2008). 501mel cells were treated with UO126 and PLX4720 for 24 and 48 hours and, relative to either untreated control cells or DMSO-treated cells, a slight increase in pigmentation was observed in cell pellets after 24 hours. Pigmentation was significantly elevated with both drugs after 48 hours (Figure 3.9A). Pigmentation is a hallmark of differentiation for cells within the melanocyte lineage, and this suggested that removal of activated MAPK-signalling had induced melanoma differentiation. In general, the MAPK pathway promotes proliferation, although MAPK signalling has been observed to promote differentiation under certain conditions (Marshall, 1995). From the rheostat model (Carreira et al., 2006), increasing levels of MITF will also promote differentiation. To confirm that the differentiation induced by MAPK inhibition was not caused by elevated MITF, the cell pellets were analysed by Western blotting. Total ERK2 was unchanged throughout the timecourse, while both inhibitors reduced levels of phospho-ERK, at both time points, relative to a Lamin B loading control. UO126 showed a more efficient inhibition of ERK phosphorylation throughout the

timecourse. There was no significant increase in total MITF at 24 hours, although the hypo-phosphorylated form of the protein was enriched, and at 48 hours, there was a loss of the hyper-phosphorylated form of MITF. This result is discussed further with Figure 3.14.

If MAPK inhibition promotes melanoma cell differentiation, it would be expected that cells treated with UO126 or PLX4720 would grow more slowly than untreated cells. The proliferation of 501mel cells was measured with an MTT assay (Figure 3.9B). Cells that were either untreated or treated with DMSO grew at a similar rate, with no significant difference between them after 5 days. However, cells treated with either UO126 or with PLX4720 grew at a significantly slower rate than control cells, indicating that MAPK inhibition does indeed reduce cell growth as part of the differentiation induced by the treatment.
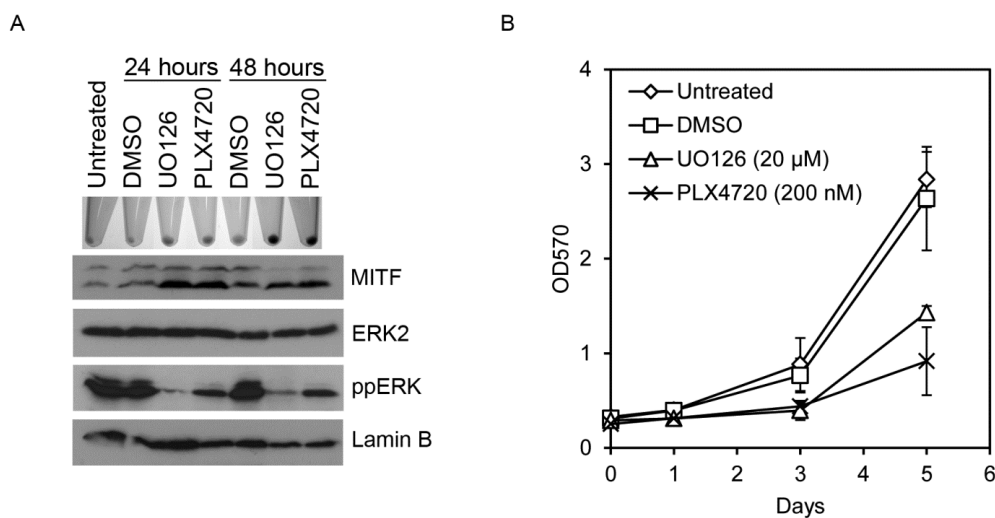
Figure 3.9. MAPK inhibition induces 501mel differentiation. (A) 501mel cells were treated or not with DMSO, UO126 (20 μM) or PLX4720 (200 nM) for the indicated times. Cell pellets were photographed and whole cell extracts were analysed by Western blotting with the indicated antibodies. Note that this panel appears as part of Figure 3.14A. (B) 1000 501mel cells were plated in 96 well plates. The next day (day 0), media was replaced with fresh media that was untreated, or contained DMSO, UO126 (20 μM) or PLX4720 (200 nM). At the indicated time points, cells were subjected to an MTT assay. Results are presented as mean ± standard error of 3 independent experiments.

The data so far suggested that MAPK inhibition promotes melanoma cell differentiation by reducing cell growth and activating pigmentation, and posed a question about how this could be taking place. It is possible that MAPK signalling could be regulating this through either MITF-phosphorylation or MITF-acetylation. Upon examination of M-box and E-box motifs in MITF target genes, those playing roles in pigmentation or other differentiation processes, such as *Tyrosinase*, *TYRP1*, *PMEL* and *DIAPH1*, all had motifs flanked by a 5'-T on one or both strands (Figure 3.10A). In target genes with roles in regulating proliferation, invasiveness, or survival, such as the *MET* proto-oncogene and *BCL2*, the M-box and E-box motifs are either flanked by no 5'-T, or only at one end of the motif (Figure 3.10B). We hypothesised
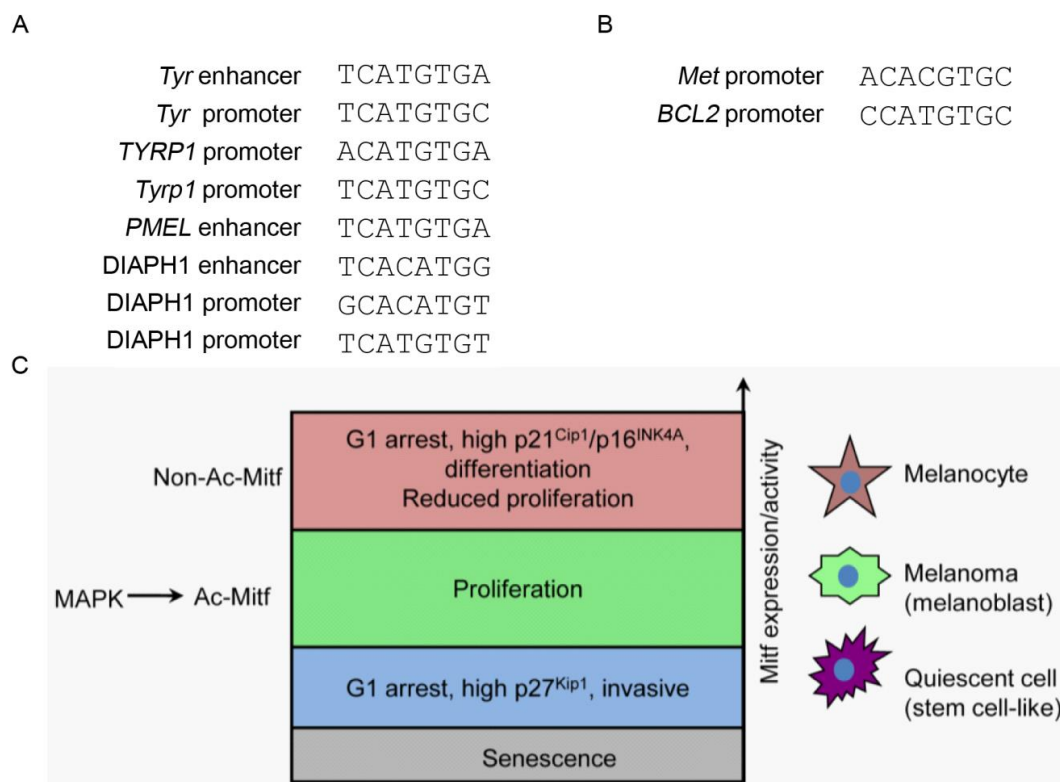
Figure 3.10. Acetylation-driven redirection of MITF binding could add to the rheostat model. (A) MITF binding sites in differentiation target genes. (B) MITF binding sites in genes regulating proliferation, survival, and invasiveness. (C) Modified rheostat model whereby in proliferative cells, Acetyl-MITF could occupy sites lacking a flanking 5'-T, whereas in differentiated cells where MAPK signalling is not active, non-acetyl-MITF would occupy sites containing a 5'-T. Adapted from Carreira et al. (2006).

that in differentiated melanocytes or melanoma cells, MITF would be bound primarily to motifs containing 5'-flanking T residues in genes promoting differentiation and pigmentation while, in proliferative or invasive melanoblasts or melanoma cells, MITF binding to sites containing no 5'-flanking T in target genes promoting proliferation, invasiveness, or survival could dominate. Because of the reactivation of MAPK-signalling in melanoma, and its activation in melanoblasts, we further hypothesised that acetylation of MITF within the DNA binding domain could be responsible for this, giving rise to an additional layer of regulation within the rheostat model (Figure 3.10C). It should be noted though that this hypothesis gives considerable scope for variation, because M-boxes and E-boxes that contain one 5'-flanking T can be found in target genes regulating both differentiation and proliferation, invasiveness, and survival.

In a preliminary investigation, 501mel cells were transfected with a luciferase reporter construct under the control of a *Tyrosinase* promoter, either the wild-type construct used earlier or two mutants (Figure 3.11A). First, both M-boxes were replaced with 5'-TCATGTGA-3', to serve as a classical differentiation motif (TA), and secondly, both M-boxes were replaced with 5'-CCATGTGC-3', to represent proliferation, survival, and invasiveness-regulating target genes (NN). In the absence of any cofactors, the reporter constructs showed different basal activities. The WT and TA reporters showed very similar levels of activation, while the NN reporter was significantly repressed relative to these (Figure 3.11B), in agreement with previous work showing that a 5'-flanking T is required for strong activation of a 5'-CATGTG-3' M-box (Aksan and Goding, 1998). It should be noted however that this experiment was conducted in the absence of a source of exogenous MITF and, as

such, that activation of the NN reporter could potentially be being repressed by another bHLH-LZ factor.

To test the hypothesis that MAPK signalling could redirect MITF DNA-binding, the experiment was repeated in the presence or absence of constitutively activated Myc-BRAF^{V600E}. In Western blots of the lysate, 501mel cells expressing Myc-BRAF^{V600E} showed up-regulation of phospho-ERK as can be seen in membranes probed for phospho-ERK as well as total ERK2, and a strong down-regulation of
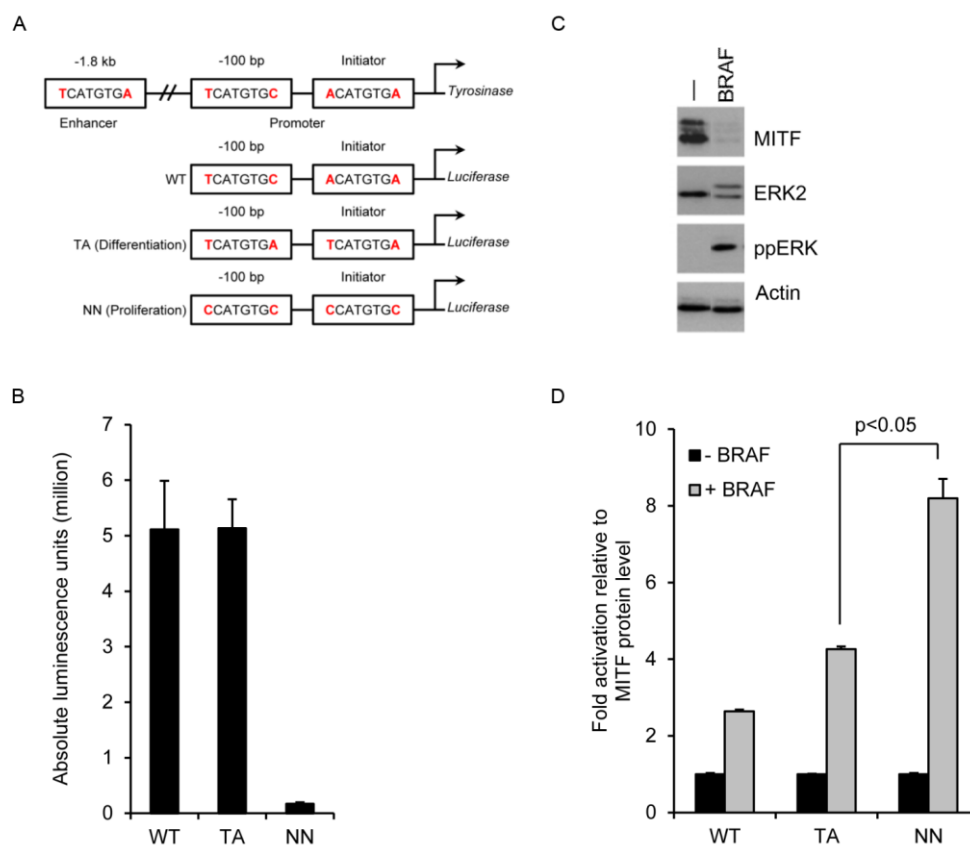
Figure 3.11. BRAF selectively promotes expression of luciferase reporters lacking 5'-T in their MITF binding sites. Luciferase assay results are shown as mean ± standard error of the mean of four independent experiments. Statistical test: two-tailed t-test. (A) Scheme of *Tyrosinase* promoter and enhancer (top), and the WT, TA and NN *Tyrosinase* luciferase reporters (below) used in this experiment. (B) 40 hours post transfection with the luciferase reporters, 501mel cells were subjected to a luciferase assay. (C) Lysates of a representative experiment where 501mel cells were transfected or not for 40 hours with Myc-BRAF^{V600E}. (D) Luciferase assay in extracts from (C) in the presence or absence of Myc-BRAF^{V600E} where 501mel cells were transfected with the indicated reporters. A 2-tailed t-test was performed as indicated.

MITF protein (Figure 3.11C), in agreement with previous studies linking activation of MAPK signalling with MITF-degradation (Wu et al., 2000; Xu et al., 2000). Luciferase activity was normalised for MITF protein-levels in the lysate, revealing that Myc-BRAF^{V600E} induced an approximately 2.5-fold activation of the WT reporter, 4-fold activation of the TA reporter, and 8-fold activation of the NN reporter compared to cells transfected only with the reporter (Figure 3.11D). While Myc-BRAF^{V600E} expression activated all three reporters, perhaps through a non-specific promotion of transcription, the fold-activation of the NN reporter was significantly greater than that of the TA reporter (2 tail t-test, p-value < 0.05). However, the absolute NN reporter activity remained very low in all conditions of the experiment.

To directly assay the effect of MITF in this system, 501mel cells were unsuitable because they express a high level of endogenous MITF, and so addition of further MITF into the system may make little difference. 501mel cells also express BRAF^{V600E}, and, although Myc-BRAF^{V600E} clearly sufficed to induce additional phospho-ERK (Figure 3.11C), it is unclear whether this is enough to truly challenge the equilibrium within the cell. 501mel cells may already be saturated for productive MAPK-signalling, and so an additional source of pathway activation may not strongly perturb downstream effectors of the pathway.

Because of this, Phoenix cells were employed as they express no endogenous MITF and, unlike the majority of melanoma cell lines, have no known constitutive activation of the MAPK pathway. Phoenix cells were transfected with the WT reporter in the presence or absence of Myc-BRAF^{V600E} and FLAG-Mitf (Figure 3.12A). Expression of Myc-BRAF^{V600E} alone failed to activate the reporter relative to cells transfected with the reporter alone, while FLAG-Mitf induced a 6.8-fold activation of the reporter. In the presence of Myc-BRAF^{V600E}, FLAG-Mitf induced
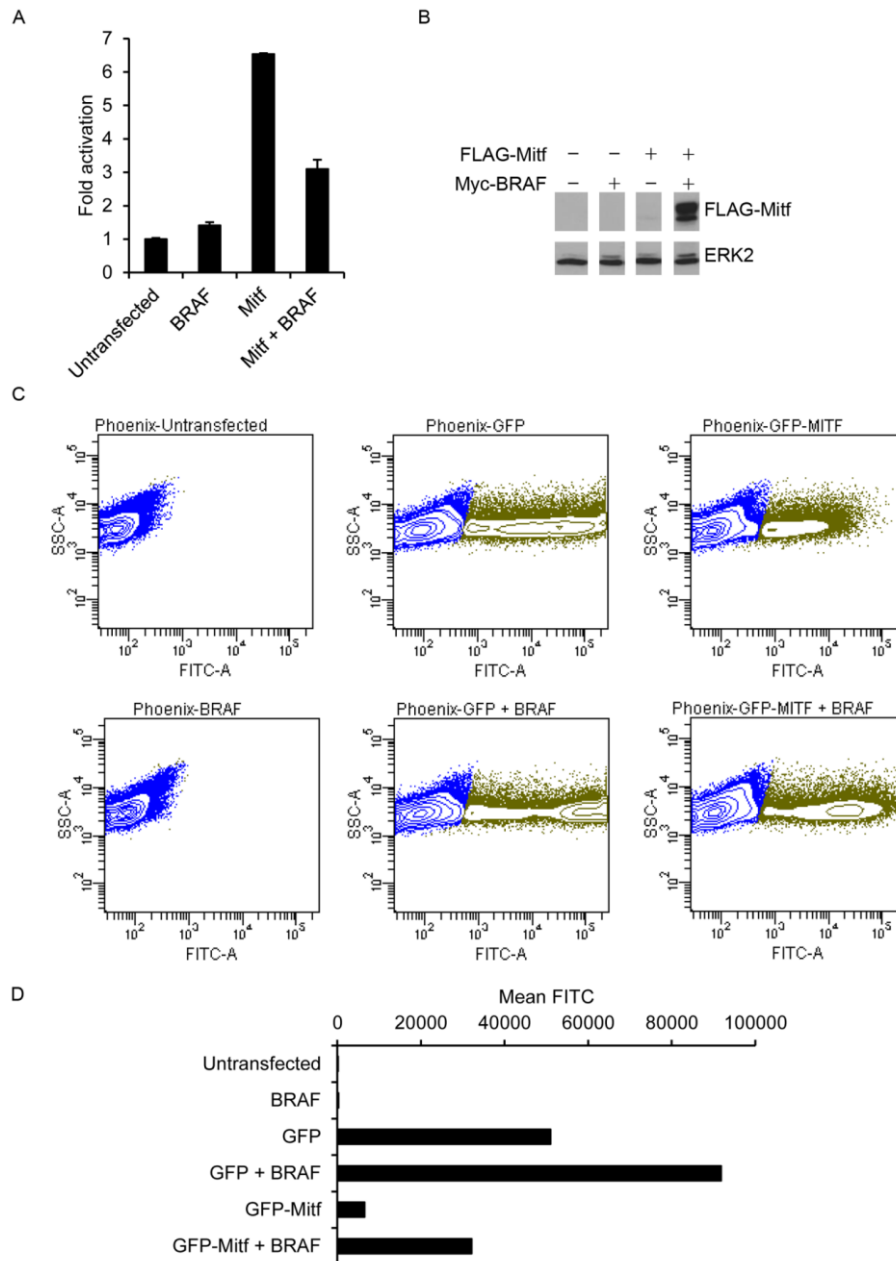
Figure 3.12. BRAF represses reporter gene activation by Mitf. The BRAF construct used in these experiments is Myc-BRAF^{V600E}. (A) Luciferase assay and (B) Western blots from Phoenix cells transfected for 40 hours with the indicated constructs. Luciferase assay results are shown as mean ± standard error of the mean of four independent experiments. (C) Phoenix cells transfected with the indicated constructs for 40 hours were subjected to flow cytometry analysis to quantify GFP content in cells. GFP$^-$ cells are coloured blue, and GFP$^+$ cells are coloured green. (D) Quantification of results from (C), presented as mean FITC count per cell.

only 3-fold activation of the reporter. After Western blotting of the lysates it was clear that Myc-BRAF^{V600E} expression led to significantly more FLAG-Mitf protein (Figure 3.12B). Without needing to normalise luciferase activity for FLAG-Mitf protein levels, it was clear that coexpression of Myc-BRAF^{V600E} together with FLAG-Mitf strongly repressed the capacity of FLAG-Mitf to activate a luciferase reporter, making Phoenix cells a poor model system in which to perform these experiments.

As has been shown with coexpression with HA-p300, coexpression of Myc-BRAF^{V600E} with FLAG-Mitf served to increase the protein level of Mitf substantially in cell lysates. This is in stark contrast to the effect of transfecting 501mel cells with Myc-BRAF^{V600E} where MITF protein levels were reduced, and suggested that BRAF was inducing additional MITF expression in these cells.

To examine this possibility, Phoenix cells were transfected with either GFP or GFP-Mitf in the presence or absence of Myc-BRAF^{V600E}, and the GFP content of the cells was examined by flow cytometry by measuring FITC fluorescence in live cells relative to the side-scattering, which measures the inner granularity of the cell (Figure 3.12C). In the absence of GFP, very low FITC fluorescence was observed in the presence or absence of Myc-BRAF^{V600E}. The GFP tag was expressed at a much higher level than GFP-Mitf. On coexpression of Myc-BRAF^{V600E}, additional GFP and GFP-Mitf was observed, without there being a large change in the number of cells expressing the fluorophore. Following quantification, Myc-BRAF^{V600E} induced 6-fold more GFP-Mitf, and almost 2-fold more GFP, indicating that Myc-BRAF^{V600E} is, at least in part, activating the CMV promoter driving expression of GFP, suggesting that this is the partial cause of the additional FLAG-Mitf in these cells (Figure 3.12D).

This data suggested that, as with HA-p300, Myc-BRAF^{V600E} could be able to repress DNA binding by Mitf. To confirm that DNA binding was indeed being

affected, nuclear extracts from Phoenix cells transfected with FLAG-Mitf and Myc-BRAF^{V600E} were prepared and analysed by Western blotting (Figure 3.13A). Myc-BRAF^{V600E} led to elevated FLAG-Mitf relative to total ERK2, and a shift of ERK2 from a mixture of unphosphorylated and phosphorylated protein to purely phosphorylated protein was observed. In an EMSA using a *Tyrosinase* enhancer M-box, induction of a FLAG-Mitf-specific band was observed when anti-FLAG antibody was included in the binding reaction (Figure 3.13B). FLAG-Mitf DNA-binding in extract from cells also transfected with Myc-BRAF^{V600E} was increased but, following normalisation for FLAG-Mitf protein level, it can be seen that additional BRAF strongly repressed the ability of FLAG-Mitf to bind to DNA (Figure 3.13C).
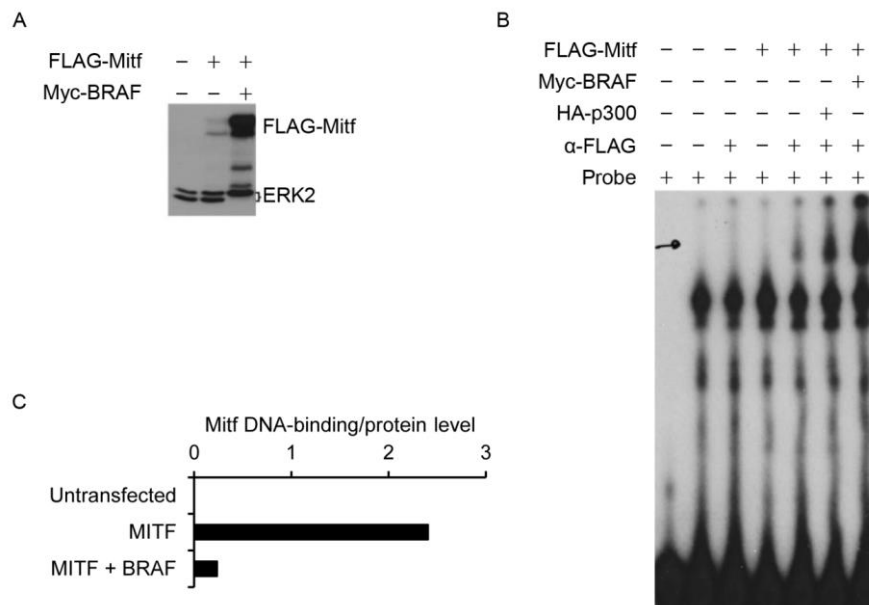
Figure 3.13. BRAF represses Mitf DNA binding. The BRAF construct used in these experiments is Myc-BRAF^{V600E}. (A) Western blot of nuclear extracts from Phoenix cells transfected with the constructs shown. (B) EMSA using nuclear extracts from (A) in the presence or absence of anti-FLAG antibody (α-FLAG) and bound to a probe containing a 5'-TCATGTG-A-3' MITF binding site. Pen-drawn arrow indicates migration of the Mitf-specific band. (C) Quantification of the ratio of the band intensity of FLAG-Mitf protein level (relative to ERK2 bands) in (A) versus FLAG-Mitf specific band in (B). Note that (A) and (B) are also used in Figure 3.4.

Taken together, the data so far suggested that MAPK-induced hyper-acetylation of Mitf could be responsible for reducing its DNA binding.

To understand the molecular mechanisms underlying the differentiation programme observed on treatment with MAPK inhibitors, 501mel cells, treated or not with DMSO, 20 μM UO126, or 200 nM PLX4720 for 24 and 48 hours, were subjected to Western blotting analysis (Figure 3.14A). In the samples, total ERK2 was unchanged while both inhibitors reduced levels of phospho-ERK, at both time points, relative to the Lamin B loading control. Inhibition by UO126 was more efficient than by PLX4720 throughout the timecourse. It was anticipated that the upper, hyper-phosphorylated form of endogenous MITF would be eliminated following MAPK inhibition, as this should prevent further phosphorylation of MITF, and it has previously been reported that phospho-S73/409 MITF is rapidly degraded (Wu et al., 2000). MITF that was freshly translated during the treatment period would not be phosphorylated, and therefore an increase in hypo-phosphorylated MITF was anticipated. As expected, 24 hours of treatment with UO126 and PLX4720 enriched the lower, hypo-phosphorylated band relative to DMSO-treated control cells, and this remained the case at 48 hours (Figure 3.14A). However, it was not until 48 hours of treatment with either inhibitor that there was any reduction in phospho-MITF. This suggested three possibilities: firstly, that MITF phosphorylated on S73/409 is not stable, in contrast to the earlier report (Wu et al., 2000); secondly, that while phosphorylation on S73/409 is necessary for the presence of the upper band, another, subsequent phosphorylation event could also be required; or thirdly, that phosphorylation of another site could be responsible for this mobility shift.

Other factors that play important roles in melanoma were also examined (Figure 3.14A). Brn-2 is a transcription factor that is up-regulated by MAPK-activity

and can promote melanoma cell proliferation and invasiveness (Goodall et al., 2004a; Goodall et al., 2008), and thus represents a further positive control for the effects of MAPK-inhibition. Brn-2 levels were reduced by treatment with UO126 as has been previously observed (Goodall et al., 2004a) and also, as expected, by PLX4720. TBX2 and TBX3 are anti-senescence factors expressed in many melanomas, and were unchanged by either inhibitor, although there was a very slight decrease in TBX2 in
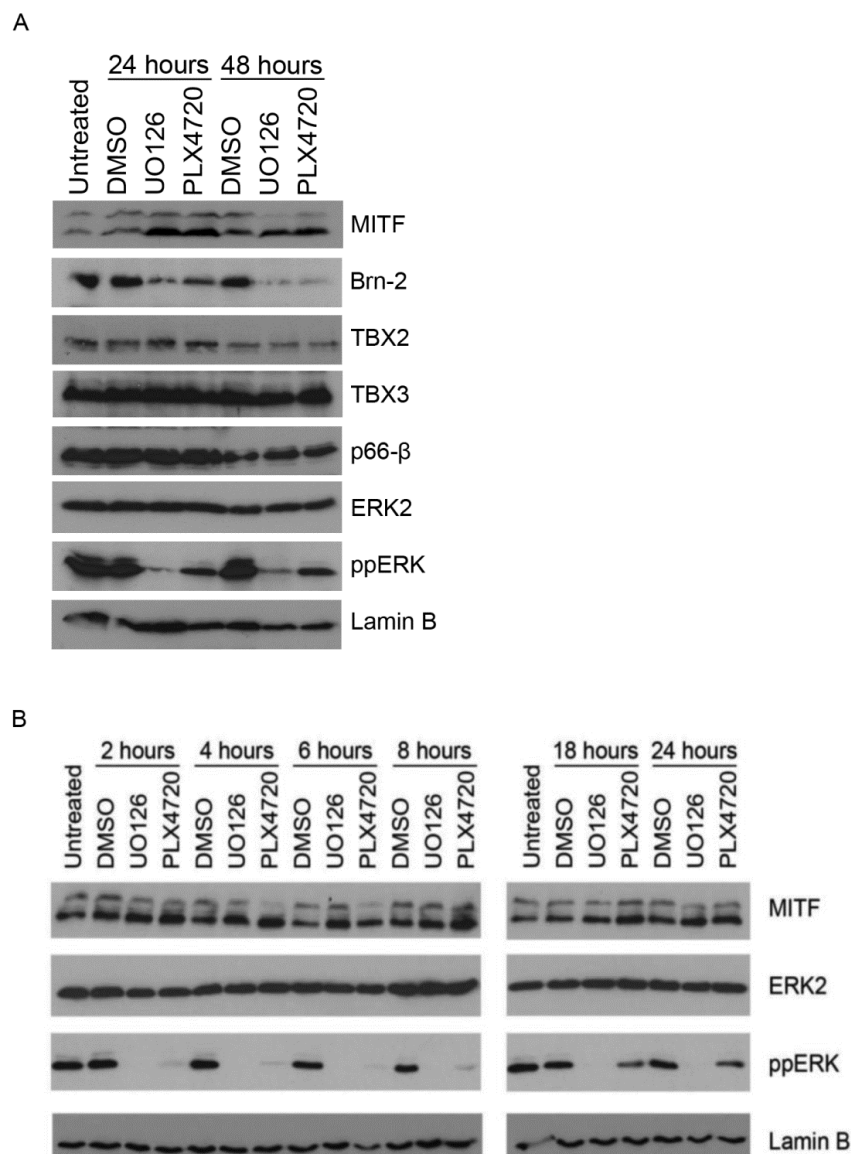
Figure 3.14. The effects of MAPK inhibition in 501mel cells. 501mel cells were either left untreated, or treated with DMSO, UO126 (20 μM) or PLX4720 (200 nM), for times as shown before whole cell extracts were subjected to Western blotting with the indicated antibodies.

cells treated with DMSO or drug at 48 hours. The transcriptional repressor p66-β, a member of the Mi-2/nucleosome remodelling and deacetylase (NuRD) complex (Brackertz et al., 2002), has been shown to interact with MITF and is required for *MITF* expression (Luis Sanchez, personal communication). As with TBX2, treatment with DMSO was sufficient to reduce p66-β levels after 48 hours; there was no further reduction with either inhibitor at this time point.

In an attempt to examine the functional effects of MAPK signalling on MITF acetylation in a fashion uncoupled from its phosphorylation status, 501mel cells were treated with UO126 and PLX4720 for shorter times, up to 24 hours (Figure 3.14B). Total ERK2 was unchanged throughout the experiment and phospho-ERK was strongly repressed after just 2 hours treatment with both inhibitors, again more efficiently by UO126, relative to the Lamin B loading control. After 18 and 24 hours, phospho-ERK in PLX4720-treated cells had recovered to almost the level in untreated cells, whereas the original level of inhibition was retained in UO126-treated cells. This could perhaps be due to PLX4720 being less stable in cell growth media than UO126, although there is no data available to confirm or refute this. MITF levels did not vary significantly throughout the experiment until 24 hours, when the lower band of MITF was enriched relative to the upper, as before. There was a slight decrease in hyper-phospho-MITF after 4 and 6 hours of PLX4720 treatment, but after 8 hours treatment the effect was reversed, so it is not thought to have been a significant effect.

3.3.1 Genome-wide binding of MITF in the presence and absence of PLX4720

Having determined that before 24 hours there is no major effect on MITF phosphorylation status, we wished to assess the effect of PLX4720 on MITF *in vivo*. To this end, 501mel cells stably expressing HA-Mitf (501.HA-Mitf) at a similar level to endogenous MITF (Figure 3.15A) were employed for chromatin

immunoprecipitation (ChIP) coupled to deep sequencing (ChIP-Seq) using an anti-HA antibody. The upper two bands detected by the anti-MITF antibody are HA-Mitf, while the lower two are endogenous MITF. Parental 501mel cells could not be used because there is no antibody available against endogenous MITF that works reliably for ChIP. 501.HA-Mitf cells were treated for 8 hours with 200 nM PLX4720 (Figure 3.15B), which achieved a strong reduction in phospho-ERK signal relative to ERK2. The anti-HA ChIP was performed in cells treated with ethanol (referred to as Mitf) or PLX4720 (Mitf.PLX4720 hereafter; Figure 3.15B), and in parental 501mel cells (501neg) to serve as a negative control population. DNA recovered from the ChIP was used for 50 bp single-end sequencing. The read libraries were filtered to remove PCR duplicates and randomly sampled to the size of the smallest library (Table 3.1).

To visualise HA-Mitf binding in these experiments, wiggle files were prepared and uploaded to UCSC. Binding to *Tyrosinase*, the prototypical MITF target gene that plays a key role in pigmentation, was observed in the presence and absence
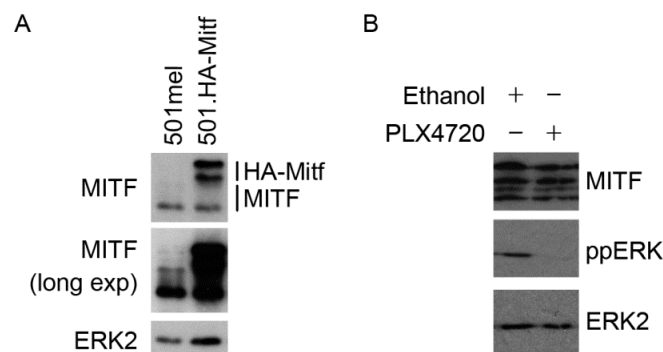
Figure 3.15. ChIP-Seq sample preparation. (A) Western blot comparing 501mel and 501.HA-Mitf cells. Endogenous MITF and HA-Mitf bands are indicated. (B) 501.HA-Mitf cells were treated or not with PLX4720 (200 nM) for 8 hours before being harvested for ChIP. A sample was taken for Western blotting with the indicated antibodies.

Table 3.1. ChIP-Seq sequencing statistics.

Sample	Aligned reads	Unique reads	Subsampled reads
501mel	35794085	29237190	29237190
Mitf	52228313	44724616	29237190
Mitf.PLX4720	48441638	39641393	29237190

of PLX4720 treatment (Figure 3.16A). The 501neg sample showed no enrichment at these sites, suggesting that the binding seen is specific to HA-Mitf. Three MITF binding sites have previously been described for *Tyrosinase*, two 5'-TCATGTGC-3' motifs in the core promoter approximately 100 bp apart, and an enhancer site 1.8 kb upstream from the transcription start site (TSS) that contains a 5'-TCATGTGA-3' motif. Additionally, binding was observed in intron 1 of *Tyrosinase*, containing a 5'-TCACATGG-3' motif, and two regions further upstream, located approximately -9 kb and -7 kb from the TSS. The -9kb region did not contain a canonical MITF binding site, while the -7 kb region contained a 5'-TCACATGA-3' motif. Binding to the -7 kb region was increased 2.5-fold in the presence of PLX4720, but the remaining four regions, including the three previously described sites, were unchanged. The fact that binding to *Tyrosinase* was largely unchanged was surprising as, given the earlier results, it was anticipated that enhanced binding should be observed on the 5'-TCATGTGA-3' -1.8 kb enhancer element. Therefore *PMEL*, a transmembrane glycoprotein required for melanosome biogenesis, was examined (Figure 3.16B). *PMEL* expression is controlled by MITF binding to an enhancer site in intron 1 of the gene, with a 5'-TCATGTA-3' motif, which also allows MITF to promote expression of *CDK2* (Du et al., 2003; Du et al., 2004). Binding at this location was observed, but was unchanged in the presence or absence of PLX4720.

MITF binding sites that have been previously described were not necessarily occupied in these experiments. For example, *BCL2*, whose function downstream of MITF has been suggested to be essential for survival of the melanocyte lineage (McGill et al., 2002), contains a 5'-CCATCTGC-3' MITF binding site in its promoter. This motif was a key part of the hypothesis surrounding differentiation versus non-differentiation target genes outlined earlier, but the promoter region was
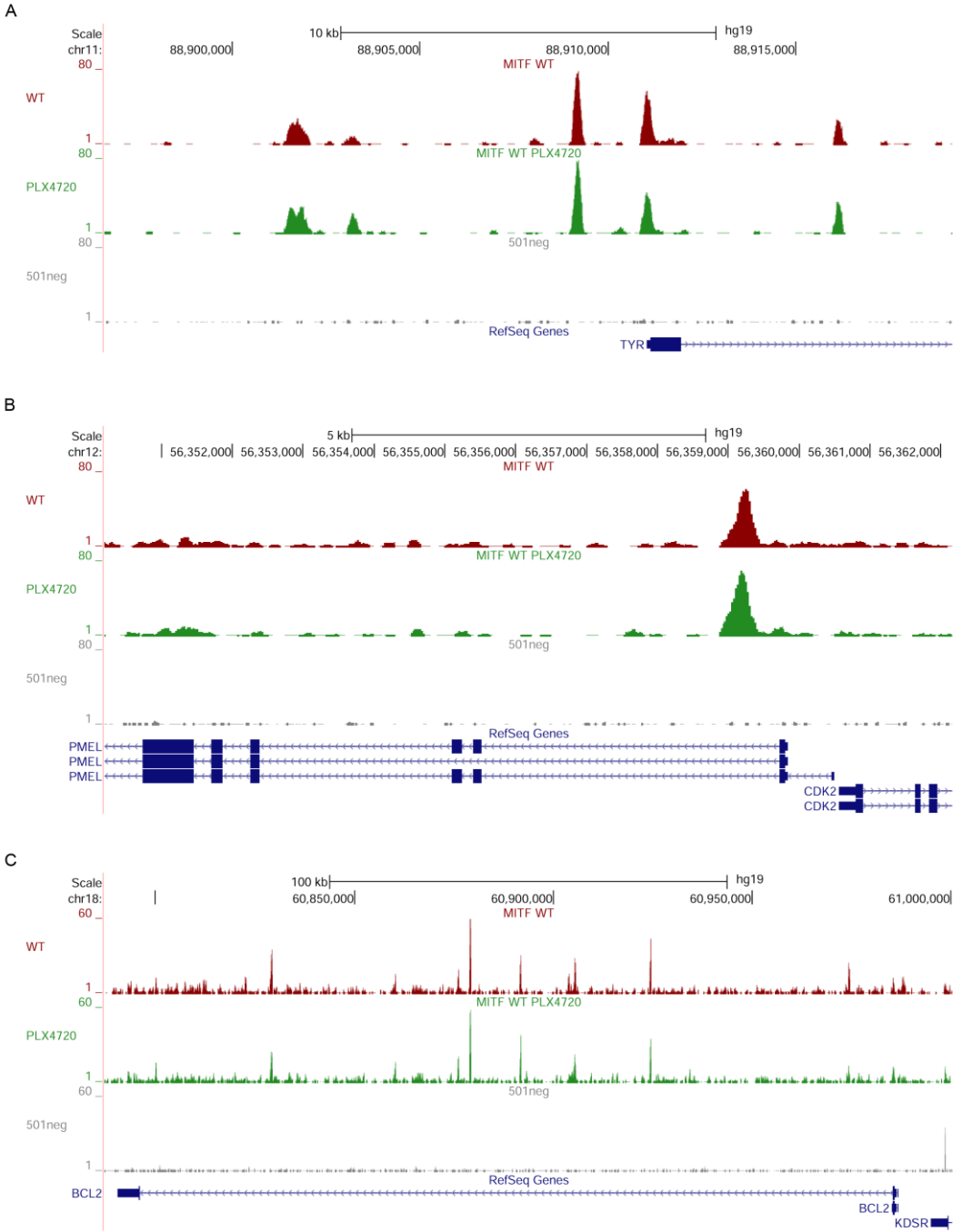
Figure 3.16. HA-Mitf ChIP-Seq from cells treated or not with PLX4720. UCSC screenshots of binding to (A) *Tyrosinase*, (B) *Pmel*, (C) *BCL2*. "WT" track is Mitf. "PLX4720" track is Mitf.PLX4720.

only occupied at a background level by either Mitf or Mitf.PLX4720 (Figure 3.16C). However, several intronic bound regions were observed, containing 5'-TCATGTGA-3' motifs, which suggests that MITF could occupy different sites, and likely regulate different targets, in different cell contexts. These regions were unchanged between Mitf and Mitf.PLX4720. Immediately upstream of the *BCL2* promoter is the terminus of the *KDSR* gene, encoding 3-ketodihydrosphingosine reductase. Within the 3'-untranslated region (3'-UTR) of *KDSR* was a region enriched in the 501neg sample (Figure 3.16C), showing the importance of controlling for non-specific binding in ChIP-Seq experiments.

To date, MITF has been shown to have the ability to bind the *MITF-M* promoter in complex with LEF-1 without being able to directly bind the *MITF-M* promoter (Saito et al., 2002; Yasumoto et al., 2002). On examination of *MITF*, a number of bound regions could be seen throughout the gene, including at -10 and -7.5 kb from the *MITF-M* TSS, and at a region in exon 2 of *MITF* (Figure 3.17A), the point from which all isoforms of *MITF* are common. LEF-1 binds the *MITF* promoter at 3 sites in between -200 and +1, and a minor enrichment could be seen here, relative to the background signal. In the exon 2 region and the -10 kb region, canonical MITF binding motifs were found, all containing a 5'-T on one strand of the motif. This finding suggests that, as well as indirectly influencing its own expression, MITF could also have the capacity to directly auto-regulate its expression, which has not been shown before.

Potential novel MITF target genes were also identified from this assay. Lysosome-associated membrane glycoprotein 1 (LAMP1) is required for fusion of lysosomes with phagosomes (Huynh et al., 2007), and *LAMP1* expression is often elevated in melanoma (Kuzbicki et al., 2006). A strong HA-Mitf peak of

approximately 3 times the size of the larger peaks in *Tyrosinase* was observed close to

the *LAMP1* TSS that was invariant between Mitf and Mitf.PLX4720 (Figure 3.17B),

and closer examination revealed two motifs, both 5'-TCACGTGA-3', located in the

5'-untranslated region (5'-UTR) and very close to the TSS.

This preliminary investigation suggested that there might not be large

differences induced in genome-wide HA-Mitf binding following treatment with

PLX4720, either in terms of quantitative changes in binding or the motifs being

targeted. To begin to characterise the binding observed, regions statistically enriched

Figure 3.17. HA-Mitf ChIP-Seq from cells treated or not with PLX4720.
UCSC screenshots of binding to (A) *MITF*, (B) *LAMP1*. "WT" track is Mitf.
"PLX4720" track is Mitf.PLX4720.

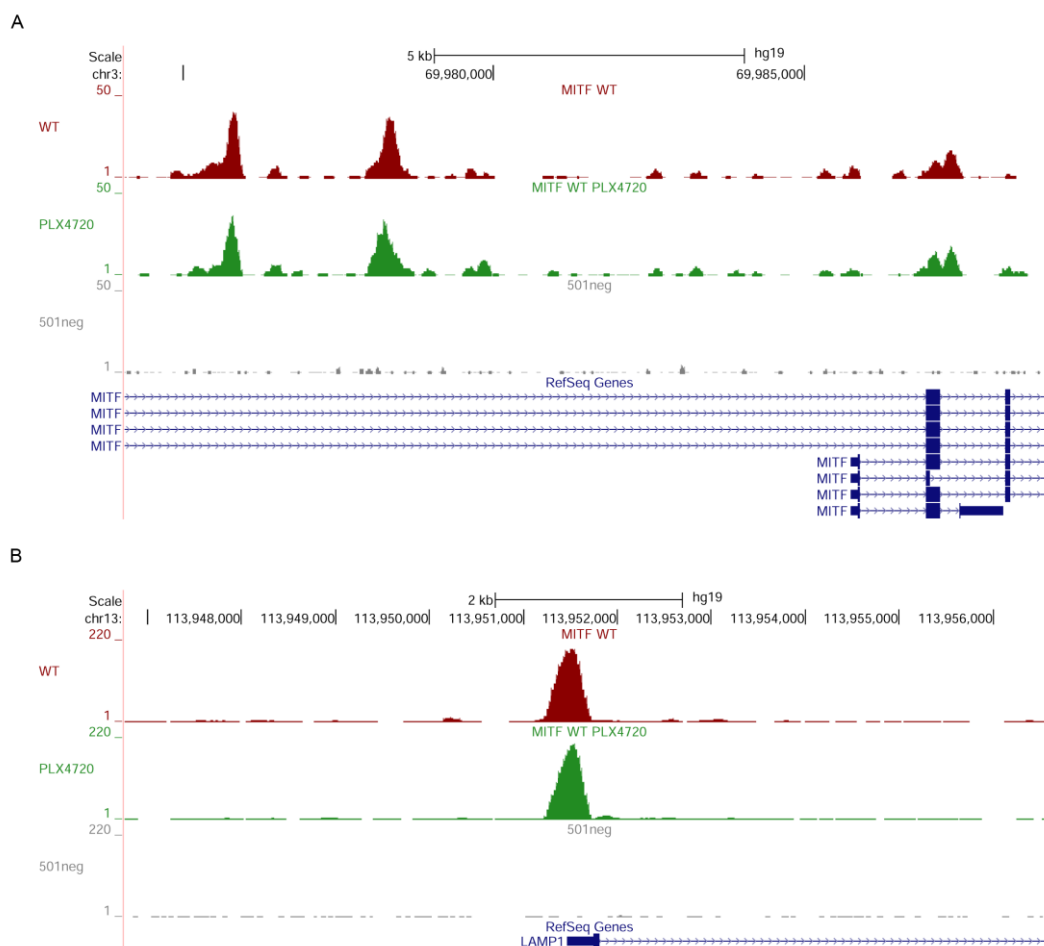for binding in the treated and untreated samples relative to the 501mel negative control, termed peaks, were determined, with a q-value cut-off of 10^{-10}. 41,070 Mitf and 38,467 Mitf.PLX4720 bound regions were identified, which had the same mean height (Table 3.2).

To characterise the genome-wide binding patterns in the Mitf and Mitf.PLX4720 samples, Mitf bound regions were ranked by binding density around the summit, with rank 1 being the lowest. Read density ±500 kb from the Mitf summit coordinates was calculated in 10 bp bins for both samples (Figure 3.18A). There appeared to be a good correlation between binding in Mitf and Mitf.PLX4720 samples around the summits of Mitf binding regions at all ranks, with a very similar reduction in binding intensity as peak rank increases. In a reverse calculation that ranked Mitf.PLX4720 summits, exactly the same effect could be seen (Figure 3.18B). These results suggested that binding between the two samples was very similar, and that regions bound by each sample tend to have a similar degree of binding. To probe this further, the raw genome-wide ChIP-Seq reads were compared using a pair-wise correlation calculation (Figure 3.18C). The genome was divided into 100 kb bins, and the median read counts compared in them for Mitf and Mitf.PLX4720. A strong correlation was found between Mitf and Mitf.PLX4720 (Pearson correlation coefficient R=0.99). When the analysis was restricted to windows defined by Mitf

Table 3.2. ChIP-Seq peak statistics

Sample	Mitf	Mitf.PLX4720
MACS2 binding regions	41,070	38,467
Mean binding region height	40	40
Uniquely bound regions	7,443	4,841
Peaks (>40)	14,362	13,105
Unique filtered peaks	2,511 (34*)	1,246 (6*)
Gene-associated filtered peaks	9,037	8,322
Filtered peak-associated genes	5,559	5,244
Conserved with Strub et al., 2011	3,055	3,099
Unique genes	650	337

* Numbers in brackets represent the unique peaks when peaks > 40 in one sample were intersected with all binding regions in the other.
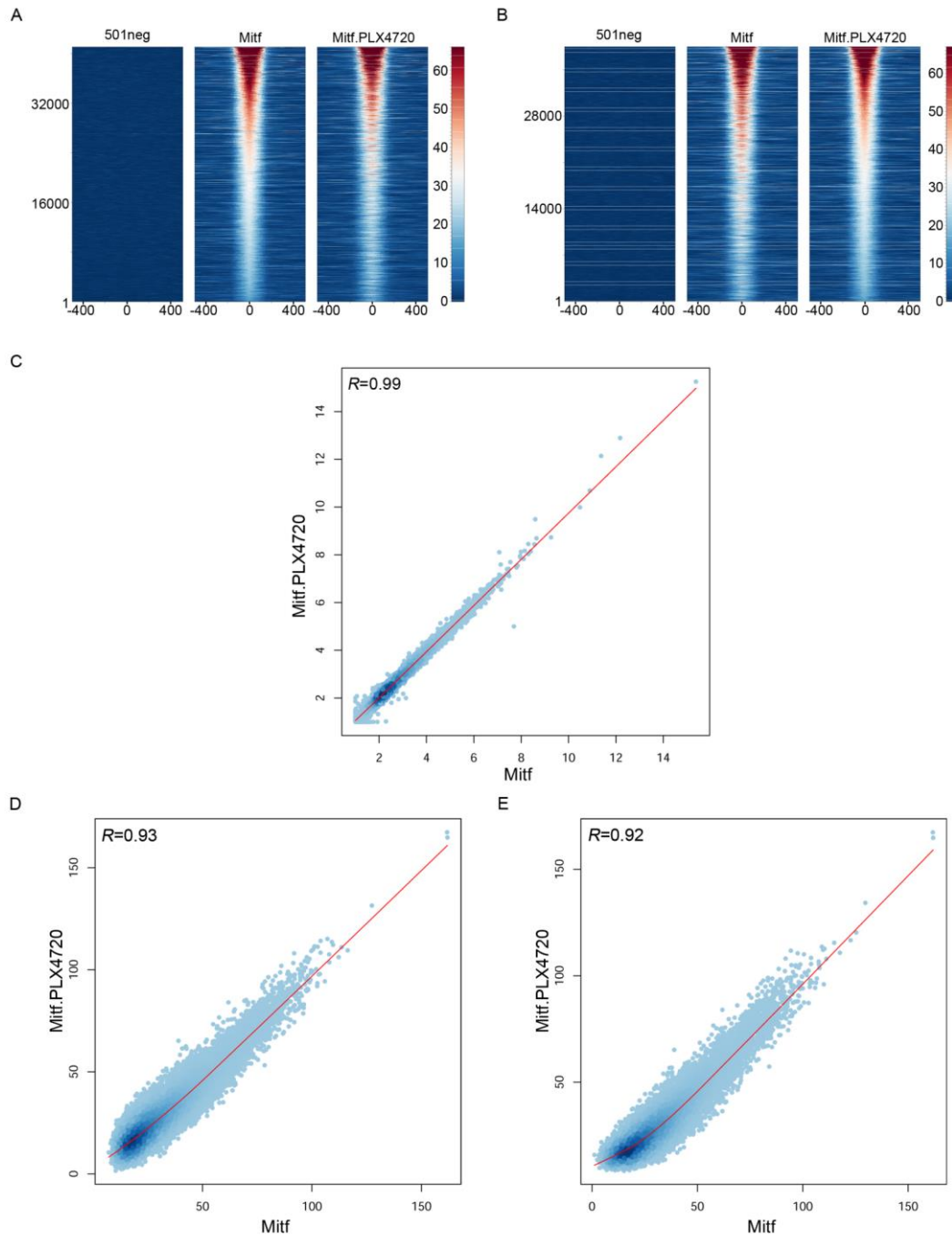
Figure 3.18. Genome-wide ChIP-Seq sample comparison. (A) Mitf peaks were ranked based on binding strength (y-axis; rank 1 = weakest) and raw binding density profiled ± 500 bp from the summit for 501neg, Mitf and Mitf.PLX4720 (x-axis). Density was coloured from blue (0, lowest) to red (66, highest), scale bar shown at right. (B) As for (A) but using Mitf.PLX4720 peaks as a starting point. (C) Pair-wise genome-wide correlation between Mitf and Mitf.PLX4720 based on the median read density in 100 kb windows. Pearson correlation coefficient is shown top left. (D) As in (C) but restricted to bases in Mitf peaks rather than binning the entire genome. (E) As in (D) but restricted to bases in Mitf.PLX4720 peaks.

bound regions, a very strong correlation was again seen for binding density in the presence and absence of PLX4720 (Pearson correlation coefficient R=0.93; Figure 3.18D). If Mitf.PLX4720 peaks were used to score the samples, the Pearson correlation was similar (R=0.92; Figure 3.18E). The difference in correlation coefficients between these analyses likely arises because the vast majority of the genome is excluded in the peak-based analysis, permitting small local variations to have a larger effect. The different scales arise because the majority of bases in each 100 kb will be weakly occupied, while peak-covered bases by their nature are more highly occupied. Together, this data suggests that there was not a large change in HA-Mitf binding induced following treatment with PLX4720.

Peak height was calculated using the "pileup" option of MACS2, which counts reads intersecting the coordinates assigned to the summit. Regions were divided into bins based on peak height in 10 read increments. The overall distribution of peak heights was very similar between these regions, with the most populous bin containing peaks between 20 and 30 reads in height (Figure 3.19A). There were slightly more Mitf regions in each bin than Mitf.PLX4720, reflecting the modest difference in peak count between the samples. No peaks were detected in either sample with height less than 10.

The binding regions in each sample were assigned to different categories to ascertain where they were localised genome-wide (Figure 3.19B). Mitf and Mitf.PLX4720 peaks were almost identically distributed, with around 40% of peaks not occurring within 10 kb of the start or end of a RefSeq gene. 36% of peaks were intronic, while 13% were located up to 10 kb upstream of the TSS and 6% lay within 10 kb downstream of the transcription termination site (TTS). The remaining peaks were distributed between exons (2%), the 5'-UTR (2%), and the 3'-UTR (1%). A

surprising feature of this analysis was the large proportion of intronic peaks. However, it is likely to be true as repetition of the analysis with a different software package returned very similar proportions of intronic peaks (CisGenome; data not shown). The intronic peaks could present potential enhancers, and predominantly intronic/intergenic occupancy has previously been observed in other bHLH proteins, for example MYOD (Fong et al., 2012).
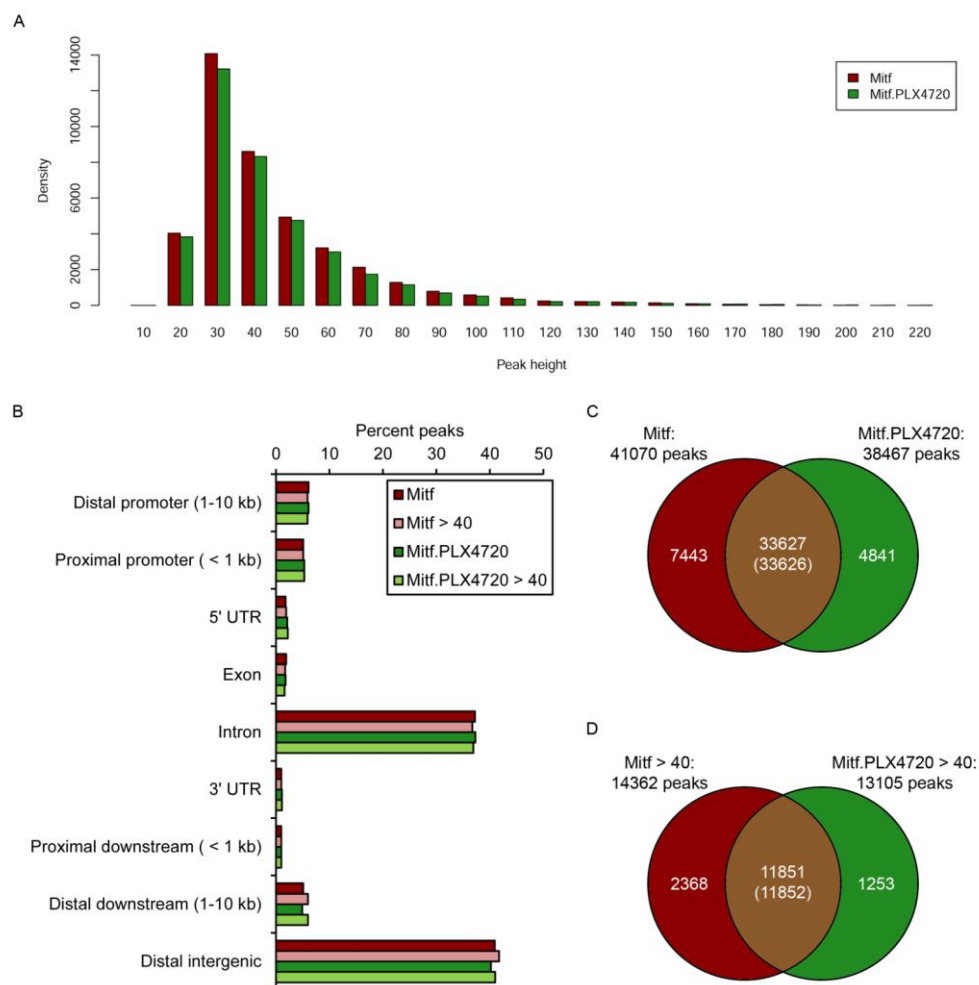
Figure 3.19. Mitf and Mitf.PLX4720 peaks are very similar. (A) Mitf and Mitf.PLX4720 peaks were divided into 22 bins of equal width based on increasing peak height, and histograms plotted. (B) The distribution of all peaks and peaks with height > 40 for Mitf and Mitf.PLX4720 was analysed. (C) Venn diagram showing the proportion of common and unique peaks between all Mitf and Mitf.PLX4720 peaks. In the centre, the number outside the brackets denotes the number of Mitf peaks, and the number inside the brackets denotes the number of Mitf.PLX4720 peaks. (D) As in (C) but using peaks with height > 40 as a starting

In Mitf and Mitf.PLX4720, more bound regions were identified than there are genes in the genome. Therefore, a conservative height filter of 40 reads was applied to each sample, to leave only the most significant peaks. The cut-off is likely to be set too high to catch all genuine binding events, but will minimise the false-positive rate and hence the noise in the analysis. Known peaks in genes such as *Tyrosinase* were retained as was the novel binding site at *LAMP1*. Not all the *MITF-M* or *BCL2* bound regions were recovered. Post-filtering, 14,362 Mitf and 13,105 Mitf.PLX4720 peaks were retained for further analysis. Removal of the smaller peaks from the sample made very little difference to the distribution of peaks (Figure 3.19B), although there was a minor increase in binding in distal downstream and intergenic sites at the expense of intronic binding.

Next, the peak coordinates of Mitf and Mitf.PLX4720 peaks were intersected (Figure 3.19C, Table 3.2). 33,627 Mitf peaks overlapped with 33,626 Mitf.PLX4720 peaks, giving a conservation rate of 82% and 87% respectively between the samples. Among peaks with height greater than 40, 11,851 Mitf peaks overlapped with 11,852 Mitf.PLX4720 peaks (Figure 3.19D, Table 3.2), at a conservation rate of 82% and 90% respectively. Because peaks could change in height between the samples and span the 40-read cut-off, peaks higher than 40 from one sample were intersected with all peaks from the other. In this more stringent identification of unique filtered peaks, only 34 Mitf peaks and 6 Mitf.PLX4720 peaks were unique, further adding to the idea that the binding profile of HA-Mitf in the presence and absence of PLX4720 is very similar. To find out the gene occupancy of Mitf and Mitf.PLX4720, peaks with height greater than 40 were associated with a gene if they lay within 20 kb of the gene body (Table 3.2). Mitf was associated with 5,559 genes, of which 650 were uniquely occupied using the criteria used in Figure 3.19D, while Mitf.PLX4720 was associated

with 5,244 genes, of which 337 were unique. 3,055 of the 5,559 Mitf-occupied genes and 3,099 of the 5,244 Mitf.PLX4720-occupied genes were shared with the previously published MITF ChIP-Seq dataset (Strub et al., 2011).

Because the genome-wide binding between the samples appeared so similar (Figure 3.18), boxplots were drawn of the total, unique, and common sets of peaks of any height, from both samples, to see if there was a peak height difference among them (Figure 3.20). It revealed that, for each comparison, Mitf and Mitf.PLX4720 were very similar, and that the unique peaks were clustered toward the small end of the peak scale. The maximum peak height among Mitf unique peaks was 51, while for Mitf.PLX4720 it was just 47. This suggests that the unique peaks between the samples are perhaps unlikely to make a major contribution to the effect of the presence or absence of PLX4720 on HA-Mitf binding in this experiment.
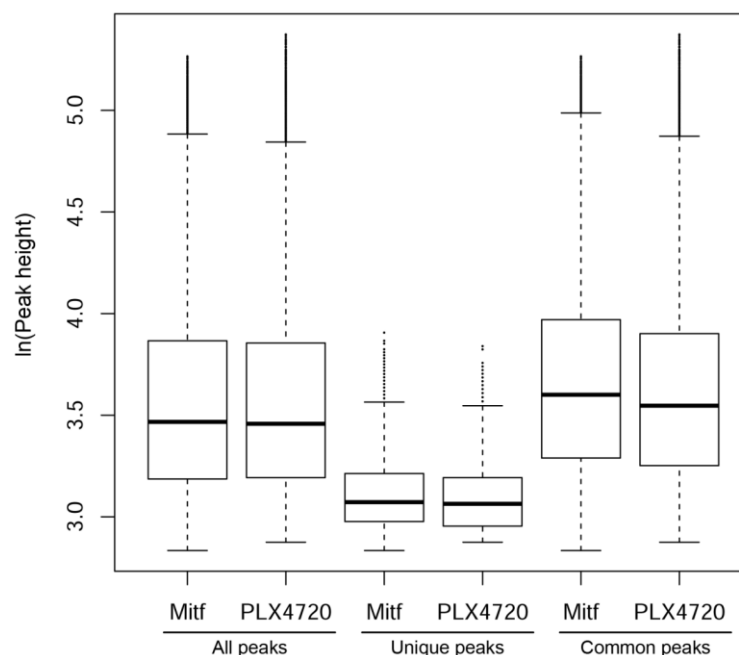
Figure 3.20. Unique Mitf and Mitf.PLX4720 peaks are small. Boxplots of peak heights for all, unique and common peaks for Mitf and Mitf.PLX4720, as shown. The peak height scale is natural-log transformed to enhance clarity. The box shows the interquartile range (IQR), with the median value the line transecting the box. Values falling outside the IQR but within the range of IQR ± 1.5×IQR are shown by the dashed line whisker. Remaining values are outliers represented by dots.

In both samples, peaks that were either filtered or unfiltered by height had shown similar proportions of binding less than 1 kb upstream of the TSS or within the 5'-UTR. To examine this more closely, histograms were plotted showing the summit density of all Mitf and Mitf.PLX4720 peaks with summits lying in a 2 kb window centred at the TSS (Figure 3.21A). Both samples had maximal occupancy in the first 100 bp upstream of the TSS, followed closely by the first 100 bp downstream of the TSS. In bins further away from the TSS, the summit density decreased quickly. The peaks higher than 40, the enrichment at the TSS was even more pronounced (Figure 3.21B). The first 100 bp upstream of the TSS contained by far the most peak summits, again followed by the first 100 bp downstream of the TSS. This indicated that, like many transcription factors, at a genome-wide level MITF tends to be located very close to the TSS of genes that it occupies.

Earlier, it was hypothesised that PLX4720 treatment should promote binding to E/M-boxes that are flanked by 5'-T residues. However, on visual inspection of the published binding sites used to form this hypothesis, binding was unchanged in the Mitf and Mitf.PLX4720 ChIP-Seq samples. To assess whether this hypothesis was likely to be true or not, the top 900 peaks in each sample were used to predict, *de novo*, the consensus motif occupied by HA-Mitf in each case. For both Mitf and Mitf.PLX4720, it was virtually identical, centred on an invariant core of 5'-TCACGTGA-3' for each (Figure 3.21C, D), indicating that, for the most significant sites occupied, there is very little difference in motif occupancy in these samples. The uniquely occupied peaks in each sample were clustered at the small end of the peak height spectrum. To ask whether these peaks discriminated better than the total sets of peaks, the *de novo* analysis was repeated (Figure 3.21 E,F). The motif was very similar for both, centred on 5'-CA[C/T]GTG-3', with the only difference being a
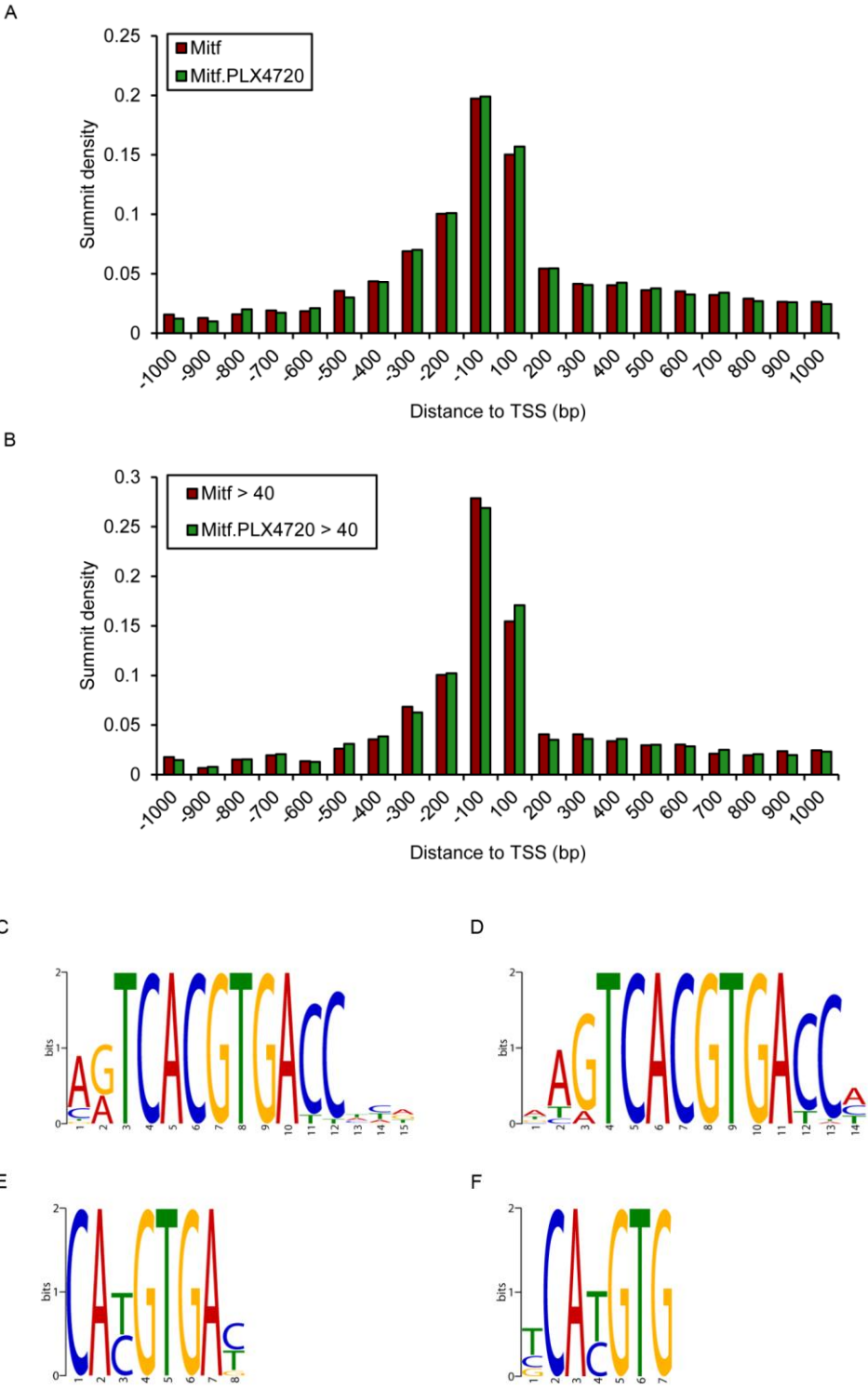
Figure 3.21. Mitf and Mitf.PLX4720 are enriched at the TSS and have a similar *de novo* predicted motif. (A) Summits of all Mitf and Mitf.PLX4720 peaks within 1 kb of a TSS were assigned to bins based on the distance to the TSS. (B) As (A) but using peaks higher than 40 as input. (C) *De novo* motif prediction was performed on the 60 bp surrounding the summit of the top 900 Mitf peaks. (D) As (C) but using the top 900 Mitf.PLX4720 peaks. (E),(F) As (C) but using the top 900 unique Mitf (E) and Mitf.PLX4720 (F) peaks.

requirement for 3'-A in the Mitf peaks. However, given the lowly stature of the unique peaks, it is hard to assign a functional consequence of this apparent difference.

To extend the motif occupancy analysis to all the peaks that were bound in each sample, all of the 5'-CATGTG-3' and 5'-CACGTG-3' motifs in the genome were identified. From this list of coordinates the motifs that fell within Mitf and Mitf.PLX4720 peaks were extracted. A total of 51,872 motifs were identified in 35,541 Mitf peaks, while 48,115 motifs were identified in 33,001 Mitf.PLX4720 peaks. For peaks whose height exceeded 40, Mitf occupied 21,407 motifs in 13,637 peaks, while Mitf.PLX4720 occupied 19,528 motifs in 12,330 peaks. On plotting the percentage of total, common and unique peaks in either the complete sets of peaks or peaks higher than 40, it was clear that the vast majority of peaks contained at least 1 motif (Figure 3.22A). The percentage of unique Mitf.PLX4720 peaks containing a motif was approximately 10% lower than in the other sets of peaks at each height cut-off, while the number of peaks containing motifs was 10-15% greater for peaks higher than 40 than for the set of total peaks. In contrast, in a set of control peaks matched for length and distance from the TSS, only around 20% peaks contained a 5'-CA[C/T]GTG-3' motif, indicating that MITF peaks are strongly enriched in relation to the genome for these elements.

The relative heights of the subsets of total, common, and unique peaks with and without motifs were analysed next (Figure 3.22B). Among each set of Mitf peaks examined, peaks without motifs were clustered in the smaller bins, being virtually absent once peak height exceeded 60, while peaks containing motifs persisted to the highest bins. The distribution of peak heights in the same analysis for Mitf.PLX4720 was almost identical to that of Mitf (Figure 3.22C), further suggesting that there is little difference in motif binding between these samples. Because there was a small,

yet appreciable, percentage of peaks lacking a 5'-CA[C/T]GTG-3' motif, it was possible that either HA-Mitf was binding to degenerate motifs or as a cofactor for another transcription factor. To investigate this, the 60 bp around the summits of the most significant peaks lacking motifs was used for *de novo* consensus motif
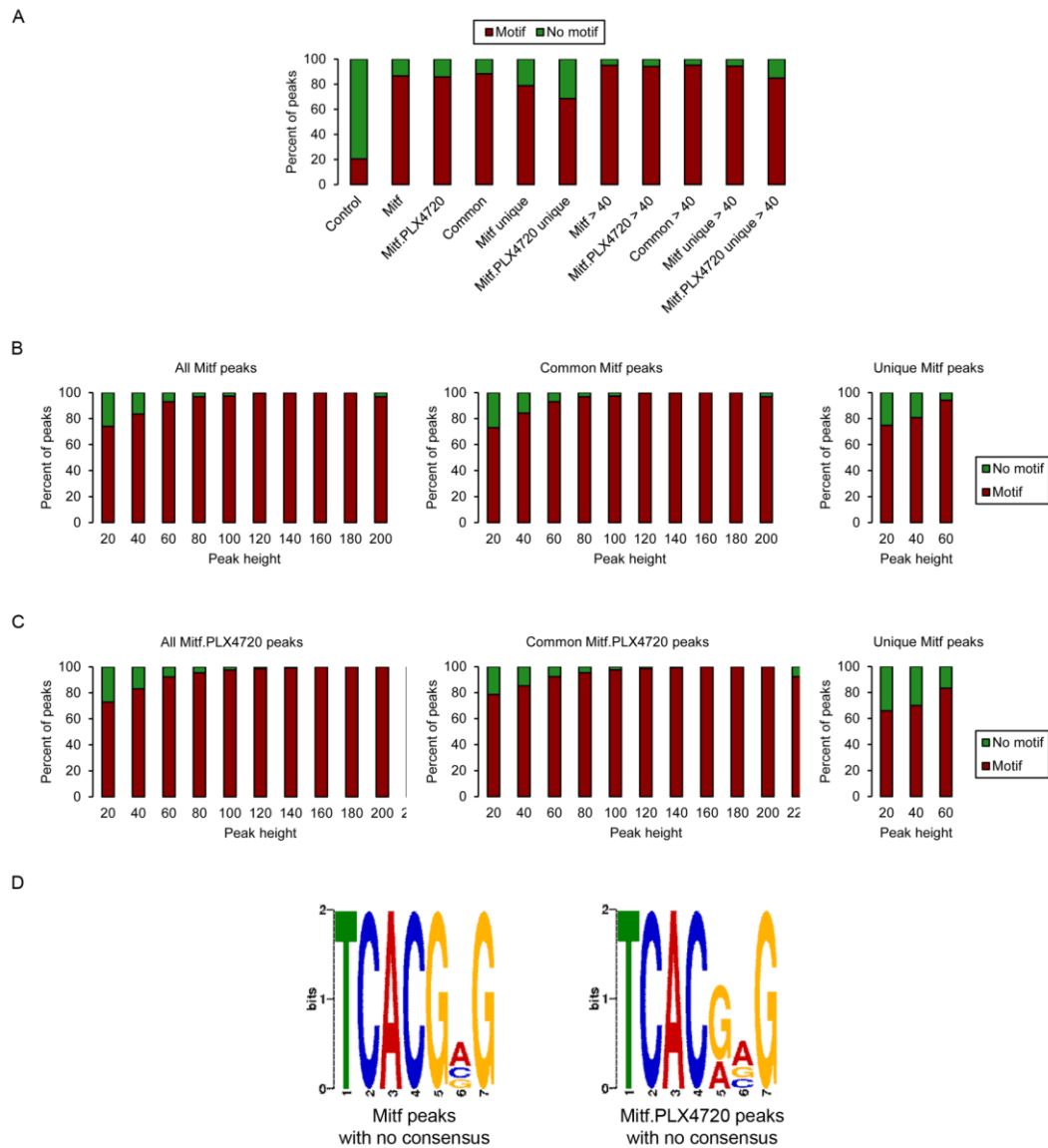
Figure 3.22. Motif preferences in different height Mitf and Mitf.PLX4720 peaks. (A) The percentage of Mitf and Mitf.PLX4720 peaks at either any height or height > 40 with or without a 5'-CA[C/T]GTG-3' motif was counted for the total, common, and unique peaks. Values for a random matched control set of peaks are also shown. (B) Charts of Mitf peaks (all, left; common with Mitf.PLX4720, centre; or unique, left) at any height with or without a 5'-CA[C/T]GTG-3' motif. Bars are presented as the percentage of peaks at each height with or without a motif. (C) As in (B) but analysing Mitf.PLX4720 peaks.

prediction (Figure 3.22D). As shown, the consensus for both Mitf and Mitf.PLX4720 was a very similar near E-box (5'-CANNTG-3'), suggesting that these peaks arise as a result of HA-Mitf binding to degenerate motifs.

Next, the precise motifs bound by Mitf and Mitf.PLX4720 were analysed. By chance, a randomly chosen hexameric sequence would be expected to arise every 4096 bp. The human genome contains approximately 3 Gbp of DNA, meaning that ~750,000 instances of a random, unconstrained hexameric sequence such as 5'-CACGTG-3' would be expected to occur in the genome. However, 3-fold fewer (276,439) instances were identified (Figure 3.23A). For 5'-CATGTG-3' motifs on the bottom strand, the top strand will read 5'-CACATG-3', and, for this hexamer where the middle two bases are constrained to a choice of two, the motif would be expected to arise every 1,024 bp, or ~3,000,000 times throughout the genome. Only two thirds of this number (2,175,744) was found, so both motifs are relatively under-represented according to random chance. It is possible that sequences with the potential to be bound by transcription factors have been evolutionarily selected against in attempt to ward off promiscuous binding events. The distribution of different flanking sequences among these motifs was very similar. Approximately 6% of both 5'-CATGTG-3' and 5'-CACGTG-3' motifs were flanked by T on both strands, and around 30% by T on one strand with the remainder containing no 5'-T (Figure 3.23A).

Next, the relative enrichment of each motif relative to the frequency of that motif in the genome was assessed for Mitf and Mitf.PLX4720 peaks (Figure 3.23B). The overall distribution between Mitf and Mitf.PLX4720 motif preference in all and common peaks was very similar. In keeping with the consensus motif predictions (Figure 3.21), 5'-TCACGTGA-3' was the most strongly enriched; 29% are occupied by Mitf, suggesting that Mitf has a very high affinity for this motif *in vivo*. 5'-

A
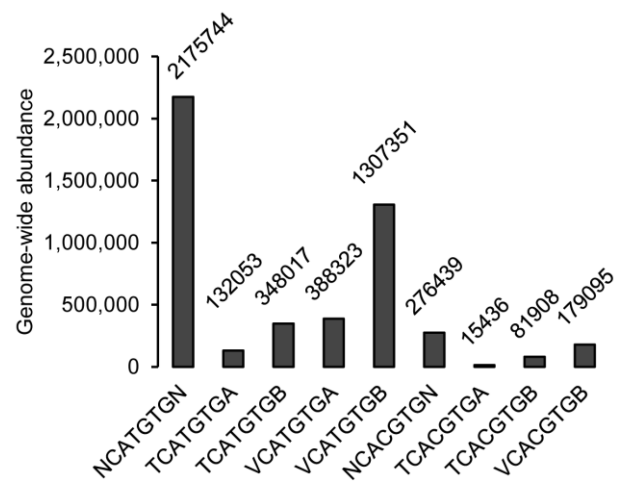
B
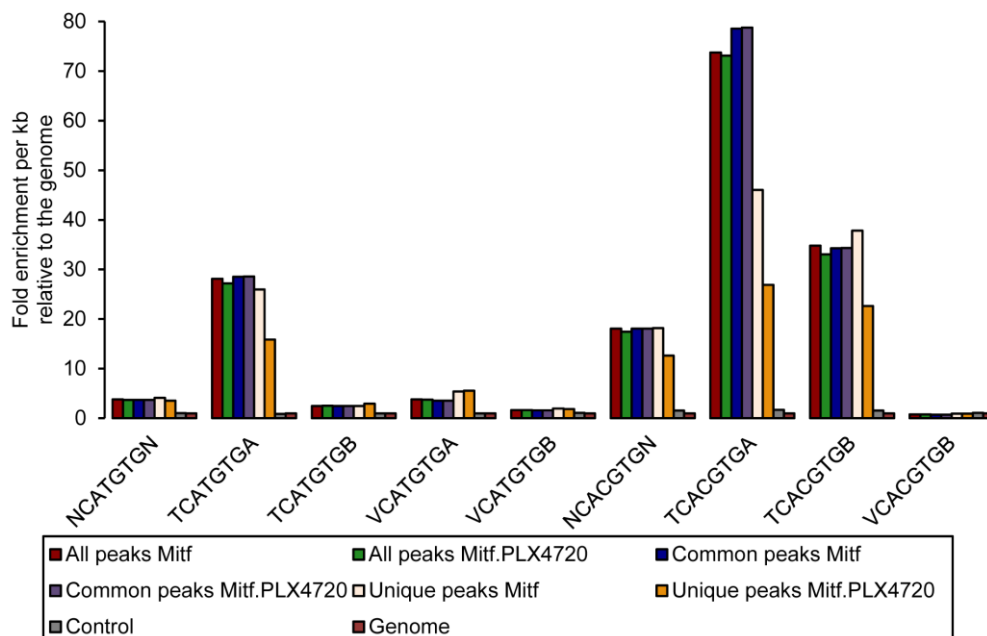
Figure 3.23. Comparing relative motif occupancy by Mitf and Mitf.PLX4720.
(A) Genome-wide occurrences of the indicated motifs were counted (N=any base;
V=A, C, or G; B=T, C, or G). Note that every motif is counted twice: once as
N…N, and once with its specific flanking bases. (B) The instances of each motif
per kb of peak sequence is expressed relative to the occurrences of that motif per
kb of the genome for Mitf and Mitf.PLX4720 peaks of any height (total, unique
and common), as well as for a set of matched control peaks (based on all Mitf
peaks; similar enrichments were obtained by matching to other sets of peaks, not
shown).

TCATGTGA-3' and 5'-TCACGTGB-3' were similarly enriched over the genomic background in Mitf and Mitf.PLX4720 all and common peaks; these three motifs together comprise 58% of motifs occupied by HA-Mitf. The other combinations of flanking sequences are not enriched more frequently than would be expected by random chance.

The unique peaks contained slightly different ratios of motifs to the total sets. 5'-TCACGTG-3' was most affected, with its enrichment in Mitf and Mitf.PLX4720 reduced by 30-fold and 50-fold respectively compared to the total set of peaks. 5'-TCATGTG-A-3' and 5'-TCACGTGB-3' were unchanged in the Mitf unique peaks, while their enrichment was reduced in the Mitf.PLX4720 peaks.

Thus, contrary to the initial hypothesis that treatment with PLX4720 should redirect HA-Mitf to motifs containing 5'-T, this data suggests the opposite might be the case, as 5'-TCA[C/T]GTGA-3' and 5'-TCACGTGB-3' are less enriched among peaks uniquely bound by Mitf.PLX4720. It is hard to assess the significance of this finding, however, because the difference is very slight and apparent only in the peaks unique to each sample. It could therefore simply reflect a decrease in binding to these motifs in smaller peaks.

Because the unique peaks were so small, it was anticipated that the overall biological roles of genes associated with the Mitf and Mitf.PLX4720 samples should be the same. In two cases, a gene was associated with an Mitf peak but not an Mitf.PLX4720 peak; the difference in the peak-associated genes for the samples is 315, while the difference in uniquely occupied genes between the samples is 313. Thus the impact of a peak just falling within the 20 kb cut-off for association with a gene in one sample but not in the other will be minimal in relation to the number of genes associated with each sample.

To find out the biological roles of the genes occupied by Mitf and Mitf.PLX4720, the 1,000 most significantly occupied genes were analysed for enriched Kyoto Encyclopedia of Genes and Genomes (KEGG) pathways and gene ontology (GO) terms (Figure 3.24). The identified regulated pathways and terms generally had at least 10% of their number bound in the sample. There were small differences in the pathways and terms enriched in the samples. The actin cytoskeleton KEGG pathway was enriched in Mitf but not Mitf.PLX4720. However, actin binding was enriched in the GO analysis for both samples, so it could be that the cytoskeleton
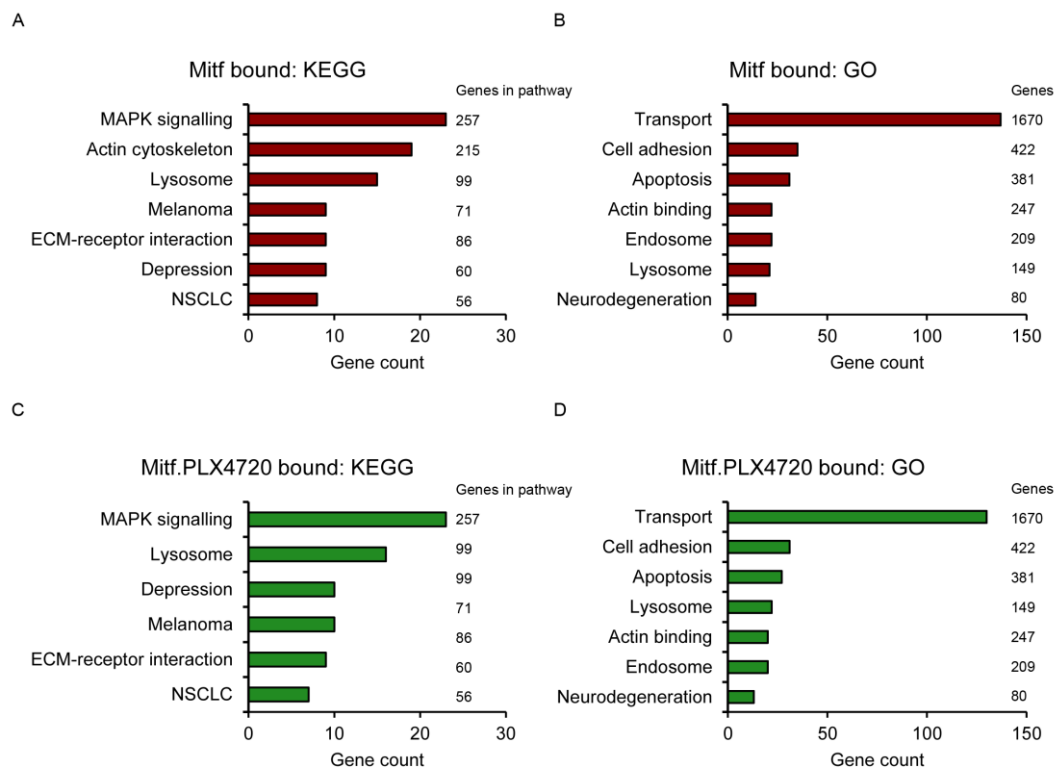
Figure 3.24. Gene ontology analysis of Mitf and Mitf.PLX4720 binding. Bars on Mitf graphs are red; bars on Mitf.PLX4720 graphs are green. The top 1,000 Mitf and Mitf.PLX4720 peaks were analysed for significantly enriched Kyoto Encyclopedia of Genes and Genomes (KEGG) pathways or Gene Ontology (GO) terms as shown. All terms reported had p-value < 0.1. ECM: extra-cellular matrix; NSCLC: non-small-cell lung cancer. Numbers at the end of each bar represent the total gene count in the KEGG pathway or GO term.

pathway just failed to make the cut-off for the KEGG analysis. Indeed, analysis of a longer list of Mitf.PLX4720 genes did enrich the actin cytoskeleton (not shown).

Vesicular terms (endosomes and lysosomes) were enriched in both samples. It was interesting that lysosomal-regulating genes feature so prominently among the genes bound by Mitf, because TFEB, another member of the MiT subfamily of bHLH-LZ factors, has been identified as the master regulator of the lysosomal pathway (Sardiello et al., 2009). MITF and TFEB can heterodimerise (Hemesath et al., 1994), and they bind to exactly the same sequences *in vitro* and *in vivo* as one another (Sardiello et al., 2009; Figure 3.21C). This suggests, for the first time, that MITF could be a major regulator of the lysosomal pathway, which is used to break down waste materials in the cell. Little is known about the role of lysosomes in melanoma, although some lysosomal genes such as *LAMP1* are overexpressed in melanoma (Kuzbicki et al., 2006). Melanosomes are lysosome-related organelles that are derived from the endosomal membrane and can fuse with lysosomes (Raposo and Marks, 2007). In addition, a number of lysosomal-storage diseases, such as Hermansky-Pudlak Syndrome, are characterised by abnormal pigmentation (Huizing et al., 2000). It would not therefore be a surprise to find that MITF is able to control the genes driving the lysosomal pathway. HA-Mitf was also bound to a large number of transport-related genes that play a role in a wide range of processes, including metabolite transport in and out of the cell and shuttling between different organelles. Given the pivotal role of MITF throughout development, it is not surprising that nutrient processing would be regulated by MITF.

3.3.2 Identification of MITF- and PLX4720-regulated genes by RNA-Seq

The presence or absence of a binding site does not necessarily indicate that a gene is regulated by MITF, just that it has the potential to be. To determine which

genes were MITF-regulated in 501mel cells, MITF was knocked down using siRNA, with siRNA against *Luciferase* (siCTR) as a control, and cells were harvested after 72 hours (Figure 3.25A). A good knock-down was achieved, and paired end RNA deep sequencing (RNA-Seq) was performed on RNA extracted from 501mel cells transfected with each siRNA as well as untransfected 501mel negative control cells. To compare the gene expression levels in these samples, correlation analysis was performed. A very strong correlation between all three samples was observed (501mel vs siCTR Pearson correlation coefficient R=0.96 [Figure 3.25B], 501mel vs siMITF Pearson correlation coefficient R=0.96 [Figure 3.25C], siCTR vs siMITF Pearson correlation coefficient R=0.97 [Figure 3.25D]), indicating that, for most genes, the expression level was very similar. The linear runs of points in the bottom left corner represent the genes that were zero in one sample but with a low non-zero RPKM in the other.

To directly compare the global expression levels in the three samples, the $\log_2$ ratio between two samples was plotted against the $\log_2$ RPKM of one of the samples as shown (siCTR vs 501mel [Figure 3.25D], siMITF vs 501mel [Figure 3.25E], siMITF vs siCTR [Figure 3.25F]). As in the previous set of graphs, the linear runs of points are the genes that were zero in one sample but with a low non-zero RPKM in the other. The graphs revealed that a modest number of genes were likely differentially expressed, but that the majority of the genes in the genome were non-regulated by either siRNA.

Mitf peak height was plotted against expression level in 501mel cells for expressed peak-associated genes from the Mitf ChIP-Seq sample (Figure 3.26A), revealing a wide spread of expression values for a given peak height. A weak Pearson correlation coefficient (R=0.0187) was calculated, suggesting that the height of an
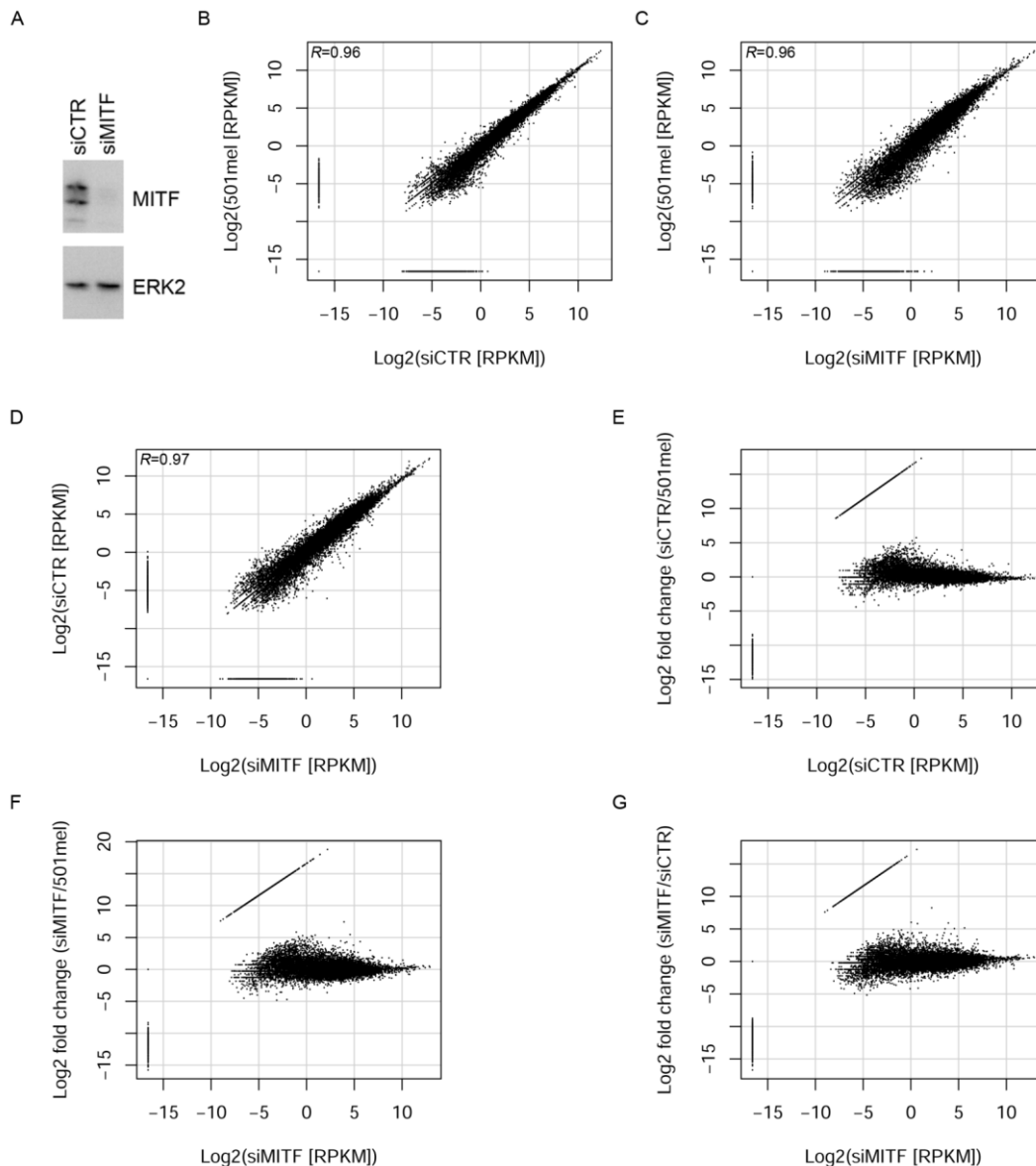
Figure 3.25. siMITF RNA-Seq in 501mel cells. (A) 501mel cells transfected for 72 hours with siCTR or siMITF were analysed by Western blotting with the indicated antibodies. (B) Log-transformed RPKM values comparing siCTR and 501mel RNA-Seq samples. Pearson correlation coefficient is shown top-left. All RPKM were increased by 0.00001 to allow comparisons for genes where one value was zero. (C) As (B) but comparing siMITF and 501mel. (D) As in (B) but comparing siMITF and siCTR. (E) Log-transformed plot showing the fold-change between siCTR and 501mel RPKM values versus siCTR PRKM. (F) As (E) but comparing siMITF and 501mel. (G) As (E) but comparing siMITF and siCTR.

Mitf peak at a gene does not correlate with the expression level of that gene. However, it appeared that there was a general association between the presence of a peak and the expression level of a gene.

On analysis of differentially expressed genes between the siCTR and siMITF samples, 809 RefSeq genes were down-regulated by siMITF of which 291 were Mitf-bound, and 665 genes were up-regulated of which 205 were occupied by Mitf peaks higher than 40 (Figure 3.26B), indicating that the many of de-regulated genes on MITF knockdown can also be bound by MITF. While 35% of regulated genes were occupied by HA-Mitf with peaks taller than 40, only 25% of non-regulated genes were occupied by HA-Mitf, suggesting that HA-Mitf-occupancy is more associated with mis-regulation than a lack of mis-regulation. It would be expected that, were the peak height cut-off to be reduced, the number of directly bound and regulated genes should increase. Indeed, when this analysis was conducted with all the Mitf peaks (data not shown), 637 down-regulated genes were occupied, and 518 down-regulated genes were occupied, suggesting that MITF could potentially directly regulate most of the genes that are de-regulated following the siRNA transfection. The total number of de-regulated genes, however, is still small compared with the number of occupied genes. It is possible that some genes are occupied with an occupancy that has little functional consequence, or that some could be regulated under different conditions that are not mimicked by MITF-depletion.

To find out the biological functions of the genes de-regulated by MITF-depletion, KEGG and GO analysis was carried out, identifying pathways and terms with more than 5-10% of their constituent members subject to regulation. Among down-regulated genes (Figure 3.26C, D), lysosomes were a prevalent KEGG pathway, suggesting that MITF does indeed regulate lysosome biogenesis and
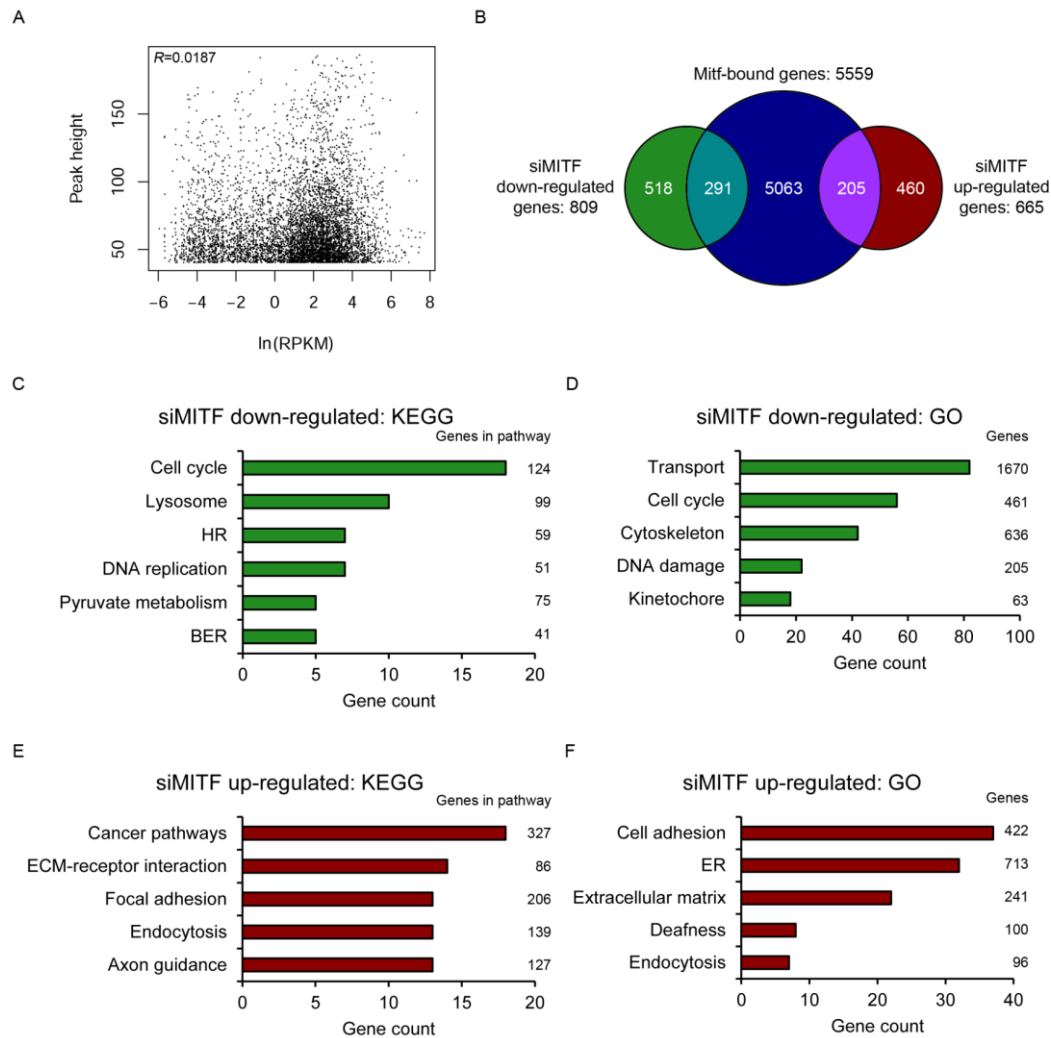
Figure 3.26. Analysis of MITF-regulated genes. (A) Scatter plot of Mitf peak height gene-associated peaks against the natural-logarithm of the RPKM. Pearson correlation coefficient is shown at top-left. (B) Genes with a greater than 2-fold expression difference between siCTR and siMITF RNA-Seq samples were compared with Mitf-occupied genes. (A) KEGG pathways enriched in siMITF down-regulated genes. (B) GO terms enriched in siMITF down-regulated genes. (C) KEGG pathways enriched in siMITF up-regulated genes. (D) GO terms enriched in siMITF up-regulated genes. BER: base excision repair; ER: endoplasmic reticulum; HR: homologous recombination. In GO and KEGG graphs, all reported terms had p-value < 0.1. siMITF down-regulated graphs are coloured green; siMITF up-regulated graphs are coloured red. Numbers at the end of each bar represent the total gene count in the KEGG pathway or GO term.

function. Cell cycle regulation by CDK2 (Du et al., 2004) and DNA-replication have previously been characterised as being MITF-regulated (Strub et al., 2011). Two directly bound and regulated genes that regulate the cell cycle that have not previously been identified as MITF-regulated are CDK4 and CDK6 which, in complex with cyclin D, phosphorylate and inactivate Rb, permitting progression to S-phase. MITF has previously been shown to influence the cytoskeleton through regulation of *Diaph1* (Carreira et al., 2006). Among the up-regulated genes (Figure 3.26 E, F) were genes that regulated focal adhesion, axon migration and interaction with the extracellular environment, in keeping with the idea that MITF-depletion in cells promotes the adoption of an invasive phenotype (Carreira et al., 2006). This data suggests that MITF could actively suppress invasiveness by directly repressing these genes, rather than by up-regulating another gene which, in turn, down-regulates invasiveness-promoting genes.

To enable similar comparisons to be made for PLX4720 treatment, RNA-Seq experiments were performed in 501mel cells treated or not with DMSO or 200 nM PLX4720 for 12 hours. Correlation calculations were performed between all 3 RNA-Seq samples, and they were found to be well correlated (501mel vs DMSO Pearson correlation coefficient R=0.97, 501mel vs PLX4720 Pearson correlation coefficient R=0.97, DMSO vs PLX4720 Pearson correlation coefficient R=0.97; Figure 3.27A). The linear runs of points in the bottom left corner represent the genes that were zero in one sample but with a low non-zero RPKM in the other.

To directly compare the global expression levels in the three samples, the $\log_2$ ratio between two samples was plotted against the $\log_2$ RPKM of one of the samples as shown (Figure 3.27B). As in the previous set of graphs, the linear runs of points are the genes that were zero in one sample but with a low non-zero RPKM in
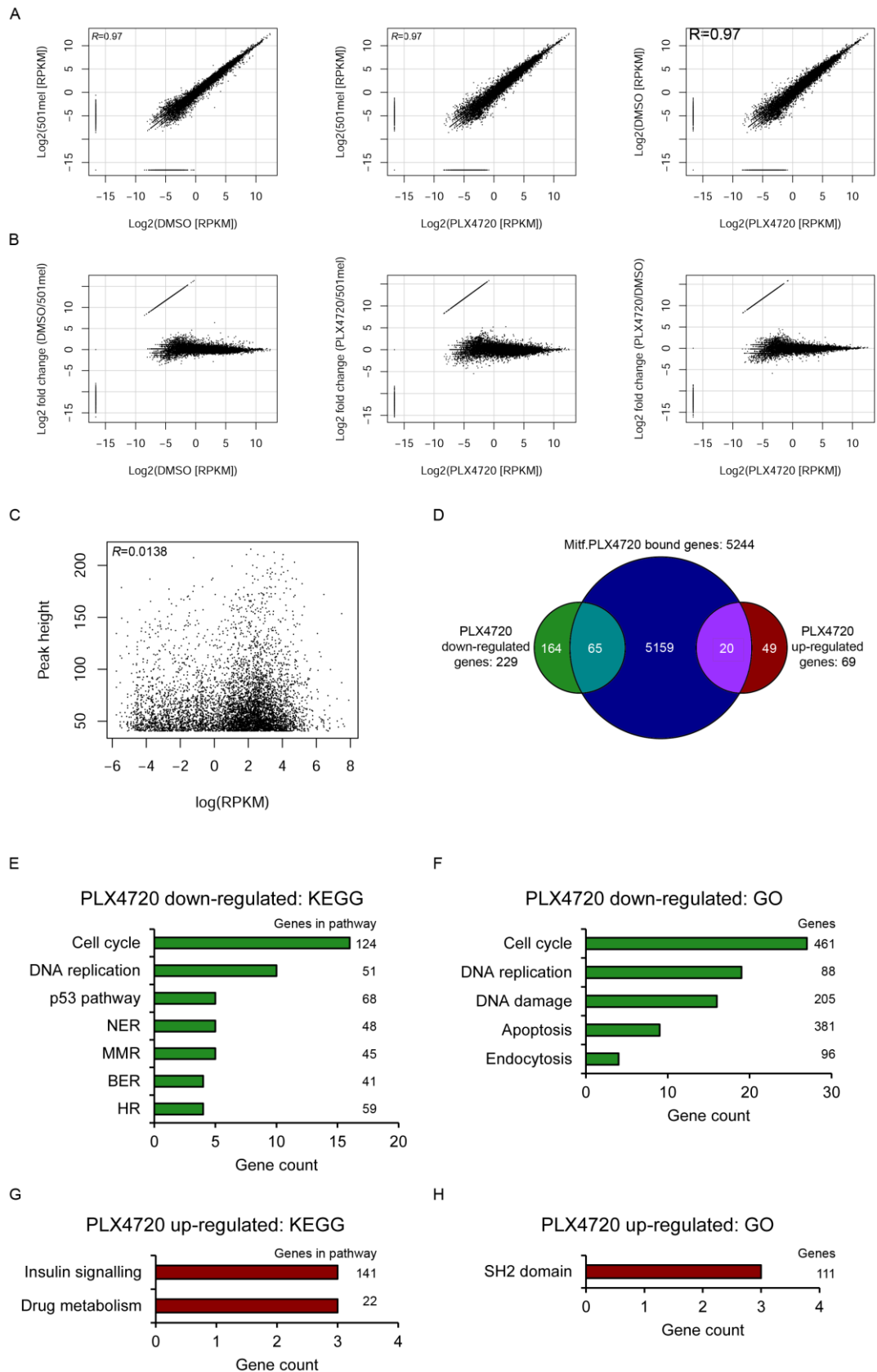
Figure 3.27. PLX4720 RNA-Seq in 501mel cells. [Legend continues at bottom of next page.]

the other. The graphs revealed that a modest number of genes were likely differentially expressed, but that the majority of the genes in the genome were non-regulated by either DMSO or PLX4720.

Plotting peak height for Mitf.PLX4720 against expression level in the presence of PLX4720 for expressed peak-associated genes (Figure 3.27C) revealed a similar distribution to the Mitf plot (Figure 3.26A). A similar correlation was observed (Figure 3.27C; Pearson correlation coefficient R=0.0138), suggesting that the overall relationship between HA-Mitf binding and gene expression is similar in these samples, and that the presence of a peak is positively associated with gene expression, while the height of the peak is less important.

Next, genes with a two-fold expression difference between the PLX4720 and DMSO RNA-Seq samples were identified as being differentially expressed, and they were compared genes occupied by Mitf.PLX4720 (Figure 3.27D). Of 229 genes significantly down-regulated by PLX4720 treatment, 65 were occupied by

Figure 3.27. PLX4720 RNA-Seq in 501mel cells. (A) 501mel cells were treated or not with DMSO or PLX4720 (200 nM) for 12 hours before being harvested and RNA prepared for RNA-Seq analysis. Untreated cells are represented as 501mel. Graphs display correlations between DMSO-501mel (left), PLX4720-501mel (middle), and PLX4720-DMSO log-transformed RPKM. Pearson correlation coefficient is shown top-left. All RPKM were increased by 0.00001 to allow comparisons for genes where one value was zero. (B) Log-transformed plots showing fold-change between DMSO vs 501mel RPKM plotted against DMSO RPKM (left), fold-change between PLX4720 vs 501mel RPKM plotted against PLX4720 RPKM (middle), and fold-change between PLX4720 vs DMSO RPKM plotted against PLX4720 RPKM (right). (C) Scatter plot of Mitf.PLX4720 peak height gene-associated peaks against the natural-logarithm of the RPKM in the PLX4720 RNA-Seq. Pearson correlation coefficient is shown at top-left. (D) Genes with a greater than 2-fold expression difference between DMSO and PLX4720 RNA-Seq samples were compared with Mitf.PLX4720-occupied genes. (E),(F) KEGG and GO analysis of PLX4720 down-regulated genes. Bars are coloured green. (G),(H) KEGG and GO analysis of PLX4720 up-regulated genes. Bars are coloured red. All de-regulated terms in (E)-(H) have p-value < 0.1. MMR: mismatch repair, NER: nucleotide excision repair; SH2: Src homology 2. Numbers at the end of each bar represent the total gene count in the KEGG or GO entry.

Mitf.PLX4720. Only 69 genes were up-regulated by PLX4720, of which 20 were occupied by Mitf.PLX4720. This suggested that MITF could, at least in part, be mediating the response to PLX4720 treatment in 501mel cells. To identify the biological roles of the genes de-regulated following PLX4720 treatment, KEGG and GO analysis was performed. Down-regulated genes (Figure 3.27E,F), were predominantly associated with cell cycle progression and DNA damage, which would be expected given that MAPK is a growth-promoting pathway and, in order for cell cycle progression, DNA damage cannot go unrepaired. Very few enriched terms were identified among PLX4720 up-regulated genes, with few genes associated with them (Figure 3.27 G, H), which most likely reflects the small number of genes identified that were up-regulated.

Comparative analysis of the ChIP-Seq and RNA-Seq data had suggested that Mitf-binding could be positively correlated with gene expression level. To test this idea, genes and their associated peaks were divided into expressed and non-expressed bins, in the presence and absence of PL4720. Approximately 40% of RefSeq genes were expressed in both RNA-Seq samples, and Mitf binding was more strongly associated with expressed genes than non-expressed ones (Figure 3.28A). To analyse this further, expressed genes were divided into 10 bins of equal size but increasing expression level, and gene density among them plotted (Figure 3.28B). In both ChIP-Seq samples, more bound genes were associated with the lowest expressed group than the next most expressed group, but between groups 2 and 6 there was an increase in the number of peaks assigned to each group. The highly expressed groups of genes (6 through 10) had similar numbers of peaks associated with them. Because there is a general upwards trend in the number of bound genes associated with each expression group, this data suggests that Mitf binding has a positive influence on transcription.

However, given that 665 genes were up-regulated by siMITF, of which 205 were

associated with Mitf peaks higher than 40, and 518 with an Mitf peak of any height

and can presumably thus be directly repressed by MITF, it is possible that some of the
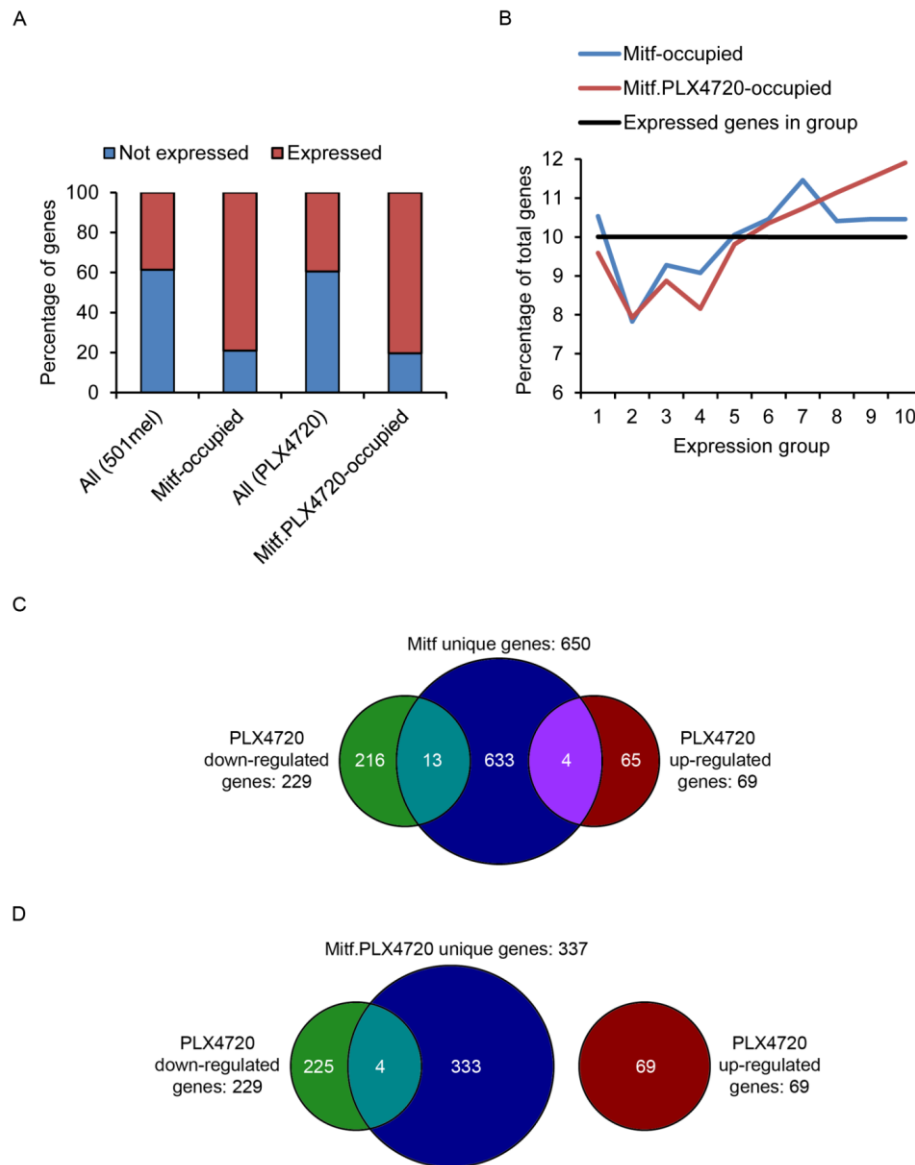
Figure 3.28. Relationship between HA-Mitf occupancy and gene expression.
(A) Genes in 501mel and PLX4720 RNA-Seq were categorised as expressed or not expressed, and genes associated with Mitf and Mitf.PLX4720 ChIP-Seq peaks respectively divided into these groups. (B) Expressed 501mel and PLX4720 genes from (A) were divided into 10 bins of equal size and increasing expression level, and genes associated with ChIP-Seq peaks from each sample were divided into these bins. (C) Genes uniquely occupied by Mitf were compared with genes de-regulated by PLX4720. (D) Genes uniquely occupied by Mitf.PLX4720 were compared with genes de-regulated by PLX4720.

40% of peaks in non-expressed genes, or the peaks in weakly-expressed genes, could be play a repressive role that was not relieved by siMITF transfection in this cell line.

3.4 Discussion

ERK-mediated phosphorylation of p300 has previously been shown, and has been confirmed here, to activate the acetyl-transferase activity of p300 (Chen et al., 2007). Previous work in our laboratory showed that MITF was acetylated by p300/CBP in a MAPK-dependent fashion. MITF is also phosphorylated on two sites following activation of the MAPK pathway (Hemesath et al., 1998), but these events are not required for MITF acetylation, suggesting that the MAPK-dependency could arise from MAPK signalling being necessary for strong p300 activation. In melanocyte development, MAPK signalling is a major growth-promoting pathway that is subsequently down-regulated on differentiation. In almost all melanoma patients, the MAPK pathway is constitutively activated (Brose et al., 2002; Davies et al., 2002), suggesting that, in melanoma, MITF should have increased acetylation levels. Two lysines that may be acetylated are in the MITF DNA binding basic region, and four more can be found throughout the bHLH-LZ of the protein. This led to a hypothesis that MAPK-driven acetylation of MITF could regulate the ability of MITF to bind to different subsets of its target genes. If true, this would add to the rheostat model of MITF activity (Carreira et al., 2006), and could explain how MITF is able to promote proliferation in actively growing cells—where there is active MAPK signalling—yet restrict growth in differentiated or quiescent, stem-like cells. In MITF target genes playing roles in differentiation, the bound E-box appeared to always be flanked by 5'-T on at least one residue, whereas this requirement seemed to be more lax for genes with roles in proliferation and survival that would be anticipated to be expressed when MITF is in the middle of the rheostat.

Following initial experiments showing that MAPK can promote expression from luciferase reporters that have binding sites lacking a 5'-T, genome-wide profiling of Mitf binding was carried out in 501mel cells using epitope-tagged Mitf, in the presence and absence of PLX4720. However, in the ChIP-Seq experiments, there was essentially no difference found in motif preference by Mitf in the treated or untreated state. There are a number of possible explanations for this. First, that 501mel cells can use an alternate RAF level activation that allows them to retain some MAPK signalling capacity. Melanoma cells can bypass BRAF inhibition through up-regulation of CRAF, and it is possible that 501mel cells are able to respond to BRAF inhibition by activating a different RAF. Given that UO126 is able to reduce ERK phosphorylation far more efficiently than PLX4720, this could be a likely candidate, and ChIP-Seq experiments in the presence and absence of UO126 will be conducted to see whether MEK inhibition is a more effective means of looking for MAPK-directed redirection of HA-Mitf DNA binding.

A second possibility is that 8 hours of treatment was insufficient to redirect MITF DNA binding. However, extending the treatment for longer would start to interfere with Mitf phosphorylation, which would also be expected to impact on where Mitf is bound, and so extending the treatment time is not considered a viable option. Alternately, it could be that there is no discernible difference in *in vivo* binding induced by PLX4720 treatment. However, the fact that MAPK blockade was observed to induce melanoma differentiation renders this unlikely. If the same result is found from UO126 ChIP-Seq, further time course ChIP experiments will be required to ask whether and when there is any difference in Mitf binding with time. This will need to be correlated with Mitf phosphorylation status to allow an informative conclusion to be drawn.

A third possible option is that, although there was no significant change observed in the absolute HA-Mitf occupancy between PLX4720 treated and untreated cells in the ChIP-Seq experiments, there could have been a difference in the binding kinetic. It has been shown that the longer a transcription factor is present at a binding site, the more likely that gene is to be expressed (Lickwar et al., 2012). These authors demonstrate that, following induction of an inducible Myc-tagged Rap1 construct, FLAG-Rap1 is competed away from its binding sites and replaced with Myc-Rap1. Crucially, however, the total Rap1 occupancy at sites genome-wide is unchanged. It is thus possible that PLX4720-treatment triggers changes in the binding kinetics of HA-Mitf that are not detectable here. This idea could be tested by introducing an inducible FLAG-Mitf construct into the 501.HA-Mitf cell line, and measuring HA-Mitf and FLAG-Mitf occupancy following induction in the presence and absence of MAPK blockade.

One final possibility is that there was a difference in the relative peak height between the samples in peaks containing different motifs rather than a pure shift in Mitf binding. However, following genome-wide profiling across bound motifs, there was no difference observed in the presence and absence of PLX4720, strongly suggesting that there was indeed little difference between these samples.

Many genes differentially regulated in RNA-Seq experiments following siMITF and siCTR transfection were bound by HA-Mitf in the ChIP-Seq. Down-regulated genes are associated with the cell cycle (e.g. CDK1, CDK2, CDK4, CDK6), DNA replication (e.g. LIG1), DNA damage repair (e.g. BRCA2, CHK1, MDM4, LIG1), and kinetochore function (e.g. PLK1, 8 CENP complex proteins). Together, this set of genes suggests that MITF plays a major role in cell cycle progression by promoting DNA damage repair as well as promoting faithful mitotic passage, which

together will help to prevent the genome from being destabilised. Previous work has established that loss of MITF leads to accumulation of DNA damage and can promote entry to a senescent state (Giuliano et al., 2010), and recent genome-wide MITF profiling found a similar biological effect of MITF loss (Strub et al., 2011).

Pigmentation genes were not de-regulated in the siMITF RNA-Seq but these, along with genes playing roles in Waardenburg syndrome, deafness, and albinism, which can result from defective MITF expression or functioning, were bound. Except for deafness these terms did not appear in the KEGG and GO analysis of the top 1,000 bound genes, but analysing 3,000 genes led to the inclusion of pigmentation terms in the enriched list (data not shown). This suggests that other proteins would still be driving expression of these genes. Indeed, the bHLH-LZ protein upstream stimulatory factor 1 (USF1) is also able to occupy the MITF sites in the *Tyrosinase* promoter, and it is a major promoter of *Tyrosinase* expression (Galibert et al., 2001).

Hitherto, MITF has not been suggested to be a transcriptional repressor, except in the previous genome-wide study (Strub et al., 2011), and the same has been observed here. Genes associated with focal adhesion (e.g. SHC4, PTEN), axon migration (e.g. EPHA3, EPHB3), and interaction with the extracellular environment (e.g. 6 collagens, MMP16, the TGF-β family bone morphogenic protein 4) were up-regulated following MITF knock-down, in agreement with the notion that MITF may also be able to repress gene expression. Brn-2, which is repressed by MITF-mediated induction of the micro-RNA miR-211 (Boyle et al., 2011), is up-regulated after MITF silencing. The genes and pathways up-regulated on loss of MITF promote adoption of an invasive, metastatic phenotype, particularly genes such as SHC4 (Fagiani et al., 2007) and BMP4 (Rothhammer et al., 2005) that promote melanoma metastasis. It was interesting to note that the anti-senescent protein TBX2, which has been shown to

be regulated by MITF (Carreira et al., 2000), was bound in the ChIP-Seq and also up-regulated in the siMITF RNA-Seq, likely in an attempt to ward off senescence.

In addition, a potential metabolic shift was suggested from this work, lactose dehydrogenase A and D were bound and directly regulated by MITF. Further suggesting a metabolic role for MITF, transporters such as GLUT1 were bound and regulated, along with binding observed to many other transporter genes. These observations suggest that MITF could well be a major metabolic regulator in melanoma cells. It will be necessary in the future to correlate MITF function with metabolism through metabolome profiling in siCTR and siMITF transfected cells to determine whether MITF can control metabolism.

MITF could also be a major regulator of lysosomes (ten genes, including TFEB and LAMP1, regulating lysosome biogenesis and maturation, are directly bound and regulated by MITF). TFEB has been identified as the master regulator of lysosomes, binding a 5'-GTCACGTGAC-3' motif in the promoters of these genes (Sardiello et al., 2009), and it is a closely related protein to MITF. The bHLH-LZ are almost perfectly conserved between these proteins, and they have been observed to heterodimerise *in vitro* (Hemesath et al., 1994). It is thus not surprising that HA-Mitf was observed bound to many lysosome gene promoters, and further work will be required to investigate whether MITF plays a functional role in lysosomal biogenesis. This is the first time that a potential role for MITF has been identified in lysosome regulation, although some lysosomal genes were identified, but not noted, as putative MITF targets in the recently published MITF ChIP-Seq (Strub et al., 2011).

The work in this chapter has shown that Mitf is deacetylated by HDAC1 and HDAC4. It also shows for the first time that SIRT1 is a major suppressor of p300 protein level, and hence acetylation within the cell, although it has previously been

reported that SIRT1 can deacetylate and inhibit p300 (Bouras et al., 2005). This is an interesting finding, because SIRT1 is dependent on NAD^+ as a cofactor and thus functions as a metabolic sensor for the NAD^+:NADH ratio inside the cell. NAD^+/NADH links the Krebs cycle with oxidative phosphorylation. In starving cells, SIRT1 will be activated, and it has been shown that this promotes cell survival (Cohen et al., 2004). In a starving cell, therefore, SIRT1 would be expected to abolish p300 protein levels, which would result in deacetylation of MITF and thus, presumably, a switch in which metabolic target genes it regulates.

The work in this chapter uses over-expressed Mitf and acetyltransferase constructs. In the future, it will be important to confirm endogenous MITF acetylation in cells in the absence of excess acetyltransferases, and that its acetylation status is regulated by the MAPK signalling pathway. Hitherto this has been hampered by poor reagents, notably an MITF antibody that works reliably in IP. It may be possible to circumvent this issue with the HA-Mitf stable cell line. However, this construct, like all the other MITF constructs used here, is derived from the murine cDNA rather than the human sequence, so some care is needed. The human and mouse proteins are highly similar and have identical bHLH-LZ domains, so this is not seen as a problem. MITF DNA-binding is inhibited by its hyper-acetylation. If K205 and K206 are both acetylated, the positively charged basic region will be largely neutralised, which would be expected to disrupt MITF-DNA interaction. In addition to examining the global effects of MITF acetylation on its DNA binding, the role of site-specific MITF acetylation will also need to be examined. This is addressed in Chapter 4.

Chapter 4 – MITF-K243 acetylation may be required for specific DNA binding

4.1 Introduction

In Chapter 3, it was shown that hyper-acetylation of Mitf by p300, or induced by BRAF^{V600E}, inhibited Mitf DNA binding and the potential of Mitf to activate target genes. This effect may have been caused by acetylation of both K205 and K206, which lie in the basic region and bind within the major groove of the E/M-box. Understanding the effects of acetylation on MITF DNA binding activity by looking at overall acetylation was difficult because there were numerous acetylation sites that could have been functional. As discussed in Section 3.4, a genome-wide change in MITF DNA binding following treatment with PLX4720, the specific inhibitor of BRAF^{V600E}, also could not be observed. Therefore, to gain a better understanding of the effects of MAPK-driven acetylation of MITF on the ability of MITF to bind and activate different fractions of its target genes, it was necessary to examine the role of individual DNA binding amino acids in MITF.

The crystal structure of MITF revealed that certain amino acids within the bHLH-LZ play important roles in recognising different MITF binding sites (Pogenberg et al., 2012). In particular, R217 was found to be important for binding to a 5'-GCACGTGC-3' E-box motif, while I212 was crucial for mediating binding to a 5'-TCATGTGC-3' M-box. H209 was important for binding to both motifs. However, beyond the change in the cores of the motifs, these sequences also differ in the base 5' to the CA(C/T)GTG motif, as well as in bases further from the core. It is thus hard to draw conclusions about the role of these amino acids in the base-specificity of MITF DNA binding. Further, while the study identified some interactions regulating the capacity of MITF to interact with different sequences, it did not address how MITF can be stimulated to recognise different target sequences. In this chapter, the role of K243 and its acetylation in mediating DNA binding by MITF-K243 is investigated.

4.2 The *in vitro* role of MITF-K243

To begin the assessment of the potential role of different acetylation sites in Mitf, the lysine residues that can be acetylated were mutated to arginine. The side chains of both amino acids are both basic with a similar shape: lysine has a 4-carbon aliphatic chain capped with an amino group, and arginine a 3-carbon aliphatic chain capped with a guanidinium group. Arginine substitution is frequently used experimentally as a mimic of non-acetylated lysine, while glutamine is often used as a structurally similar mimic of acetyl-lysine with similar biological properties. For example, an $H4^{K16Q}$ mutant was found to behave in the same fashion as the unmutated residue in preventing formation of heterochromatin, and it was later shown that this is mediated by H4K16-acetylation (Hecht et al., 1995; Shogren-Knaak et al., 2006).

Mitf can be acetylated on at least ten lysines, and lysine-arginine point mutations were created in the FLAG-Mitf expression vector at sites that can be acetylated (Figure 4.1A). The mutants were expressed in Phoenix cells in the presence of HA-p300 and analysed by anti-FLAG immunoprecipitation (Figure 4.1B). Different amounts of each protein were detected following Western blotting, along with varying acetyl-lysine signals. However, it was clear that, while FLAG-Mitf^{WT} had strong acetylation induced by coexpression with HA-p300, none of the single-site mutants abolished the ability of FLAG-Mitf to be acetylated by HA-p300. Following normalisation of the relative levels of total and acetylated lysine in the protein (Figure 4.1C), it was clear that K91R, K205R, K233R, K243R or K248R mutation all reduced the level of FLAG-Mitf acetylation approximately two-fold relative to the wild-type protein, while K206R or K225R mutation repressed Mitf-acetylation approximately five-fold. This suggests that either K206 and K225 are major acetylation targets of p300, and that K91, K205, K233, K243, and K248 all also make a contribution to

Mitf-acetylation, or that one or more of these sites must be acetylated for Mitf to be acetylated at others. Acetylation was slightly reduced in the K21R and K43R mutants and slightly elevated in the K33R mutant. K91R showed a small downward mobility
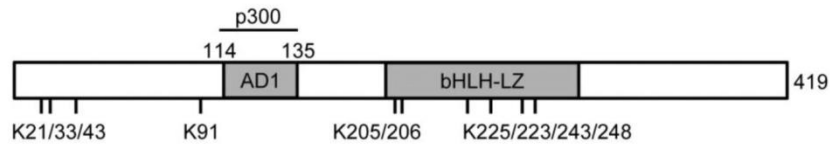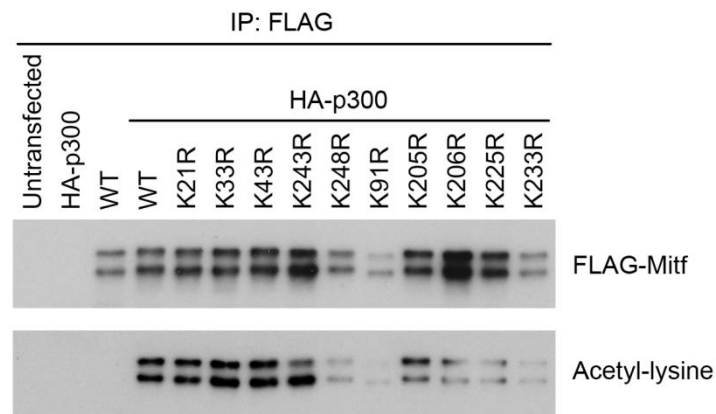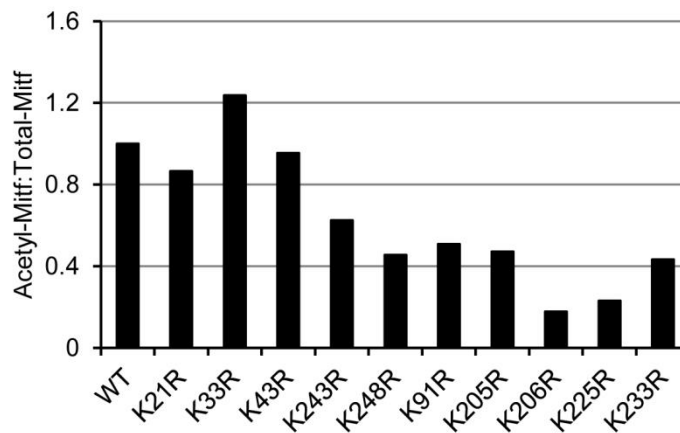
Figure 4.1. Acetyl-lysine point mutants of Mitf can all be acetylated. (A) Scheme showing sites of acetylation of Mitf, the p300 interaction domain within Mitf, and the point mutants used here. (B) Lysates from Phoenix cells, 40 hours post-transfection with the indicated constructs, were subjected to anti-FLAG IP followed by Western blotting with the indicated antibodies. (C) Quantification of Western blots in (B), showing the ratio of acetylated to total FLAG-Mitf.

shift relative to the other mutants, suggesting that this mutation might disrupt an additional post-translational modification.

While FLAG-Mitf[K243R] showed reduced overall acetylation relative to FLAG-Mitf[WT], there was also a shift in the phosphorylation pattern of the protein (Figure 4.1B). More hypo-phosphorylated FLAG-Mitf[K243R] was detected than hyper-phosphorylated FLAG-Mitf[K243R]. The same pattern was true for the acetylated protein, but to a greater extent, suggesting that acetyl-K243 might principally be found in the hyper-phosphorylated upper band of the protein.

While Mitf-K206 and Mitf-K225 appear to be more major acetylation targets than Mitf-K243 *in vitro*, MITF-K243 was chosen for further investigation for a number of reasons. First, with the exception of MAD and MAX, it is conserved at the start of helix 2 in human bHLH proteins (Figure 4.2A). MITF-K206 is less well conserved, and MITF-K225 is not conserved outside of the MiT subfamily of bHLH proteins. MITF-K243 is also conserved in murine Mitf and in the yeast bHLH proteins CBF1 and PHO4. Secondly, it has been observed in bHLH crystal structures that the K243-equivalent can contact the phosphate backbone (Ferre-D'Amare et al., 1993; Ferre-D'Amare et al., 1994), and the same is the case for Mitf (Pogenberg et al., 2012). In the Mitf crystal structure, the backbone amide group of K243 makes a potential hydrogen bond contact with the phosphate group of the cytosine at beginning of the hexameric core of the E/M-box (C-3), while the side chain amino group contacts the phosphate group from the adenosine at -2 (A-2) to the centre of the motif (Figure 4.2B). Because the lysine-phosphate hydrogen bond is a charged interaction, neutralisation of the MITF-K243 side chain by acetylation would thus reduce MITF affinity for DNA. Therefore, the Ac-K243-MITF should only be able to interact with highly specific binding sites. Moreover, G244 has been determined to be

physiologically relevant in mice, where an *Mi^b* (G244E) mutation reduces the DNA-affinity of Mitf *in vitro* and results in a brown-coated mouse rather than the wild-type mouse (Steingrimsson et al., 1996). In addition, a recent study identified somatic *MITF* mutations in melanoma patients, one of which was MITF^G244R (Cronin et al., 2009). MITF^G244R was less able to activate a *Tyrosinase* luciferase reporter than MITF^WT, suggesting that the interaction of this protein with DNA is also reduced.
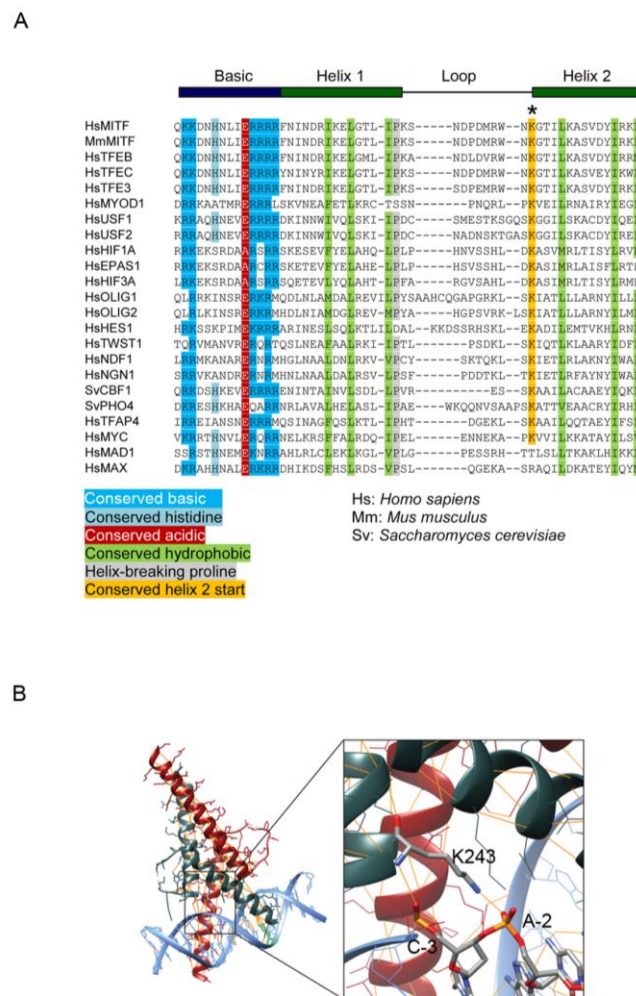
Figure 4.2. K243 is conserved in bHLH proteins and contacts DNA. (A) Clustal W multiple sequence alignment of the bHLH domains of the indicated proteins. * indicates the position of the K243-equivalent residue. (B) Crystal structure of the bHLH of Mitf (Pogenberg et al., 2012) bound to a CACGTG motif, showing the interaction between K243 and the backbone.

A *Tyrosinase* reporter luciferase assay was conducted in Phoenix cells expressing FLAG-MITF, the levels of which were examined by Western blotting (Figure 4.3A). FLAG-Mitf^{K243R} were expressed at a higher level than the other constructs, a result that was reproducible using independently prepared constructs (data not shown). This suggested that MITF-K243 might play a role in regulating Mitf stability, either by preventing ubiquitylation of K243, or by interfering with one of the published ubiquitylation events, or interaction with a cofactor that regulates Mitf stability. After normalisation of luciferase activity for the level of FLAG-Mitf in the cell lysate, it was apparent that FLAG-Mitf^{K243R} and FLAG-Mitf^{G244R} had reduced capacity (2-tail t-tests $p<0.001$ and $p<0.01$, respectively) to activate the *Tyrosinase* reporter relative to FLAG-Mitf^{WT}, while FLAG-Mitf^{K243Q} had enhanced ability to
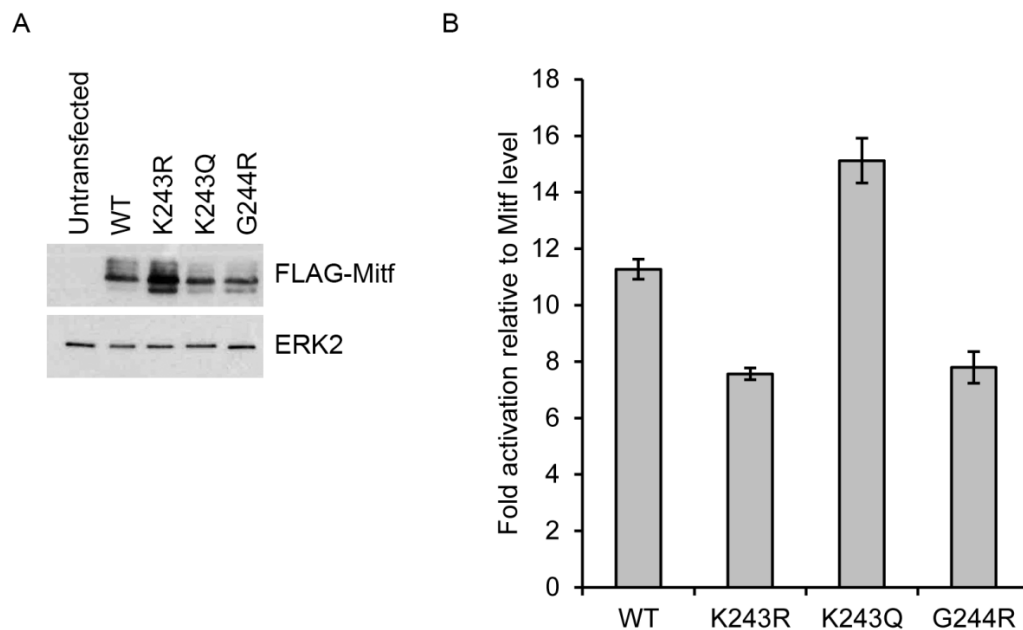
Figure 4.3. K243 and G244 mutants show altered activation of a *Tyrosinase* reporter. (A) Lysates from Phoenix cells transfected for 40 hours with the indicated constructs were subjected to Western blotting with the indicated antibodies. (B) Lysates from (A) were used in a luciferase assay, and luciferase activity normalised for the Mitf content of the lysate. Results are presented as mean ± standard error of the mean of three independent experiments.

activate the reporter relative to FLAG-Mitf^{WT} (2-tail t-test $p<0.05$; Figure 4.3B). The K243-mutations suggest that acetyl-K243-MITF may in fact be able to better activate specific MITF elements in its target genes compared to non-acetyl-K243-MITF. G244R is likely to be a structurally severe mutation, as arginine will impose greater packing constraints on the surrounding amino acids than glycine, and thus could disrupt proper formation of helix 2. It is therefore not surprising that FLAG-Mitf^{G244R} therefore shows reduced ability to activate the reporter, and suggests that it could impact on MITF behaviour in a manner similar to non-acetyl-K243-MITF.

One of the problems with the analysis of the experiments in Chapter 3 was the gain in Mitf protein levels following coexpression with p300 or BRAF^{V600E}, and the same is true here. It is hard to assign a biological role to a point mutation in a protein when the levels of that protein are also changing within the experiment. Therefore, an *in vitro* approach using recombinant protein was adopted to interrogate the role of K243 in the regulation of Mitf DNA binding. His-Mitf.180-296, the Mitf protein fragment used to determine the crystal structure of Mitf (Pogenberg et al., 2012), was purified that was WT, K243R, K243Q, or G244R. This encompasses the entire bHLH-LZ of Mitf. Analysis of the elution fractions revealed that the fourth and fifth sequential elutions appeared pure by Coomassie staining (Figure 4.4A, showing a representative gel for His-Mitf^{WT}.180-296; gels for mutant proteins are not shown). These fractions were used for further analysis and their volumes adjusted to equalise their His-Mitf.180-296 concentration (Figure 4.4B). The ability of the proteins to bind to either a *Tyrosinase* enhancer M-box probe (*Tyr* CAT), or to an oligonucleotide with a 5'- CACGTG-3' (*Tyr* CAC; Figure 4.4C), was assessed by EMSA (Figure 4.4D). In mock-purified protein from an un-transformed bacterial culture, a band was induced close to the probe that was present in protein-containing lanes. This is likely due to
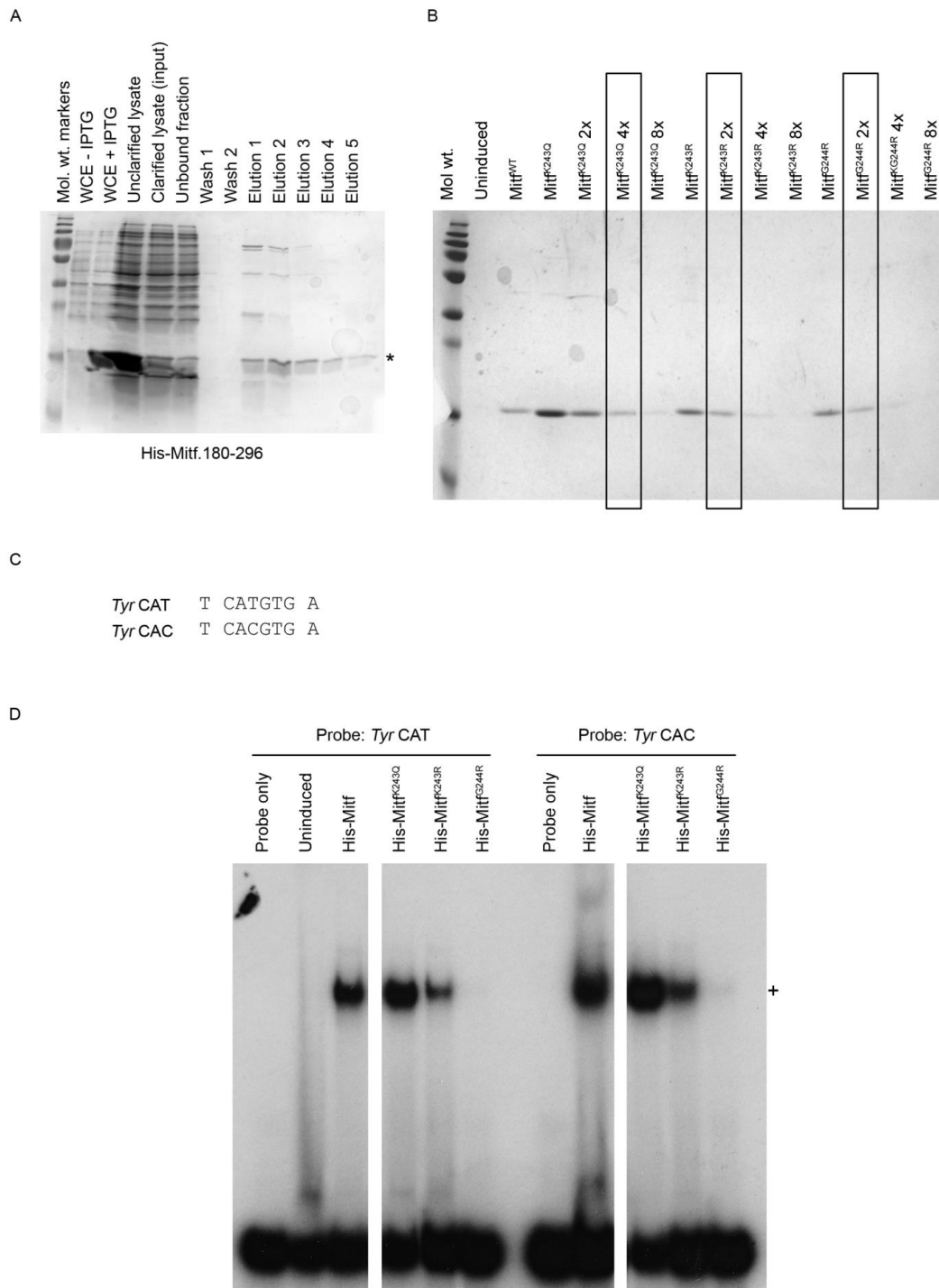
Figure 4.4. Purification and DNA binding of recombinant Mitf bHLH-LZ. (A) Aliquots of each fraction of the purification were retained and analysed by Coomassie staining. WCE: whole cell extract. * denotes the resolution of the His-Mitf.180-296 protein, around the 15 kDa marker. (B) Equalisation of pure protein fractions as judged by Coomassie staining. Serial dilutions of each protein were analysed by Coomassie staining. Boxed lanes indicate the chosen dilutions with similar protein to Mitf^{WT} levels. (C) MITF binding sites in the radiolabelled oligonucleotides used in EMSA. Full sequences can be found in Chapter 2. (D) EMSA using the indicated proteins and radiolabelled probes. + indicates the Mitf-specific band.

the elution fractions used not being completely homogeneous. In lanes containing purified Mitf, a specific band was induced. His-Mitf.180-296 that was WT, K243R, or K243Q bound the *Tyr* CAC probe approximately twice as strongly as each individual protein bound to the *Tyr* CAT probe. His-Mitf^{WT}.180-296 protein bound slightly more strongly than His-Mitf^{K243R}.180-296 to both probes, while the acetyl-mimetic His-Mitf^{K243Q}.180-296 bound slightly more strongly than His-Mitf^{WT}.180-296. In these experiments, it should be emphasised that the wild-type His-Mitf^{WT}.180-296 protein was not acetylated, and that the His-Mitf^{K243R} mutation therefore assesses the impact of changing in amino acid at this position rather than a lack of acetylation. The acetyl to non-acetyl comparison was made between His-Mitf^{WT}.180-296 and His-Mitf^{K243Q}.180-296. This experiment showed that His-Mitf^{K243Q}.180-296 binds to E/M-boxes with a greater affinity than His-Mitf^{WT}.180-296. This suggests that acetyl-K243-MITF would bind to specific MITF binding sites more strongly than non-acetyl-K243-MITF, in agreement with Figure 4.3. Although this result is in apparent contradiction of Figures 3.4 and 3.5, where p300-mediated FLAG-Mitf hyper-acetylation led to reduced DNA-binding potential, this experiment just probes the effects of K243-acetylation rather than all acetylation sites at the same time. It quite possible that the inhibitory effects of coexpression with p300 seen before arise from double acetylation of Mitf-K205/6, as both these residues are DNA-binding within the E/M-box.

Surprisingly, only negligible binding was seen by His-Mitf^{G244R}.180-296 to either probe, which was confirmed by repetition with independent protein preparations (data not shown). The difference in the ability of the full-length protein to activate the luciferase reporter—and hence by extension bind DNA—and the recombinant bHLH-LZ to bind DNA could be explained if structural changes induced

by the G244R mutation can be partially compensated for by a stabilising influence of the N- or C-terminus of the protein being in close proximity to helix 2. This would still enable the mutant protein to function at a reduced level, while the absence of this stabilising intra-molecular (or inter-molecular from the second protomer of the dimer) interaction in the recombinant protein could largely prevent it from binding to DNA. This is beyond the scope of the project, and the role of the G244R mutant is not considered beyond this point. However, given the phenotype of the Mi^b mouse, it will be important to return to the role of this residue in the future.

The presence of 5'-T has been shown to be required for strong MITF binding to 5'-CATGTG-3' M-boxes but not for binding to 5'-CACGTG-3' E-boxes (Aksan and Goding, 1998). To explore whether K243Q substitution affected the ability of His-Mitf.180-296 to bind DNA, probes were designed by changing the 5'-T and 3'-A flanking residues in the *Tyr* CAT and CAC oligonucleotides for flanking residues that gave a 5'-T on one or other strand, or no 5'-T for each sequence (Figure 4.5A).

First, the effect of varying flanking sequence of a 5'-CATGTG-3' M-box was tested by EMSA. The recombinant proteins were bound to a 5'-TCACGTGA -3' radiolabelled E-box probe and increasing amounts of cold competitor sequences were titrated into the binding reaction (Figure 4.5B). Note that only the bound DNA bands are shown in this figure, but in all cases the probe was in excess. The *Tyr* CAC sequence was chosen as the probe because the relative binding of the 3 proteins to both sequences was the same, but stronger for *Tyr* CAC than for *Tyr* CAT (Figure 4.4C). Although direct comparison between these gels is difficult because of the different strength exposures, it is possible to compare the relative competition within the same gel. His-Mitf^WT.180-296 showed similar competition with both the CAC and

A

Tyr CAT	T CATGTG A	1
Tyr CAT_Tt	T CATGTG t	2
Tyr CAT_Tc	T CATGTG c	3
Tyr CAT_cA	c CATGTG A	4
Tyr CAT_cc	c CATGTG c	5
Tyr CAC	T CACGTG A	6
Tyr CAC_Tt	T CACGTG t	7
Tyr CAC_Tc	T CACGTG c	8
Tyr CAC_cA	c CACGTG A	9
Tyr CAC_cc	c CACGTG c	10

B

Probe= T CACGTG A

C

Probe= T CACGTG A
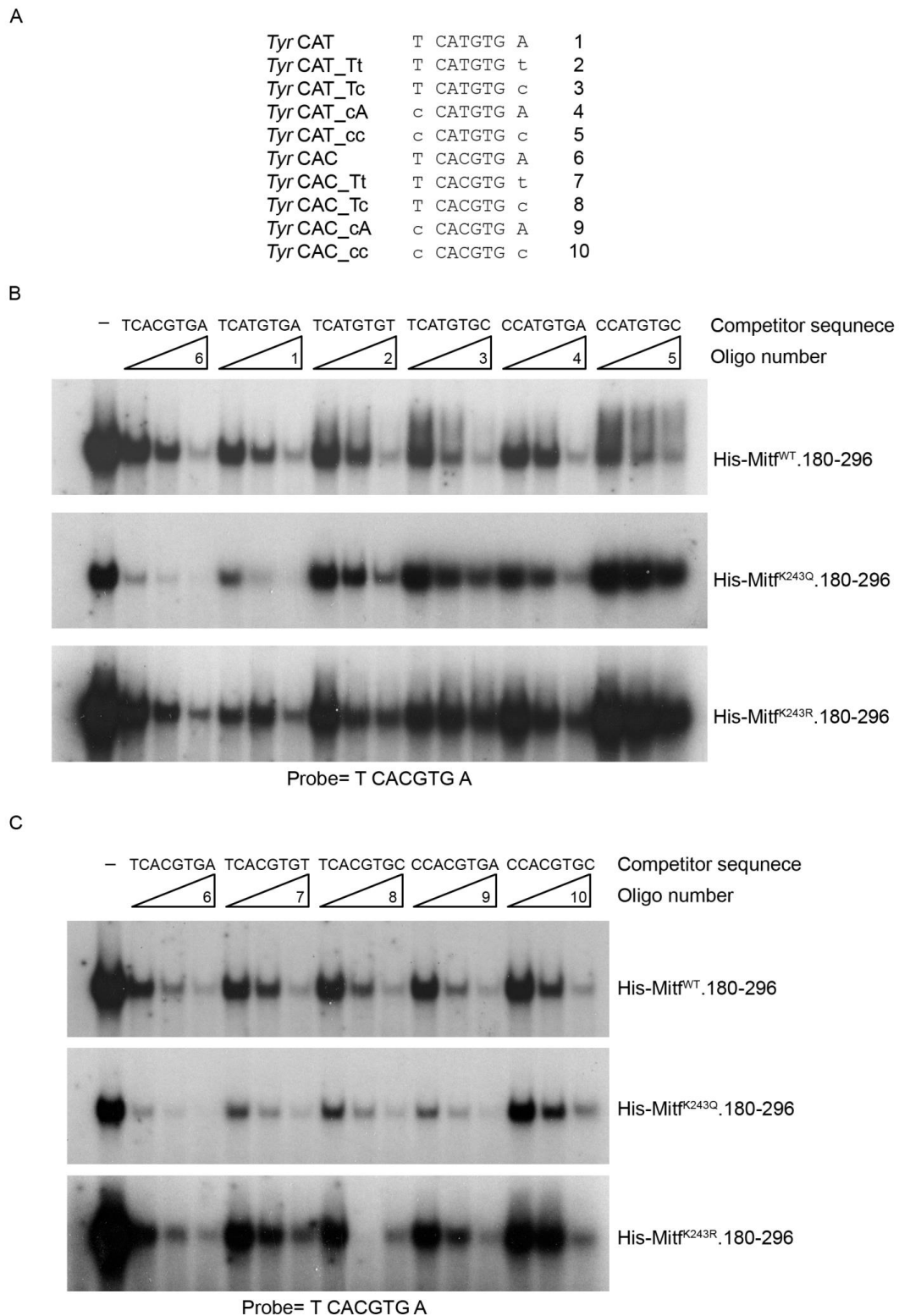
Figure 4.5. Flanking sequence requirement of His-Mitf^{K243Q} DNA binding. (A) MITF binding sites in the oligonucleotides used in this assay (B), (C) EMSA using the indicated proteins and titrations (3, 10, 30 ng) of the shown unlabelled competitor. The probe was *Tyr* CAC. Note that only the bound DNA is shown, but in all cases the probe was in excess.

CAT competition series. Binding to 5'-TCATGTGT-3', 5'-TCATGTGC-3', and 5'-CCATGTGA-3' sequences was slightly reduced compared to CAT, indicating that binding to 5'-CATGTG-3' is strongest when it is flanked by T on both strands. As was previously reported (Aksan and Goding, 1998), very little binding was observed to the 5'-CCATGTGC-3' competitor, which lacks a 5'-T on both strands. The appearance of a smear in an EMSA, as can be seen with some tracks in the His-Mitf^{WT} gel, indicates that the protein:DNA complex starts to dissociate while the gel is running, which can occur if the interaction is weak. The binding pattern for His-Mitf^{K243Q}.180-296 was different to His-Mitf^{WT}.180-296. A less strong shift was seen in this exposure than for His-Mitf^{WT}.180-296. Competition by 5'-TCACGTGA-3' was stronger and more complete than competition by 5'-TCATGTGA-3', and seemed to be stronger than the equivalent competition of His-Mitf^{WT}.180-296. Binding to all competitors with altered flanking sequences was reduced relative to competition by 5'-TCATGTGA-3'. Some competition was seen with 5'-TCATGTGT-3'and 5'-CCATGTGA-3', and almost none with 5'-TCATGTGC-3' and 5'-CCATGTGC-3'. For His-Mitf^{K243R}.180-296, competition by 5'-TCACGTGA-3'and 5'-TCATGTGA-3'was closer to the His-Mitf^{WT}.180-296 competition than His-Mitf^{K243Q}.180-296 competition. For motifs lacking 5'-T on both strands (oligos 2 – 5), His-Mitf^{K243R}.180-296 competition was closer to that seen with His-Mitf^{K243Q}.180-296. This result suggests that MITF-K243 may be important in determining the ability of MITF to bind to 5'-CATGTG-3' motifs that deviate from the canonical 5'-TCATGTGA-3'; in particular 5'-CCATGTGA-3' and 5'-CCATGTGC-3'. Because 5'-T is required for strong binding to 5'-CATGTG-3', these motifs represent more degenerate flanking sequences than oligos 2 and 3.

The experiment was repeated using a 5'-TCACGTGA-3' (*Tyr* CAC) radiolabelled E-box probe and varying the flanking sequences around a 5'-CACGTG-3' E-box for competitor DNA (Figure 4.5C). As before, 5'-TCACGTGA-3' could compete all three proteins away from the probe, but competition was most efficient for His-Mitf^{K243Q}.180-296. For His-Mitf^{WT}.180-296 and His-Mitf^{K243R}.180-296, competition by 5'-TCACGTGT-3', 5'-TCACGTGC-3', and 5'-CCACGTGA-3' was similar to competition by 5'-TCACGTGA-3', while these competitors appeared less efficient at competing His-Mitf^{K243Q} away from the probe. For 5'-CCACGTGC-3', the competition was reduced for all three proteins relative to 5'-TCACGTGA-3', and to a greater level for His-Mitf^{K243Q}. However, all three did bind to this sequence, unlike the 5'-CCATGTGC-3' competitor. The His-Mitf^{WT}.180-296 competition pattern confirms that a 5'-T is dispensable for binding to 5'-CACGTG-3' *in vitro* (Aksan and Goding, 1998). Because binding of His-Mitf^{K243Q} to the non-5'-TCACGTGA-3' competitors was reduced relative to His-Mitf^{WT}.180-296, this suggests that acetyl-K243-MITF could have a greater relative affinity for 5'-CACGTG-3' flanked by 5'-T on both strands than for other flanking sequences.

Mitf-K243 interacts with the first and second phosphate groups of the core hexameric binding site (Figure 4.2B). To investigate whether these bases are important for regulating binding by MITF, a series of oligonucleotides was designed containing increasingly degenerate E-boxes (Figure 4.6A). The oligonucleotides were titrated as cold competitors into a binding reaction between the recombinant proteins and a 5'-TCACGTGA-3' (*Tyr* CAC) radiolabelled E-box probe (Figure 4.6B). His-Mitf^{WT}.180-296 protein was efficiently competed away from the probe by CAC, and it showed slightly reduced competition to M1. A little competition was seen with M2, but M3, M4 and M5 failed to compete, indicating that it is possible to remove one

base from the end of the core binding site before Mitf binding is strongly inhibited. His-Mitf^{K243Q}.180-296 bound the CAC competitor more strongly than His-Mitf^{WT}.180-296, but failed to bind to any of the mutant competitors. This indicated that the intact CACGTG binding site is required to bind His-Mitf^{K243Q}.180-296, and suggested that acetyl-K243-MITF may have a stricter dependency on the edges of the binding site than non-acetyl-K243-MITF. If the side-chain interaction with the phosphate at -2 to the E-box centre is lost for Mitf^{K243Q} or acetyl-K243-MITF, then the amide backbone interaction with the phosphate at -3 would become more important for determining whether or not the protein will bind. His-Mitf^{K243R}.180-296 showed a very similar pattern of binding to CAC, M1, and M2 as His-Mitf.180-296,
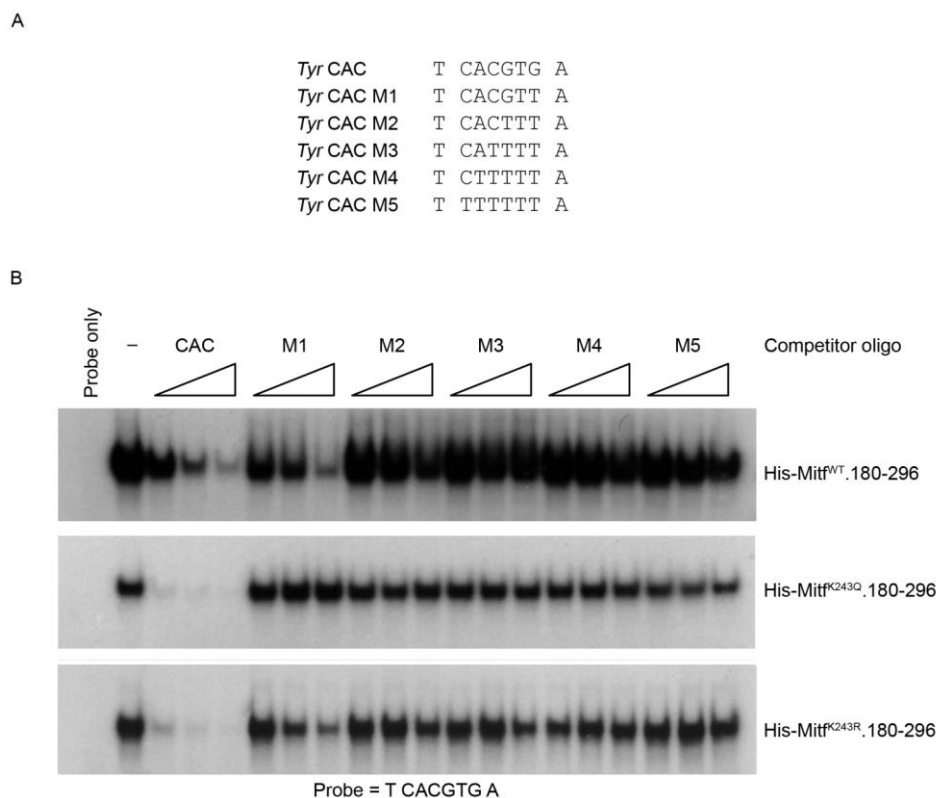
Figure 4.6. Flanking sequence requirement of His-Mitf^{K243Q} DNA binding. (A) MITF binding sites in the oligonucleotides used in this assay. (B) EMSA using the indicated proteins and titrations (3, 10, 30 ng) of the shown unlabelled competitor. The probe was CAC. Note that only the bound DNA is shown here, but in all cases the probe was in excess.

while also failing to bind M3, M4 or M5. This result suggests that, unlike acetyl-K243-MITF, non-acetyl-K243-MITF can bind to less canonical motifs.

The results thus far indicated that Mitf^{K243Q} has a reduced DNA affinity but a greater specificity (and binding strength) for canonical MITF binding sites. To test this hypothesis, increasing amounts of sonicated salmon sperm DNA were titrated into an EMSA binding reaction between the recombinant proteins and a *Tyr* CAC radiolabelled probe (Figure 4.7A). The salmon sperm DNA is genomic in origin, and thus represents a pool of non-specific DNA. His-Mitf^{WT}.180-296 and His-Mitf^{K243R}.180-296 proteins showed a very similar pattern of competition from increasing concentrations of salmon sperm DNA. His-Mitf^{K243Q}.180-296, however, required the presence of significantly more salmon sperm DNA in the binding reaction before any competition could be seen. No reduction in His-Mitf^{K243Q}.180-296 binding was seen until 156 ng of salmon sperm DNA were in the reaction, whereas just 2 ng of salmon sperm DNA were required to begin to compete His-Mitf^{WT}.180-296 and His-Mitf^{K243R}.180-296.

Together, these results indicate that the Mitf^{K243Q} bHLH-LZ forms a strong interaction with 5'-TCACGTGA-3' or 5'-TCATGTGA-3' motifs, and they suggest that it has reduced affinity for non-specific DNA yet greater affinity for MITF-specific sites than the Mitf^{K243R} or Mitf^{WT} bHLH-LZ domains. The same should be true of acetyl-K243-MITF, and future work must seek to clarify this biochemically.

As an initial means of testing whether this finding could be recapitulated *in vivo*, nuclear extracts were prepared from Phoenix cells expressing full-length FLAG-Mitf (WT, K243Q or K243R) in the absence or presence of HA-p300. Similar amounts of FLAG-Mitf proteins were recovered in the absence of HA-p300 and in the presence of HA-p300, although coexpression with HA-p300 led to an increase in

nuclear extractable FLAG-Mitf in the cells (data not shown). These extracts were used for a salmon sperm DNA competition EMSA with a *Tyr* CAC radiolabelled probe (Figure 4.7B). Anti-FLAG antibody was included in the reaction to allow detection of Mitf-specific binding. The supershifted bands are shown in the figure. While a faint doublet is seen in each gel resolving in a similar location to the supershifted bands,
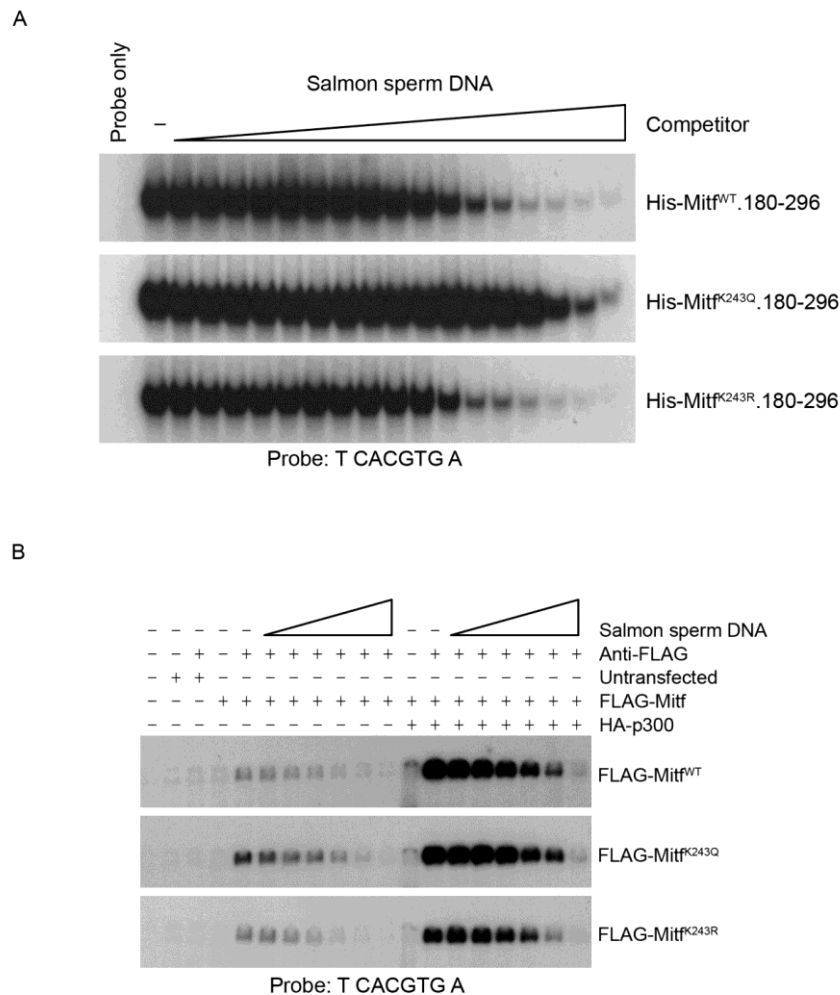
Figure 4.7. Mitf K243–acetylation imposes greater DNA binding sequence specificity. (A) Recombinant proteins were incubated or not with a 4-fold, 17 point dilution series of salmon sperm DNA, from 10 µg to 2.3 fg, before being subjected to EMSA with a *Tyr* CAC radiolabelled probe. (B) Nuclear extracts from Phoenix cells transfected with FLAG-Mitf constructs in the presence or absence of HA-p300 as were incubated or not with anti-FLAG and a 5-fold, 6 point dilution series of salmon sperm DNA, from 20 µg to 6.4 ng, before being subjected to EMSA with a *Tyr* CAC radiolabelled probe. Note that in both figures only the bound DNA is shown, but in all cases the probe was in excess.

the Mitf-specific bands are clearly distinguishable from these, particularly in the presence of HA-p300. As with the recombinant proteins, for approximately the same amount of FLAG-Mitf in the binding reaction, greater binding was seen from FLAG-Mitf^{K243Q} than FLAG-Mitf^{K243R}. In the titration, more salmon sperm DNA was required to compete the acetyl-mimetic FLAG-Mitf^{K243Q} from the probe than FLAG-Mitf^{K243R} required. FLAG-Mitf^{WT} displayed a competition pattern between the two mutants, suggesting that a proportion of the FLAG-Mitf from these cells may be acetylated at K243. In the presence of HA-p300, more binding was seen from all 3 proteins, in keeping with the enhanced protein levels in the Western blot. As in the absence of HA-p300, a higher salmon sperm DNA concentration was required to compete FLAG-Mitf^{K243Q} from the probe than FLAG-Mitf^{K243R}. In contrast to the absence of HA-p300, the FLAG-Mitf^{WT} competition profile was almost identical to that of FLAG-Mitf^{K243Q}. This suggested that the wild-type protein had been acetylated on K243, and that K243-acetylation, in the full-length protein that has been otherwise post-translationally modified in cells, has a similar effect to a K243Q mutation in recombinant bHLH-LZ proteins. However, it is important to note that the difference between Q and R substitution in this assay is reduced, which suggests that another factor or acetylation site could play a role in determining DNA binding specificity.

4.3 The *in vivo* role of MITF-K243

Having established that Mitf-K243 plays an important role in regulating Mitf DNA binding affinity and specificity, we next wished to investigate the biological role of this amino acid and its modification. To do this, 501mel cells were stably transfected with HA-Mitf^{K243R} or HA-Mitf^{K243Q} in the presence of puromycin selection. Clones were screened for those expressing HA-Mitf at a similar level to endogenous MITF. Achieving a comparable expression level was important to permit

a physiologically relevant analysis of the role of these substitution mutations, and also to facilitate comparison with the 501.HA-Mitf stable cell line used in Chapter 3. The clones meeting this requirement were retained for further analysis (Figure 4.8).

To begin analysing these cell lines, the subcellular distribution of HA-Mitf was examined by immunofluorescence with an anti-HA antibody (Figure 4.9). 501mel cells stained with anti-HA showed only background signal and, when the image was adjusted to maximise signal intensity, revealed that the secondary antibody was excluded from the nucleus in the absence of HA-tagged proteins in the cell (data not shown). After imaging the stable cell lines, including 501.HA-Mitf, it was clear that every cell in all lines expressed HA-Mitf that was predominantly nuclear, as judged by DAPI counterstaining. A small degree of extra-nuclear staining was detected in each cell line. In all cells, HA-Mitf was excluded from some regions of the nucleus. DAPI does not stain nucleoli and, since in some samples DAPI-free nuclear regions
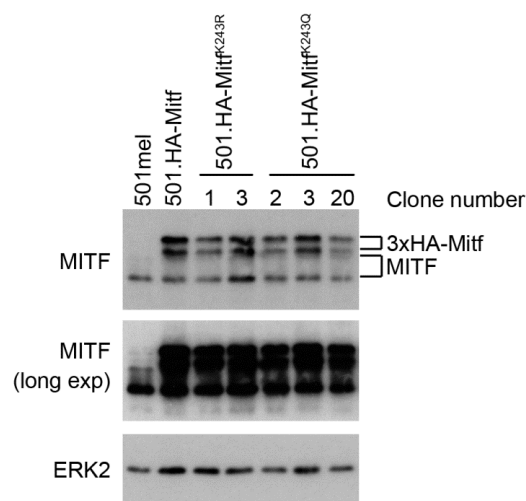
Figure 4.8. Establishing HA-Mitf^{K243R} and HA-Mitf^{K243Q} stable cell lines. 501mel cells were stably transfected with expression vectors encoding HA-Mitf^{K243R} or HA-Mitf^{K243Q} in the presence of a puromycin resistance vector. Clones from each transfection expressing a similar amount of HA-Mitf to the endogenous protein were selected by Western blotting.
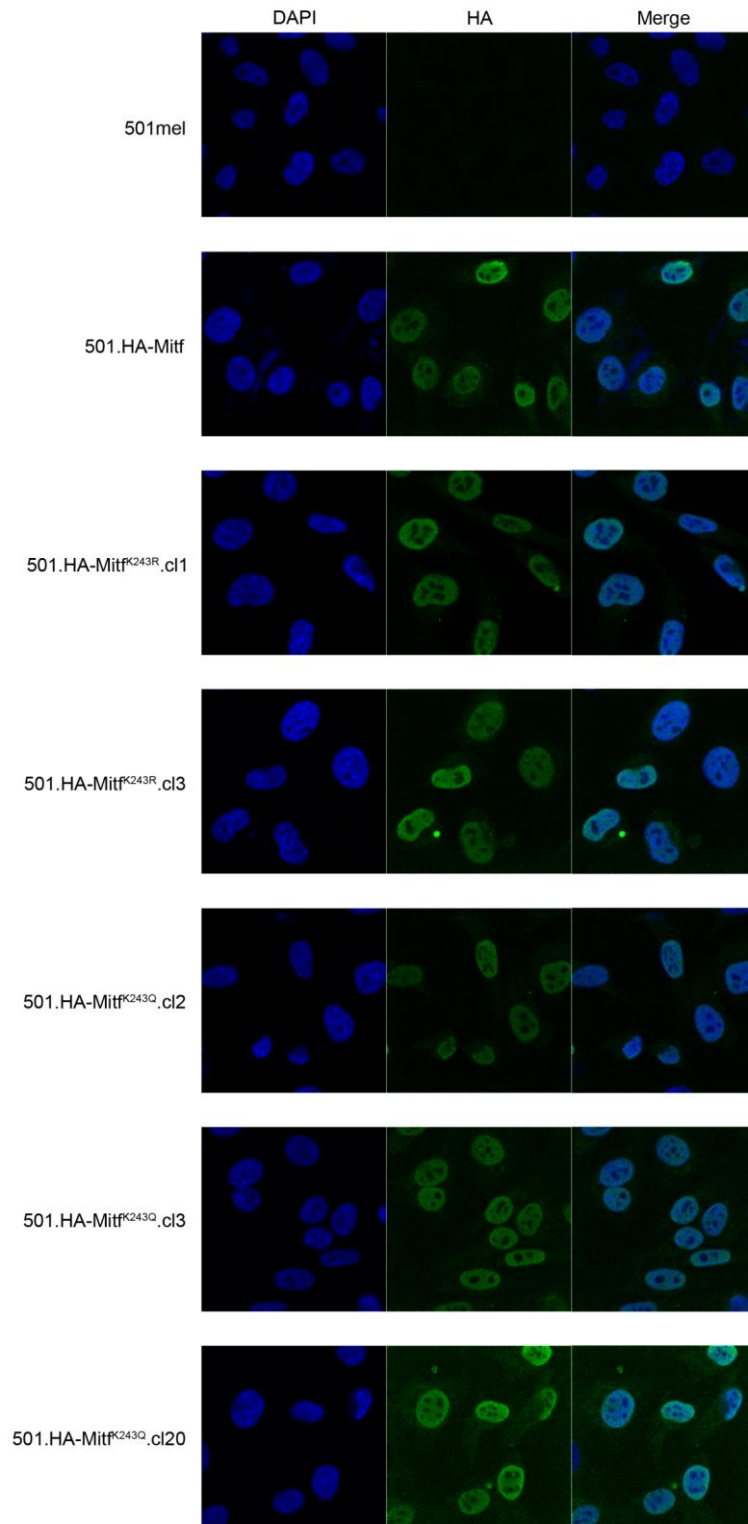
Figure 4.9. Subcellular localisation of HA-Mitf in stable cell lines is similar. Stable cell lines were stained with anti-HA antibody followed by an Alexa-Fluor-488 secondary antibody and counterstaining with DAPI. Slides were analysed by confocal microscopy.

(presumably nucleoli) were co-localised with HA-Mitf-free regions, it is likely that HA-Mitf cannot enter the nucleolus. It was concluded that there is no major difference in subcellular distribution of HA-Mitf^{WT}, HA-Mitf^{K243R}, or HA-Mitf^{K243R}. In addition to unchanged HA-Mitf subcellular localisation was unchanged, the stable cell lines looked morphologically similar (Figure 4.10).

To investigate whether HA-Mitf^{K243Q} increased migratory behaviour, scratch-wound healing assays were performed (Figure 4.11). After 12-15 hours, the wound made in the 501mel culture had closed by 50%. Interestingly, 501.HA-Mitf^{WT} wounds took approximately 40 hours to reach the same degree of closure. It is possible that, with the double-titre of MITF, these cells are less migratory than 501mel cells due to being pushed further up the rheostat. 501.HA-Mitf^{K243R} cells half-closed the wound in
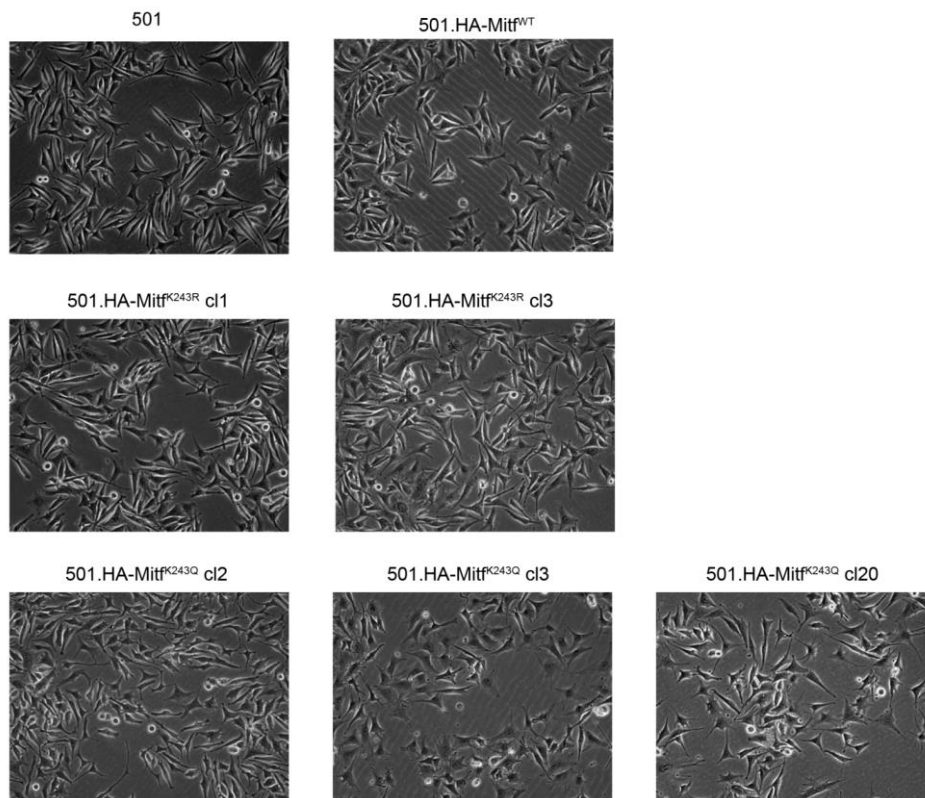
Figure 4.10. HA-Mitf^{K243Q} cell lines have similar morphology. Subconfluent cultures were examined by phase-contrast microscopy and photographed.

around 35 hours, also significantly more slowly than 501mel cells. Both 501.HA-Mitf and 501.HA-Mitf^{K243R} cell lines continued to close the wound more slowly than 501mel cells. 501-HA-Mitf^{K243Q} half-closed the wound after 20 hours, which,
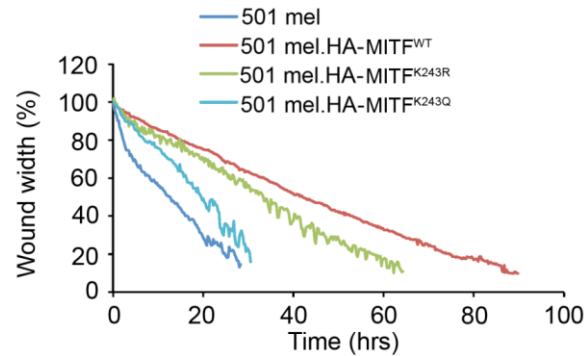
Figure 4.11. HA-Mitf^{K243Q} cell lines enhance wound closure. Stable cell lines were grown to confluence and wounds created with a pipette tip. Timelapse microscopy was used to track wound closure. Each line represents the average of at least 3 biological replicate experiments and, for Mitf^{K243R} and Mitf^{K243Q} mutants, the individual cell lines' results are averaged for greater clarity.
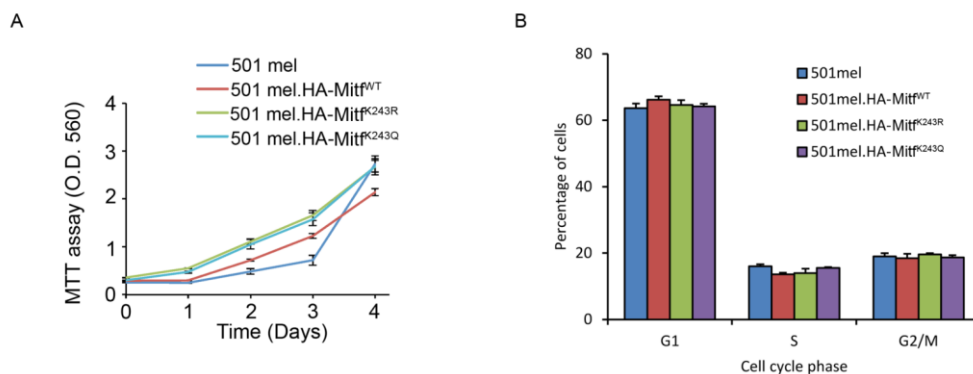
Figure 4.12. HA-Mitf stable cell lines grow at similar rates. For Mitf^{K243R} and Mitf^{K243Q} cell lines, the individual cell lines' results are averaged for greater clarity. (A) 1000 cells were plated in 96-well plates. The next day (day 0) and at subsequent times as shown, cells were subjected to an MTT assay. Data points represent the mean ± standard error of the mean of three independent experiments. (B) Cultures of the indicated cell lines were grown to 50% confluence and cell cycle phase measured by flow cytometry using propidium iodide as a DNA-dye. Results are presented as the mean ± standard error of three independent experiments.

although slower than 501mel, was a difference that was diminished at later time points. This suggested that 501-HA-Mitf^{K243Q} cells are more migratory than 501.HA-Mitf^{K243R} or 501.HA-Mitf^{WT} cells, but not quite as migratory as 501mel cells. One possible reason for the difference between 501mel and 501-HA-Mitf^{K243Q} cells is that, although Mitf^{K243Q} (and presumably acetyl-K243-MITF) could be promoting migration, the addition of extra Mitf to the cell may still up-regulate some of the processes that make 501.HA-Mitf cells less migratory than 501mel cells.

As well as cell migration, closure of a scratch-wound can be affected by proliferation. Therefore, we next examined the proliferation rate of these cell lines. with an MTT assay (Figure 4.12A). There was no discernible difference between 501.HA-Mitf^{K243Q} and 501.HA-Mitf^{K243R} cells throughout the assay, while both grew slightly faster than 501.HA-Mitf cells. 501mel cells grew more slowly than the other three cell lines for the first three days and then their growth accelerated to close the difference. Taken together, this data suggests that there is little difference in the growth rates of these cell lines, indicating that the difference in scratch-wound closure was due to cell migration rather than proliferation. Given that MITF influences cell cycle progression, it was possible that one of these mutations had an impact on the cell cycle without leading to an overall effect on proliferation. Therefore, the cell cycle distribution of each cell line was measured (Figure 4.12B). There was no significant difference between any of the cell lines tested. In all cell lines, around 60-65% of cells were in G1, with a similar split of the remainder between S and G2/M.

4.4 The genome-wide role of MITF-K243

To study the effect of Mitf^{K243R} mutation, 501.HA-Mitf^{K243R}.cl1 cells were used in a ChIP-Seq assay to allow comparison with the 501neg and HA-Mitf samples

from Chapter 3. Uniquely aligned HA-Mitf^{K243R} reads were randomly subsampled to the same number as in the 501neg and HA-Mitf samples (Table 4.1).

Following sequencing analysis, visual inspection of the data revealed that binding of HA-Mitf^{K243R} differed significantly from that of HA-Mitf. Binding was much reduced at the *Tyrosinase* locus (Figure 4.13A). At the promoter, which contains two 5'-TCATGTGC-3' M-boxes on opposite strands that face towards each other, and at the intronic binding site, which contains a 5'-TCACATGG-3' motif, binding is almost entirely lost in HA-Mitf^{K243R} compared to HA-Mitf. The enhancer region at -1.8 kb from the TSS, containing a 5'-TCATGTGA-3' motif, had three-fold reduced binding while the -9 kb region, which does not contain a canonical MITF element, had 1/3 reduced binding in HA-Mitf^{K243R} relative to HA-Mitf. The loss of binding at this locus was surprising, because activation of the *Tyrosinase* promoter luciferase reporter was similar by each protein (Figure 4.3). Therefore, anti-HA ChIP was performed in 501.HA-Mitf and 501.HA-Mitf^{K243R}.cl1 cell lines, and the recovered DNA was used for qPCR directed against the *Tyrosinase* -1.8 kb enhancer element (Figure 4.13B). Amplicons -1 kb from the *Tyrosinase* TSS and the *Protamine* (*Prm*) promoter, which is not known to be bound by MITF, were used as negative control regions. As expected, in neither cell line was enrichment seen in the control regions relative to the input fraction, while the *Tyrosinase* enhancer was enriched. In this assay, binding in 501.HA-Mitf^{K243R}.cl1 was reduced 2.5-fold relative to binding in 501.HA-Mitf cells, in good agreement with the ChIP-Seq result, suggesting that the ChIP-Seq reflects *in vivo* binding.

Table 4.1. ChIP-Seq sequencing statistics.

Sample	Aligned reads	Unique reads	Subsampled reads
501mel	35794085	29237190	29237190
HA-Mitf	52228313	44724616	29237190
HA-Mitf^{K243R}	49737394	43470835	29237190
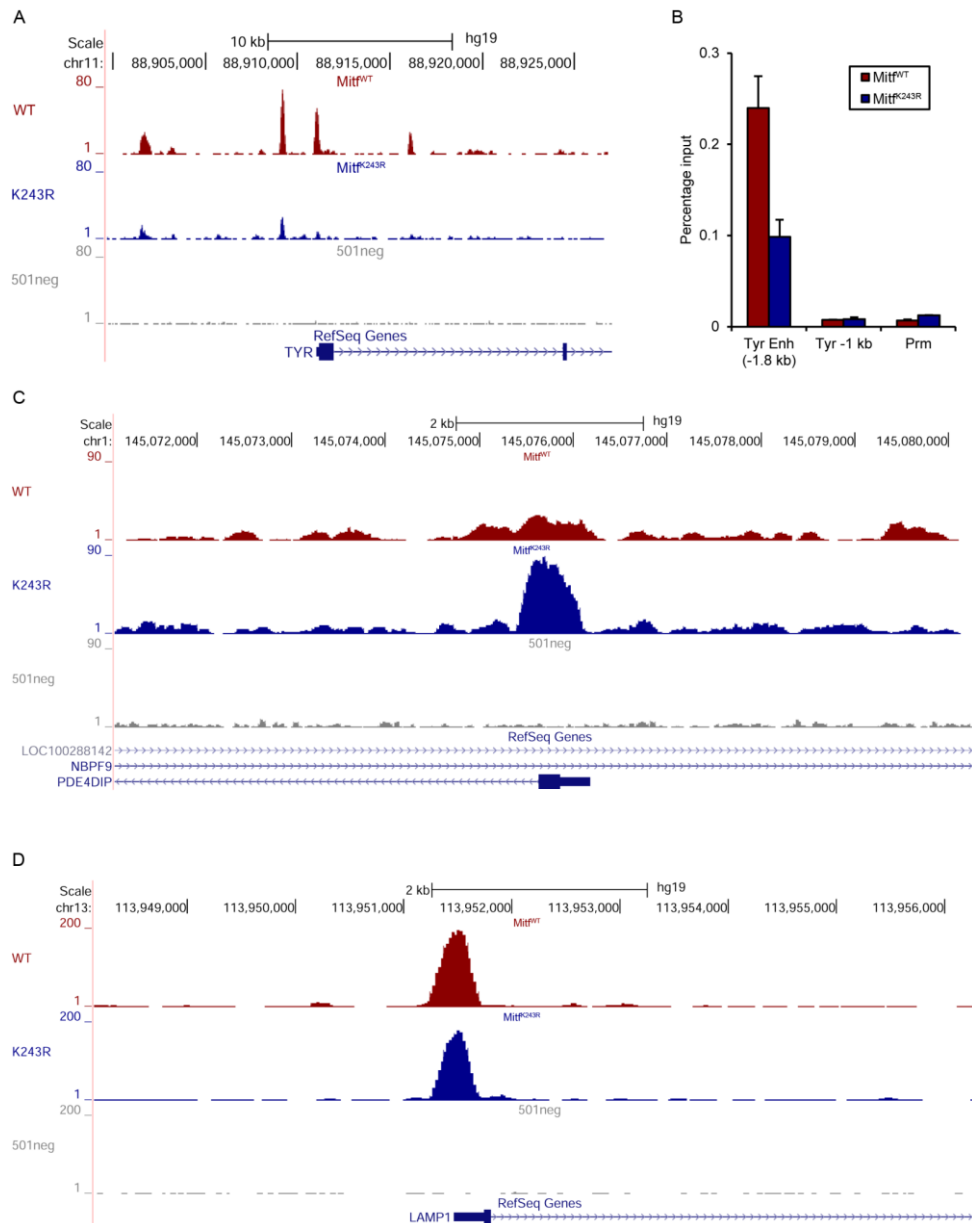
Figure 4.13. HA-Mitf and HA-Mitf^K243R binding varies at some loci. (A), (C), (D) Screenshots from the UCSC Genome Browser showing raw read density of HA-Mitf, HA-Mitf^K243R and 501neg ChIP-Seq samples at different locations (A: *Tyrosinase*; B: *PDE4DIP*; C: *LAMP1*), as indicated by the RefSeq Genes track at the bottom of each image. (B) Anti-HA ChIP in 501.HA-Mitf and 501.HA-Mitf^K243R.cl1 cell lines was performed, following by qPCR analysis against the indicated regions. Tyr: *Tyrosinase*, Prm: *Protamine*. Results are presented as the percentage of the input fraction from each cell line that was recovered, and show the mean of two independent experiments (performed in technical duplicate) ± the standard deviation.

Table 4.2. ChIP-Seq peak statistics

Sample	HA-Mitf	HA-Mitf^{K243R}
MACS2 binding regions	41,070	42,461
Mean binding region height	40	23
Uniquely bound regions	34,871	36,334
Peaks (>40)	14,362	1,308
Unique filtered peaks	13,378	325
Gene-associated filtered peaks	9,037	1,180
Filtered peak-associated genes	5,559	1,098
Unique genes	4,641	174

At some locations, increased HA-Mitf^{K243R} binding was seen relative to HA-Mitf, such as at the promoter of *PDE4DIP*, encoding phosphodiesterase 4D interacting protein (Figure 4.13C). Here, binding by HA-Mitf^{K243R} was approximately 3-fold greater than HA-Mitf. This site is also an intronic region of *NBPF9*, encoding Neuroblastoma breakpoint family member 9. Analysis of the sequence underlying the peak revealed that there was no canonical MITF binding site in the vicinity. Not all binding sites were different between the samples. For example, binding across the *LAMP1* TSS, which contains two 5'-TCACGTGA-3' motifs in the 5'-UTR, was very similar in both samples (Figure 4.13D).

Visual inspection of the data revealed that many locations had different binding in one or other sample. To allow detailed analysis of the differences in these samples, statistically enriched binding regions were identified in the HA-Mitf^{K243R} sample using default MACS2 settings. As before, after peak-calling a q-value threshold of 10^{-10} was applied to the data, which returned 42,461 HA-Mitf^{K243R} binding regions, as compared with 41,070 HA-Mitf peaks (Table 4.2).

To ask whether HA-Mitf and HA-Mitf^{K243R} binding differed genome wide, HA-Mitf-bound regions were ranked according to raw read density in a 1 kb window centred on the summit (rank 1 being the weakest), and the raw read density in 10 bp bins throughout the window calculated and plotted for HA-Mitf and HA-Mitf^{K243R} (Figure 4.14A). While HA-Mitf bound regions showed a smooth decline in read
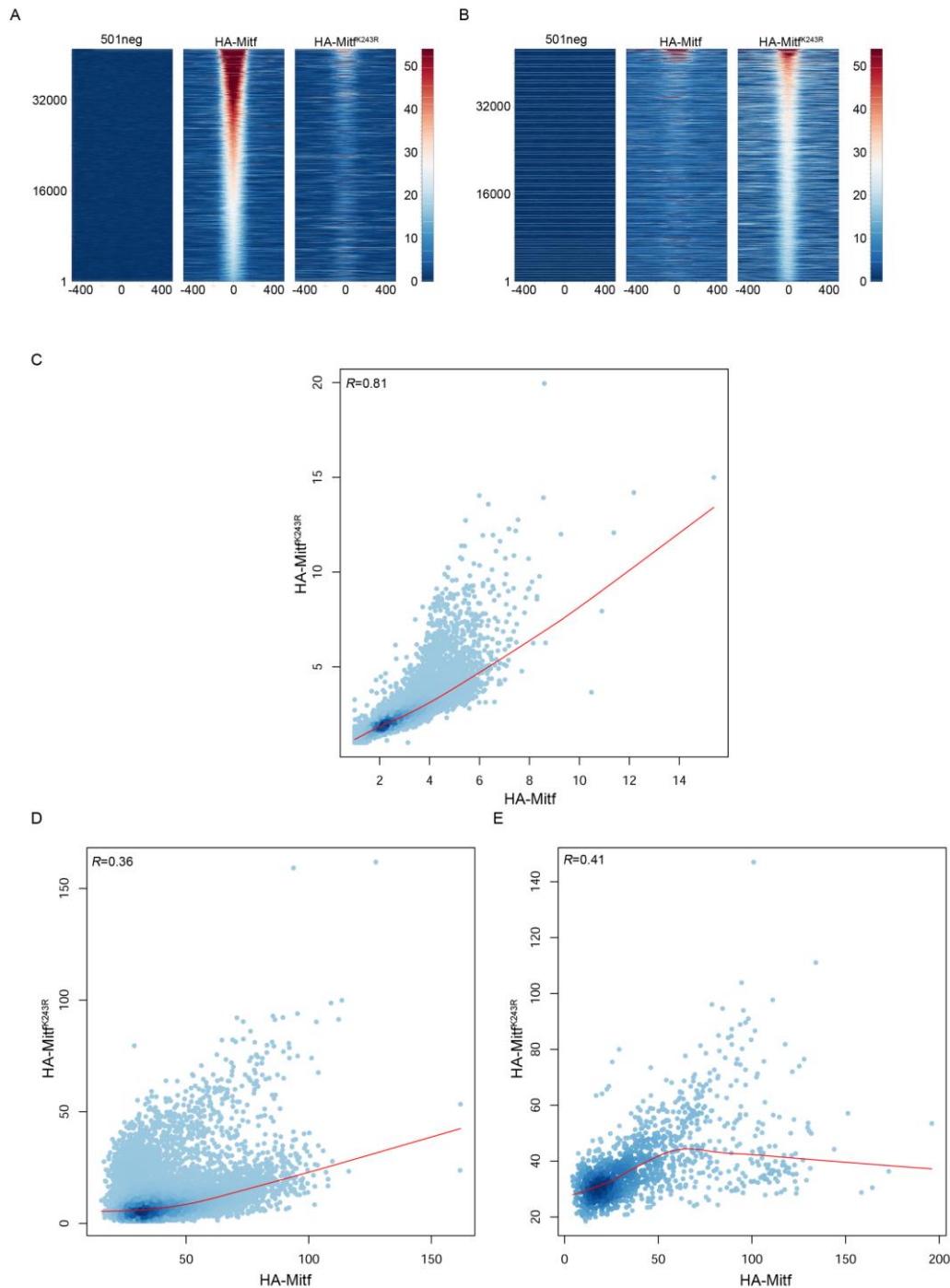
Figure 4.14. HA-Mitf and HA-Mitf^{K243R} binding is poorly correlated genome wide. (A) HA-Mitf bound regions were ranked based on binding strength (rank 1 = weakest) and raw binding density profiled ±500 bp from the summit for 501neg, HA-Mitf and HA-Mitf^{K243R}. Scale bar showing colours used from blue (weakest) to red (maximal) is shown at the left. A polynomial best fit line is plotted. (B) As (A) but using coordinates of HA-Mitf^{K243R} bound regions as a starting point. (C) Pairwise genome-wide correlation analysis between HA-Mitf and HA-Mitf^{K243R} occupancy based on median read density in 100 kb windows. Pearson correlation is shown top left. (D), (E) As (C) but restricted to bases comprising HA-Mitf binding sites (D) or HA-Mitf^{K243R} binding sites (E) rather than the entire genome.

density as rank decreased, there was little concordance with read density in HA-Mitf^{K243R}: there was no region of strong overlap, with the high-read density HA-Mitf^{K243R} regions evenly distributed throughout the HA-Mitf peaks. In a reverse calculation ranking HA-Mitf^{K243R} bound regions, a slightly better overlap between the samples was observed (Figure 4.14B). The decline in read density about the summit in HA-Mitf^{K243R} was sharper than for HA-Mitf, with fewer bound regions reaching maximal density (Figures 4.14A and 4.14B are coloured on the same intensity scale). A small set of the strongest HA-Mitf^{K243R} peak regions showed similarly high read density in HA-Mitf but, as binding strength decreased, the degree of similarity between the samples became very small. Combined, these results suggested that the binding patterns of HA-Mitf and HA-Mitf^{K243R} are dissimilar. To investigate this, the raw ChIP-Seq reads were compared in a genome-wide pairwise correlation calculation. The genome was divided into 100 kb bins, and the median read counts compared in them for HA-Mitf and HA-Mitf^{K243R}. A good correlation was found between the samples (Pearson correlation coefficient R=0.81; Figure 4.14C), reflecting the fact that, although the HA-Mitf and HA-Mitf^{K243R} binding sites appear very different, the vast majority of the genome is unoccupied in each sample. When the analysis was restricted to windows defined by Mitf bound regions, a weaker correlation was observed (Pearson correlation coefficient R=0.36; Figure 4.14D). Some bases had a well-correlated density in this sample, presumably corresponding to overlapping peaks, while the majority of bases (those surrounding the polynomial best-fit line) had less coverage by HA-Mitf^{K243R} than HA-Mitf. A slightly improved correlation was seen using the bases in HA-Mitf^{K243R} bound regions (Pearson correlation coefficient R=0.41; Figure 4.14E), with a similar pattern in the plot. Together, this data suggests that there is a poor correlation between HA-Mitf binding

and HA-Mitf^{K243R} binding. The difference in correlation coefficients between these analyses likely arises because the vast majority of the genome is excluded by the peak-based analysis, permitting small local variations to have a larger effect, while the different scales arise because the majority of bases in each 100 kb window are weakly occupied, while peak-covered bases by their nature are more highly occupied.

To examine the possibility that HA-Mitf^{K243R} binding strength is reduced relative to HA-Mitf , peaks in each sample were divided into bins based on peak height in 10-read increments, and histograms of the frequency of peaks within each sample plotted (Figure 4.15A). As expected, the peak height distribution for HA-Mitf was more skewed than for HA-Mitf^{K243R}. In HA-Mitf, the most populous bin contained peaks of height 21-30 reads and, while the same was true for HA-Mitf^{K243R}, there were more HA-Mitf^{K243R} peaks in it. The 11-20 read bin contained a similar number of HA-Mitf^{K243R} peaks to the 21-30 read bin, while there were very few HA-Mitf peaks. No peaks in either sample were less than 10 reads high at the summit, and the decline in frequency of peaks at greater heights in HA-Mitf^{K243R} was faster than for HA-Mitf.

To ascertain where the binding regions were localised genome-wide, they were divided into different categories (Figure 4.15B). HA-Mitf^{K243R} binding was more dense around gene bodies, with a near three-fold reduction in peaks more than 10 kb away from a gene (distal intergenic). The majority of this loss was offset by a large gain in exonic binding in HA-Mitf^{K243R}. There was reduced intronic binding in HA-Mitf^{K243R} and a modest gain in binding around the TTS (3' UTR, downstream). There was a two- to three-fold increase in binding to the proximal promoter and 5' UTR by HA-Mitf^{K243R} which, coupled with the intronic and TTS changes, suggests that many of the additional exonic regions could be located in exon 1, although this data cannot

confirm this idea. Separate examination of HA-Mitf^{K243R} peaks smaller than 40 revealed an identical distribution of peaks to the total set of peaks (data not shown); this was expected because just 3% of HA-Mitf^{K243R} peaks are higher than 40. It is possible that, if binding by HA-Mitf^{K243R} is weaker than by HA-Mitf, that HA-
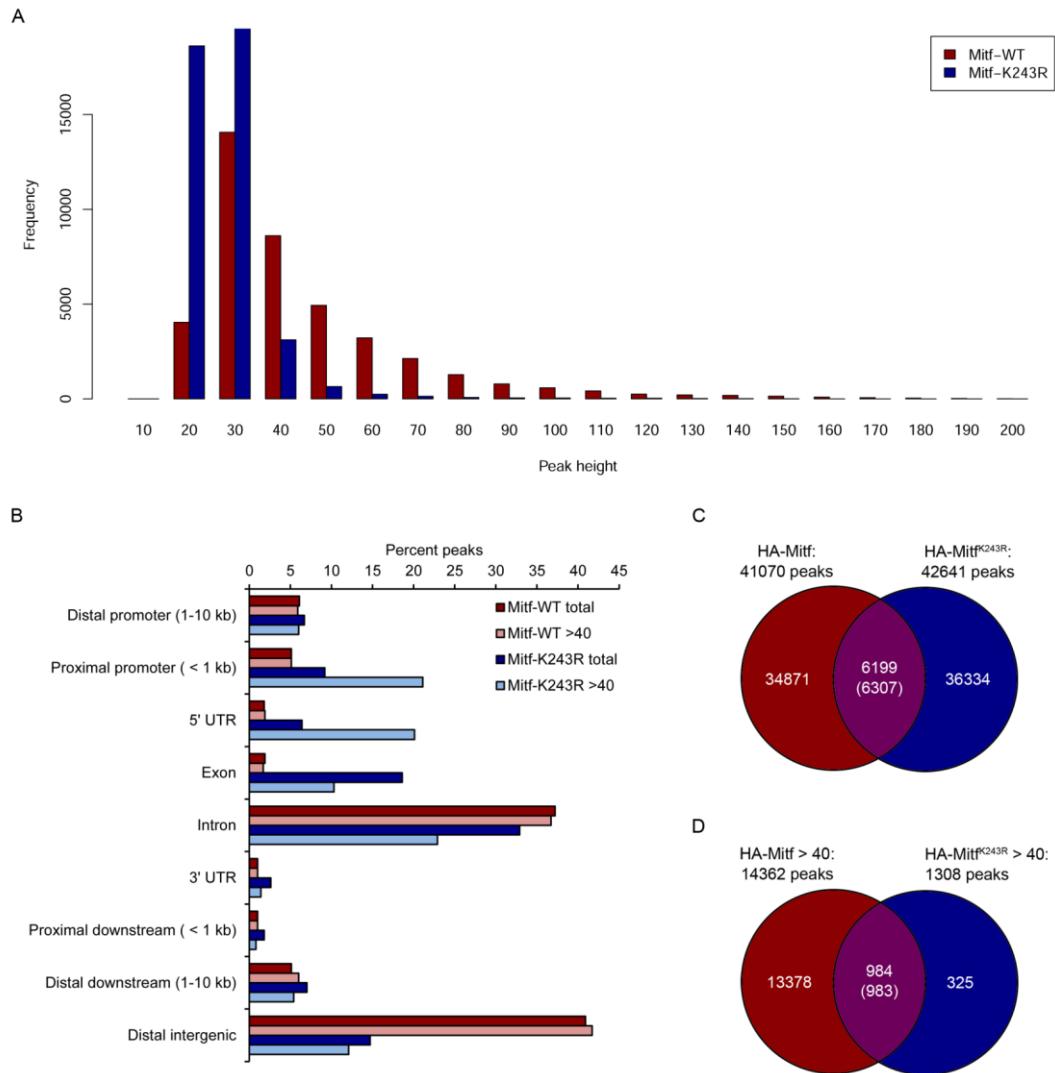
Figure 4.15. HA-Mitf^{K243R} peaks are smaller, differently distributed, and poorly overlapping with HA-Mitf peaks. (A) HA-Mitf and HA-Mitf^{K243R} peaks were divided into 20 bins of equal width based on increasing peak height, and histograms plotted. (B) The distribution of all HA-Mitf and HA-Mitf^{K243R} peaks, and peaks with height > 40, was analysed. (C) Venn diagram showing the proportion of common and unique peaks between all HA-Mitf and HA-Mitf^{K243R} peaks. In the centre, the number outside the brackets denotes the number of HA-Mitf peaks, and the number inside the brackets denotes the number of HA-Mitf^{K243R} peaks. (D) As in (C) but using peaks with height > 40 as a starting point.

Mitf^{K243R} binding is more restricted to areas of open chromatin than HA-Mitf, although this analysis cannot confirm this idea.

As in Chapter 3, because there are more bound regions in both these samples than genes in the genome, a conservative height filter of 40 reads was applied to leave only the most significant peaks in each sample. This cut-off is likely to be set too high to catch every real binding event, but will encompass the major binding sites. After filtering, 14,362 HA-Mitf peaks and 1,308 HA-Mitf^{K243R} peaks remained (Table 4.2). Analysis of the distribution of these remaining peaks revealed that the HA-Mitf peaks were very similarly distributed between the total and filtered peaks (Figure 4.15B). In HA-Mitf^{K243R}, however, there was a further loss of binding in introns and a reduction in exonic peaks. This was compensated for by a two- to three-fold gain in binding in the proximal promoter and 5' UTR.

In confirmation of the notion that overall binding between these samples was different, total peak coordinates were intersected (Figure 4.15C and Table 4.2). Just 6,199 HA-Mitf peaks overlapped with 6,307 HA-Mitf^{K243R} peaks, a conservation rate of 15%. The majority of bound regions were unique for each sample. The disparity in the number of common peaks in each sample indicates that a number of HA-Mitf bound regions must intersect multiple HA-Mitf^{K243R} regions. For peaks greater than 40, 984 HA-Mitf filtered peaks overlapped with 983 HA-Mitf^{K243R} peaks, a conservation rate of 6% for HA-Mitf and 75% for HA-Mitf^{K243R} that reflects the different numbers of peaks in the samples. To find out what genes were bound in each sample, filtered peaks were associated with a gene if they lay within 20 kb of the gene body (Table 4.2), and the peak coordinates intersected (Figure 4.15D). HA-Mitf was associated with 5,559 genes, of which 4,641 were uniquely occupied, while HA-Mitf^{K243R} was associated with 1,098 genes, of which 174 were uniquely occupied.

This data suggested that Mitf, particularly HA-Mitf^{K243R}, was enriched around the TSS. To examine this, histograms were plotted showing summit density of all HA-Mitf and HA-Mitf^{K243R} peaks with summits lying in a 2 kb window centred on the TSS (Figure 4.16A). While HA-Mitf was centred at -1 to -100, and showed a faster decline downstream from the TSS than upstream from this bin, the opposite was true for HA-Mitf^{K243R}. This sample was centred in the +1 to +100 bin, and showed a rapid decline upstream from the TSS, while coverage downstream of the TSS remained high. In peaks higher than 40, however, both samples were maximally enriched in the -1 to -100 bin, with a similar upstream decline in density (Figure 4.16B). Downstream from the TSS, HA-Mitf^{K243R} was more enriched than HA-Mitf in the +1 to +100 bin; both samples had relatively low enrichment further downstream.

So far, HA-Mitf binding has been seen to be very different from HA-Mitf^{K243R} binding. Mitf^{K243R} bound more degenerate sequences *in vitro* than Mitf^{K243Q}. To see whether the same might be true for HA-Mitf and HA-Mitf^{K243R}, 60 bp regions around the summit of the top 900 peaks in each sample were subjected to *de novo* motif prediction. The most enriched motif in each sample was very similar, comprising a 5'-TCACGTGAC-3' element, with a mix of G/A upstream and preferentially C downstream (Figure 4.16C, D). The identified motifs, at various levels of enrichment, were all centred on 5'-CACGTG-3' rather than 5'-CATGTG-3', suggesting that in the most significant, and hence largest, peak regions, it tends to be an E-box that is bound rather than an M-box.

To begin to understand motif preferences between HA-Mitf and HA-Mitf^{K243R}, peaks were divided between those containing a 5'-CACGTG-3' or 5'-CATGTG-3' motif for both the total and filtered sets of peaks, or those lacking such a motif (Figure 4.17A). The vast majority of peaks bound by HA-Mitf contain at least
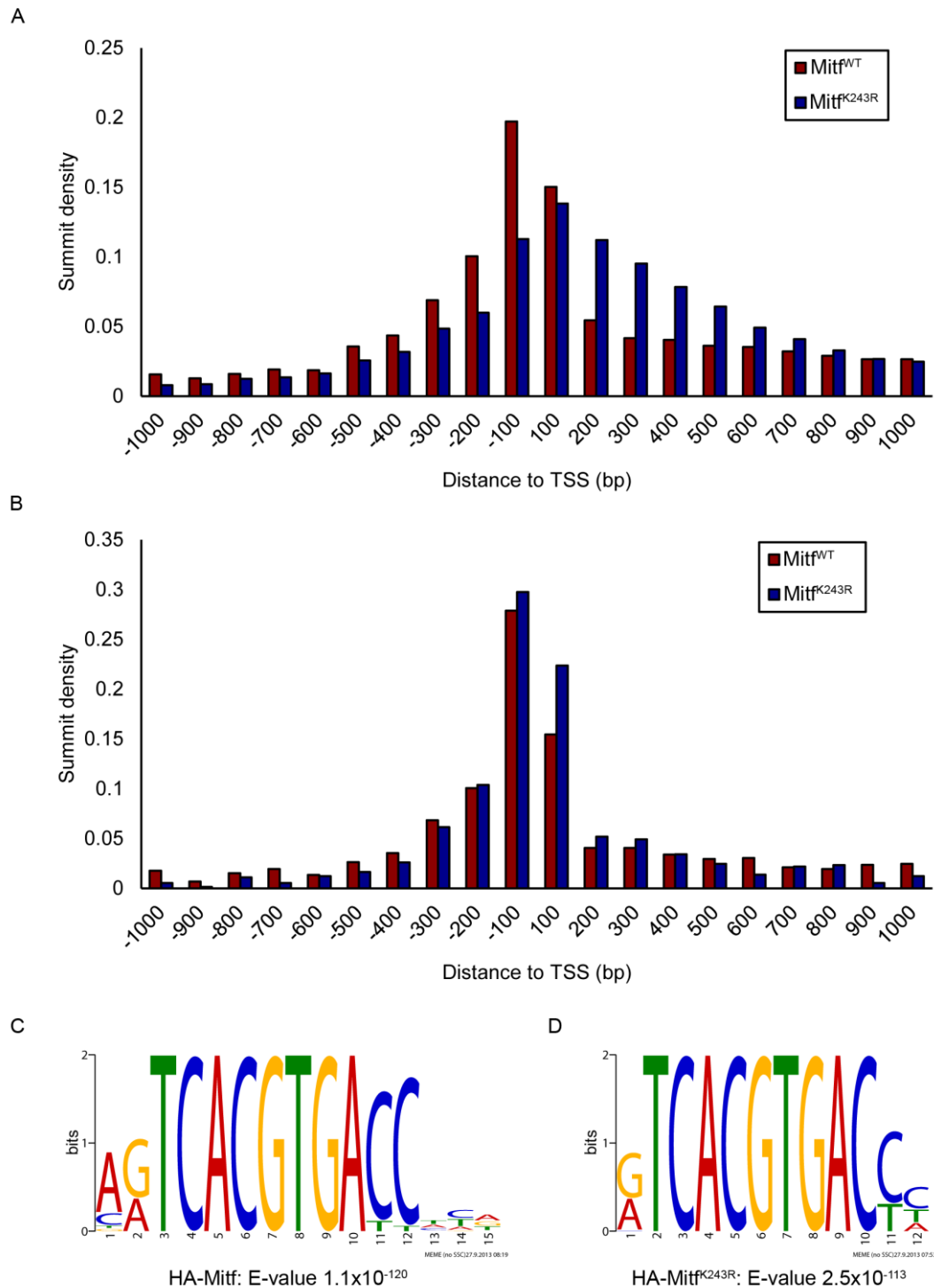
Figure 4.16. HA-Mitf and HA-Mitf[K243R] are enriched at the TSS and have a similar *de novo* predicted consensus motif. (A) Summits of all HA-Mitf and HA-Mitf[K243R] peaks within 1 kb of a TSS were assigned to bins based on the distance to the TSS. (B) As (A) but using peaks higher than 40 as input. (C) *De novo* motif prediction was performed on the 60 bp surrounding the summit of the top 900 HA-Mitf peaks. (D) As (C) but using the top 900 HA-Mitf[K243R] peaks.

one motif, and the percentage lacking a motif decreases in the filtered peaks. For HA-Mitf^{K243R}, more peaks in the total peak set have no motif, indicating that, since the total peak count in each sample is similar, HA-Mitf^{K243R} binding is more degenerate. Indeed, the ratio of motif:no motif is similar to that of a length- and location-matched set of control regions, suggesting that HA-Mitf^{K243R} does not occupy specific motifs with a much greater frequency than would be expected at random. In the filtered peaks, however, only 24% of peaks lack a motif, indicating that the peaks missing motifs are predominantly the smaller ones. The common and unique filtered peaks for each sample were examined in the same way (Figure 4.17B). 85% of common peaks contained a motif, compared to 96% of HA-Mitf-unique peaks. However, only 51% of HA-Mitf^{K243R}-unique peaks were motif-containing, indicating that, as with lower peaks, sites that were not also occupied by HA-Mitf were less likely to contain a canonical binding motif.

Next, the relationship between peak height and motif prevalence was investigated. Peaks were binned by height and the percentage of peaks with or without a motif in each bin plotted for HA-Mitf and HA-Mitf^{K243R} (Figure 4.17C). This revealed that, for both samples, the peaks lacking motifs are clustered at the lower end of the peak spectrum. The smallest height bin is the only one containing proportionally more peaks that lack a motif than contain one. However, HA-Mitf^{K243R} peaks lack motifs at much higher frequency than HA-Mitf peaks, and peaks lacking motifs in this sample persist at relatively high frequency until much greater peak height than for HA-Mitf. Indeed, HA-Mitf bins contain comparatively few peaks lacking a motif at any height. When common peaks in each sample were examined (Figure 4.17D), it was anticipated that the motif pattern should be similar for HA-Mitf and HA-Mitf^{K243R}. However, the common peaks closely resembled the total set of
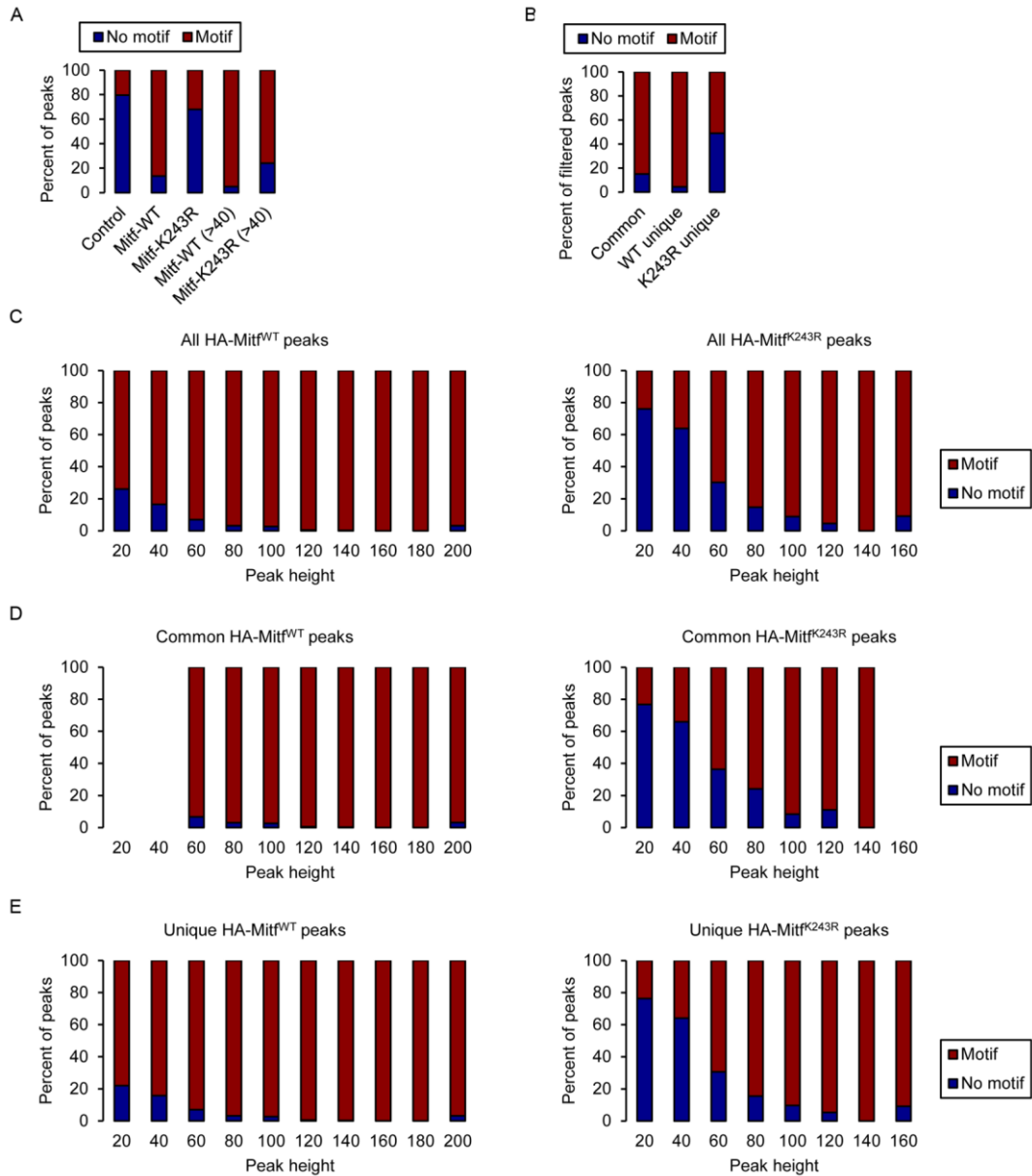
Figure 4.17. HA-Mitf peaks are more associated with E/M-box motifs than HA-Mitf^K243R. (A) Peaks in the total or >40 peaksets for HA-Mitf and HA-Mitf^K243R were divided by presence or absence of a 5'-CA[C/T]GTG-3' motif. Control peaks are length and location matched. (B) Common and unique HA-Mitf and HA-Mitf^K243R peaks higher than 40 were divided by presence or absence of a 5'-CA[C/T]GTG-3' motif. (C) Charts of HA-Mitf (left) and HA-Mitf^K243R peaks (right) at a given height with or without a 5'-CA[C/T]GTG-3' motif. Bars are presented as the percentage of peaks at each height with or without a motif. (D) As in (C) but analysing common peaks. (E) As in (C) but analysing unique peaks.

peaks for each sample, despite comprising only approximately 15% of the peaks from each sample. This suggests that, although these peaks overlap, they do not share a majority overlap and that, for the most part, the HA-Mitf^{K243R} binding is offset from the HA-Mitf peak. When unique peaks were considered (Figure 4.17E), again the motif:no motif ratios at each peak height were very similar to the total set of peaks. Taken together, this result adds further to the notion that the binding profile of HA-Mitf^{K243R} is largely distinct to and more degenerate than that of HA-Mitf, with HA-Mitf^{K243R} being less prevalent at motif-containing loci.

We next wished to find out if there was a difference in motif binding preference in each sample. Instances of different flanking sequence for 5'-CACGTG-3' and 5'-CATGTG-3' motifs were counted for HA-Mitf and HA-Mitf^{K243R} peaks and normalised for the total number of motifs bound in each sample (Figure 4.18A). HA-Mitf bound more 5'-CATGTG-3' than 5'-CACGTG-3' motifs. Half of 5'-CATGTG-3' motifs were 5'-TCATGTGA-3' motifs, whereas statistically only 1/16 should have had these precise flanking bases. 5'-VCATGTGB-3' comprised about a quarter of the 5'-CATGTG-3' motifs. Among 5'-CACGTG-3' motifs, half were 5'-TCACGTGB-3' and a quarter each were 5'-TCACGTGA-3' and 5'-VCACGTGB-3'. HA-Mitf^{K243R} bound approximately even numbers of 5'-NCATGTGN-3' and 5'-NCACGTGN-3' motifs, of which 60% were 5'-VCA[C/T]GTGB-3'. Among motifs flanked by 5'-T most contained a single 5'-T. The analysis was repeated for peaks higher than 40 (Figure 4.18B). In HA-Mitf higher than 40, the motifs were very similarly distributed to the total set of peaks, but there was a rise in 5'-TCACGTGA-3' at the expense of 5'-TCACGTGB-3' motifs. In HA-Mitf^{K243R} peaks higher than 40, 73% were 5'-CACGTG-3', with a similar split between 5'-TCACGTGA-3', 5'-TCACGTGB-3', and 5'-VCACGTGB-3'. Among the small number of 5'-CATGTG-3' motifs bound
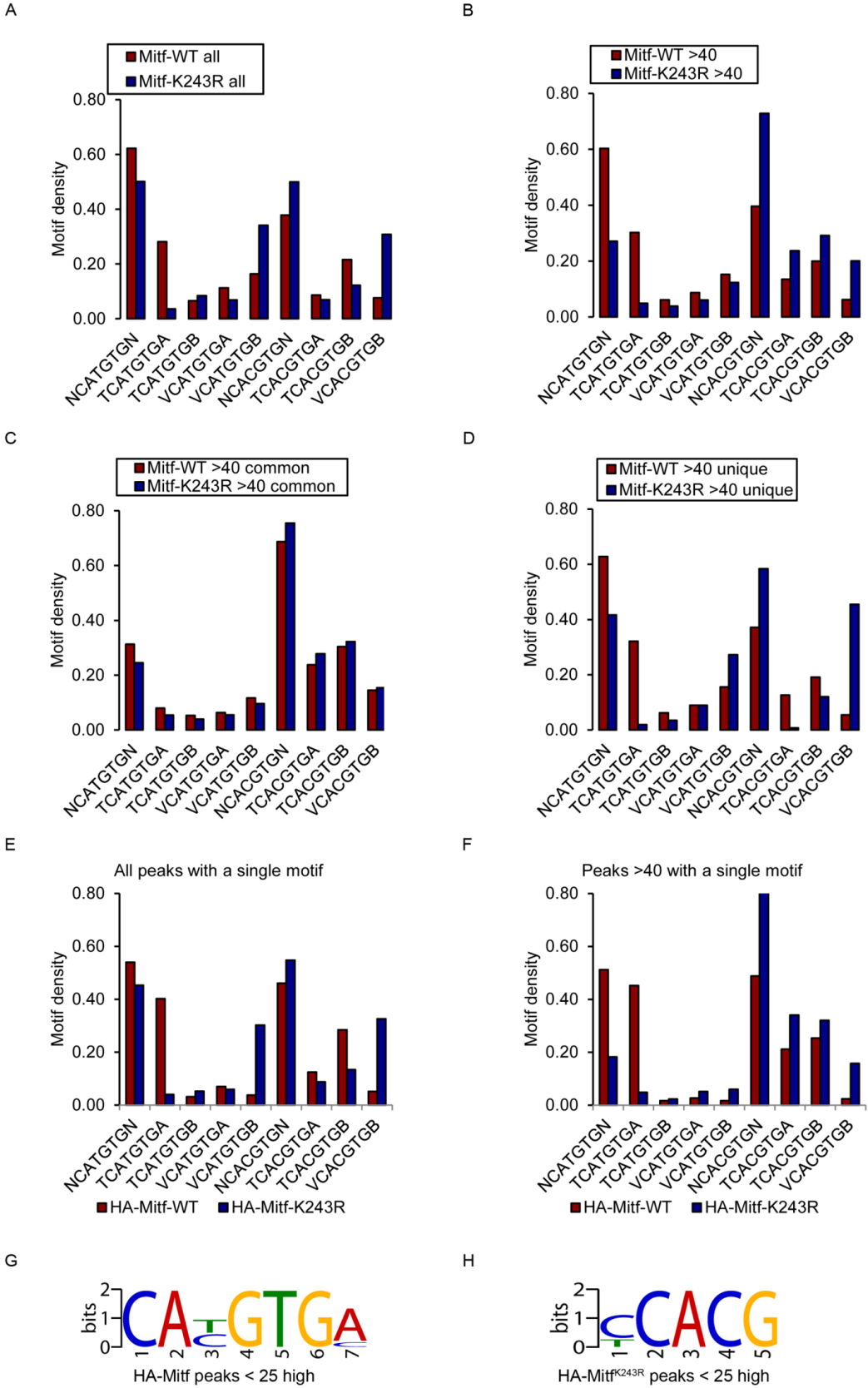
Figure 4.18. HA-Mitf^{K243R} peaks are more enriched in CACGTG and do not contain 5'-TCA[C/T]GTGA-3' motifs. [Legend continues on next page.]

by the mutant, more 5'-VCATGTGB-3' motifs were occupied than 5'-TCATGTGA-3', 5'-TCATGTGB-3', or 5'-VCATGTGA-3' motifs. Among commonly occupied peaks (Figure 4.18C), the distribution of motifs is similar to that of the total set of HA-Mitf^{K243R} peaks, with most motifs being 5'-TCACGTGA-3' or 5'-TCACGTGB-3'. This observation makes sense because 83% of motifs bound by HA-Mitf^{K243R} are in peaks commonly bound by HA-Mitf. Among uniquely occupied peaks a striking difference in motif binding distribution was seen (Figure 4.18D). HA-Mitf unique peaks contained predominantly 5'-CATGTG-3' motifs, of which the majority were 5'-TCATGTGA-3'. Most of the rest were 5'-TCACGTGB-3', 5'-VCATGTGB-3', and 5'-TCACGTGA-3' motifs. In HA-Mitf^{K243R} peaks, however, half of all motifs bound were 5'-VCACGTGB-3', a 10-fold gain over HA-Mitf peaks. There was a small increase in binding to 5'-VCATGTGB-3' motifs. The most dramatic change was seen in binding to 5'-TCATGTGA-3' and 5'-TCACGTGA-3', which were almost entirely unoccupied by HA-Mitf^{K243R}.

From manual inspection of the data, some peaks contain multiple motifs. These motifs could potentially act additively or synergistically, or indeed not all the motifs under a peak actually be occupied, the latter of which cannot be determined with an experiment of this resolution. Therefore the analysis was repeated in HA-Mitf

Figure 4.18. HA-Mitf^{K243R} peaks are more enriched in CACGTG and do not contain 5'-TCA[C/T]GTGA-3' motifs. Note the sum density of each series in this figure is 2 because each motif was counted twice, once as N…N, and once with the specified flanking sequences. (A) The proportion of different flanking sequences as shown for 5'-CACGTG' and 5'-CATGTG-3' motifs in all HA-Mitf and HA-Mitf^{K243R} peaks was assessed. (B) The proportion of different flanking sequences as shown for 5'-CACGTG' and 5'-CATGTG-3' motifs in HA-Mitf and HA-Mitf^{K243R} peaks > 40 was assessed. (D) As (A) but using common peaks > 40. (D) As (A) but using unique peaks > 40. (E) As (A) but using peaks containing just a single motif. (F) As (A) but using peaks > 40 that contain a single motif. (G) 60 bp around the summit of the top 900 HA-Mitf peaks with height < 25 was submitted for *de novo* motif discovery. (H) As (G) but using HA-Mitf^{K243R} peaks.

(24520) and HA-Mitf^{K243R} (10099) peaks that contain a single motif (Figure 4.18E). HA-Mitf bound a greater proportion of 5'-TCATGTGA-3' and 5'-TCACGTGB-3' in its single motif peaks and slightly more 5'-TCACGTGA-3' with a compensating reduction in other motifs. HA-Mitf^{K243R} bound similar ratios of motifs. When peaks containing a single motif and higher than 40 were analysed (Figure 4.18F), a difference was observed. HA-Mitf again bound to a greater proportion of 5'-TCATGTGA-3', 5'-TCACGTGA-3' and 5'-TCACGTGB-3' in single motif peaks. HA-Mitf^{K243R} bound almost no 5'-NCATGTGN-3' motifs in its single motif peaks over 40, with most peaks containing a single 5'-TCACGTGN-3' motif. This is consistent with the idea that 5'-TCACGTGN-3' is the highest specificity binding site, to which Mitf^{K243R} can bind against genome-wide competition from non-specific sequences.

From the *in vitro* analysis (Figure 4.5), it is not the case that HA-Mitf^{K243R} cannot bind these sequences. This, in turn, suggests that, because the affinity of non-acetyl-K243 Mitf for general DNA or degenerate E/M-boxes is greater than that of acetyl-K243 (K243Q) Mitf, HA-Mitf^{K243R} is being titrated away from the highly specific binding sites such as those flanked by 5'-T on both strands of the motif by less specific binding sites. To test this, consensus motifs were predicted *de novo* for the 900 most significant peaks with height less than 25. For HA-Mitf (Figure 4.18G), the consensus was 5'-CA[C/T]GTGA-3', which is close to the consensus predicted for the highest affinity binding sites. This suggests that HA-Mitf peaks retain specific binding sites until low heights (below the height cut-off employed here). Interestingly a mix of 5'-CACGTG-3' and 5'-CATGTG-3' motifs were recovered, further adding to the idea that 5'-CATGTG-3' is not found in the highest affinity sites. For HA-Mitf^{K243R} (Figure 4.18H), however, only a degenerate 5'-CACG-3' consensus could

be observed. This is the same level of degeneracy as could be bound by His-Mitf^{K243R}.180-296 *in vitro*. Together, this data strongly supports the notion that HA-Mitf^{K243R} is rapidly titrated away from high affinity binding sites as peak height decreases.

From visual inspection of the sequences underlying the peaks, some peaks, often large ones such as those found at the *LAMP1* TSS (Figure 4.13D), were seen to contain multiple motifs. To test this across all binding sites, HA-Mitf and HA-Mitf^{K243R} peaks higher than 40 were first divided by those containing 0, 1, 2 or 3+ motifs. Among both samples, most peaks contained 1 motif (Figure 4.19A), while there was a greater proportion of HA-Mitf^{K243R} than HA-Mitf peaks with 0 motifs. Peaks with 2 or 3+ motifs were, as expected, less abundant in both samples, but they were similarly abundant between each sample. Next, peaks were separated by height and, within each bin, the proportion containing 0, 1, 2 or 3+ motifs was assessed. For HA-Mitf (Figure 4.19B), very few peaks in each bin lacked a motif. The proportion of peaks containing 1 motif dropped by almost half between the smallest and largest peaks, while the proportion of peaks containing 2 motifs increased by a third. However, peaks containing 3 or more motifs had a five-fold increase in prevalence between the smallest and largest peaks. Among HA-Mitf^{K243R} peaks the proportion of peaks at a given height lacking a motif was greater than for HA-Mitf (Figure 4.19C). The proportion of peaks containing 1 motif in each of the first 4 bins was similar, before declining with further increases in peak height. For peaks containing 2 motifs, abundance rose to become the relatively most abundant in the 121 to 140 peak height bin, while peaks with 3 or more motifs rose in abundance, then diminished, before climbing to be the most prevalent in the very highest peaks. This result indicated that

A

B

C
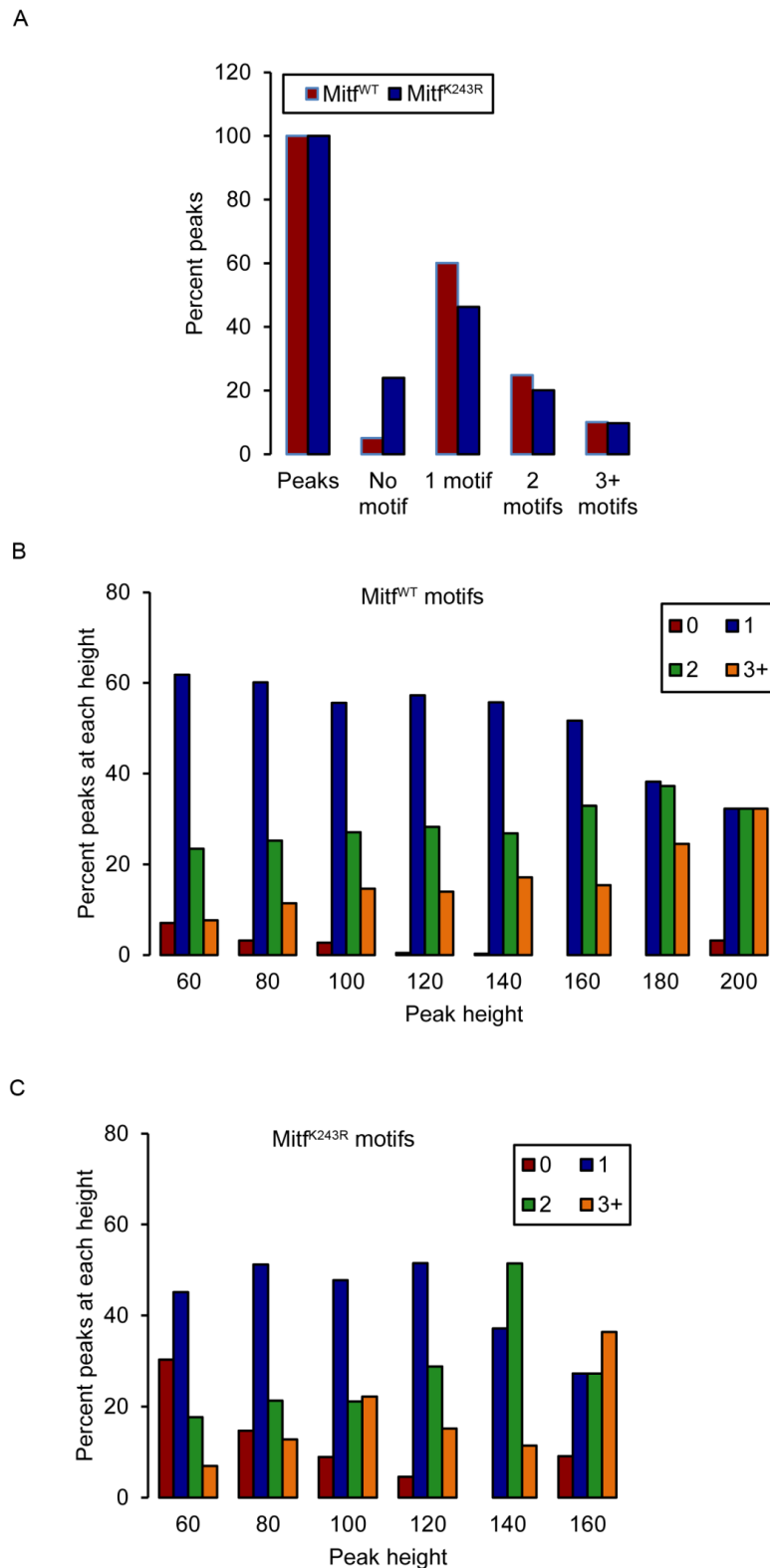
Figure 4.19. Higher peaks contain more motifs. (A) The percentage of HA-Mitf and HA-Mitf^{K243R} peaks > 40 with the indicated number of motifs was counted. (B) For HA-Mitf peaks, the percentage of peaks containing the indicated numbers of motifs in each peak height bin was assessed. (C) As in (B) but using HA-Mitf^{K243R} peaks.

the larger an HA-Mitf peak is, the more likely it is to contain multiple motifs and that, although the distribution is different for HA-Mitf^{K243R}, the same rule holds true.

The data so far suggests that HA-Mitf^{K243R} is titrated away from specific MITF binding sites as a result of its increased affinity for DNA, and it predicts that acetyl-K243 MITF should be bound to high specificity sites. However, some very high affinity sites are still occupied by HA-Mitf^{K243R}, so it is not the case that all high affinity sites are not bound by HA-Mitf^{K243R}. We have found that hair follicles in mice restrict acetylation to proliferating cells, as judged by pan-acetyl-lysine and Ki-67 staining (Rasmus Freter, personal communication). Therefore Ac-K243-MITF will only be found in proliferating cells, meaning that the very high affinity sites bound by HA-Mitf^{K243R} will form a repertoire of acetylation-independent targets genes.

In a preliminary examination of these very high affinity binding sites, peaks that had a height greater than 100 were extracted to represent the acetylation-independent genes, corresponding to approximately the top 10% of peaks in each sample. 1,430 HA-Mitf and 112 HA-Mitf^{K243R} peaks were in these datasets, of which 110 peaks were commonly bound between the two samples (Figure 4.20A). Lowering the peak height threshold would increase the number of common peaks. However, as well as being commonly bound by each protein, the truly acetylation-independent genes should also be bound with similar affinity. Although there will be variation in the peak height of intersecting peaks of height greater than 100, because the maximal peak size in either set is close to but not quite 200, there cannot be more than a two-fold difference in binding in the peak, which is generally taken as the threshold for assessing differential binding or expression.

Among the peaks higher than 100, one of the two HA-Mitf^{K243R} unique peaks lacked a motif and the other contained a single 5'-TCATGTGB-3' motif (Figure
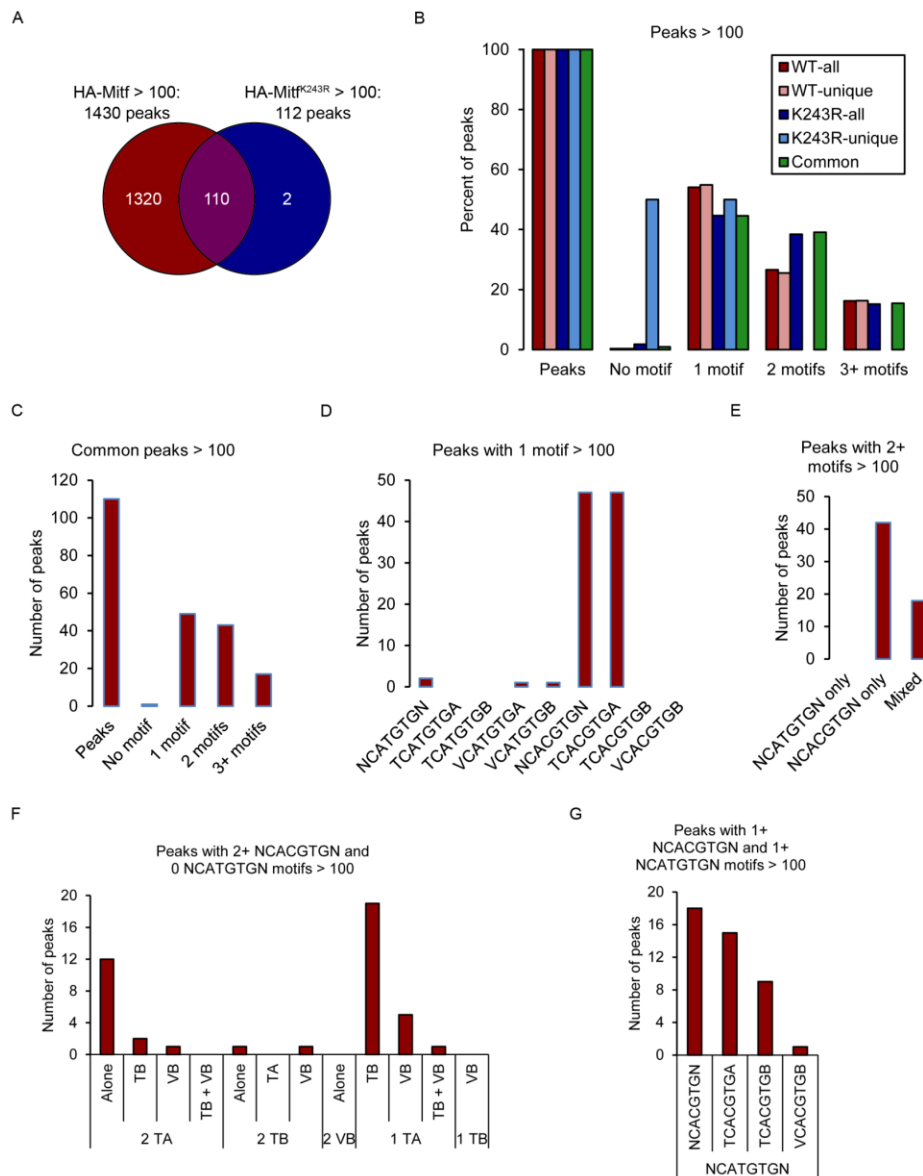
Figure 4.20. Motif analysis in peaks higher than 100. (A) HA-Mitf and HA-Mitf^{K243R} peaks with height greater than 100 were intersected. (B) The number of motifs occurring in all, common, and unique peaks higher than 100 was assessed. (C) The number of peaks containing the indicated number of motifs in commonly bound peaks higher than 100 was assessed. (D) Common peaks containing just 1 instance of the shown motifs were counted. (E) Common peaks containing 2 or more occurrences of only 5'-NCATGTGN-3' or 5'-NCACGTGN-3' motifs, or at least 1 of each, were counted. (F) For common peaks containing 2 or more 5'-NCACGTGN-3' motifs and no 5'-NCATGTGN-3', different combinations of flanking sequences of 5'-CACGTG-3' motifs were assessed. (G) As (F) but for the mixed peaks from (E).

4.20B). Around 50%-60% of peaks in the other sets examined (HA-Mitf total and unique, HA-Mitf^{K243R} total, and the commonly occupied loci) contained 1 motif, and a decreasing proportion had either 2 or 3+ motifs. Among the common peaks, which are essentially an identical set to the total HA-Mitf^{K243R} peaks, a greater proportion of peaks contain 2 motifs than contain the HA-Mitf total or unique peaks, and there are slightly fewer instances of 3+ motifs. To begin to search for a motif-binding signature in high affinity MITF target genes, the common peaks were examined (Figure 4.20C, also a series in Figure 4.20B). Of 110 common peaks, 49 contained 1 motif, 43 contained 2 motifs and 17 contained 3+ motifs. Just 1 peak contained no motif at all. When the 49 peaks containing just 1 motif were examined (Figure 4.20D), 47 contained 5'-TCACGTGA-3' motifs, clearly suggesting that this is the one to which HA-Mitf^{K243R} is most likely to bind in the class of acetylation-independent target genes. Among peaks containing 2 or more motifs, none contained just 5'-NCATGTGN-3' motifs, 42 contained just 5'-NCACGTGN-3' motifs, and 18 contained more than 1 of each (Figure 4.20E), further suggesting that 5'-CACGTG-3' is the major motif in K243 acetylation-independent targets. Next, the 42 peaks containing 2 or more 5'-NCACGTGN-3' motifs were examined for flanking sequence preference (Figure 4.20F). 19 contained at least 1 5'-TCACGTGA-3' and 1 or more 5'-TCACGTGB-3' motif, and 12 contained just 5'-TCACGTGA-3' motifs, suggesting that 5'-TCACGTGN-3' is the major requirement within these very strong peaks. Similarly, among the 18 mixed motif peaks from Figure 4.20E, all contained at least 1 5'-TCACGTGN-3' motif alongside their 5'-NCATGTGN-3' motif (Figure 4.20G). Taken together, this data also suggests that the highest affinity MITF binding sites will contain multiple motifs, and that, where there is only one MITF binding site,

there might be a binding site close by for another factor with which MITF can interact. Further work will be required to investigate this notion.

To find out if there were significant biological differences in the genes bound by each sample, the 1,000 most significantly occupied genes were analysed for enriched KEGG pathways (Figure 4.21A, B). While lysosomes, melanoma, and MAPK signalling were shared between the samples, uniquely enriched HA-Mitf pathways included the cytoskeleton and interactions with the extra-cellular matrix (Figure 4.21A), and uniquely enriched HA-Mitf^{K243R} terms were for metabolic pathways (Figure 4.21C). Following GO analysis of these lists of genes (Figure 4.21B, D), proteins involved in transport, many of them metabolite transporters, were significantly enriched in both samples, along with the lysosome and endosomal pathways. Actin-binding and apoptosis-regulating proteins were enriched in HA-Mitf (Figure 4.21C), while the endoplasmic reticulum and albinism were enriched in HA-Mitf^{K243R} (Figure 4.21D). This suggested that, like HA-Mitf, HA-Mitf^{K243R} can play a major role in regulating lysosomes and metabolism. These genes could therefore be controlled by MITF in an acetylation-independent manner, and their expression would be dependent on *MITF* expression levels.

To understand how these processes might be differentially regulated between HA-Mitf and HA-Mitf^{K243R}, genes associated with common and unique peaks higher than 40 were analysed. Among common peaks (Figure 4.21E), enriched KEGG pathways such as lysosomes also appear in one or both of the HA-Mitf and HA-Mitf^{K243R} lists. Some terms, such as depression, ECM-receptor interaction and sugar metabolism, are absent. The same is true for GO terms associated with common peaks (Figure 4.21F). GO terms enriched in one or both of the individual lists, such as lysosomes and transport, are enriched in the common peaks. The actin binding term in
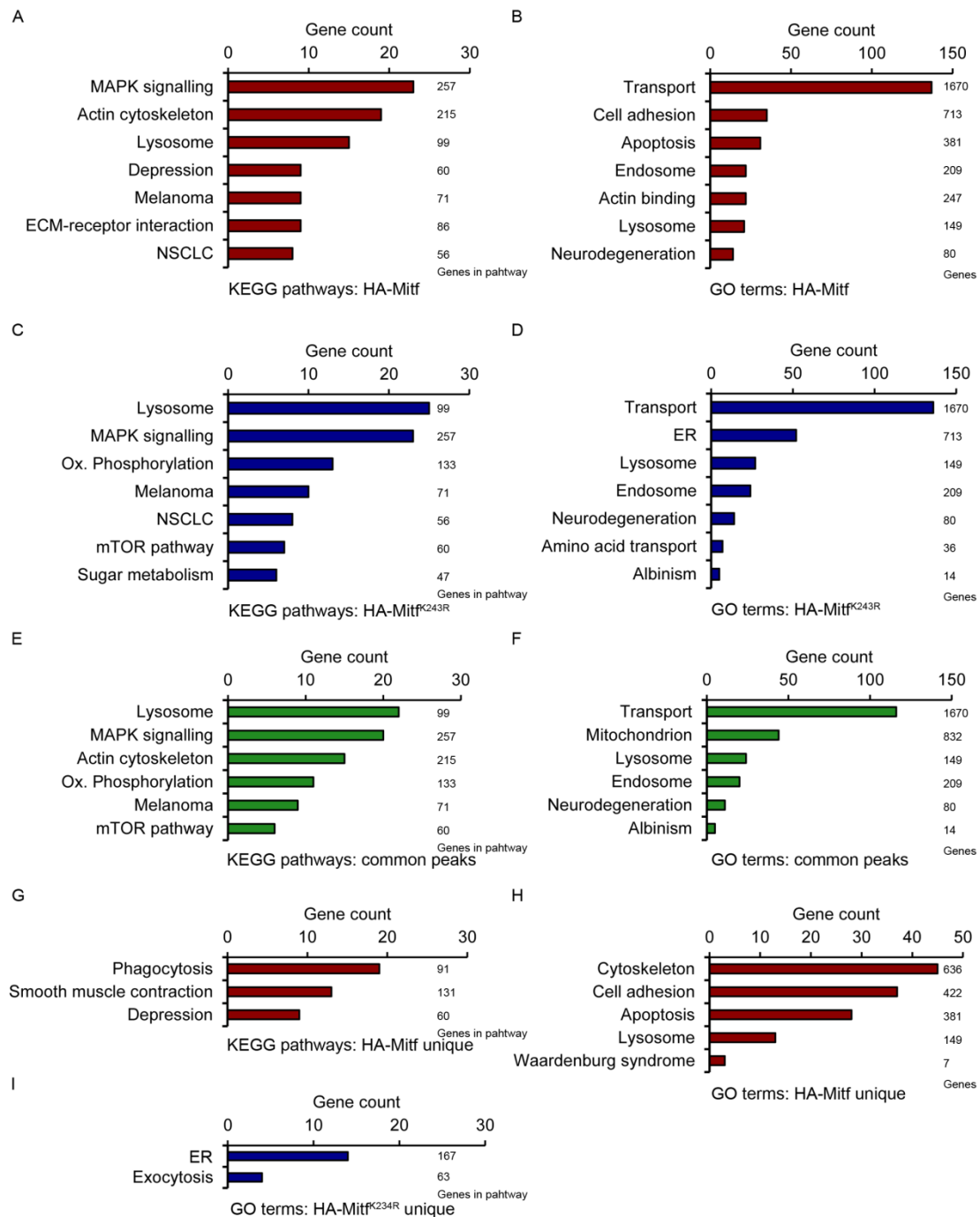
Figure 4.21. Gene ontology analysis of HA-Mitf and HA-Mitf^K243R binding.
Bars on HA-Mitf graphs are red, bars on HA-Mitf^K243R graphs are blue, and bars on graphs for common peaks are green. (A)-(D) The top 1000 genes from HA-Mitf and HA-Mitf^K243R peaks were analysed for significantly enriched KEGG pathways and GO terms as indicated. All terms reported terms had p-value < 0.1. (E)-(I) As for (A) but using common and unique HA-Mitf and HA-Mitf^K243R peaks. There were no enriched KEGG pathways in the HA-Mitf^K243R unique peaks.

the HA-Mitf gene list does not appear in the common peaks, while mitochondria are significantly enriched in the common peaks. The top 1,000 unique HA-Mitf genes were analysed, in keeping with the number of genes used in Figures 4.21A-D. Enriched KEGG pathways included depression, which is present in the set of all HA-Mitf genes but absent from the common ones (Figure 4.21G) and GO terms included cell adhesion and apoptosis, which were again absent from the common genes (Figure 4.21H). Lysosomes were also enriched in this list, which suggests that either HA-Mitf is able to bind more lysosome-genes, or that the binding sites in these genes fall below the peak height cut-off of 40. Among the 174 unique genes bound by HA-Mitf^{K243R}, no KEGG pathways were enriched and, in GO terms (Figure 4.21I), the ER and exocytosis were enriched (the former of which appears in the list of total genes [Figure 4.21D] but not the common genes [Figure 4.21F]).

Waardenburg syndrome is enriched in the unique HA-Mitf GO terms and, if a larger gene list of HA-Mitf unique genes is submitted for analysis, terms such as melanogenesis are enriched (not shown). This combined data further suggests that, although MITF is essential for the pigmentation process, other functions that are not cell-type specific, such as regulation of metabolism and lysosomes, are similarly important. The commonly enriched processes further support the idea that a major acetylation-independent role of MITF is the regulation of metabolism and lysosomes.

Association of a ChIP-Seq peak with a gene does not necessarily mean that the gene will be directly regulated. Gene expression measurements must be correlated with ChIP-Seq data to be able to infer whether a gene is directly regulated. Therefore, total RNA was extracted from the 501.HA-Mitf, 501.HA-Mitf^{K243R}.cl1 and 501.HA-Mitf^{K243Q}.cl2 cell lines, and genome-wide gene expression levels were analysed in triplicate with microarrays. Following normalisation of the readings, global

expression levels were compared by Pearson correlation analysis between the averaged expression values for each cell line. In all 3 combinations of cell lines a very strong correlation was observed (*R*=0.99 comparing 501.HA-Mitf with 501.HA-Mitf^{K243R}.cl1 [Figure 4.22A], *R*=0.98 comparing 501.HA-Mitf with 501.HA-Mitf^{K243Q}.cl2 [Figure 4.22B], and *R*=0.99 comparing 501.HA-Mitf^{K243R}.cl1 with 501.HA-Mitf^{K243Q}.cl2 [Figure 4.22C]). Genes whose expression clearly varied between two cell lines were observed in each case. To make an initial comparison of the array data from each cell line, principal component analysis (PCA) was employed; PCA transforms multi-dimensional datasets onto a series of new orthogonal
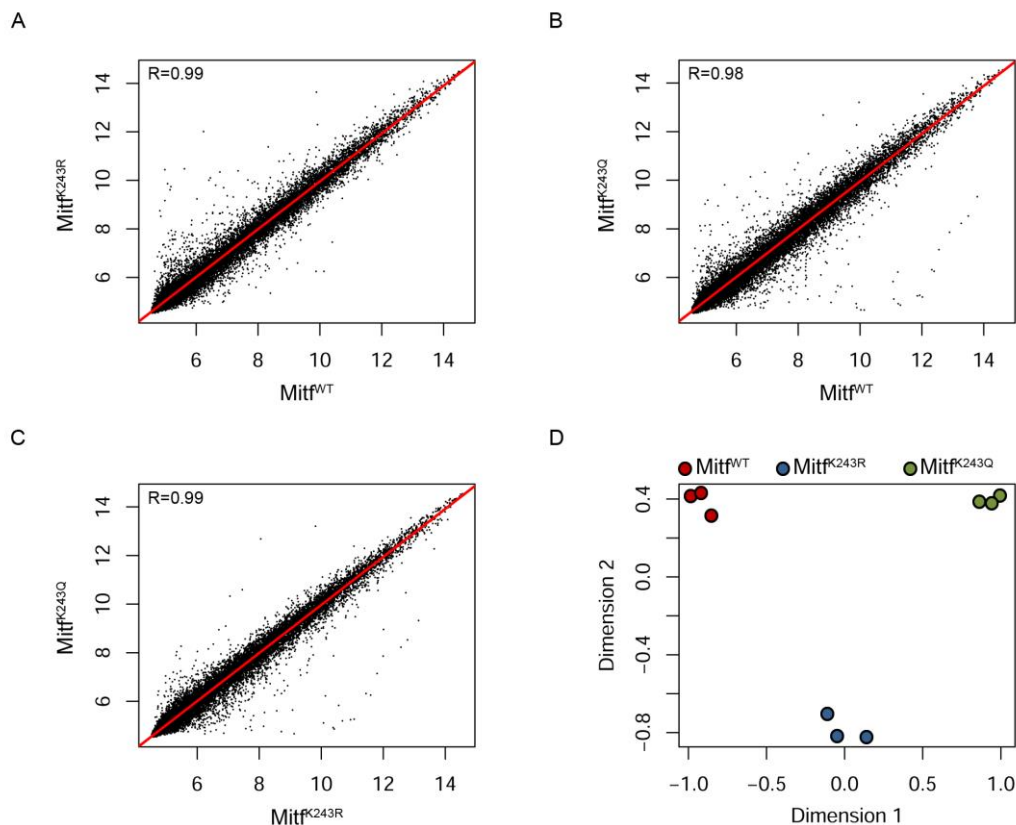
Figure 4.22. Microarray analysis of 501.HA-Mitf, 501.HA-Mitf^{K243R}.cl1 and 501.HA-Mitf^{K243Q}.cl2 cell lines. (A)-(C) Averaged, per-gene normalised expression values for triplicate measurements on the indicated cell lines for 21,509 RefSeq genes encoding both coding and non-coding genes were plotted and a best-fit line calculated. Pearson correlation coefficient calculated is shown top-left. (D) Principal component analysis was performed on per-gene, normalised expression values for all 3 replicates in each cell line.

coordinate systems (principal components, or dimension). As the dimension number increases, the variance among the data points along it decreases. Thus, in this example, dimension 1 is the component which has the greatest variance among the three cell lines. Analysis of the expression levels between the repeats of the arrays revealed that the replicates of the cell lines clustered together, and that the cell lines were separated in analytic space (Figure 4.22D). To ascertain whether these differences led to functional changes in gene expression between cell lines, genes with more than two-fold difference in expression between any two cell lines were identified. 21,509 RefSeq genes, both coding and non-coding, were analysed in this experiment. Of these, 1,119, or 5.2%, were identified as differentially expressed (Table 4.3). To look for coordinated patterns of gene expression, the differential genes were plotted in a clustered heatmap (Figure 4.23A). On the x-axis, replicates of each cell line clustered together, and 501.HA-Mitf^{K243R}.cl1 was found to be closer to 501.HA-Mitf^{K243Q}.cl2 than to 501.HA-Mitf. A block of genes was up-regulated in each cell line relative to the other two. There appeared to be some genes that were up-regulated in two cell lines relative to the third, in particular a set of genes up-regulated in 501.HA-Mitf^{K243R}.cl1 and 501.HA-Mitf^{K243Q}.cl2 relative to 501.HA-Mitf. This is presumably why these two cell lines were linked together in the clustering analysis.

After examining the genes that were differentially regulated, a large degree of overlap in differentially expressed genes was found (Figure 4.23B). In any comparison, more than half of the differentially expressed genes were found to be

Table 4.3. Differential gene expression[*]

Comparison	WT – K243R	WT – K243Q	K243R – K243Q
Up-regulated	119	229	206
Unchanged	21129	21065	21214
Down-regulated	261	215	89

[*] For comparison WT – K243R, up-regulated genes are up-regulated in WT relative to K243R, and down-regulated genes are down-regulated in WT relative to K243R. The same is the case for comparisons WT – K243Q and K243R – K243Q.
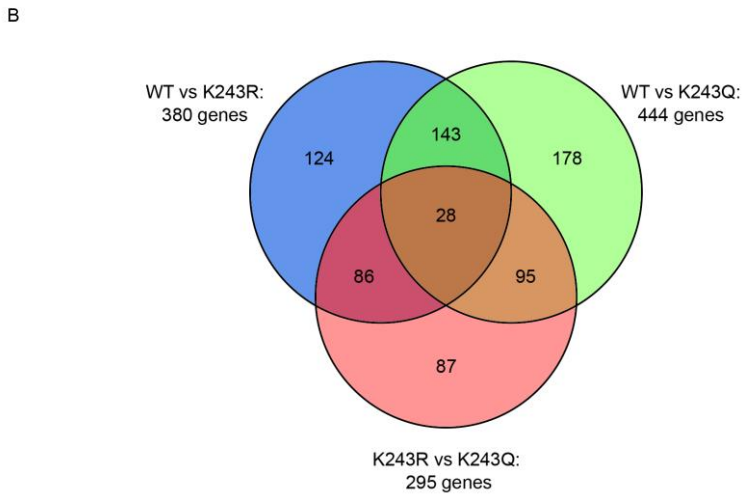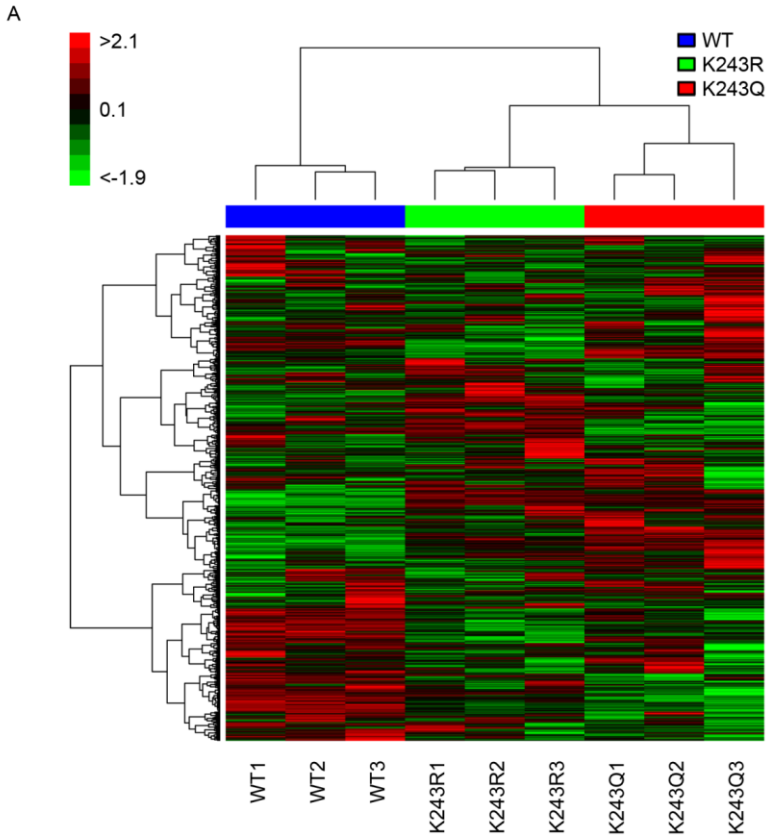
Figure 4.23. Differential gene expression analysis. (A) Heatmap of genes that had a greater than 2-fold change between any two samples. Genes were hierarchically clustered based on expression level and arrays were clustered based on similarity using Pearson correlation analysis. The scale bar is shown in the top-left corner. (B) Genes that had a greater than 2-fold change in expression between HA-Mitf and HA-Mitf^{K243R} (WT vs K243R), HA-Mitf and HA-Mitf^{K243Q} (WT vs K243Q), and HA-Mitf^{K243R} and HA-Mitf^{K243Q} (K243R vs K243Q) arrays were analysed for genes that were de-regulated between 2 or 3 of the comparisons.

differentially expressed in another comparison. Although this is a crude measure because the analysis does not account for the direction of the change in each case, it shows that, for many differentially expressed genes, the expression changes in any 2 cell lines relative to a third one. A small number of genes (27) were found to be differentially expressed among all three comparisons.

5% of genes are de-regulated between at least two of the cell lines. We next wished to establish whether there was a link between HA-Mitf or HA-Mitf^{K243R} occupancy of a site in a gene and the expression of that gene. The height of peaks in each sample that were associated with a gene was plotted against the normalised expression level from the microarray data. A very weak correlation was found between HA-Mitf peak height and 501.HA-Mitf gene expression levels (Pearson correlation coefficient R=0.04; Figure 4.24A), while a slightly stronger but still very poor correlation was found between HA-Mitf^{K243R} peak height and 501.HA-Mitf^{K243R}.cl1 gene expression levels (Pearson correlation coefficient R=0.11; Figure 4.24B).

This data suggested that there was not a strong link between the degree of binding at a gene and its expression for either HA-Mitf or HA-Mitf^{K243R}. The same was observed in Chapter 3 for HA-Mitf peak height in comparison to RNA-Seq-derived expression levels, and has previously been found with the yeast transcription factor Rap1 (Lickwar et al., 2012). However, this does not preclude a more general relationship between occupancy (ignoring the peak height) and expression level. Therefore, genes were split into expressed and not expressed categories. In the microarray data the normalised expression values across all arrays ranged from 4.4 to 14.7, encompassing a pre-normalisation array detection range of 83.3 to 29,990.8; no probe had a detection level of 0. In the RNA-Seq experiments in Chapter 3,

approximately 40% of genes were expressed in the parental 501mel cells under varying conditions, and it would be surprising if there was a large deviation from this figure in the stable cell lines. Therefore, a normalised expression cut-off of 5.298 was chosen as the dividing line between expressed genes and not expressed genes, which corresponded to a raw detection signal of approximately 200 and removed the 60% of genes with the weakest detection signal.
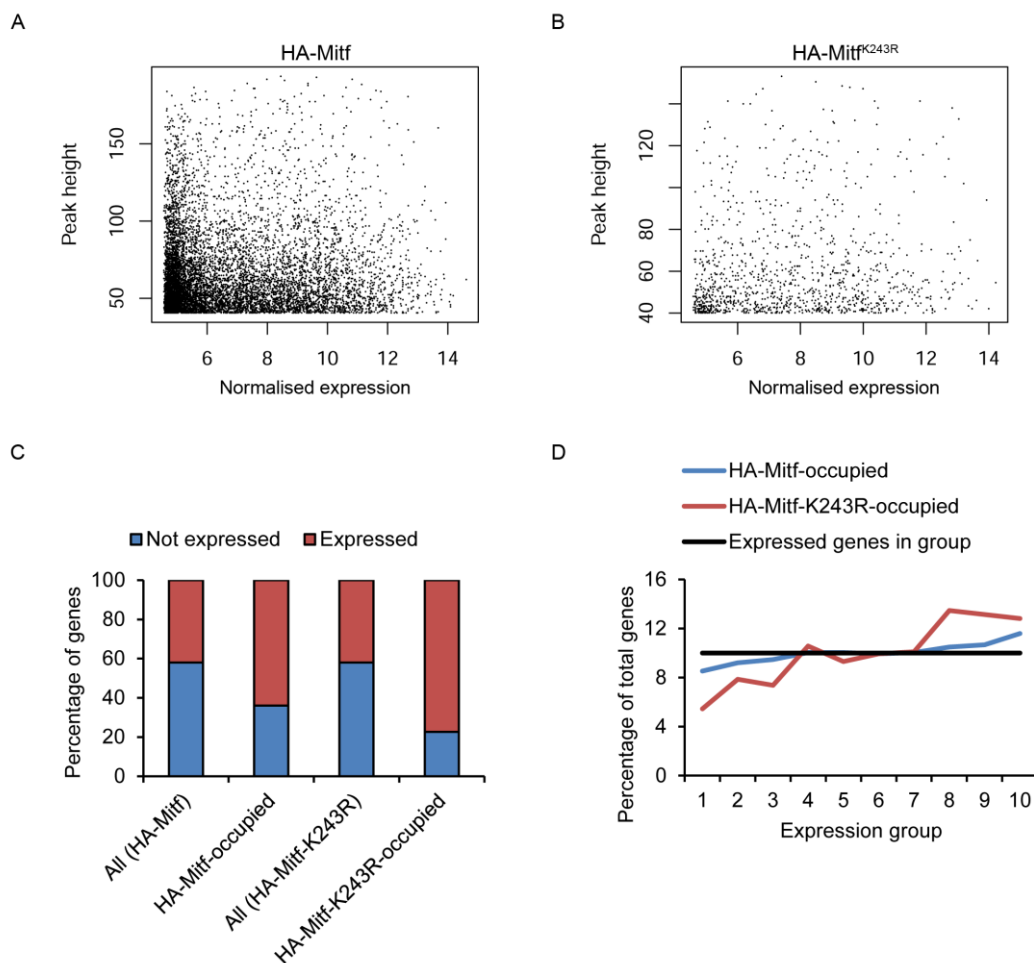
Figure 4.24. HA-Mitf and HA-Mitf^{K243R} binding is positively associated with gene expression. (A) Scatterplot of the peak height for genes bound by HA-Mitf and the normalised expression level of that gene in the HA-Mitf microarrays. (B) As for (A), but for HA-Mitf^{K243R} ChIP-Seq and microarray experiments. (C) For HA-Mitf and HA-Mitf^{K243R} microarrays, genes were categorised as expressed or not expressed, and genes associated with ChIP-Seq peaks from each sample were divided into these groups. (D) Expressed genes in HA-Mitf and HA-Mitf^{K243R} microarrays were divided into 10 bins of equal size and increasing expression level, and genes associated with ChIP-Seq peaks from each sample were divided into these bins.

Next, HA-Mitf and HA-Mitf^{K243R} peaks associated with a gene were divided among these bins (Figure 4.24C). Both proteins are more likely to bind to expressed genes than non-expressed genes: 64% of gene-associated HA-Mitf peaks and 77% of gene-associated HA-Mitf^{K243R} peaks were associated with expressed genes. This suggested that both proteins could positively influence gene expression, and that HA-Mitf^{K243R} binding is more associated with expressed genes. An alternate explanation is that both proteins (and particularly HA-Mitf^{K243R}) are associated with regions of open chromatin, which tend to be around genes that are actively transcribed. To investigate a link between occupancy and expression, the expressed genes from 501.HA-Mitf and 501.HA-Mitf^{K243R}.cl1 cells were each divided into 10 equally sized bins of increasing expression level, and the proportion of bound and expressed genes falling into each bin measured (Figure 4.24D). As expression level increased, the percentage of HA-Mitf peaks falling into the bin increased steadily. The rise in association with HA-Mitf^{K243R} peaks with increasing expression level was steeper than for HA-Mitf. The bin with lowest expression (group 1) contained only 5% of the HA-Mitf^{K243R} peaks, compared to 8.5% of HA-Mitf peaks. The number of peaks in each bin increased to 10% and remained there until bin 8, when there was an increase to 10.5% in HA-Mitf but to 13.5% in HA-Mitf^{K243R}. This result suggests that HA-Mitf^{K243R} binding is associated with more highly expressed genes than HA-Mitf. It should be noted that this analysis does not take into account genes that may be repressed by either protein, as some of the genes either categorised as being non-expressed or with very low expression could be repressed by MITF.

Some caution is needed due to the much smaller peak pool for HA-Mitf^{K243R}. As there appears to be a link between the occupancy and expression level but not between peak height and expression level, it could be that the relationship between

occupancy and expression level has been skewed as a result. However, on inspection of Figure 4.24A, there is no apparent increase in correlation between peak height and expression level for the highest portion of HA-Mitf peak heights, suggesting that the relationship found here for HA-Mitf^{K243R} is not an artefact of reduced sample size.

The lists of genes bound by HA-Mitf and HA-Mitf^{K243R} were compared with the lists of differentially regulated genes in the 3 comparisons made (Figure 4.25), indicating that some genes de-regulated in all 3 comparisons are bound by HA-Mitf and HA-Mitf^{K243R}. A greater number of genes bound by HA-Mitf than were bound by HA-Mitf^{K243R} were de-regulated in one of the comparisons. This is likely a reflection of the numbers of genes that are bound by each sample. However, the number of genes that are bound and de-regulated is low. It could well be that this effect is due to the high peak height threshold of 40, and that reducing the cut-off would increase the numbers. Alternately, it could be that the endogenous MITF in the stable cell lines is able to mask any transcriptional effects of the HA-Mitf.

Finally, the biological roles of the de-regulated genes between the different cell lines were investigated by gene ontology analysis. In genes up-regulated in 501.HA-Mitf relative to 501.HA-Mitf^{K243R}.cl1, cytoskeletal proteins were enriched (Figure 4.26A), while the ER and differentiation were down-regulated (Figure 4.26B). Some ABC and sugar transporters were also down-regulated. This suggests that, although metabolic regulation seems to be an important role of MITF, the wild-type and K243R proteins could be directing subtly different metabolic programmes. The major set of genes up-regulated in 501.HA-Mitf relative to 501.HA-Mitf^{K243Q} were metal binding, along with a number of genes involved in the degradation of valine, leucine, and isoleucine (Figure 4.26C). A large number of transport-related genes were down-regulated in 501.HA-Mitf relative to 501.HA-Mitf^{K243Q}, as well as genes
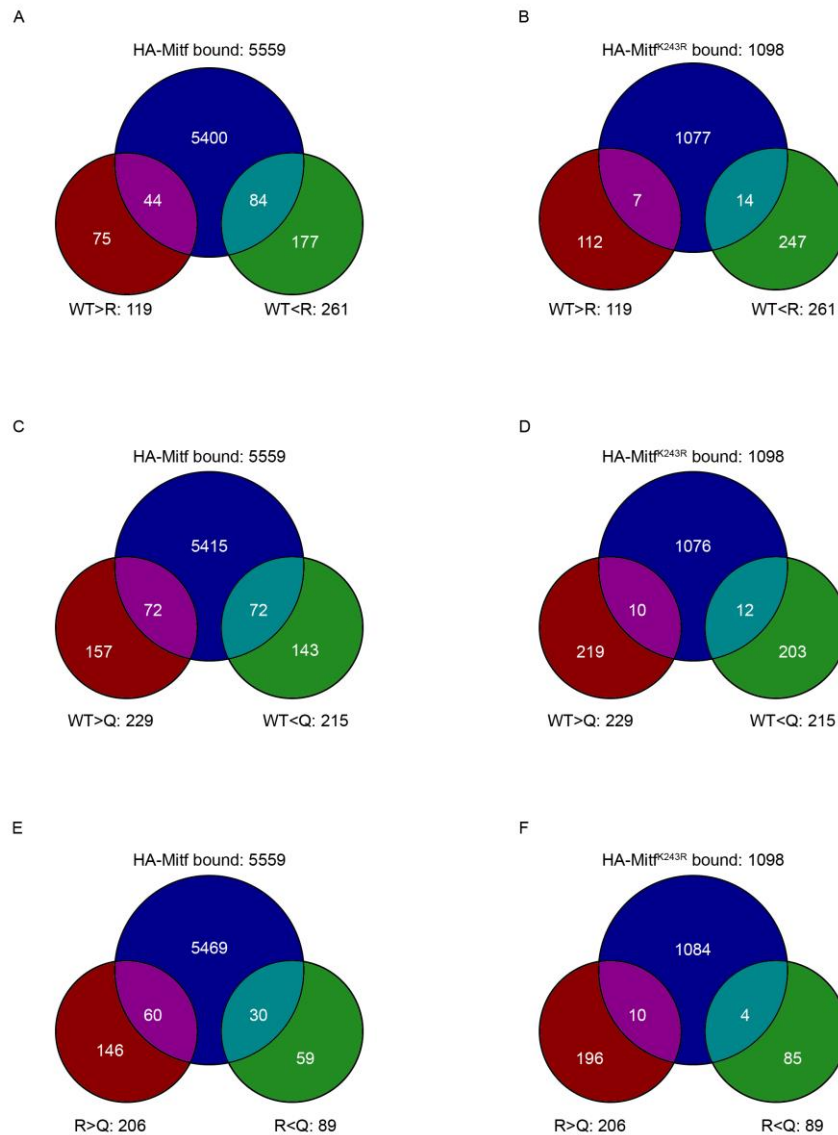
Figure 4.25. Comparison of HA-Mitf and HA-Mitf^{K243R} bound genes with differentially expressed genes. (A),(B) WT vs K243R differentially expressed genes were compared with HA-Mitf (A) and HA-Mitf^{K243R} (B) bound genes. (C),(D) WT vs K243Q differentially expressed genes were compared with HA-Mitf (C) and HA-Mitf^{K243R} (D) bound genes. (E),(F) K243R vs K243Q differentially expressed genes were compared with HA-Mitf (E) and HA-Mitf^{K243R} (F) bound genes.

involved in purine metabolism (Figure 4.26D). Interestingly, ER and ABC transporters were also down-regulated, implying that these sets of genes are commonly de-regulated by the mutant proteins and that they thus might form an acetylation status-independent set of target genes. In genes up-regulated in 501.HA-Mitf^{K243R} relative to 501.HA-Mitf^{K243Q}, sugar transport and differentiation terms were enriched, in common with the genes up-regulated in 501.HA-Mitf^{K243R} relative to the 501.HA-Mitf cell line, suggesting that these genes are regulated by acetyl-K243 MITF (Figure 4.26E). Finally, calcium-related genes and ion transporters were down-regulated in 501.HA-Mitf^{K243R} relative to 501.HA-Mitf^{K243Q} (Figure 4.26F).

4.5 Discussion

In this chapter, the function of site-specific acetylation of MITF has been examined. Mutation analysis suggested that K206 and K225 could be major acetylation targets of p300 as judged by a strong reduction in acetyl-Mitf signal in Western blotting, while mutation of the other sites throughout the bHLH-LZ also reduced the overall detectable acetylation level of Mitf. This suggested no single major acetylation site within Mitf must be acetylated in order for the others to be acetylated, although it is possible that there is a hierarchical nature to the acetylation pattern generated that cannot be determined from this experiment. Ongoing and future work in the laboratory will seek to clarify the roles of these acetylation events in targeting of MITF to different subsets of target genes or through regulating interaction with MITF-cofactors.

The remainder of the chapter focussed on the role of MITF-K243. Through *in vitro* and *in vivo* studies, it appears that this amino acid controls MITF DNA binding specificity via its acetylation status which, in turn, is controlled by whether a cell is proliferating. In proliferative cells, acetyl-K243-MITF (Mitf^{K243Q}) binds to
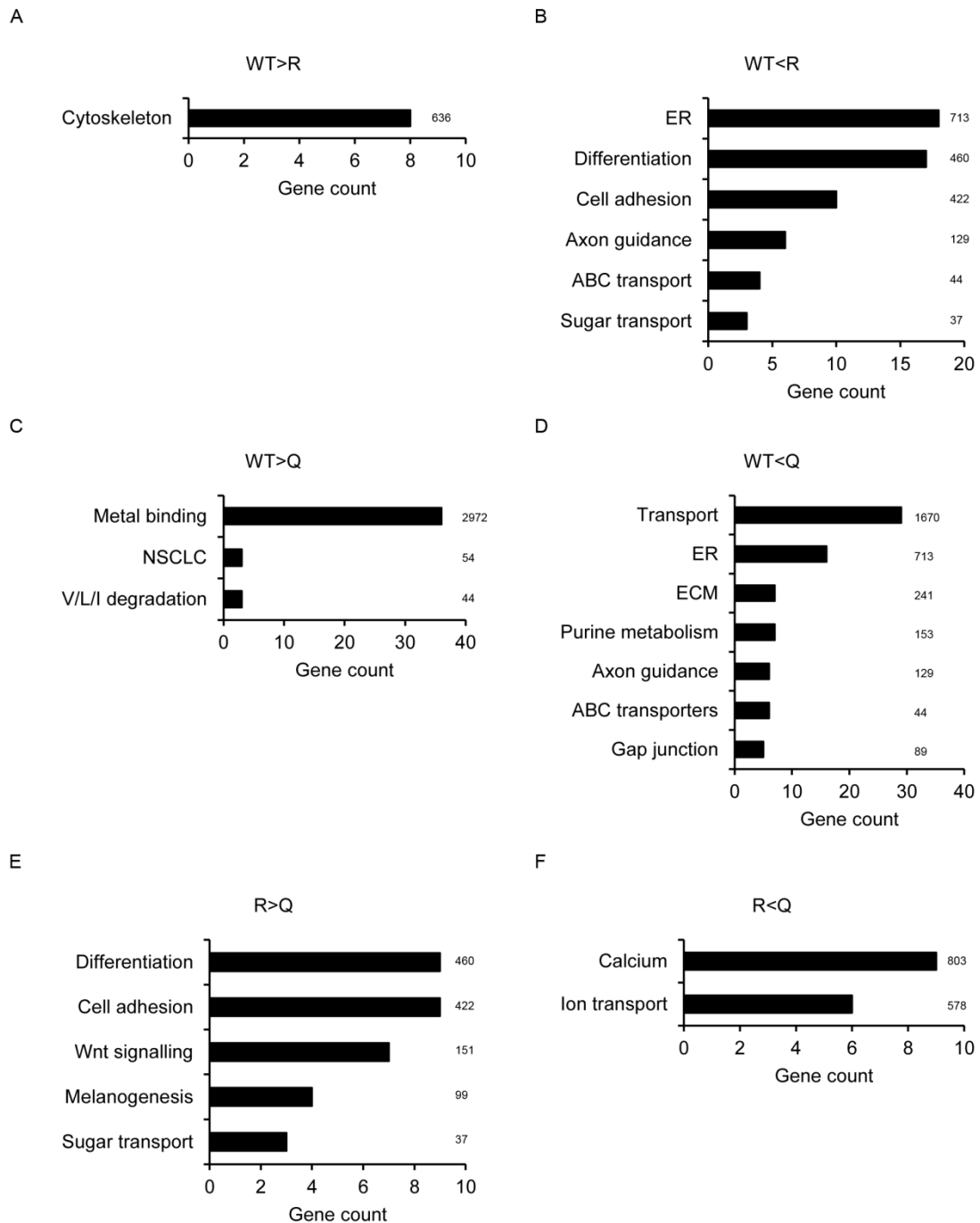
Figure 4.26. Gene ontology analysis of differentially expressed genes in the microarray experiments. KEGG and GO analysis was performed for the comparisons and direction of expression change as indicated. Graphs show combined KEGG pathways and GO terms. All enriched terms had p-value < 0.1. In graph titles, the arrow indicate the direction of up-regulation in the comparison i.e. WT>R indicates genes up-regulated in 501.HA-Mitf relative to 501.HA-Mitf[K243R].

DNA with low affinity, and is thus only capable of binding to sites for which MITF has high affinity. The non-acetyl-K243-MITF (Mitf^{K243R}) found in non-proliferative cells has a greater affinity for DNA than the acetylated protein, and it also has reduced DNA binding specificity. It is therefore titrated by the genome, and remains bound to only the highest affinity sites that are MITF-occupied. This set of very high affinity genes forms a group of acetylation-independent genes. This model and its implications will be further addressed in Chapter 6. Many of the acetylation-independent genes appear to regulate nutritional processing. Therefore, metabolome profiles of the stable cell lines generated in the present work will be assembled, to determine the concentrations of all metabolic pathway compounds in the cell. This will allow elucidation of any shift in metabolic preference following MITF-K243 acetylation.

In the ChIP-Seq analysis, HA-Mitf^{K243R} appeared more associated with (expressed) genes than HA-Mitf^{WT}. To test whether this reflects a stronger association with open chromatin, regions of open chromatin will be determined in each cell line by two complementary methods. First, nucleosome position will be determined by digesting chromatin with MNase to yield mononucleosomes followed by deep sequencing of the protected DNA. Secondly, formaldehyde-assisted isolation of regulatory elements (FAIRE) will be performed to identify regions depleted of nucleosomes or other protecting proteins, the DNA from which will remain in the aqueous phase following phenol-chloroform extraction. This will allow for deep sequencing of this DNA. FAIRE-Seq and MNase-Seq do not return exactly the same regions, so combining the data from the procedures will permit a more confident identification of regions of open chromatin.

One limitation of the analysis undertaken here is that, when considering whether peaks were the same or not between the samples, only the peak coordinates were accounted for. Therefore in the future, the heights of the peaks that overlap will be taken into consideration to identify a set of differentially bound genes. It will also be vital to perform ChIP-Seq on the 501.HA-Mitf^{K243Q}.cl2 cell line, to complement the Mitf^{K243R} ChIP-Seq dataset. Further, it remains to be confirmed that acetyl-K243-MITF does indeed bind DNA with greater specificity than non-acetyl-K243-MITF. This will be achieved by chemical acetylation as outlined in Chapter 6.

Chapter 5 – A MAPK-p300 feedback loop

5.1 Introduction

To help a cell respond to the many stimuli that it must integrate, there are multiple levels of interaction between different signal transduction pathways. For example, the MAPK PI3K/Akt and pathways may both be activated by RAS, and they have been demonstrated to interact with one another. The MAPK pathway inhibits the adoption of a myogenic fate by precursor cells and thus inhibits differentiation. However, it was shown that the PI3K/Akt pathway promotes muscle differentiation, as Akt phosphorylates and inhibits RAF to promote differentiation (Rommel et al., 1999; Zimmermann and Moelling, 1999). It has also been shown that RAF can induce cell cycle arrest through inhibition of PI3K/AKT, mediated by up-regulation of the EphA2 receptor (Westbrook et al., 2002; Menges and McCance, 2008).

Numerous post-translational modifications of MITF have been described, but little is known about how these modifications affect one another. MAPK signalling activates p300, by ERK-mediated phosphorylation of p300 (Chen et al., 2007). Given that feedback loops are common in biology, it is possible that p300 could also impact on MAPK activity. As well as activating p300, which in turn acetylates MITF in a MAPK-dependent fashion (Figure 3.1), MAPK activation results in phosphorylation of MITF S73 and S409. In turn, MITF-S73/409 have been reported to promote MITF degradation (Hemesath et al., 1998; Wu et al., 2000; Xu et al., 2000). Previous work in our laboratory revealed that phosphorylation of MITF-S73/409 is not required for acetylation of MITF (Figure 3.1), but it could be that individual acetylation sites are impacted by one or other phosphorylation, or indeed by other post-translational modifications of MITF. Here we investigate the effects of abrogation of acetylation on MITF.

5.2 p300/CBP-inhibition activates MAPK signalling

In an attempt to complement our earlier studies on activation of MAPK-driven MITF acetylation, p300/CBP was inhibited using small molecules. Historically, small molecule inhibitors of acetyltransferases tended to have broad off-target effects, but a new generation of more specific molecules has recently been introduced. One such compound, C646, a selective inhibitor of p300 and CBP with K_i of 400 nM, was employed (Bowers et al., 2010). These authors treated different melanoma cell lines with 10-25 µM doses of the compound, and some cell lines showed an effect on proliferation following treatment alongside reduction of H3 and H4 acetylation. Because we were interested in the immediate effects of inhibiting acetylation of MITF, a short treatment was employed to try to minimise the confounding effects of growth arrest. Therefore, 501mel cells were treated or not for 1 hour with a range of C646 concentrations that spanned and subjected to Western blotting (Figure 5.1A). Surprisingly, treatment with doses of 10 µM, the dose used by Bowers et al. (2010) to reduce melanoma cell growth), or greater led to a shift of MITF from a roughly equal mix of hyper-phosphorylated (upper band, phosphorylated on S73 and S409) and hypo-phosphorylated (lower band, lacking phosphorylation on S73 and S409) forms to almost entirely the upper band of MITF. This suggested that MAPK-signalling was activated by C646, which was confirmed by an increase in phospho-ERK relative to an actin loading control. The increase in phospho-ERK was reflected in a blot for total ERK2, which displayed a similar upward mobility shift.

Next, 501mel cells were treated for a range of times with DMSO, or with 20 µM or 50 µM C646, and analysed by Western blotting for MITF, ERK2 and phospho-ERK. As before, MITF was shifted to the upper band following treatment with both

concentrations of C646 at all the time points, although by 7 hours treatment with 50 μM C646 there was a loss of MITF protein (Figure 5.1B). Activation of MAPK was again seen by an increase in phospho-ERK with both concentrations of C646, reaching maximal intensity after 3 hours. 50 μM C646 failed to generate such a strong
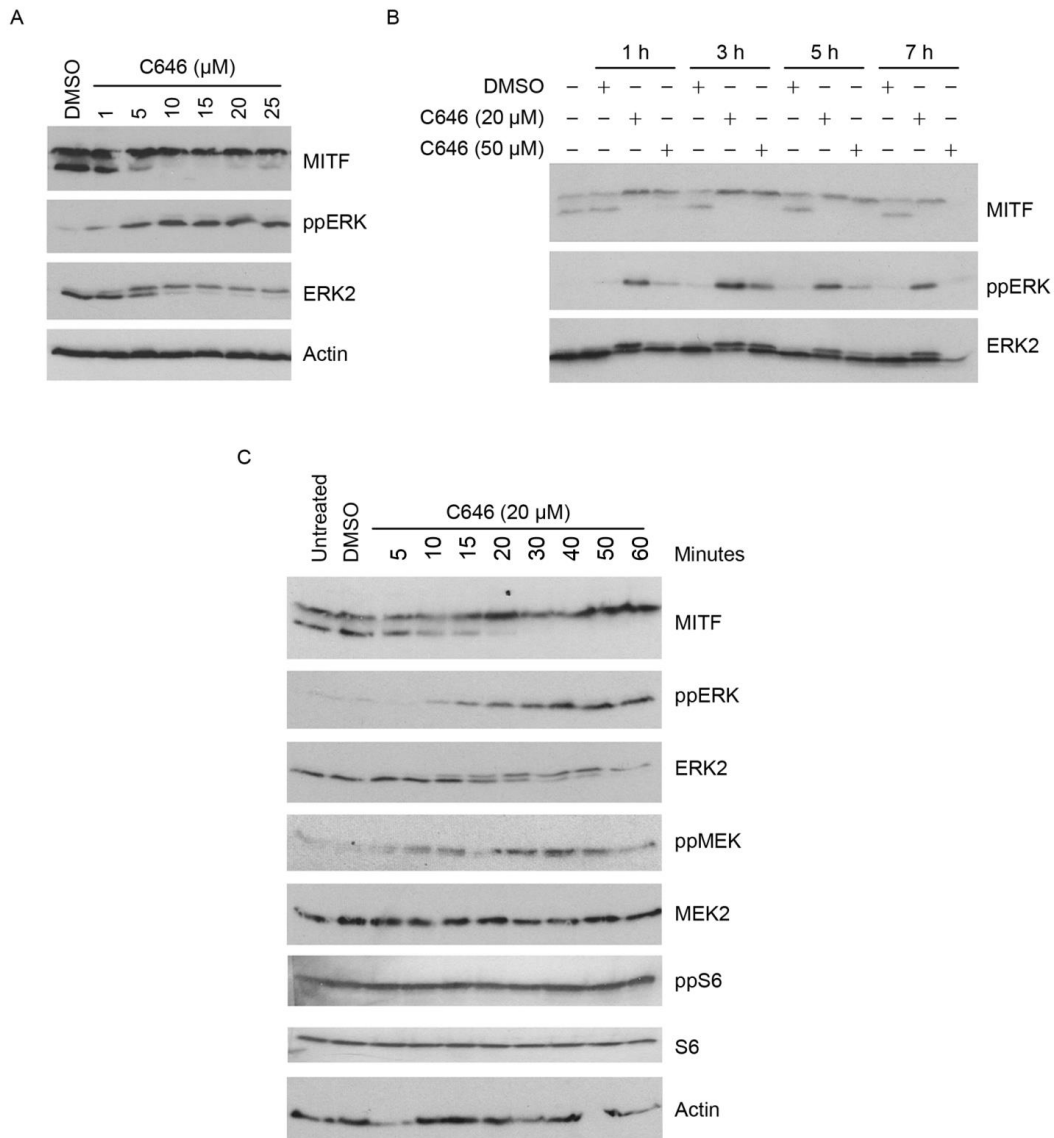
Figure 5.1. p300/CBP inhibition activates MAPK signalling in 501mel cells. (A) 501mel cells were treated with DMSO or increasing doses of C646 for 1 hour before whole cell extracts were subjected to Western blotting with the indicated antibodies. (B) 501mel cells were treated or not with DMSO or C646 (20 μM or 50 μM) for the times indicated before being analysed as in (A). (C) 501mel cells were either left untreated, treated with DMSO for 1 hour, or treated with C646 (20 μM) for the times indicated before being analysed as in (B).

activation of phospho-ERK compared to 20 μM, although the MITF mobility shift was comparable to that seen with a 20 μM treatment. Phospho-ERK almost disappeared from cells by 7 hours treatment with 50 μM C646; this was accompanied by a decrease in total ERK2. Together with cell death apparent in the dish by this time (data not shown), this suggested that the higher concentration of the drug was too toxic for cells to tolerate and was unsuitable for further use.

The data so far indicated that MAPK signalling was activated upon C646 treatment as judged by an increase in phospho-ERK. To assess the speed of the process, 501mel cells were treated with 20 μM C646 for periods of up to 1 hour (Figure 5.1C). Actin was used as the loading control. A rapid increase in MAPK activation throughout the time-course was seen, with the bulk of the phospho-ERK increase occurring between 10 and 40 minutes, and with the mobility shift in total ERK2 between 10 and 60 minutes. MITF phosphorylation became strongly apparent after 20 minutes, with complete phosphorylation occurring by 30 minutes after treatment began. Activation of the MAPK pathway on p300/CBP-inhibition suggested that the acetylation of a component of the pathway could be the cause, either an inhibitory acetylation of a kinase or as an activating acetylation of a phosphatase, such that this restraint is removed and MAPK activity increases after p300/CBP-inhibition.

To see whether the MAPK pathway activation was at the level of ERK or upstream in the pathway, membranes were probed for total MEK and MEK phosphorylated on S217/221 (phospho-MEK; Figure 5.1C). Total MEK was unchanged throughout the time course, while phospho-MEK increased after just 5 minutes of treatment to a maximum after 30 minutes and then appeared to decrease slightly at 60 minutes. This response was faster than ERK phosphorylation, demonstrating that the activation of the pathway must take place upstream of ERK.

MAPK-PI3K crosstalk is known to occur, and it was possible that the acetylation event was modulating the PI3K pathway. Because crosstalk can take place at various levels between the two pathways, and because the acetylation event could potentially have been affecting any of these points of crosstalk, PI3K pathway activation was examined by Western blotting for S6 ribosomal protein, which is phosphorylated and activated by Akt following PI3K activation. Neither total S6 nor active S6 (phosphorylated on S235/236) changed throughout the timecourse (Figure 5.1C), suggesting that the PI3K pathway was not affected by C646, and C646 was directly affecting the MAPK pathway.

Cancer cell lines frequently carry numerous mutations, which can mis-regulate signal transduction pathways. For example, the 501mel cells used so far have an activating BRAF^{V600E} mutation, a mutation leading to aberrant β-catenin nuclear accumulation (Rubinfeld et al., 1997), and mutant p53 (Lu et al., 2013). To establish whether C646 treatment was having a *bona fide* effect on the MAPK pathway, or whether it is a phenomenon restricted to 501mel cells, a range of human melanoma cell lines with different mutational statuses in MAPK pathway proteins and the murine melanoma cell line B16F10 were tested by treatment with 20 µM C646 for 1 hour (Figure 5.2A). Full details of the known mutations in these cell lines are given in Table 2.1. Western blotting for MITF revealed that, where there was detectable protein (501mel, SKmel28, MDA-MB-435, Me235, SKmel3, SKmel30 and B16F10), phosphorylation of MITF following C646-treatment could be seen relative to solvent-treated controls. B16F10 did not exhibit the total phosphorylation of MITF that is seen in the human melanoma cell lines, but rather showed a shift in ratio from predominantly the lower band to a roughly equal ratio of hyper- to hypo-phosphorylated MITF.
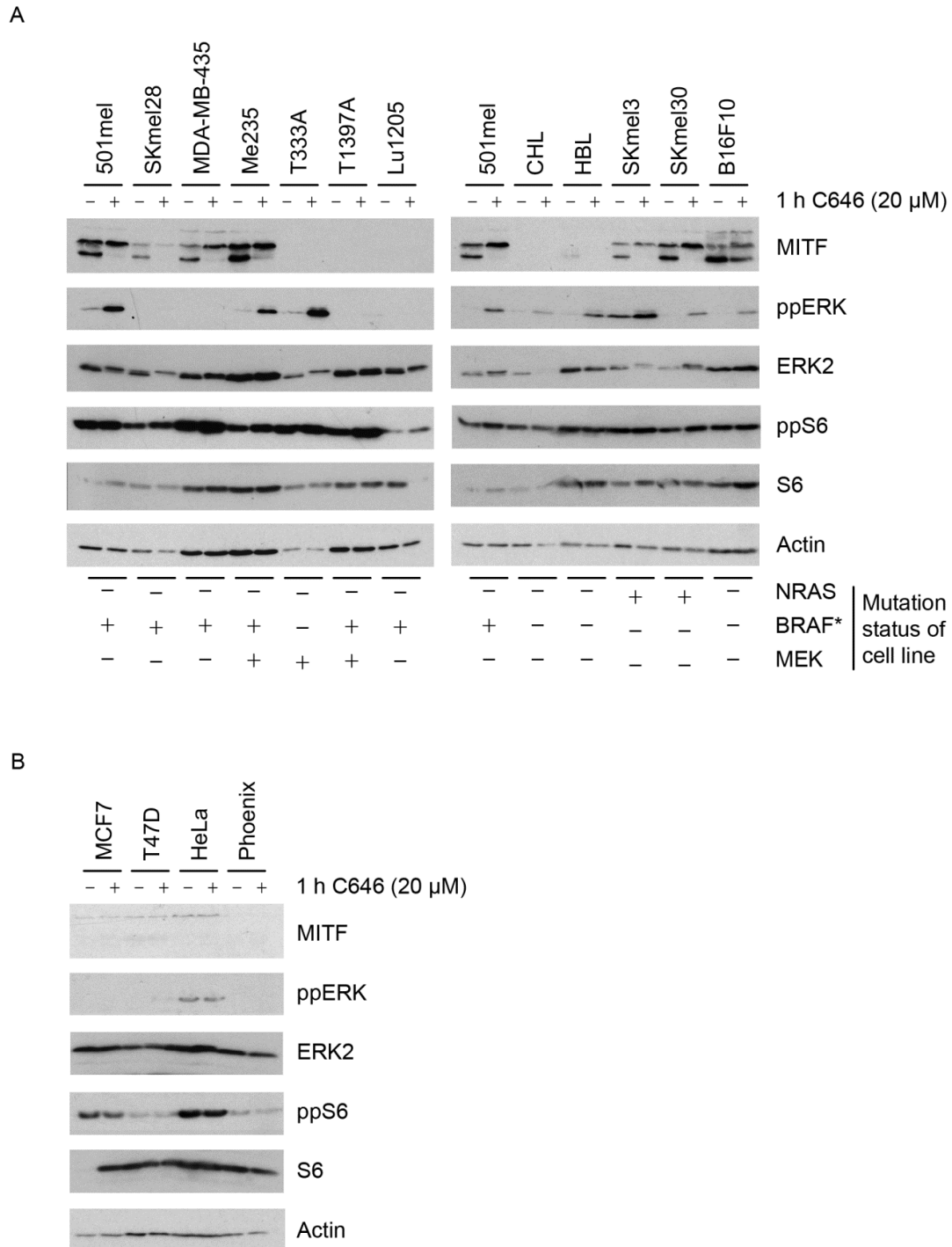
Figure 5.2. p300/CBP inhibition specifically activates MAPK signalling. (A) Melanoma cell lines were treated with either DMSO or 20 µM C646 for 1 hour as shown, before whole cell lysates were subjected to Western blotting with the indicated antibodies. Mutation status of cell line: + indicates a known mutation in this protein; − indicates either that the protein is wild-type, or (for MEK) that there is no sequence data available. *: BRAF mutants are all V600E, except Me235 which are K601E. (B) Cell lines were treated and analysed as in (A).

MAPK activation was assessed by ERK phosphorylation relative to an actin loading control (Figure 5.2A). Not all cell lines had detectable phospho-ERK but, where they did (501mel, Me235, T333A, CHL, HBL, SKmel3, SKmel30 and B16F10), although the basal level of phospho-ERK was variable among them, enhanced phospho-ERK was seen following C646 treatment, as compared with the Actin loading control. Additionally, three cell lines (SKmel28, MDA-MB-235 and Lu1205) showed a mobility shift in total ERK2, suggesting that these cells also activated MAPK signalling in response to C646 treatment, although this was not visible by blotting for phospho-ERK. Of the cell lines tested, only Lu1205 failed to show increased ERK phosphorylation following treatment.

To ascertain whether PI3K signalling was affected in any of these cell lines following C646-treatment, S6 phosphorylation was examined (Figure 5.2A). Despite having variable baseline levels of total S6 and phospho-S6, there was no additional phospho-S6 induced in these cell lines. This added to the notion that the PI3K/AKT pathway does not play any role in the response to C646, which is mediated solely through the MAPK pathway.

The results so far indicated that, in melanoma cell lines, MAPK activation is seen in response to treatment with C646. With the exception of CHL and HBL cells, these cell lines all harbour activating mutations in at least one component of the NRAS-BRAF-MEK cascade. However, many melanomas also contain mutations in receptor tyrosine kinases (RTK) such as Kit (Beadling et al., 2008), albeit at lower frequency than BRAF mutation. Kit activates both the MAPK and PI3K pathways and its mutation is mutually exclusive with NRAS and BRAF mutation (Beadling et al., 2008), just as is the case for NRAS and BRAF mutation. It is entirely possible, but not known, that CHL and HBL cells could contain RTK mutations. This raises two

possibilities. Firstly, it could be that activation of MAPK signalling by C646 is specific to melanoma cells or, secondly, that it is a response specific to cells with activated MAPK pathway components.

To investigate this, four further, non-melanocyte lineage cell lines with a range of transformation backgrounds were tested. T47D and MCF7 are breast cancer cell lines. T47D have p53 and PI3KC alpha subunit mutations, while MCF7 have deleted *CDKN2A* and a PI3KC alpha subunit mutation. Both cell lines are wild-type for Kit, NRAS, HRAS, KRAS and BRAF (source: COSMIC; cancer.sanger.ac.uk). HeLa is a cervical cancer cell line, which was transformed by HPV18 integration (Schwarz et al., 1985). HPV18 expresses oncoproteins E6 and E7, which bind and inactivate the p53 and Retinoblastoma proteins respectively, thus blocking cell cycle arrest and apoptosis and permitting uncontrollable cell division. In HeLa, E6 and E7 are over-expressed because, as a result of the integration, the viral gene *E2*, which inhibits E6 and E7, was inactivated (Schwarz et al., 1985). Recent deep-sequencing to assemble a haplotype-resolved HeLa genome sequence revealed that *c-Myc* expression was activated by HPV18 integration (Adey et al., 2013), perhaps explaining why HeLa cells are so aggressive. Phoenix cells are derived from 293T cells and are thus transformed by adenovirus E1a and the SV40 T antigen. Thus all four cell lines are likely free from activating mutations in the MAPK pathway. In Western blots, none of these cells expressed MITF, as expected (Figure 5.2B). Just one cell line, HeLa, had detectable levels of phospho-ERK in the absence of C646 treatment, and MCF7, HeLa, and Phoenix cells showed no increase in its levels following treatment with 20 μM C646 for 1 hour relative to an Actin loading control. There was a scarcely detectable level of phospho-ERK in T47D cells following treatment, although given the low level of the detection observed it is hard to assess

the significance of this observation. There was no change in total ERK2 in any of these cell lines, further suggesting that they do not activate, or least do not significantly activate, MAPK signalling following C646 treatment. Finally, none of the four cell lines showed changes in either phospho-S6 or total S6 following C646 treatment. As with the melanoma cell lines, however, there was a variable basal level of total S6 and phospho-S6 among them.

Taken together, this data suggests that C646 mediates its effects through the MAPK pathway in melanoma cells, but does not activate MAPK signalling in non-melanoma cells that do not have constitutively activated MAPK pathway components. However, we cannot distinguish between the C646 response being a melanoma-specific phenomenon or an activated-MAPK-specific phenomenon. Further investigation in non-melanoma cell lines with activating mutations in the MAPK pathway, such as are found in colon cancer, is required to definitively establish this.

Previous experiments established that the MAPK activation observed following C646 treatment must occur no lower in the MAPK pathway than MEK (Figures 5.1-2). Because the MAPK pathway begins to be activated just 5 minutes after treatment (Figure 5.1C), it was considered more likely that the effect was being mediated by post-translational modification than by a transcriptional mechanism. Within the activation loop of kinases is a lysine residue conserved in over 95% of kinases (Hanks and Hunter, 1995). This lysine plays a key role in coordinating ATP-binding; the lysine reportedly changes its conformation in the presence and absence of ATP to allow ATP to dock in the active site (De Bondt et al., 1993). It has been recently shown that acetylation by CBP of this conserved lysine residue in MEKK2 (K385), a MAPK component that functions at the BRAF level of the cascade, inhibits the kinase activity of this protein (Choi et al., 2012). The same mechanism

A

```
            *
hsBRAF   477  HG-DVAVKMLNVTAP  490
hsMEKK2  378  TGRELAVKQVQFDPD  392
hsCDK9    41  TGQKVALKKVLMENE   55
```

B

CDK9.ATP

C

BRAF V600E.Vemurafenib

D

BRAF WT.Sorafenib

E

BRAF V600E.Sorafenib
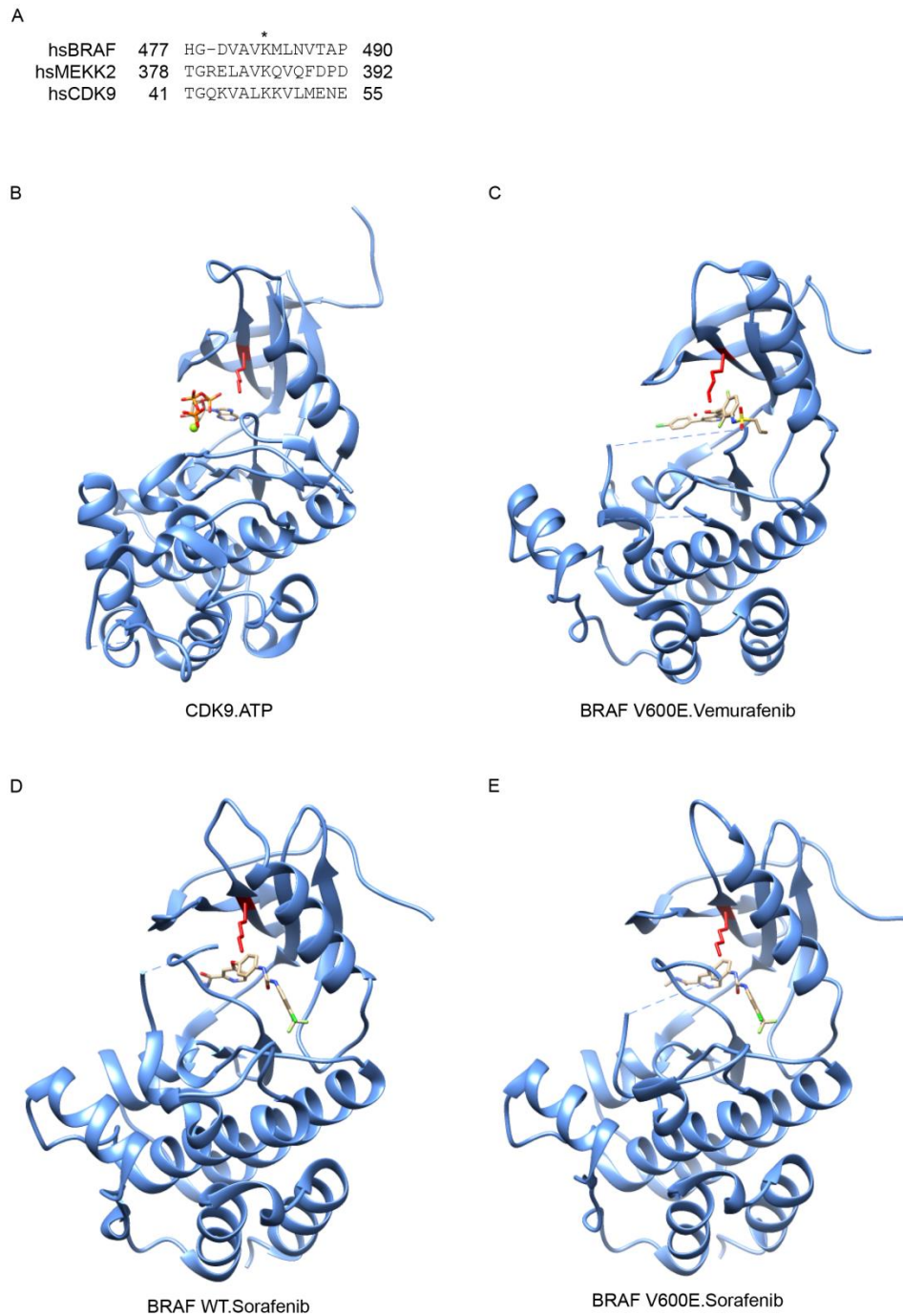
Figure 5.3. A conserved lysine in the active sites of kinases can be acetylated in CDK9, inhibiting kinase activity. (A) Alignment of kinases showing the conserved lysine (marked with *). (B)-(E) Atomic coordinates were downloaded from the Protein Data Bank and structures visualised in Chimera 1.8. (B) CDK9 (blue) complexed with ATP and Mg^{2+} (3BLQ); K48 in red (Baumli et al., 2008). (C) $BRAF^{V600E}$ (blue) complexed with vemurafenib (PLX4032; 3OG7); K483 in red (Bollag et al., 2010). (D), (E) $BRAF^{WT}$ (D; 1UWH) and $BRAF^{V600E}$ (E; 1UWJ) complexed with sorafenib (BAY439006); K483 in red (Wan et al., 2004).

has been reported in cyclin-dependent kinase 9 (CDK9), the catalytic component of the positive transcription elongation factor b complex, which activates transcription through phosphorylation of S2 of the heptapeptide repeats (YSPTSPS) of the RNA polymerase II C-terminal domain (Cho et al., 2001). In CDK9, the conserved lysine in the activation loop is K48 (Figure 5.3B), which can been seen in a co-crystal structure with ATP to be in close proximity to the ATP alpha-phosphate moiety (Baumli et al., 2008). CDK9 K48 may be acetylated by the histone acetyltransferase GCN5, a modification that severely diminishes the kinase activity of CDK9 (Sabo et al., 2008). In melanoma cells BRAF is the major RAF kinase, and it phosphorylates and activates MEK. BRAF contains this conserved lysine (K483) in its activation loop (Figure 5.3A), and we hypothesised that a similar mechanism to that observed with MEKK2 or CDK9 could take place with BRAF. To examine this possibility, crystal structures of BRAF were visualised (Wan et al., 2004; Bollag et al., 2010). In a structure of BRAF^{V600E} complexed with vemurafenib (PLX4032; Figure 5.3B), and in structures of both wild-type (Figure 5.3C) and V600E (Figure 5.3D) BRAF complexed with sorafenib (BAY439006), another clinically approved RAF inhibitor, K483 can be seen protruding from the activation loop into the active site in a similar 3D space to CDK9. This suggests that if BRAF could be acetylated at this site, it will also likely be inhibitory; acetylation neutralises the charge of the lysine side-chain, reducing its affinity for the negatively-charged ATP alpha-phosphate.

To ask whether BRAF could be acetylated, FLAG-BRAF WT and FLAG-BRAF^{V600E} were expressed in Phoenix cells in the presence or absence of HA-p300. Following FLAG-immunoprecipitation and Western blotting for pan-acetyl-lysine, it could be seen that p300 can acetylate both forms of the kinase (Figure 5.4, data from Kao-Chin Ngeow). This suggested that, by inhibiting p300/CBP in cells, an inhibitory

acetylation event on BRAF is prevented, thereby permitting hyper-activation of the MAPK pathway. Further work will be required to confirm whether BRAF-K483 is indeed acetylated by p300, that this modification, if it exists, is inhibitory, and that BRAF-K483 can be acetylated in the absence of exogenous acetyl-transferase.

5.3 p300/CBP-inhibition induces senescence in melanoma cells

In the course of earlier experiments p300/CBP inhibition was seen to activate MAPK signalling (Figure 5.1). Because aberrant MAPK activation is known to induce senescence in melanocytes as a protective mechanism against melanoma development (Michaloglou et al., 2005; Gray-Schopfer et al., 2006), and because loss of p300 in melanocytes also leads to senescence (Bandyopadhyay et al., 2002), it was hypothesised that these could be linked. In this hypothesis, p300-mediated acetylation, and presumed inhibition, of BRAF would block excessive activation of the MAPK pathway even in the presence of oncogenic mutations such as BRAF^{V600E}. This would provide the cell with a potential means of suppressing senescence, alongside other
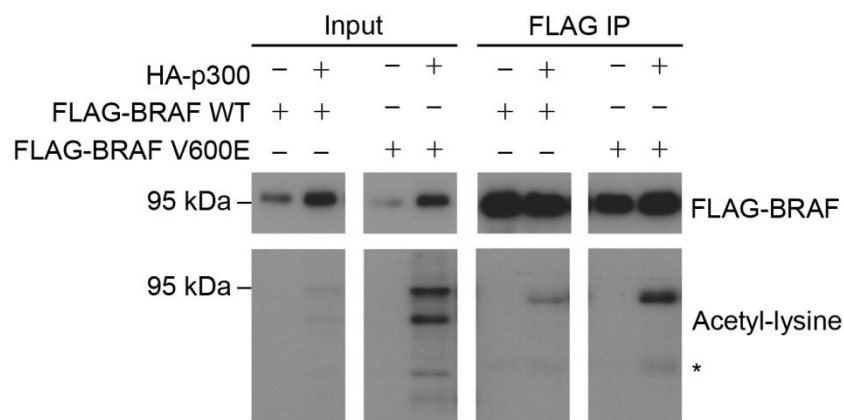
Figure 5.4. BRAF is acetylated by p300. Phoenix cells were transfected with the constructs indicated for 40 hours before harvesting and immunoprecipitation with anti-FLAG-conjugated agarose beads. Input and IP fractions were probed by Western blotting with the indicated antibodies. 95 kDa marker indicates the mobility of FLAG-BRAF. * marks the presence of IgG in the IP lanes. Data from Kao-Chin Ngeow.

changes such as inactivation of p16^{INK4A}. Additionally it was observed that, following treatment with a high dose of C646, melanoma cells had a tendency to die (Figure 5.1B), suggesting that C646 could be toxic to cells. While it is unlikely that the molecule itself is directly DNA-damaging, p300 has been shown to play a role in the DNA-damage response. For example, p300 acetylates p53-K382 following UV-irradiation, which enhances sequence-specific DNA binding of p53 (Sakaguchi et al., 1998), and p300-mediated acetylation of H3K56 increases at damaged loci following genotoxic insult (Vempati et al., 2010). Thus, following p300-inhibition, the repair of DNA damage of both endogenous and exogenous sources would be expected to be hindered.

Following treatment with agents inducing DNA double-strand damage such as strand breaks or UV-mediated crosslinks, histone H2AX at the sites of damage is phosphorylated on S139 within 5 minutes (Rogakou et al., 1998). The ability of melanoma cells to repair DNA damage following C646 treatment was assessed by immunofluorescence for γ-H2AX foci. Following 3 hours of treatment, up-regulation of γ-H2AX was seen in 501mel cells (Figure 5.5A), suggesting that inhibition of p300 in these cells was preventing DNA-damage repair. The coverslips were also stained for MITF to see whether there was any change in sub-cellular localisation of MITF following treatment, but MITF localisation did not change following C646 treatment, as judged by DAPI counterstaining.

Treatment with C646 activates MAPK signalling, which tends to promote cell growth, but also leads to accumulation of DNA damage, which would inhibit growth. To confirm which of these happens in response to C646 treatment, growth of 501mel cells in the presence of 20 μM C646 was measured with an MTT assay. Untreated or DMSO-treated cells grew as expected, while cells treated with C646

completely failed to grow; indeed, the MTT reading decreased slightly from day 0 (Figure 5.5B). It should be noted that while MTT is a measure of mitochondrial viability and thus not a direct measure of cell proliferation, visual inspection of the wells throughout the experiment confirmed that 501mel cells fail to proliferate in the presence of C646 (data not shown).
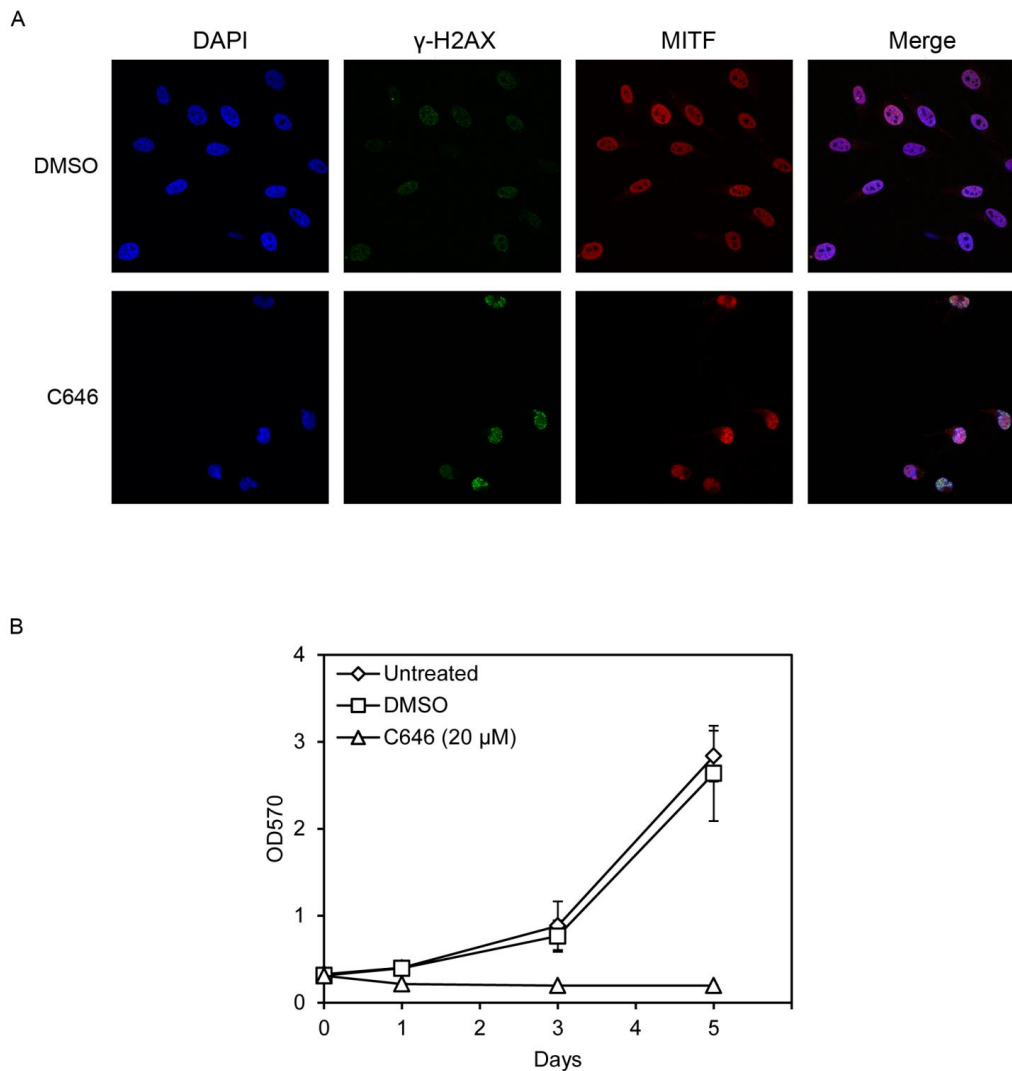
Figure 5.5. C646 is toxic to 501mel cells. (A) 501mel cells plated on coverslips were treated with DMSO or C646 (20 μM) for 3 hours, stained with antibodies against γ-H2AX and MITF, and counterstained with DAPI, as shown, before being analysed by confocal microscopy. (B) 1,000 501mel cells were plated in 96 well plates. The next day (day 0), media was replaced with fresh media, or media containing DMSO or C646 (20 μM). At the indicated times, cells were subjected to an MTT assay. Each data point is the average of 3 independent experiments ± standard error of the mean.

Two important proteins that can suppress senescence in melanoma cells are TBX2 (Jacobs et al., 2000; Prince et al., 2004; Vance et al., 2005), and TBX3 (Brummelkamp et al., 2002; Rodriguez et al., 2008). p300-down-regulation in melanocytes induces senescence (Bandyopadhyay et al., 2002) and, to see whether the same may occur in melanoma cells, we treated 501mel cells with 20 µM C646 for a range of times to assess levels of the suppressors of senescence TBX2/3 (Figure 5.6). In a Western blot analysis, MITF was phosphorylated in response to C646 treatment as was previously observed (Figure 5.1B), demonstrating that the treatment had been effective. The anti-senescent protein TBX3 was reduced following 12 hours of treatment compared to DMSO-treated control cells, relative to the actin loading control. Another anti-senescence factor, TBX2, appeared to decrease slightly in C646-treated cells. This result suggested that C646-mediated inhibition of p300 could induce senescence in 501mel cells, which has been confirmed by senescence-associated-β-galactosidase (SA-β-gal) assays (Rhoda Alani, Boston University, personal communication). An SA-β-gal assay is a marker of the overexpression and accumulation of lysosomal β-galactosidase that occurs in senescing cells (Lee et al., 2006), and is a widely used assay as a correlate of the induction of senescence.
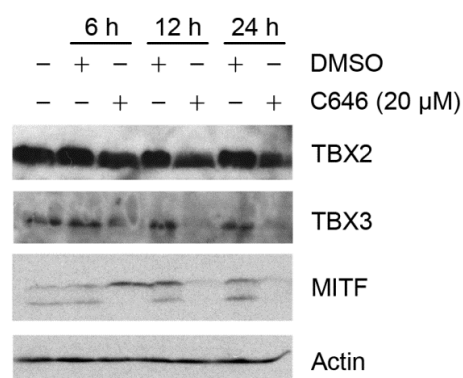
Figure 5.6. C646 down-regulates anti-senescence factors. 501mel cells were treated or not for the indicated times with DMSO or C646 (20 µM) before whole cell lysates were analysed by Western blotting with the indicated antibodies.

5.4 Discussion

In melanocytes, abrogation of p300 expression has been demonstrated to lead to the induction of senescence (Bandyopadhyay et al., 2002). Together with collaborators (Rhoda Aline, Boston University), we show here that chemical inhibition of p300/CBP can induce senescence in 501mel cells, as demonstrated by a failure to proliferate, elevated γ-H2AX, an increase in SA-β-gal staining, and down-regulation of the anti-senescence factors TBX2 and TBX3. These collective results demonstrate that p300 can play an anti-senescent role in the melanocyte lineage. It is known that the MAPK pathway activates p300 acetyl-transferase activity following phosphorylation of p300 by ERK2. Oncogenic MAPK activation in melanocytes induces senescence. Because loss of p300 also triggers a senescent programme, MAPK-mediated p300 activation could act as a restraint on senescence.

It has also been shown here that the small molecule inhibitor of p300/CBP, C646, activates the MAPK pathway in cells in a fashion specific either to melanoma cells or to cells with genetically activated MAPK pathway components. This suggests that p300/CBP inhibits MAPK signalling. A likely candidate mechanism for this inhibition could be acetylation of a highly conserved lysine residue in the activation loop of BRAF. This raises the possibility of an advantageous negative feedback loop coupling BRAF and p300 activities. In healthy cells, when MAPK is activated by mitogenic signalling, one way in which it can promote cell growth is through stimulation of p300, which will lead to a general activation of transcription. It will, in turn, lead to inhibition of BRAF and a natural limit will be placed on the degree of pathway activation, which will prevent hyper-proliferation (Figure 5.7A). In an oncogenic situation, however, the MAPK pathway is constitutively activated, and the cell will enter senescence as a means of preventing excessive proliferation. The

negative feedback loop can be turned to tumorigenic advantage here too: if MAPK activates p300, which in turn inhibits BRAF, then even constitutively activated MAPK should be inhibited by p300-mediated acetylation, which could help the cell to escape senescence and continue proliferating (Figure 5.7B). Importantly, BRAF-acetylation was observed in both wild-type BRAF and BRAF^{V600E}, demonstrating that the process is independent of activating mutations within the MAPK pathway. While it has been shown here that p300/CBP inhibition does indeed activate the MAPK pathway, it will be necessary to extend these studies into other melanoma cell lines to confirm the senescent phenotype induced, and to show that it is MAPK-mediated through experiments coupling C646 and MAPK inhibitors. It will also be important in the future to confirm that BRAF K483 is acetylated by p300, and identify any other
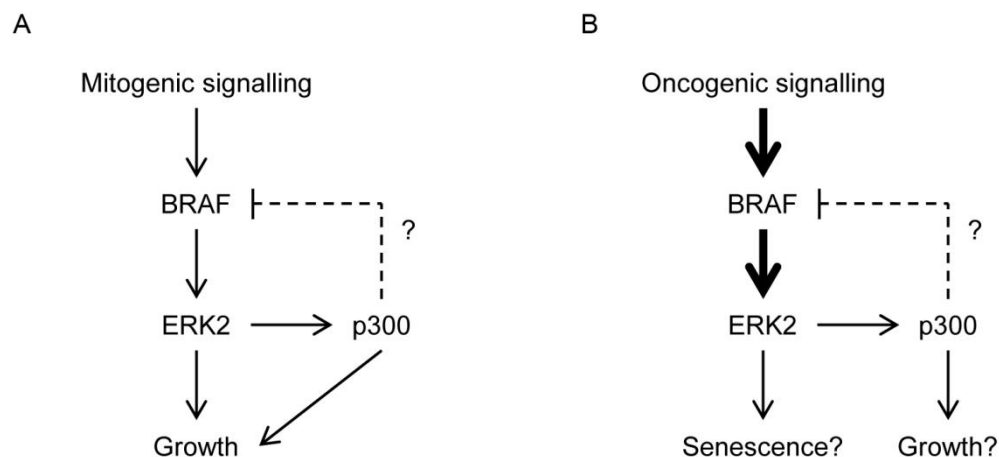
Figure 5.7. Hypothesis of the effects of p300 activity on MAPK activity under different conditions. (A) Under healthy conditions, mitogenic signalling stimulates growth by activating BRAF and the MAPK pathway. ERK2 will also be stimulated to activate p300, which is hypothesised to inhibit BRAF by acetylation of its active site. (B) Under oncogenic activation, constitutive activation of MAPK, usually by BRAF mutation, will result in induction of senescence. Because mutant BRAF can still be acetylated, it is hypothesised that acetylation can still inhibit it, and that this will provide a restraint on entering senescence. This could, in turn, give the cell sufficient time to find further means of senescent escape, such as loss of p16^{INK4A}.

acetylated residues within the protein, and to show with *in vitro* kinase assays that acetyl-K483 BRAF is inhibited compared to protein with the unmodified residue.

MITF has been shown to have an anti-senescent role through up-regulation of TBX2 in melanoma cells (Carreira et al., 2000), and loss of MITF in melanoma cells following siRNA-mediated MITF depletion has been shown to induce senescence (Giuliano et al., 2010). C646 treatment in 501mel cells led to loss of MITF following rapid MAPK activation and MITF phosphorylation, which raised the possibility that the senescence induced by C646 could, at least partially, arise from loss of MITF and consequent changes in MITF target gene expression.

Following C646 treatment in WM852 melanoma cells and microarray profiling, a signature showing transcriptional silencing of genes regulating cell cycle progression, DNA replication and DNA repair, along with up-regulation of tumour suppressor genes such as p53, has been identified (Byungwoo Ryu, Boston University, personal communication). As a preliminary approach to asking whether any of these genes could also be MITF-regulated, the list of mis-regulated genes forming this signature was compared with genome-wide MITF ChIP-Seq and siRNA MITF RNA-Seq data collected earlier. When compared with genes whose expression is down-regulated following depletion of MITF in 501mel cells, 60 genes that are down-regulated on C646 treatment are also down-regulated following siMITF, while none of the C646-upregulated genes are upregulated in MITF-depleted cells (Figure 5.8A). This suggested that some genes induced by MITF could also play an important role in suppression of OIS in melanoma cells. Among genes that are up-regulated in MITF-depleted cells, one gene, *CITED2*, is up-regulated by C646 (Figure 5.8B). CITED2 is a p300/CBP co-activator that functions as a bridge to the AP-2 family of transcription factors and plays a role in neural tube development (Sun et al., 1998;

Bamforth et al., 2001). It is not unexpected that cells might respond to loss of p300/CBP activity by up-regulation of a p300/CBP co-activator. Taken together, this data suggests that, in 501mel cells, MITF could be acting to suppress the senescent phenotype observed following treatment with C646, by directly binding and up-regulating expression of certain genes, as well as through repression of *CITED2*.

HA-Mitf binds approximately four times more genes whose expression is unaffected by siRNA depletion of MITF than those that are MITF-bound and directly MITF-regulated. The fact that in 501mel cells depleted for MITF for 72 hours the
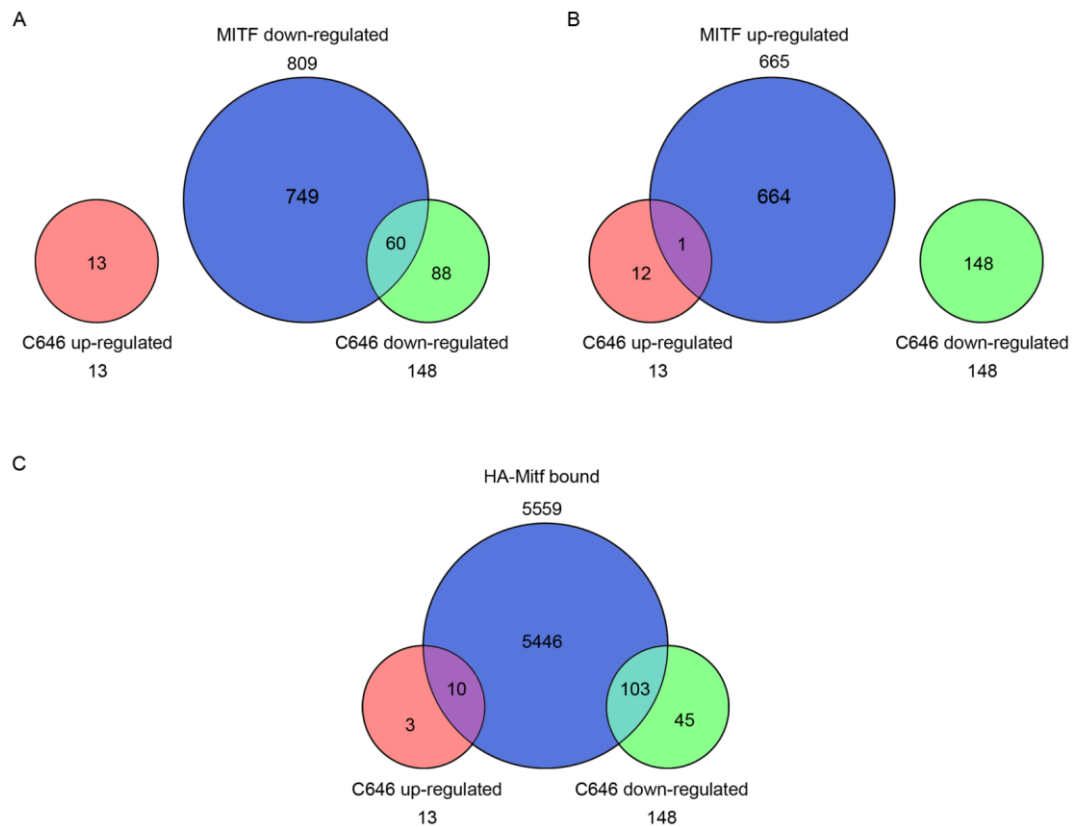
Figure 5.8. Expression of genes regulated by C646 treatment could be controlled by MITF. Microarray analysis to determine C646 regulated genes was carried out in WM852 cells (Byungwoo Ryu, Boston University). HA-Mitf ChIP-Seq and siCTR vs siMITF RNA-Seq was carried out in 501mel cells as described in Chapter 3. (A),(B) C646-regulated genes were compared with genes down-regulated (A), or up-regulated (B), following siMITF transfection. (C) C646-regulated genes were compared with genes bound by HA-Mitf.

expression of these genes is unchanged does not mean that they will not be regulated by MITF under certain cellular contexts, or in different cell lines. Thus all 5,559 bound genes have the potential to be MITF-regulated. By comparing genes bound by MITF with the C646-regulated genes, 10 out of 13 genes up-regulated by C646 have MITF peaks associated with them, and 103 out of 148 genes down-regulated by C646 are associated with MITF peaks (Figure 5.8C). Given that MITF highly occupies 5,559 out of 21,509 RefSeq genes, by chance it would be expected that 41 C646-regulated genes should be occupied by MITF; the fact that 161 are suggests that MITF does have the potential to influence the expression of many of the genes forming the signature associated with C646-treatment.

HA-Mitf ChIP-Seq and siMITF RNA-Seq was carried out in 501mel cells and the C646 microarrays in WM852 cells. Definitive conclusions cannot therefore be drawn from these comparisons, and similar experiments must be performed in the same cell lines to permit direct comparisons between the role of MITF and the effects of C646 treatment. Further, after determining whether or not C646 affects DNA-binding by MITF, a timecourse of gene expression and ChIP assays from cells treated or not with C646 must be conducted to interrogate how MITF DNA binding and target gene expression changes with time, and whether this correlates with the C646-induced gene expression changes observed.

Chapter 6 – Discussion

6.1 MITF: a global regulator of cell function

In this study we have generated a genome-wide profile of MITF DNA binding. As well as occupying many known genes in the expected binding sites such as *Pmel*/*CDK2* (which are co-regulated from an enhancer element within the first intron of *Pmel* [Du et al., 2003]) and *Tyrosinase*, MITF occupied sites in many genes that have not previously been described, including enhancer regions in *MITF* itself. One notable category of gene occupied in the ChIP-Seq and de-regulated following siMITF transfection was lysosome-regulating genes. These genes were previously thought to be the provenance of TFEB, the master regulator of lysosomes (Sardiello et al., 2009). TFEB is a member of the MiT subfamily of bHLH-LZ transcription factors, binds the same consensus sequence *in vitro* and *in vivo*, and can heterodimerise with MITF (Hemesath et al., 1994; Sardiello et al., 2009). It would be interesting to compare the genome-wide binding profiles of MITF and TFEB (this work; Sardiello et al., 2009). However, the raw TFEB ChIP-Seq data is not publically available and the processed data is only incompletely published at the time of writing, so this is an unfeasible comparison to make at present. Work is underway in our laboratory to establish a HA-TFEB cell line with which to perform ChIP-Seq.

A role for MITF in metabolic functioning of the cell has also been suggested by this work. Expression of genes such as the glucose transporting *GLUT1*, as well as metabolic enzymes such lactose dehydrogenase, appears to be regulated by MITF. Regulation of metabolism by MITF is largely uncharacterised, although it was recently shown that MAPK signalling regulates oxidative phosphorylation, using MITF as a mediator to induce PGC-1α, which regulates of mitochondrial biogenesis (Haq et al., 2013). PGC-1α, in turn, regulates *MITF* expression (Shoag et al., 2013). Given that MITF guides the developing cell from the activated MSC, through a

proliferative stage, and into a differentiated melanocyte, it would make sense if MITF was able to regulate metabolic flux in the cell, as the nutritional requirements of the cell at different stages in its development will vary.

The previous MITF ChIP-Seq and RNA-Seq experiments identified a similar set of target genes and biological processes to those found to be regulated by MITF here (Strub et al., 2011). Of the 5,559 HA-Mitf-occupied genes identified here, 3,055 out of 5,578 were commonly bound in Strub et al. (2011), while just 378 of the 1,474 differentially regulated genes following our siMITF RNA-Seq experiment were also mis-regulated among the 1,345 differential genes identified in Strub et al. (2011). However, although both studies demonstrate a reduction in MITF protein following siMITF, Strub et al. actually report a near-2-fold increase in *MITF* mRNA expression while this study down-regulates *MITF* 2.2-fold, rendering it impossible to make a truly valid comparison between the two RNA-Seq datasets. The combined ChIP-Seq and our RNA-Seq data suggest that MITF plays a major role in maintaining melanoma cell viability through promotion of faithful DNA replication and repair, and cell cycling. Low levels of MITF, as induced by siMITF transfection, can promote a phenotype switch to an invasive, metastatic state, in agreement with the rheostat model of MITF function (Carreira et al., 2006). MITF has been reported to be a lineage addiction oncogene (Levy et al., 2006). This is in keeping with the finding that many processes, such as pyruvate metabolism (see GO analysis in Chapter 3) are under the control of MITF, whereas in other cell types they must be controlled by another factor (or factors). Indeed, the majority of the targets identified in this work are not related to pigmentation, one of the originally identified roles of MITF, but to other, more general, non-cell type-specific pathways and functions. This is indicative of a key role for MITF in controlling the phenotype a cell adopts, and hence the

identity of different subpopulations of tumour cells that will exist within a heterogeneous melanoma.

6.2 An acetylation-dependent affinity switch controlling DNA binding specificity

This thesis has largely focussed on the role of MITF acetylation. Several transcription factors have been reported to be acetylated, with different effects. For example: p53 acetylation increases p53 DNA binding specificity (Gu and Roeder, 1997), as will be discussed later; c-Myc acetylation regulates its stability by decreasing c-Myc-ubiquitylation, and interaction of p300/CBP with c-Myc serves to increase transcription of c-Myc target genes (Vervoorts et al., 2003; Patel et al., 2004); and MYOD is acetylated by p300/CBP and PCAF, leading to enhanced expression of its target genes (Polesskaya et al., 2000).

Chapter 4 focussed on the role of MITF-K243 acetylation in controlling MITF function. We identify here a major affinity switch controlling the specificity of MITF DNA binding. In *in vitro* studies, Mitf^{K243Q} mutation substantially increases the DNA binding sequence specificity of Mitf as compared to a wild-type protein, while at the same time reducing the general affinity for DNA. In these experiments, the protein fragments were purified from bacteria and hence the wild-type protein was non-acetylated at K243. An Mitf^{K243R} mutant, mimicking non-acetylated Mitf, behaved very similarly to the wild-type protein, conferring upon Mitf the ability to bind degenerate M/E-box sequences that deviated from the previously identified 5'-TCA[C/T]GTGA-3' consensus binding sites, both within the core hexamer and the flanking residues.

In *in vivo* ChIP-Seq experiments, HA-Mitf^{K243R} suffered a considerable loss of binding specificity compared to HA-Mitf wild-type, as had been predicted by the *in vitro* experiments. For the same number of identified binding events, HA-Mitf^{K243R}

was titrated across the genome in low affinity sites that predominantly lacked canonical MITF binding elements. In the small number of HA-Mitf^{K243R} peaks that passed a stringent cut-off to be considered highly specific binding sites, the consensus sequence for HA-Mitf^{K243R} was 5'-GTCACGTGAC-3', the same as wild-type HA-Mitf. This suggested that, although HA-Mitf^{K243R}, and by extension non-acetyl-K243 MITF, is competed away from specific binding elements by the genomic background, HA-Mitf^{K243R} can still bind the very highest affinity sites. These sites most frequently contain multiple occurrences of either just 5'-TCACGTGA-3' motifs or a mix of 5'-TCACGTGA-3' and 5'-TCACGTGB-3' motifs, perhaps suggesting that MITF cooperates in binding to multiple elements via inter-dimer interactions. This predicts that high affinity peaks containing a single MITF motif might also contain a motif for another transcription factor with which MITF can cooperate in binding to the target.

Because HA-Mitf^{K243R} was bound to fewer sites than wild-type HA-Mitf, it could be the case that either it is able to interact with fewer specific sites and therefore binding to other motifs is elevated giving the non-specific background, or that more background, non-specific, motifs are occupied, which competes the protein away from the specific motifs. The first explanation is unlikely to be case for a number of reasons. In the *in vitro* binding experiments, the ability to bind a canonical consensus motif was similar between wild-type and mutant MITF fragments, and the difference only became apparent in the face of competition from genomic DNA. Additionally, in the ChIP-Seq data, it is not the case that all sites are less bound by HA-Mitf^{K243R}, with genes such as *LAMP1* being unaffected by the mutational status of Mitf-K243. The unaffected peaks are tall, and commonly contain multiple motifs that will combine to form a higher affinity binding site than any single motif alone can. Thus, it is most likely that HA-Mitf^{K243R} binds to a similar number of locations as the wild-type

protein, but that only the highest affinity binding sites are capable of being strongly occupied by outcompeting the genomic reservoir of degenerate sequences.

MITF-K243 forms the start of helix 2 and, with the exception of MAX and MAD, was found to be absolutely conserved in human bHLH proteins as well as numerous family members from other species. From crystal structures of bHLH family members such as MYOD, PHO4 and USF (Ferre-D'Amare et al., 1994; Ma et al., 1994; Shimizu et al., 1997), it has been noted in passing several times that the K243-eqiuvalent side chain forms a contact with the phosphate backbone. Given the conservation of this lysine throughout the family, it is surprising that it has not hitherto received more attention. In the recently solved MITF crystal structure (Pogenberg et al., 2012), the authors also identified the interaction between MITF-K243 and the E/M-box motifs they studied, but failed to pursue the role of this residue in MITF regulation, focussing instead on other bHLH amino acids.

The strong conservation of MITF-K243 implies that this affinity switch could be conserved among bHLH proteins. Recent work in our laboratory has suggested that this could be the case: K-Q and K-R substitutions in the equivalent lysine residue in USF-1 (K240) show the same behaviour in *in vitro* binding behaviour as they do in MITF (Pakavarin Louphrasitthiphol, personal communication). USF-1 is not known to be acetylated on K240, but it has been shown in the laboratory that it can indeed be acetylated by p300. USF-1 can be acetylated on K199 in response to activation of p38 signalling by a range of stresses (Corre et al., 2009), but K199R mutation fails to abolish the p300-induced acetylation, indicating that USF-1 can be multiply acetylated. Work is currently underway to identify the exact sites that are acetylated within USF-1.

The acetylation-mediated switch in MITF DNA binding affinity and specificity has a number of interesting ramifications. The number of active molecules of MITF, and indeed any other transcription factor in which a similar mechanism could occur, will likely be lower than previously thought; at many sites where MITF is DNA-bound genome wide, it will not be bound productively. Rather, non-acetyl-K243-MITF will form a highly mobile pool of protein that surveys the genome with low specificity, and likely does not remain bound to any one site for long time periods. If the switch is conserved in other bHLH proteins such as c-Myc, MYOD, or USF, these would also be expected to be titrated away from their specific binding sites in the absence of acetylation, forming a pan-genomic transcription factor reservoir.

Work in our laboratory has determined that, in the mouse hair follicle, non-proliferating, quiescent cells exhibit low levels of acetyl-lysine, while actively proliferating cells, including melanocyte lineage cells, have a robust detectable acetyl-lysine signal as detected by immunostaining (Rasmus Freter, personal communication). A similar result was observed in melanoma sections, where proliferative cells contain acetyl-lysine while non-proliferative stem-like cells do not (Rasmus Feter and Richard Lisle, personal communication).

Integration of these findings allows a model of K243-acetylation in regulating the transition between proliferating and non-proliferating melanocytes or melanoma cells to be proposed (Figure 6.1). In a proliferative cell, such as a growing cell in the hair follicle or a proliferating melanoma cell, MAPK signalling will be activated. These cells will contain elevated levels of acetyl-lysine. MITF would therefore be acetylated on K243 and MITF will have reduced affinity for DNA, but will bind with far greater specificity. MITF will no longer be able to interact with low affinity sequences, and so will interact with target genes containing a canonical 5'-

TCA[C/T]GTG-3' motif. This, however, presents a problem for the cell. If MITF binds targets containing 5'-TCA[C/T]GTG-3' motifs then, as well as regulating proliferative target genes such as *CDK2*, it would be directed to genes that control the differentiation and pigmentation programme, such as *Tyrosinase*. The problem lies in the fact that the differentiation programme and proliferation are potentially mutually exclusive. Recent work in the laboratory has revealed MITF-K206, which is located in the basic region and is also acetylated by p300, regulates a switch in binding from
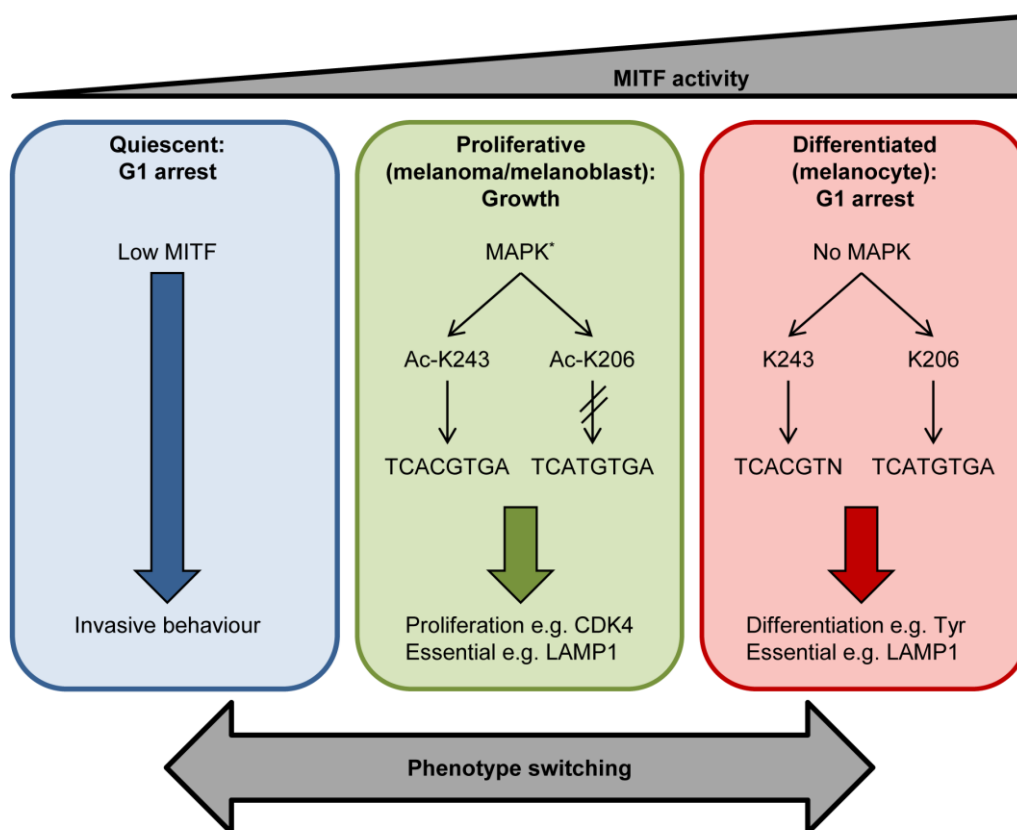
Figure 6.1. Modified rheostat model for MITF function. The rheostat model relies on MITF activity coupled to its expression level to control the phenotype adopted by a cell (Carreira et al., 2006). Quiescent cells (invasive melanoma cells or migratory melanoblasts) show invasive behaviour and G1 arrest as a result of low MITF levels (left). From this work, in proliferative melanoma cells or melanoblasts, active MAPK signalling (and Ac-K206/243) directs MITF to target both essential and pro-proliferative target genes at the expense of differentiation targets (middle). In differentiated cells, MAPK is inactive, allowing targeting of both essential and differentiation target genes.

5'-CATGTG-3' to 5'-CACGTG-3', depending on its acetylation state (Hans Friedrichsen, personal communication). Mitf^{K206Q} has a reduced affinity for 5'-CATGTG-3', but it strongly binds to 5'-CACGTG-3'. On re-inspection of motifs in characterised target genes of MITF (Cheli et al., 2010), it was observed that pigmentation and differentiation-type genes are largely the ones that contain 5'-CATGTG-3' motifs. Thus, in the proliferating, acetylation up-regulated cell, MITF should primarily be directed to bind target genes containing 5'-CACGTG-3' motifs, meaning that the differentiation genes will not be activated and the cell will be able to proliferate.

In a non-proliferating cell (quiescent and invasive or differentiated), MITF will presumably be in an unacetylated state, given the global lack of acetylation in these cells. It will therefore be able to interact with more degenerate sequences, such as 5'-TCACGTN-3', displaying a high affinity yet lower specificity for DNA. The genes that are activated will therefore be those with very high affinity binding sites that can retain MITF occupancy against the titrating effect of the genomic reservoir. These are K243-acetylation independent target genes, such as *LAMP1*, which typically contain multiple motifs: frequently 2 or more 5'-TCACGTGA-3' motifs or a mix of 5'-TCACGTGA-3' and 5'-TCACGTGB-3'. Because MITF is not acetylated in these cells and hence will be non-acetyl-K206, the protein would also be able to bind to 5'-CATGTG-3' motifs as well as the 5'-CACGTG-3' motifs, and hence promote differentiation via binding to target genes such as *Tyrosinase*.

This model presents the cell with a simple mechanism for rapid integration of pro-proliferative signalling into the network of stimuli to which it must respond and adapt, and adds to the phenotype switching model of melanoma progression (Hoek and Goding, 2010). MITF that is titrated across the genome and bound to non-specific

sites will be acetylated following emergence of pro-proliferative signals, and it will be immediately restricted to its specific binding sites. Because the protein is already in the nucleus, the response will be faster than if it were to translocate from the cytosol, such as is the case following NF-κB activation. It will certainly be faster than the synthesis of new protein, as happens following inhibition of MDM2 and activation of the p53 pathway.

In keeping with our observations on the lack of global acetylation in quiescent cells in the hair follicle and in melanoma sections, it has been reported that epidermal stem cells, both within the hair follicle and in intra-follicular regions, show reduced H4 acetylation (Frye et al., 2007). Following activation of the stem cell, H4 acetylation becomes detectable but is lost again on terminal differentiation (Frye et al., 2007). Therefore this could be a general mechanism that operates in many cell types and one not simply restricted to cells of the melanocyte lineage.

The genome, in the absence of pro-proliferative signalling, will be decorated with MITF that is bound to low affinity sites. Because MITF shows low affinity for these sequences, it is unlikely to reside for a long time at them, and instead will dissociate and translocate elsewhere. Thus, given that the duration of transcription factor residency has been shown to correlate with gene expression level in the case of Rap1 (Lickwar et al., 2012), it is highly likely that this low affinity binding is non-productive and does not promote gene expression.

Increasing evidence suggests that use of transcription factor acetylation to modulate DNA binding specificity is emerging, although the idea presented here that lack of acetylation results in genome-wide titration away from specific binding sites is novel. Acetylation of the C-terminus of p53 increases its DNA binding specificity (Gu and Roeder, 1997). These acetylation events have been shown to occur in response to

DNA damage (Sakaguchi et al., 1998; Liu et al., 1999). It has further been shown that p53-K120 can be acetylated in response to DNA damage, and that this acetylation promotes apoptosis rather than cell cycle arrest (Sykes et al., 2006; Tang et al., 2006). p53-K120 is a DNA binding residue (Kitayner et al., 2006), as is MITF-K243, and it was recently revealed that acetylation of p53-K120 led to enhanced discrimination between random DNA and p53-specific binding sites (Arbely et al., 2011). This fits well with a finding that p53 can slide along DNA in search of specific binding sites (Tafvizi et al., 2011). It thus seems likely that the genome will, at any given time, be highly occupied in a non-productive manner by transcription factors that are either transiently bound to non-specific sites, or actively scanning for specific binding sites. Post-translational modifications such as acetylation, which tends to reduce the affinity of protein-DNA interactions, would therefore promote association with specific sequences.

It is known that MITF plays a key role in maintaining genome integrity (Giuliano et al., 2010; Beuret et al., 2011; Strub et al., 2011) by regulating DNA-damage repair genes, a finding that is reproduced here following HA-Mitf ChIP-Seq and siMITF RNA-Seq. If MITF is widely distributed throughout the genome, and if it forms transient, non-specific interactions with DNA rather than being located at specific binding sites, then there should be MITF molecules bound in the vicinity following the induction of DNA damage. Indeed, work in our laboratory has shown that MITF influences the DNA damage response, that it accumulates at sites of DNA damage and that it is phosphorylated and stabilised by ATM and Chk2 (Romuald Binet, personal communication). The N-terminus of MITF appears to contain a mono-ubiquitin binding domain (Luis Sanchez, personal communication), permitting MITF to bind nucleosomes with histones H2A, H2B, or H2AX that have been mono-

ubiquitylated following DNA damage (Bergink et al., 2006; Wu et al., 2009; Moyal et al., 2011; Pan et al., 2011). This will prevent MITF from diffusing away from the DNA-damaged site, at which MITF acts as a binding site for DNA-damage repair complexes. One example is the chromatin remodelling Mi2-NuRD complex that has been shown to interact with MITF (Luis Sanchez, personal communication), and is known to play a role in the DNA-damage response (Polo et al., 2010). In this way, the genomic titration of MITF, and potentially other transcription factors that are titrated by the genome, can function as a guardian of the genome.

6.3 An acetylation-phosphorylation feedback loop

Previous work in our laboratory found that acetylation of MITF requires MAPK signalling, but that it is independent of the MAPK phosphorylation events on MITF. A hypothesis was formed that activated MAPK signalling, such as that which is found in proliferating hair follicle cells or melanoma cells, would result in MITF-acetylation. This would make MITF more likely to bind and promote expression of genes that promote proliferation. However, in non-proliferative quiescent cells, MAPK signalling is not activated and MITF will be unacetylated, which would promote binding to and expression of pigmentation genes.

Following ChIP-Seq experiments in the presence and absence of PLX4720, no change could be identified in MITF binding to either proliferative or differentiation target genes, as was discussed in Chapter 3. Integration of the data presented here with other results from the laboratory, however, suggests that MITF-K206 acetylation status could be critical for determining the ability of MITF to regulate differentiation-specific genes, which appear to contain predominantly 5'-CATGTG-3' motifs.

It is known that MAPK activates p300 acetyltransferase activity (Chen et al., 2007), which has been confirmed in this study. Given that data from us and others

suggests that high global acetylation levels could be restricted to proliferating cells (our unpublished data; Frye et al., 2007), and that, in the melanocyte lineage, these are the cells that contain active MAPK signalling, it could be that MAPK signalling upstream of p300 is required in general for up-regulation of acetylation, rather than just for a boost in p300 activity as was reported (Chen et al., 2007). In Chapter 5, it was found that chemical inhibition of p300/CBP led to almost immediate activation of the MAPK pathway and consequently to induction of senescence. A mechanism was proposed whereby BRAF-K483 acetylation within the loop region of the active site inhibits the kinase activity of this protein, which will act as a barrier against induction of oncogene-induced senescence.

We also identified SIRT1 as a potential regulator of p300 stability. Under conditions of nutrient deprivation, glycolytic flux will be reduced leading to elevated NAD^+, which will result in increased SIRT1 activity. Under such conditions, high SIRT1 activity will cause a loss of p300, meaning that MITF will be unacetylated regardless of the state of MAPK signalling, and it will drive the expression of genes that are acetylation-independent. This finding couples the regulation of metabolic pathways such as glycolysis to the release of MITF from the genomic reservoir.

6.4 Future directions

6.4.1 MITF acetylation

Further work will be required to determine the precise sites in MITF that are deacetylated by HDAC1 and HDAC4. This will be achieved by incubating peptide arrays containing peptides that are acetylated or not, covering the range of acetylatable lysines in MITF, with recombinant HDAC1 and HDAC4 enzymes. Future work will also seek to characterise the role of other acetylation sites. It is

hypothesised here that K225 acetylation would inhibit interaction with β-catenin. Investigation of the basic region acetylation sites (K205, K206) is underway, as outlined above.

6.4.2 MITF-K243 function

MITF-K243 has a key role in regulating MITF function, as K243-acetylation status determines the specificity of the MITF-DNA interaction. ChIP-Seq experiments using an HA-Mitf^{K243Q} stable cell line are underway, which will complement the already gathered data on HA-Mitf and HA-Mitf^{K243R}. It is anticipated, following *in vitro* experiments, that HA-Mitf^{K243Q} should display highly specific binding compared to the HA-Mitf^{K243R}. It will also be crucial to confirm directly that acetyl-K243 MITF behaves in the same manner as Mitf^{K243Q}, to show that MITF-K243 acetylation is important for specific DNA binding. This will be achieved by introducing a K243C mutation in a bHLH fragment of Mitf, followed by derivatisation of the thiol side chain to introduce an acetyl-lysine mimic, a method yielding modified histones recognised by acetyl-specific antibodies (Chalker et al., 2012). This acetyl-mimicking protein, along with the wild-type and mutant fragments characterised here, will be used to quantify the K_D of acetyl- and non-acetyl-K243 MITF for both random DNA and different binding sites. It will also be important to confirm whether other bHLH proteins can be acetylated on the K243-equivalent lysine residue, and whether these modifications play a similar role to the role of MITF-K243.

The microarray analysis performed in this work did not show a strong relationship between de-regulation of Mitf binding on K243R substitution and changes in gene expression. It is possible that this was not the ideal context in which to conduct gene expression measurements. The stable cell lines express endogenous MITF, so only around a quarter of the MITF dimers in the cell will be HA-Mitf

homodimers, while a quarter will be endogenous MITF homodimers. It is therefore possible that many changes induced by the HA-Mitf mutants are being masked. The stable cell lines will be used for knockdown of endogenous MITF using an shRNA designed against the 3'-UTR of *MITF*, which will not affect expression of the HA-Mitf, and will subsequently be used for RNA-Seq analysis. These studies will be coupled to functional assays such as measurements of migration and invasion; given that the HA-Mitf^{K243Q} cell lines were more migratory than HA-Mitf cell lines, the same effect should be observed following shRNA expression. Tumour formation assays in immunocompromised mice injected with the stable cell lines used here are underway, to see if the enhanced migration seen with HA-Mitf^{K243Q} might translate into greater tumorigenicity.

A putative major role in the regulation of nutrient processing, both in terms of transport, recycling of waste materials via lysosomes, and metabolic pathways, has been identified for MITF. It has recently been confirmed in the laboratory that MITF regulates lysosome biogenesis through controlling expression of genes such as *LAMP1* (Luis Sanchez, personal communication). Therefore, the metabolic function of 501mel cells in which MITF has been depleted by siRNA will be examined, along with the stable cell lines used here, to determine how MITF regulates metabolic flux in the cell, and how this might be regulated by MITF acetylation status.

6.4.3 MAPK-p300 feedback regulation, coupled to MITF acetylation

As discussed in Chapter 3, ChIP-Seq on HA-Mitf in the presence of UO126 will be performed to see whether the issue of there being no change in genome-wide occupancy following PLX4720 treatment is solved by MAPK blockade lower in the pathway. If it is not, competition ChIP experiments will be performed by introducing an inducible FLAG-Mitf into the 501.HA-Mitf cell line, and induction timecourse

experiments undertaken in the presence and absence of UO126, to investigate whether the kinetic of binding changes following treatment.

As discussed in Chapter 5, it will be essential to identify the acetylated residues within BRAF by mass spectrometry, and to confirm that the acetylated kinase is inhibited. The role of p300 in MAPK-driven OIS will be examined by conducting senescence assays in the presence and absence of C646 and UO126, to see if MAPK blockade prevents the senescence induced by C646. These findings will be correlated with HA-Mitf ChIP and gene expression analyses in the same cell line, to ask what the role of MITF in this process could be.

To examine the potential role of starvation conditions, or other conditions where nutrient content is reduced in cells, the role of acetylation-independent MITF target genes will be studied by inducing starvation conditions with minimal growth media in the Mitf-mutant stable cell lines, and by looking to see what happens to HA-Mitf gene targeting. Stem-like melanoma cells are frequently highly invasive, and it is anticipated that a highly invasive melanoma cell line, such as IGR-39, will display a metabolic shift relative to a less invasive cell line, such as IGR-37. IGR-39 is a metastatic cell line, and IGR-37 a primary tumour cell line, established from the same patient, and so these cells will provide an ideal platform in which to perform transcriptome and metabolome analysis to check whether such a shift is apparent. Further, IGR-37 express MITF while IGR-39 does not. Therefore, if an inducible MITF were introduced into IGR-39, following induction it would be expected that these cells would display reduced invasive behaviour, and alter expression of MITF-regulated metabolic regulating genes towards the pattern seen in IGR-37 cells.

6.5 Conclusion

This thesis provides evidence of a major affinity switch induced by MITF-K243 acetylation that controls MITF DNA binding behaviour, and it proposes a mechanism that enables MITF to differentiate between proliferation-promoting or differentiation-promoting target genes. In addition, it identifies a new role of MITF in regulating nutritional processing. Further, the work presented here explores a novel feedback mechanism integrating p300 and MITF-acetylation into the balance of pro-proliferative signalling and OIS induced by MAPK in melanoma. The results outlined provide a key insight into how manipulation of MITF may be used to control melanoma sub-population identity.

References

Adey, A., Burton, J.N., Kitzman, J.O., Hiatt, J.B., Lewis, A.P., Martin, B.K., Qiu, R., Lee, C. and Shendure, J., 2013. The haplotype-resolved genome and epigenome of the aneuploid HeLa cancer cell line. *Nature* 500(7461): 207-211.

Aksan, I. and Goding, C.R., 1998. Targeting the microphthalmia basic helix-loop-helix-leucine zipper transcription factor to a subset of E-Box elements In vitro and In vivo. *Mol. Cell Biol.* 18(12): 6930-6938.

Alonso, L. and Fuchs, E., 2006. The hair cycle. *J. Cell Sci.* 119(Pt 3): 391-393.

Alonso, L. and Fuchs, E., 2003. Stem cells in the skin: waste not, Wnt not. *Genes Dev.* 17(10): 1189-1200.

Amae, S., Fuse, N., Yasumoto, K., Sato, S., Yajima, I., Yamamoto, H., Udono, T., Durlu, Y.K., Tamai, M., Takahashi, K. and Shibahara, S., 1998. Identification of a novel isoform of microphthalmia-associated transcription factor that is enriched in retinal pigment epithelium. *Biochem. Biophys. Res. Commun.* 247(3): 710-715.

Amati, B., Littlewood, T.D., Evan, G.I. and Land, H., 1993. The c-Myc protein induces cell cycle progression and apoptosis through dimerization with Max. *EMBO J.* 12(13): 5083-5087.

Amati, B., Dalton, S., Brooks, M.W., Littlewood, T.D., Evan, G.I. and Land, H., 1992. Transcriptional activation by the human c-Myc oncoprotein in yeast requires interaction with Max. *Nature* 359(6394): 423-426.

Anghel, S.I., Correa-Rocha, R., Budinska, E., Boligan, K.F., Abraham, S., Colombetti, S., Fontao, L., Mariotti, A., Rimoldi, D., Ghanem, G.E., Fisher, D.E., Levy, F., Delorenzi, M. and Piguet, V., 2012. Breast cancer suppressor candidate-1 (BCSC-1) is a melanoma tumor suppressor that down regulates MITF. *Pigment Cell Melanoma Res.* 25(4): 482-487.

Arbely, E., Natan, E., Brandt, T., Allen, M.D., Veprintsev, D.B., Robinson, C.V., Chin, J.W., Joerger, A.C. and Fersht, A.R., 2011. Acetylation of lysine 120 of p53 endows DNA-binding specificity at effective physiological salt concentration. *Proc. Natl. Acad. Sci. U. S. A.* 108(20): 8251-8256.

Atchley, W.R. and Fitch, W.M., 1997. A natural classification of the basic helix-loop-helix class of transcription factors. *Proc. Natl. Acad. Sci. U. S. A.* 94(10): 5172-5176.

Attie, T., Till, M., Pelet, A., Amiel, J., Edery, P., Boutrand, L., Munnich, A. and Lyonnet, S., 1995. Mutation of the endothelin-receptor B gene in Waardenberg-Hirschsprung disease. *Hum. Mol. Genet.* 4(12): 2407-2409.

Bahadoran, P., Aberdam, E., Mantoux, F., Busca, R., Bille, K., Yalman, N., de Saint-Basile, G., Casaroli-Marano, R., Ortonne, J.P. and Ballotti, R., 2001. Rab27a: A key to melanosome transport in human melanocytes. *J. Cell Biol.* 152(4): 843-850.

Balch, C.M., Soong, S.J., Gershenwald, J.E., Thompson, J.F., Reintgen, D.S., Cascinelli, N., Urist, M., McMasters, K.M., Ross, M.I., Kirkwood, J.M., Atkins, M.B., Thompson, J.A., Coit, D.G., Byrd, D., Desmond, R., Zhang, Y., Liu, P.Y., Lyman, G.H. and Morabito, A., 2001. Prognostic factors analysis of 17,600 melanoma patients: validation of the American Joint Committee on Cancer melanoma staging system. *J. Clin. Oncol.* 19(16): 3622-3634.

Baldwin, C.T., Hoth, C.F., Amos, J.A., da-Silva, E.O. and Milunsky, A., 1992. An exonic mutation in the HuP2 paired domain gene causes Waardenburg's syndrome. *Nature* 355(6361): 637-638.

Bamforth, S.D., Braganca, J., Eloranta, J.J., Murdoch, J.N., Marques, F.I., Kranc, K.R., Farza, H., Henderson, D.J., Hurst, H.C. and Bhattacharya, S., 2001.

Cardiac malformations, adrenal agenesis, neural crest defects and exencephaly in mice lacking Cited2, a new Tfap2 co-activator. *Nat. Genet.* 29(4): 469-474.

Bandyopadhyay, D., Okan, N.A., Bales, E., Nascimento, L., Cole, P.A. and Medrano, E.E., 2002. Down-regulation of p300/CBP histone acetyltransferase activates a senescence checkpoint in human melanocytes. *Cancer Res.* 62(21): 6231-6239.

Bauer, G.L., Praetorius, C., Bergsteinsdottir, K., Hallsson, J.H., Gisladottir, B.K., Schepsky, A., Swing, D.A., O'Sullivan, T.N., Arnheiter, H., Bismuth, K., Debbache, J., Fletcher, C., Warming, S., Copeland, N.G., Jenkins, N.A. and Steingrimsson, E., 2009. The role of MITF phosphorylation sites during coat color and eye development in mice analyzed by bacterial artificial chromosome transgene rescue. *Genetics* 183(2): 581-594.

Baumli, S., Lolli, G., Lowe, E.D., Troiani, S., Rusconi, L., Bullock, A.N., Debreczeni, J.E., Knapp, S. and Johnson, L.N., 2008. The structure of P-TEFb (CDK9/cyclin T1), its complex with flavopiridol and regulation by phosphorylation. *EMBO J.* 27(13): 1907-1918.

Baxter, L.L. and Pavan, W.J., 2003. Pmel17 expression is Mitf-dependent and reveals cranial melanoblast migration during murine development. *Gene Expr. Patterns* 3(6): 703-707.

Beadling, C., Jacobson-Dunlop, E., Hodi, F.S., Le, C., Warrick, A., Patterson, J., Town, A., Harlow, A., Cruz, F., 3rd, Azar, S., Rubin, B.P., Muller, S., West, R., Heinrich, M.C. and Corless, C.L., 2008. KIT gene mutations and copy number in melanoma subtypes. *Clin. Cancer Res.* 14(21): 6821-6828.

Behrens, J., von Kries, J.P., Kuhl, M., Bruhn, L., Wedlich, D., Grosschedl, R. and Birchmeier, W., 1996. Functional interaction of beta-catenin with the transcription factor LEF-1. *Nature* 382(6592): 638-642.

Benezra, R., Davis, R.L., Lockshon, D., Turner, D.L. and Weintraub, H., 1990. The protein Id: a negative regulator of helix-loop-helix DNA binding proteins. *Cell* 61(1): 49-59.

Bennett, D.C., 2003. Human melanocyte senescence and melanoma susceptibility genes. *Oncogene* 22(20): 3063-3069.

Bentley, N.J., Eisen, T. and Goding, C.R., 1994. Melanocyte-specific expression of the human tyrosinase promoter: activation by the microphthalmia gene product and role of the initiator. *Mol. Cell Biol.* 14(12): 7996-8006.

Bergink, S., Salomons, F.A., Hoogstraten, D., Groothuis, T.A., de Waard, H., Wu, J., Yuan, L., Citterio, E., Houtsmuller, A.B., Neefjes, J., Hoeijmakers, J.H., Vermeulen, W. and Dantuma, N.P., 2006. DNA damage triggers nucleotide excision repair-dependent monoubiquitylation of histone H2A. *Genes Dev.* 20(10): 1343-1352.

Bernstein, B.E., Kamal, M., Lindblad-Toh, K., Bekiranov, S., Bailey, D.K., Huebert, D.J., McMahon, S., Karlsson, E.K., Kulbokas, E.J., 3rd, Gingeras, T.R., Schreiber, S.L. and Lander, E.S., 2005. Genomic maps and comparative analysis of histone modifications in human and mouse. *Cell* 120(2): 169-181.

Bernstein, B.E., Humphrey, E.L., Erlich, R.L., Schneider, R., Bouman, P., Liu, J.S., Kouzarides, T. and Schreiber, S.L., 2002. Methylation of histone H3 Lys 4 in coding regions of active genes. *Proc. Natl. Acad. Sci. U. S. A.* 99(13): 8695-8700.

Bertolotto, C., Lesueur, F., Giuliano, S., Strub, T., de Lichy, M., Bille, K., Dessen, P., d'Hayer, B., Mohamdi, H., Remenieras, A., Maubec, E., de la Fouchardiere, A., Molinie, V., Vabres, P., Dalle, S., Poulalhon, N., Martin-Denavit, T., Thomas, L., Andry-Benzaquen, P., Dupin, N., Boitier, F., Rossi, A., Perrot, J.L., Labeille,

B., Robert, C., Escudier, B., Caron, O., Brugieres, L., Saule, S., Gardie, B., Gad, S., Richard, S., Couturier, J., Teh, B.T., Ghiorzo, P., Pastorino, L., Puig, S., Badenas, C., Olsson, H., Ingvar, C., Rouleau, E., Lidereau, R., Bahadoran, P., Vielh, P., Corda, E., Blanche, H., Zelenika, D., Galan, P., Aubin, F., Bachollet, B., Becuwe, C., Berthet, P., Bignon, Y.J., Bonadona, V., Bonafe, J.L., Bonnet-Dupeyron, M.N., Cambazard, F., Chevrant-Breton, J., Coupier, I., Dalac, S., Demange, L., d'Incan, M., Dugast, C., Faivre, L., Vincent-Fetita, L., Gauthier-Villars, M., Gilbert, B., Grange, F., Grob, J.J., Humbert, P., Janin, N., Joly, P., Kerob, D., Lasset, C., Leroux, D., Levang, J., Limacher, J.M., Livideanu, C., Longy, M., Lortholary, A., Stoppa-Lyonnet, D., Mansard, S., Mansuy, L., Marrou, K., Mateus, C., Maugard, C., Meyer, N., Nogues, C., Souteyrand, P., Venat-Bouvet, L., Zattara, H., Chaudru, V., Lenoir, G.M., Lathrop, M., Davidson, I., Avril, M.F., Demenais, F., Ballotti, R. and Bressac-de Paillerets, B., 2011. A SUMOylation-defective MITF germline mutation predisposes to melanoma and renal carcinoma. *Nature* 480(7375): 94-98.

Bertolotto, C., Abbe, P., Hemesath, T.J., Bille, K., Fisher, D.E., Ortonne, J.P. and Ballotti, R., 1998a. Microphthalmia gene product as a signal transducer in cAMP-induced differentiation of melanocytes. *J. Cell Biol.* 142(3): 827-835.

Bertolotto, C., Abbe, P., Hemesath, T.J., Bile, K., Fisher, D.E., Ortonne, J.-P. and Ballotti, R., 1998b. Microphthalmia gene product as a signal transducer in cAMP-induced differentiation of melanocytes. *J. Cell Biol.* 142: 827-835.

Bertolotto, C., Busca, R., Abbe, P., Bille, K., Aberdam, E., Ortonne, J.-P. and Ballotti, R., 1998c. Different cis-acting elements are involved in the regulation of TRP1 and TRP2 promoter activities by cyclin AMP: pivotal role of M boxes (GTCATGTGCT) and of Microphthalmia. *Mol. Cell Biol.* 18: 694-702.

Bertolotto, C., K., B., Ortonne, J.-P. and Ballotti, R., 1996a. Regulation of tyrosinase gene expression by cAMP in B16 melanoma cells involves two CATGTG motifs surrounding the TATA box: implication of the microphthalmia gene product. *J. Cell. Sci.* 134: 747-755.

Bertolotto, C., Bille, K., Ortonne, J.P. and Ballotti, R., 1996b. Regulation of tyrosinase gene expression by cAMP in B16 melanoma cells involves two CATGTG motifs surrounding the TATA box: implication of the microphthalmia gene product. *J. Cell Biol.* 134(3): 747-755.

Beuret, L., Ohanna, M., Strub, T., Allegra, M., Davidson, I., Bertolotto, C. and Ballotti, R., 2011. BRCA1 is a new MITF target gene. *Pigment Cell Melanoma Res.* 24(4): 725-727.

Beuret, L., Flori, E., Denoyelle, C., Bille, K., Busca, R., Picardo, M., Bertolotto, C. and Ballotti, R., 2007. Up-regulation of MET expression by alpha-melanocyte stimulating hormone and MITF allows HGF to protect melanocytes and melanoma cells from apoptosis. *J. Biol. Chem.*

Blackwell, T.K. and Weintraub, H., 1990. Differences and similarities in DNA-binding preferences of MyoD and E2A protein complexes revealed by binding site selection. *Science* 250(4984): 1104-1110.

Blackwood, E.M., Luscher, B. and Eisenman, R.N., 1992. Myc and Max associate in vivo. *Genes Dev.* 6(1): 71-80.

Blackwood, E.M. and Eisenman, R.N., 1991. Max: a helix-loop-helix zipper protein that forms a sequence-specific DNA-binding complex with Myc. *Science* 251(4998): 1211-1217.

Blais, A., Tsikitis, M., Acosta-Alvear, D., Sharan, R., Kluger, Y. and Dynlacht, B.D., 2005. An initial blueprint for myogenic differentiation. *Genes Dev.* 19(5): 553-569.

Blankenberg, D., Von Kuster, G., Coraor, N., Ananda, G., Lazarus, R., Mangan, M., Nekrutenko, A. and Taylor, J., 2010. Galaxy: a web-based genome analysis tool for experimentalists. *Curr. Protoc. Mol. Biol.* Chapter 19: Unit 19 10 11-21.

Blanpain, C., Lowry, W.E., Geoghegan, A., Polak, L. and Fuchs, E., 2004. Self-renewal, multipotency, and the existence of two cell populations within an epithelial stem cell niche. *Cell* 118(5): 635-648.

Bollag, G., Hirth, P., Tsai, J., Zhang, J., Ibrahim, P.N., Cho, H., Spevak, W., Zhang, C., Zhang, Y., Habets, G., Burton, E.A., Wong, B., Tsang, G., West, B.L., Powell, B., Shellooe, R., Marimuthu, A., Nguyen, H., Zhang, K.Y., Artis, D.R., Schlessinger, J., Su, F., Higgins, B., Iyer, R., D'Andrea, K., Koehler, A., Stumm, M., Lin, P.S., Lee, R.J., Grippo, J., Puzanov, I., Kim, K.B., Ribas, A., McArthur, G.A., Sosman, J.A., Chapman, P.B., Flaherty, K.T., Xu, X., Nathanson, K.L. and Nolop, K., 2010. Clinical efficacy of a RAF inhibitor needs broad target blockade in BRAF-mutant melanoma. *Nature* 467(7315): 596-599.

Bondurand, N., Pingault, V., Goerich, D.E., Lemort, N., Sock, E., Caignec, C.L., Wegner, M. and Goossens, M., 2000. Interaction among SOX10, PAX3 and MITF, three genes altered in Waardenburg syndrome. *Hum. Mol. Genet.* 9(13): 1907-1917.

Bos, J.L., 1989. ras oncogenes in human cancer: a review. *Cancer Res.* 49(17): 4682-4689.

Bouras, T., Fu, M., Sauve, A.A., Wang, F., Quong, A.A., Perkins, N.D., Hay, R.T., Gu, W. and Pestell, R.G., 2005. SIRT1 deacetylation and repression of p300 involves lysine residues 1020/1024 within the cell cycle regulatory domain 1. *J. Biol. Chem.* 280(11): 10264-10276.

Bowers, E.M., Yan, G., Mukherjee, C., Orry, A., Wang, L., Holbert, M.A., Crump, N.T., Hazzalin, C.A., Liszczak, G., Yuan, H., Larocca, C., Saldanha, S.A., Abagyan, R., Sun, Y., Meyers, D.J., Marmorstein, R., Mahadevan, L.C., Alani, R.M. and Cole, P.A., 2010. Virtual ligand screening of the p300/CBP histone acetyltransferase: identification of a selective small molecule inhibitor. *Chem. Biol.* 17(5): 471-482.

Boyle, G.M., Woods, S.L., Bonazzi, V.F., Stark, M.S., Hacker, E., Aoude, L.G., Dutton-Regester, K., Cook, A.L., Sturm, R.A. and Hayward, N.K., 2011. Melanoma cell invasiveness is regulated by miR-211 suppression of the BRN2 transcription factor. *Pigment Cell Melanoma Res.* 24(3): 525-537.

Brackertz, M., Boeke, J., Zhang, R. and Renkawitz, R., 2002. Two highly related p66 proteins comprise a new family of potent transcriptional repressors interacting with MBD2 and MBD3. *J. Biol. Chem.* 277(43): 40958-40966.

Braun, T. and Gautel, M., 2011. Transcriptional mechanisms regulating skeletal muscle differentiation, growth and homeostasis. *Nat. Rev. Mol. Cell Biol.* 12(6): 349-361.

Brenner, M. and Hearing, V.J., 2008. The protective role of melanin against UV damage in human skin. *Photochem. Photobiol.* 84(3): 539-549.

Brose, M.S., Volpe, P., Feldman, M., Kumar, M., Rishi, I., Gerrero, R., Einhorn, E., Herlyn, M., Minna, J., Nicholson, A., Roth, J.A., Albelda, S.M., Davies, H., Cox, C., Brignell, G., Stephens, P., Futreal, P.A., Wooster, R., Stratton, M.R.

and Weber, B.L., 2002. BRAF and RAS mutations in human lung cancer and melanoma. *Cancer Res.* 62(23): 6997-7000.

Brummelkamp, T.R., Kortlever, R.M., Lingbeek, M., Trettel, F., MacDonald, M.E., van Lohuizen, M. and Bernards, R., 2002. TBX-3, the gene mutated in Ulnar-Mammary Syndrome, is a negative regulator of p19ARF and inhibits senescence. *J. Biol. Chem.* 277(8): 6567-6572.

Busca, R., Berra, E., Gaggioli, C., Khaled, M., Bille, K., Marchetti, B., Thyss, R., Fitsialos, G., Larribere, L., Bertolotto, C., Virolle, T., Barbry, P., Pouyssegur, J., Ponzio, G. and Ballotti, R., 2005. Hypoxia-inducible factor 1{alpha} is a new target of microphthalmia-associated transcription factor (MITF) in melanoma cells. *J. Cell Biol.* 170(1): 49-59.

Busca, R. and Ballotti, R., 2000. Cyclic AMP a key messenger in the regulation of skin pigmentation. *Pigment. Cell Res.* 13(2): 60-69.

Cao, Y., Yao, Z., Sarkar, D., Lawrence, M., Sanchez, G.J., Parker, M.H., MacQuarrie, K.L., Davison, J., Morgan, M.T., Ruzzo, W.L., Gentleman, R.C. and Tapscott, S.J., 2010. Genome-wide MyoD binding in skeletal muscle cells: a potential for broad cellular reprogramming. *Dev. Cell* 18(4): 662-674.

Cao, Y., Kumar, R.M., Penn, B.H., Berkes, C.A., Kooperberg, C., Boyer, L.A., Young, R.A. and Tapscott, S.J., 2006. Global and gene-specific analyses show distinct roles for Myod and Myog at a common set of promoters. *EMBO J.* 25(3): 502-511.

Carrano, A.C., Eytan, E., Hershko, A. and Pagano, M., 1999. SKP2 is required for ubiquitin-mediated degradation of the CDK inhibitor p27. *Nat. Cell. Biol.* 1(4): 193-199.

Carreira, S., Goodall, J., Denat, L., Rodriguez, M., Nuciforo, P., Hoek, K.S., Testori, A., Larue, L. and Goding, C.R., 2006. Mitf regulation of Dia1 controls melanoma proliferation and invasiveness. *Genes Dev.* 20(24): 3426-3439.

Carreira, S., Goodall, J., Aksan, I., La Rocca, S.A., Galibert, M.D., Denat, L., Larue, L. and Goding, C.R., 2005. Mitf cooperates with Rb1 and activates p21Cip1 expression to regulate cell cycle progression. *Nature* 433(7027): 764-769.

Carreira, S., Liu, B. and Goding, C.R., 2000. The gene encoding the T-box transcription factor Tbx2 is a target for the microphthalmia-associated transcription factor in melanocytes. *J. Biol. Chem.* 275: 21920-21927.

Chalker, J.M., Lercher, L., Rose, N.R., Schofield, C.J. and Davis, B.G., 2012. Conversion of cysteine into dehydroalanine enables access to synthetic histones bearing diverse post-translational modifications. *Angew Chem. Int. Ed. Engl.* 51(8): 1835-1839.

Chapman, P.B., Hauschild, A., Robert, C., Haanen, J.B., Ascierto, P., Larkin, J., Dummer, R., Garbe, C., Testori, A., Maio, M., Hogg, D., Lorigan, P., Lebbe, C., Jouary, T., Schadendorf, D., Ribas, A., O'Day, S.J., Sosman, J.A., Kirkwood, J.M., Eggermont, A.M., Dreno, B., Nolop, K., Li, J., Nelson, B., Hou, J., Lee, R.J., Flaherty, K.T. and McArthur, G.A., 2011. Improved survival with vemurafenib in melanoma with BRAF V600E mutation. *N. Engl. J. Med.* 364(26): 2507-2516.

Cheli, Y., Giuliano, S., Fenouille, N., Allegra, M., Hofman, V., Hofman, P., Bahadoran, P., Lacour, J.P., Tartare-Deckert, S., Bertolotto, C. and Ballotti, R., 2012. Hypoxia and MITF control metastatic behaviour in mouse and human melanoma cells. *Oncogene* 31(19): 2461-2470.

Cheli, Y., Ohanna, M., Ballotti, R. and Bertolotto, C., 2010. Fifteen-year quest for microphthalmia-associated transcription factor target genes. *Pigment Cell Melanoma Res.* 23(1): 27-40.

Chen, Y.J., Wang, Y.N. and Chang, W.C., 2007. ERK2-mediated C-terminal serine phosphorylation of p300 is vital to the regulation of epidermal growth factor-induced keratin 16 gene expression. *J. Biol. Chem.* 282(37): 27215-27228.

Chiaverini, C., Beuret, L., Flori, E., Busca, R., Abbe, P., Bille, K., Bahadoran, P., Ortonne, J.P., Bertolotto, C. and Ballotti, R., 2008. Microphthalmia-associated transcription factor regulates RAB27A gene expression and controls melanosome transport. *J. Biol. Chem.* 283(18): 12635-12642.

Chin, L., Garraway, L.A. and Fisher, D.E., 2006. Malignant melanoma: genetics and therapeutics in the genomic era. *Genes Dev.* 20(16): 2149-2182.

Chin, L., Pomerantz, J., Polsky, D., Jacobson, M., Cohen, C., Cordon, C., C., Horner II, J.W. and DePinho, R.A., 1997. Cooperative effects of *INK4a* and *ras* in melanoma susceptibility *in vivo*. *Genes Dev.* 11: 2822-2834.

Cho, E.J., Kobor, M.S., Kim, M., Greenblatt, J. and Buratowski, S., 2001. Opposing effects of Ctk1 kinase and Fcp1 phosphatase at Ser 2 of the RNA polymerase II C-terminal domain. *Genes Dev.* 15(24): 3319-3329.

Choi, M.C., Cohen, T.J., Barrientos, T., Wang, B., Li, M., Simmons, B.J., Yang, J.S., Cox, G.A., Zhao, Y. and Yao, T.P., 2012. A direct HDAC4-MAP kinase crosstalk activates muscle atrophy program. *Mol. Cell* 47(1): 122-132.

Clark, W.H., Jr., Elder, D.E., Guerry, D.t., Epstein, M.N., Greene, M.H. and Van Horn, M., 1984. A study of tumor progression: the precursor lesions of superficial spreading and nodular melanoma. *Hum. Pathol.* 15(12): 1147-1165.

Cohen, H.Y., Miller, C., Bitterman, K.J., Wall, N.R., Hekking, B., Kessler, B., Howitz, K.T., Gorospe, M., de Cabo, R. and Sinclair, D.A., 2004. Calorie restriction promotes mammalian cell survival by inducing the SIRT1 deacetylase. *Science* 305(5682): 390-392.

Corre, S., Primot, A., Baron, Y., Le Seyec, J., Goding, C. and Galibert, M.D., 2009. Target gene specificity of USF-1 is directed via p38-mediated phosphorylation-dependent acetylation. *J. Biol. Chem.* 284(28): 18851-18862.

Crews, S.T., Thomas, J.B. and Goodman, C.S., 1988. The Drosophila single-minded gene encodes a nuclear protein with sequence similarity to the per gene product. *Cell* 52(1): 143-151.

Cronin, J.C., Wunderlich, J., Loftus, S.K., Prickett, T.D., Wei, X., Ridd, K., Vemula, S., Burrell, A.S., Agrawal, N.S., Lin, J.C., Banister, C.E., Buckhaults, P., Rosenberg, S.A., Bastian, B.C., Pavan, W.J. and Samuels, Y., 2009. Frequent mutations in the MITF pathway in melanoma. *Pigment Cell Melanoma Res.* 22(4): 435-444.

Danen, E.H., de Vries, T.J., Morandini, R., Ghanem, G.G., Ruiter, D.J. and van Muijen, G.N., 1996. E-cadherin expression in human melanoma. *Melanoma Res.* 6(2): 127-131.

Dankort, D., Curley, D.P., Cartlidge, R.A., Nelson, B., Karnezis, A.N., Damsky, W.E., Jr., You, M.J., DePinho, R.A., McMahon, M. and Bosenberg, M., 2009. Braf(V600E) cooperates with Pten loss to induce metastatic melanoma. *Nat. Genet.* 41(5): 544-552.

Davies, H., Bignell, G.R., Cox, C., Stephens, P., Edkins, S., Clegg, S., Teague, J., Woffendin, H., Garnett, M.J., Bottomley, W., Davis, N., Dicks, E., Ewing, R., Floyd, Y., Gray, K., Hall, S., Hawes, R., Hughes, J., Kosmidou, V., Menzies, A., Mould, C., Parker, A., Stevens, C., Watt, S., Hooper, S., Wilson, R.,

Jayatilake, H., Gusterson, B.A., Cooper, C., Shipley, J., Hargrave, D., Pritchard-Jones, K., Maitland, N., Chenevix-Trench, G., Riggins, G.J., Bigner, D.D., Palmieri, G., Cossu, A., Flanagan, A., Nicholson, A., Ho, J.W., Leung, S.Y., Yuen, S.T., Weber, B.L., Seigler, H.F., Darrow, T.L., Paterson, H., Marais, R., Marshall, C.J., Wooster, R., Stratton, M.R. and Futreal, P.A., 2002. Mutations of the BRAF gene in human cancer. *Nature* 417(6892): 949-954.

De Bondt, H.L., Rosenblatt, J., Jancarik, J., Jones, H.D., Morgan, D.O. and Kim, S.H., 1993. Crystal structure of cyclin-dependent kinase 2. *Nature* 363(6430): 595-602.

de la Serna, I.L., Ohkawa, Y., Higashi, C., Dutta, C., Osias, J., Kommajosyula, N., Tachibana, T. and Imbalzano, A.N., 2006. The microphthalmia-associated transcription factor requires SWI/SNF enzymes to activate melanocyte-specific genes. *J. Biol. Chem.* 281(29): 20233-20241.

Delmas, V., Beermann, F., Martinozzi, S., Carreira, S., Ackermann, J., Kumasaka, M., Denat, L., Goodall, J., Luciani, F., Viros, A., Demirkan, N., Bastian, B.C., Goding, C.R. and Larue, L., 2007. Beta-catenin induces immortalization of melanocytes by suppressing p16INK4a expression and cooperates with N-Ras in melanoma development. *Genes Dev.* 21(22): 2923-2935.

Demunter, A., Stas, M., Degreef, H., De Wolf-Peeters, C. and van den Oord, J.J., 2001. Analysis of N- and K-ras mutations in the distinctive tumor progression phases of melanoma. *J. Invest. Dermatol.* 117(6): 1483-1489.

Dennler, S., Andre, J., Alexaki, I., Li, A., Magnaldo, T., ten Dijke, P., Wang, X.J., Verrecchia, F. and Mauviel, A., 2007. Induction of sonic hedgehog mediators by transforming growth factor-beta: Smad3-dependent activation of Gli2 and Gli1 expression in vitro and in vivo. *Cancer Res.* 67(14): 6981-6986.

Dignam, J.D., Lebovitz, R.M. and Roeder, R.G., 1983. Accurate transcription initiation by RNA polymerase II in a soluble extract from isolated mammalian nuclei. *Nucleic Acids Res.* 11(5): 1475-1489.

Dorsky, R.I., Raible, D.W. and Moon, R.T., 2000. Direct regulation of *nacre*, a zebrafish MITF homolog required for pigment cell formation, by the Wnt pathway. *Genes Dev.* 14(2): 158-162.

Dorsky, R.I., Moon, R.T. and Raible, D.W., 1998. Control of neural crest cell fate by the Wnt signalling pathway. *Nature* 396: 370-373.

Du, J., Widlund, H.R., Horstmann, M.A., Ramaswamy, S., Ross, K., Huber, W.E., Nishimura, E.K., Golub, T.R. and Fisher, D.E., 2004. Critical role of CDK2 for melanoma growth linked to its melanocyte-specific transcriptional regulation by MITF. *Cancer Cell* 6(6): 565-576.

Du, J., Miller, A.J., Widlund, H.R., Horstmann, M.A., Ramaswamy, S. and Fisher, D.E., 2003. MLANA/MART1 and SILV/PMEL17/GP100 Are Transcriptionally Regulated by MITF in Melanocytes and Melanoma. *Am J Pathol* 163(1): 333-343.

Dunn, K.J., Williams, B.O., Li, Y. and Pavan, W.J., 2000. Neural crest-directed gene transfer demonstrates Wnt1 role in melanocyte expansion and differentiation during mouse development. *Proc. Natl. Acad. Sci. U. S. A.* 97(18): 10050-10055.

Duquet, A., Polesskaya, A., Cuvellier, S., Ait-Si-Ali, S., Hery, P., Pritchard, L.L., Gerard, M. and Harel-Bellan, A., 2006. Acetylation is important for MyoD function in adult mice. *EMBO Rep.* 7(11): 1140-1146.

Dutton, K.A., Pauliny, A., Lopes, S.S., Elworthy, S., Carney, T.J., Rauch, J., Geisler, R., Haffter, P. and Kelsh, R.N., 2001. Zebrafish colourless encodes sox10 and

specifies non-ectomesenchymal neural crest fates. *Development* 128(21): 4113-4125.

Edery, P., Attie, T., Amiel, J., Pelet, A., Eng, C., Hofstra, R.M.W., Martelli, H., Bidaud, C., Munnich, A. and Lyonnet, S., 1996. Mutation of the endothelin-3 gene in the Waardenberg-Hirschsprung disease (Shah-Waardenberg syndrome). *Nature Genet.* 12: 442-444.

Epstein, D., Vekemans, M. and Goss, P., 1991. Splotch (Sp^{2H}), a mutation affecting development of the mouse neural tube, shows a deletion within the paired domain of Pax-3. *Cell* 67: 767-774.

Erbel, P.J., Card, P.B., Karakuzu, O., Bruick, R.K. and Gardner, K.H., 2003. Structural basis for PAS domain heterodimerization in the basic helix--loop--helix-PAS transcription factor hypoxia-inducible factor. *Proc. Natl. Acad. Sci. U. S. A.* 100(26): 15504-15509.

Esteller, M., 2007. Cancer epigenomics: DNA methylomes and histone-modification maps. *Nat Rev Genet* 8(4): 286-298.

Evan, G.I., Wyllie, A.H., Gilbert, C.S., Littlewood, T.D., Land, H., Brooks, M., Waters, C.M., Penn, L.Z. and Hancock, D.C., 1992. Induction of apoptosis in fibroblasts by c-myc protein. *Cell* 69(1): 119-128.

Fagiani, E., Giardina, G., Luzi, L., Cesaroni, M., Quarto, M., Capra, M., Germano, G., Bono, M., Capillo, M., Pelicci, P. and Lanfrancone, L., 2007. RaLP, a new member of the Src homology and collagen family, regulates cell migration and tumor growth of metastatic melanomas. *Cancer Res.* 67(7): 3064-3073.

Favata, M.F., Horiuchi, K.Y., Manos, E.J., Daulerio, A.J., Stradley, D.A., Feeser, W.S., Van Dyk, D.E., Pitts, W.J., Earl, R.A., Hobbs, F., Copeland, R.A., Magolda, R.L., Scherle, P.A. and Trzaskos, J.M., 1998. Identification of a novel inhibitor of mitogen-activated protein kinase kinase. *J. Biol. Chem.* 273(29): 18623-18632.

Feige, E., Yokoyama, S., Levy, C., Khaled, M., Igras, V., Lin, R.J., Lee, S., Widlund, H.R., Granter, S.R., Kung, A.L. and Fisher, D.E., 2011. Hypoxia-induced transcriptional repression of the melanoma-associated oncogene MITF. *Proc. Natl. Acad. Sci. U. S. A.* 108(43): E924-933.

Ferre-D'Amare, A., Prendergast, G.C., Ziff, E.B. and Burley, S.K., 1993. Recognition by Max of its cognate DNA through a dimeric b/HLH/Z domain. *Nature* 363(6424): 38-45.

Ferre-D'Amare, A.R., Pognonec, P., Roeder, R.G. and Burley, S.K., 1994. Structure and function of the b/HLH/Z domain of USF. *EMBO J.* 13(1): 180-189.

Filippakopoulos, P., Picaud, S., Mangos, M., Keates, T., Lambert, J.P., Barsyte-Lovejoy, D., Felletar, I., Volkmer, R., Muller, S., Pawson, T., Gingras, A.C., Arrowsmith, C.H. and Knapp, S., 2012. Histone recognition and large-scale structural analysis of the human bromodomain family. *Cell* 149(1): 214-231.

Fisher, F., Crouch, D.H., Jayaraman, P.S., Clark, W., Gillespie, D.A. and Goding, C.R., 1993. Transcription activation by Myc and Max: flanking sequences target activation to a subset of CACGTG motifs in vivo. *EMBO J.* 12(13): 5075-5082.

Flaherty, K.T., Puzanov, I., Kim, K.B., Ribas, A., McArthur, G.A., Sosman, J.A., O'Dwyer, P.J., Lee, R.J., Grippo, J.F., Nolop, K. and Chapman, P.B., 2010. Inhibition of mutated, activated BRAF in metastatic melanoma. *N. Engl. J. Med.* 363(9): 809-819.

Flores, J.F., Walker, G.J., Glendening, J.M., Haluska, F.G., Castresana, J.S., Rubio, M.P., Pastorfide, G.C., Boyer, L.A., Kao, W.H., Bulyk, M.L., Barnhill, R.L., Hayward, N.K., Housman, D.E. and Fountain, J.W., 1996. Loss of the

p16INK4a and p15INK4b genes, as well as neighboring 9p21 markers, in sporadic melanoma. *Cancer Res.* 56(21): 5023-5032.

Fong, A.P., Yao, Z., Zhong, J.W., Cao, Y., Ruzzo, W.L., Gentleman, R.C. and Tapscott, S.J., 2012. Genetic and epigenetic determinants of neurogenesis and myogenesis. *Dev. Cell* 22(4): 721-735.

Fraga, M.F., Ballestar, E., Villar-Garea, A., Boix-Chornet, M., Espada, J., Schotta, G., Bonaldi, T., Haydon, C., Ropero, S., Petrie, K., Iyer, N.G., Perez-Rosado, A., Calvo, E., Lopez, J.A., Cano, A., Calasanz, M.J., Colomer, D., Piris, M.A., Ahn, N., Imhof, A., Caldas, C., Jenuwein, T. and Esteller, M., 2005. Loss of acetylation at Lys16 and trimethylation at Lys20 of histone H4 is a common hallmark of human cancer. *Nat. Genet.* 37(4): 391-400.

Freeman, S.E., Hacham, H., Gange, R.W., Maytum, D.J., Sutherland, J.C. and Sutherland, B.M., 1989. Wavelength dependence of pyrimidine dimer formation in DNA of human skin irradiated in situ with ultraviolet light. *Proc. Natl. Acad. Sci. U. S. A.* 86(14): 5605-5609.

Frye, M., Fisher, A.G. and Watt, F.M., 2007. Epidermal stem cells are defined by global histone modifications that are altered by Myc-induced differentiation. *PLoS One* 2(8): e763.

Fuchs, E. and Raghavan, S., 2002. Getting under the skin of epidermal morphogenesis. *Nat Rev Genet* 3(3): 199-209.

Fuse, N., Yasumoto, K., Takeda, K., Amae, S., Yoshizawa, M., Udono, T., Takahashi, K., Tamai, M., Tomita, Y., Tachibana, M. and Shibahara, S., 1999. Molecular cloning of cDNA encoding a novel microphthalmia-associated transcription factor isoform with a distinct amino-terminus. *J. Biochem (Tokyo)* 126(6): 1043-1051.

Fuse, N., Yasumoto, K.-i., Suzuki, H., Takahashi, K. and Shibahara, S., 1996. Identification of a melanocyte-type promoter of the microphthalmia-associated transcription factor gene. *Biochem. Biophys. Res. Commun.* 219: 702-707.

Galibert, M.D., Yavuzer, U., Dexter, T.J. and Goding, C.R., 1999. Pax3 and regulation of the melanocyte-specific TRP-1 promoter. *J. Biol. Chem.* 274: 26894-26900.

Galibert, M.D., Carreira, S. and Goding, C.R., 2001. The Usf-1 transcription factor is a novel target for the stress- responsive p38 kinase and mediates UV-induced Tyrosinase expression. *EMBO J.* 20(17): 5022-5031.

Garraway, L.A., Widlund, H.R., Rubin, M.A., Getz, G., Berger, A.J., Ramaswamy, S., Beroukhim, R., Milner, D.A., Granter, S.R., Du, J., Lee, C., Wagner, S.N., Li, C., Golub, T.R., Rimm, D.L., Meyerson, M.L., Fisher, D.E. and Sellers, W.R., 2005. Integrative genomic analyses identify MITF as a lineage survival oncogene amplified in malignant melanoma. *Nature* 436(7047): 117-122.

Giardine, B., Riemer, C., Hardison, R.C., Burhans, R., Elnitski, L., Shah, P., Zhang, Y., Blankenberg, D., Albert, I., Taylor, J., Miller, W., Kent, W.J. and Nekrutenko, A., 2005. Galaxy: a platform for interactive large-scale genome analysis. *Genome Res.* 15(10): 1451-1455.

Giuliano, S., Cheli, Y., Ohanna, M., Bonet, C., Beuret, L., Bille, K., Loubat, A., Hofman, V., Hofman, P., Ponzio, G., Bahadoran, P., Ballotti, R. and Bertolotto, C., 2010. Microphthalmia-associated transcription factor controls the DNA damage response and a lineage-specific senescence program in melanomas. *Cancer Res.* 70(9): 3813-3822.

Goecks, J., Nekrutenko, A. and Taylor, J., 2010. Galaxy: a comprehensive approach for supporting accessible, reproducible, and transparent computational research in the life sciences. *Genome Biol.* 11(8): R86.

Goel, V.K., Ibrahim, N., Jiang, G., Singhal, M., Fee, S., Flotte, T., Westmoreland, S., Haluska, F.S., Hinds, P.W. and Haluska, F.G., 2009. Melanocytic nevus-like hyperplasia and melanoma in transgenic BRAFV600E mice. *Oncogene* 28(23): 2289-2298.

Goodall, J., Carreira, S., Denat, L., Kobi, D., Davidson, I., Nuciforo, P., Sturm, R.A., Larue, L. and Goding, C.R., 2008. Brn-2 represses microphthalmia-associated transcription factor expression and marks a distinct subpopulation of microphthalmia-associated transcription factor-negative melanoma cells. *Cancer Res.* 68(19): 7788-7794.

Goodall, J., Wellbrock, C., Dexter, T.J., Roberts, K., Marais, R. and Goding, C.R., 2004a. The Brn-2 transcription factor links activated BRAF to melanoma proliferation. *Mol. Cell Biol.* 24(7): 2923-2931.

Goodall, J., Martinozzi, S., Dexter, T.J., Champeval, D., Carreira, S., Larue, L. and Goding, C.R., 2004b. Brn-2 expression controls melanoma proliferation and is directly regulated by beta-catenin. *Mol. Cell Biol.* 24(7): 2915-2922.

Gorden, A., Osman, I., Gai, W., He, D., Huang, W., Davidson, A., Houghton, A.N., Busam, K. and Polsky, D., 2003. Analysis of BRAF and N-RAS mutations in metastatic melanoma tissues. *Cancer Res.* 63(14): 3955-3957.

Goulding, M.D., Chalepakis, G., Deutsch, U., Erselius, J.R. and Gruss, P., 1991. Pax-3, a novel murine DNA binding protein expressed during early neurogenesis. *EMBO J.* 10(5): 1135-1147.

Gray-Schopfer, V.C., Cheong, S.C., Chong, H., Chow, J., Moss, T., Abdel-Malek, Z.A., Marais, R., Wynford-Thomas, D. and Bennett, D.C., 2006. Cellular senescence in naevi and immortalisation in melanoma: a role for p16? *Br. J. Cancer* 95(4): 496-505.

Gregory, R.C., Taxman, D.J., Seshasayee, D., Kensinger, M.H., Bieker, J.J. and Wojchowski, D.M., 1996. Functional interaction of GATA1 with erythroid Kruppel-like factor and Sp1 at defined erythroid promoters. *Blood* 87(5): 1793-1801.

Grill, C., Bergsteinsdottir, K., Ogmundsdottir, M.H., Pogenberg, V., Schepsky, A., Wilmanns, M., Pingault, V. and Steingrimsson, E., 2013. MITF mutations associated with pigment deficiency syndromes and melanoma have different effects on protein function. *Hum. Mol. Genet.* 22(21): 4357-4367.

Gu, W. and Roeder, R.G., 1997. Activation of p53 Sequence-Specific DNA Binding by Acetylation of the p53 C-Terminal Domain. *Cell* 90(4): 595-606.

Guldberg, P., thor Straten, P., Birck, A., Ahrenkiel, V., Kirkin, A.F. and Zeuthen, J., 1997. Disruption of the MMAC1/PTEN gene by deletion or mutation is a frequent event in malignant melanoma. *Cancer Res.* 57(17): 3660-3663.

Halaban, R., Zhang, W., Bacchiocchi, A., Cheng, E., Parisi, F., Ariyan, S., Krauthammer, M., McCusker, J.P., Kluger, Y. and Sznol, M., 2010. PLX4032, a selective BRAF(V600E) kinase inhibitor, activates the ERK pathway and enhances cell migration and proliferation of BRAF melanoma cells. *Pigment Cell Melanoma Res.* 23(2): 190-200.

Hallsson, J.H., Haflidadottir, B.S., Stivers, C., Odenwald, W., Arnheiter, H., Pignoni, F. and Steingrimsson, E., 2004. The basic helix-loop-helix leucine zipper transcription factor mitf is conserved in Drosophila and functions in eye development. *Genetics* 167(1): 233-241.

Hanahan, D. and Weinberg, R.A., 2011. Hallmarks of cancer: the next generation. *Cell* 144(5): 646-674.

Hanks, S.K. and Hunter, T., 1995. Protein kinases 6. The eukaryotic protein kinase superfamily: kinase (catalytic) domain structure and classification. *FASEB J.* 9(8): 576-596.

Haq, R., Shoag, J., Andreu-Perez, P., Yokoyama, S., Edelman, H., Rowe, G.C., Frederick, D.T., Hurley, A.D., Nellore, A., Kung, A.L., Wargo, J.A., Song, J.S., Fisher, D.E., Arany, Z. and Widlund, H.R., 2013. Oncogenic BRAF regulates oxidative metabolism via PGC1alpha and MITF. *Cancer Cell* 23(3): 302-315.

Hari, L., Brault, V., Kleber, M., Lee, H.Y., Ille, F., Leimeroth, R., Paratore, C., Suter, U., Kemler, R. and Sommer, L., 2002. Lineage-specific requirements of beta-catenin in neural crest development. *J. Cell Biol.* 159(5): 867-880.

Hart, M.J., de los Santos, R., Albert, I.N., Rubinfeld, B. and Polakis, P., 1998. Downregulation of beta-catenin by human Axin and its association with the APC tumor suppressor, beta-catenin and GSK3 beta. *Curr. Biol.* 8(10): 573-581.

Hatzivassiliou, G., Song, K., Yen, I., Brandhuber, B.J., Anderson, D.J., Alvarado, R., Ludlam, M.J., Stokoe, D., Gloor, S.L., Vigers, G., Morales, T., Aliagas, I., Liu, B., Sideris, S., Hoeflich, K.P., Jaiswal, B.S., Seshagiri, S., Koeppen, H., Belvin, M., Friedman, L.S. and Malek, S., 2010. RAF inhibitors prime wild-type RAF to activate the MAPK pathway and enhance growth. *Nature* 464(7287): 431-435.

Hayward, N., 2000. New developments in melanoma genetics. *Curr. Oncol. Rep.* 2(4): 300-306.

Hecht, A., Laroche, T., Strahl-Bolsinger, S., Gasser, S.M. and Grunstein, M., 1995. Histone H3 and H4 N-termini interact with SIR3 and SIR4 proteins: a molecular model for the formation of heterochromatin in yeast. *Cell* 80(4): 583-592.

Heidorn, S.J., Milagre, C., Whittaker, S., Nourry, A., Niculescu-Duvas, I., Dhomen, N., Hussain, J., Reis-Filho, J.S., Springer, C.J., Pritchard, C. and Marais, R., 2010. Kinase-dead BRAF and oncogenic RAS cooperate to drive tumor progression through CRAF. *Cell* 140(2): 209-221.

Hemesath, T.J., Price, E.R., Takemoto, C., Badalian, T. and Fisher, D.E., 1998. MAP kinase links the transcription factor Microphthalmia to c-Kit signalling in melanocytes. *Nature* 391(6664): 298-301.

Hemesath, T.J., Steingrimsson, E., McGill, G., Hansen, M.J., Vaught, J., Hodgkinson, C.A., Arnheiter, H., Copeland, N.G., Jenkins, N.A. and Fisher, D.E., 1994. Microphthalmia, a critical factor in melanocyte development, defines a discrete transcription factor family. *Genes Dev.* 8(22): 2770-2780.

Hershey, C.L. and Fisher, D.E., 2005. Genomic analysis of the Microphthalmia locus and identification of the MITF-J/Mitf-J isoform. *Gene* 8: 8.

Hertwig, P., 1942. Neue Mutationen und Koppelungsgruppen bei der Hausmaus. *Zeitschrift für Induktive Abstammungs- und Vererbungslehre* 80(1): 220-246.

Hingorani, S.R., Jacobetz, M.A., Robertson, G.P., Herlyn, M. and Tuveson, D.A., 2003. Suppression of BRAF(V599E) in human melanoma abrogates transformation. *Cancer Res.* 63(17): 5198-5202.

Hirobe, T., 2005. Role of keratinocyte-derived factors involved in regulating the proliferation and differentiation of mammalian epidermal melanocytes. *Pigment Cell Res.* 18(1): 2-12.

Hodgkinson, C.A., Nakayama, A., Li, H., Swenson, L.B., Opdecamp, K., Asher, J.H., Arnheiter, H. and Glaser, T., 1998. Mutation at the anophthalmic white locus in

Syrian hamsters: haploinsufficiency in the Mitf gene mimics human Waardenburg syndrome type 2. *Hum. Mol. Genet.* 7(4): 703-708.

Hodgkinson, C.A., Moore, K.J., Nakayama, A., Steingrimsson, E., Copeland, N.G., Jenkins, N.A. and Arnheiter, H., 1993. Mutations at the mouse *microphthalmia* locus are associated with defects in a gene encoding a novel basic-helix-loop-helix-zipper protein. *Cell* 74(2): 395-404.

Hodis, E., Watson, I.R., Kryukov, G.V., Arold, S.T., Imielinski, M., Theurillat, J.P., Nickerson, E., Auclair, D., Li, L., Place, C., Dicara, D., Ramos, A.H., Lawrence, M.S., Cibulskis, K., Sivachenko, A., Voet, D., Saksena, G., Stransky, N., Onofrio, R.C., Winckler, W., Ardlie, K., Wagle, N., Wargo, J., Chong, K., Morton, D.L., Stemke-Hale, K., Chen, G., Noble, M., Meyerson, M., Ladbury, J.E., Davies, M.A., Gershenwald, J.E., Wagner, S.N., Hoon, D.S., Schadendorf, D., Lander, E.S., Gabriel, S.B., Getz, G., Garraway, L.A. and Chin, L., 2012. A landscape of driver mutations in melanoma. *Cell* 150(2): 251-263.

Hoek, K.S. and Goding, C.R., 2010. Cancer stem cells versus phenotype-switching in melanoma. *Pigment Cell Melanoma Res.* 23(6): 746-759.

Hoek, K.S., Eichhoff, O.M., Schlegel, N.C., Dobbeling, U., Kobert, N., Schaerer, L., Hemmi, S. and Dummer, R., 2008. In vivo switching of human melanoma cells between proliferative and invasive states. *Cancer Res.* 68(3): 650-656.

Hoek, K.S., Schlegel, N.C., Brafford, P., Sucker, A., Ugurel, S., Kumar, R., Weber, B.L., Nathanson, K.L., Phillips, D.J., Herlyn, M., Schadendorf, D. and Dummer, R., 2006. Metastatic potential of melanomas defined by specific gene expression profiles with no BRAF signature. *Pigment Cell Res.* 19(4): 290-302.

Hornyak, T.J., Hayes, D.J., Chiu, L.Y. and Ziff, E.B., 2001. Transcription factors in melanocyte development: distinct roles for Pax- 3 and Mitf. *Mech. Dev.* 101(1-2): 47-59.

Hoth, C.F., Milunsky, A., Lipsky, N., Sheffer, R., Clarren, S.K. and Baldwin, C.T., 1993. Mutations in the Paired Domain of the Human Pax3 Gene Cause Klein-Waardenburg Syndrome (Ws-Iii) as Well as Waardenburg Syndrome Type-I (Ws-I). *Am. J. Hum. Genet.* 52(3): 455-462.

Hsu, M., Andl, T., Li, G., Meinkoth, J.L. and Herlyn, M., 2000. Cadherin repertoire determines partner-specific gap junctional communication during melanoma progression. *J. Cell Sci.* 113 (Pt 9): 1535-1542.

Hsu, M.Y., Wheelock, M.J., Johnson, K.R. and Herlyn, M., 1996. Shifts in cadherin profiles between human normal melanocytes and melanomas. *J. Invest. Dermatol. Symp. Proc.* 1(2): 188-194.

Huang da, W., Sherman, B.T. and Lempicki, R.A., 2009. Systematic and integrative analysis of large gene lists using DAVID bioinformatics resources. *Nat. Protoc.* 4(1): 44-57.

Huber, W.E., Price, R., Widlund, H.R., Du, J., Davis, I.J., Wegner, M. and Fisher, D.E., 2003. A tissue restricted cAMP transcriptional response: SOX10 modulates MSH-triggered expression of MITF in melanocytes. *J. Biol. Chem.* 278: 45224-45230.

Hughes, A.E., Newton, V.E., Liu, X.Z. and Read, A.P., 1994. A gene for Waardenburg syndrome type 2 maps close to the human homologue of the microphthalmia gene at chromosome 3p12-p14.1. *Nat. Genet.* 7(4): 509-512.

Hughes, M.J., Lingrel, J.B., Krakowsky, J.M. and Anderson, K.P., 1993. A helix-loop-helix transcription factor-like gene is located at the *mi* locus. *J. Biol. Chem.* 268: 20687-20690.

Huizing, M., Anikster, Y. and Gahl, W.A., 2000. Hermansky-Pudlak syndrome and related disorders of organelle formation. *Traffic* 1(11): 823-835.

Hussussian, C.J., Struewing, J.P., Goldstein, A.M., Higgins, P.A., Ally, D.S., Sheahan, M.D., Clark, W.H., Jr., Tucker, M.A. and Dracopoli, N.C., 1994. Germline p16 mutations in familial melanoma. *Nat. Genet.* 8(1): 15-21.

Huynh, K.K., Eskelinen, E.L., Scott, C.C., Malevanets, A., Saftig, P. and Grinstein, S., 2007. LAMP proteins are required for fusion of lysosomes with phagosomes. *EMBO J.* 26(2): 313-324.

Ikeya, M., Lee, S.M., Johnson, J.E., McMahon, A.P. and Takada, S., 1997. Wnt signalling required for expansion of neural crest and CNS progenitors. *Nature* 389(6654): 966-970.

Jackson, I.J., 1994. Molecular and Developmental Genetics of Mouse Coat Color. *Annu. Rev. Genet.* 28: 189-217.

Jacobs, J.J., Keblusek, P., Robanus-Maandag, E., Kristel, P., Lingbeek, M., Nederlof, P.M., van Welsem, T., van De Vijver, M.J., Koh, E.Y., Daley, G.Q. and van Lohuizen, M., 2000. Senescence bypass screen identifies TBX2, which represses cdkn2a (p19ARF) and is amplified in a subset of human breast cancers. *Nat. Genet.* 26(3): 291-299.

Jacquemin, P., Lannoy, V.J., O'Sullivan, J., Read, A., Lemaigre, F.P. and Rousseau, G.G., 2001. The transcription factor onecut-2 controls the microphthalmia-associated transcription factor gene. *Biochem. Biophys. Res. Commun.* 285(5): 1200-1205.

Javelaud, D., Alexaki, V.I., Pierrat, M.J., Hoek, K.S., Dennler, S., Van Kempen, L., Bertolotto, C., Ballotti, R., Saule, S., Delmas, V. and Mauviel, A., 2011. GLI2 and M-MITF transcription factors control exclusive gene expression programs and inversely regulate invasion in human melanoma cells. *Pigment Cell Melanoma Res.* 24(5): 932-943.

Javelaud, D., Alexaki, V.I. and Mauviel, A., 2008. Transforming growth factor-beta in cutaneous melanoma. *Pigment Cell Melanoma Res.* 21(2): 123-132.

Ji, H., Jiang, H., Ma, W., Johnson, D.S., Myers, R.M. and Wong, W.H., 2008. An integrated software system for analyzing ChIP-chip and ChIP-seq data. *Nat. Biotechnol.* 26(11): 1293-1300.

Jukic, D.M., Rao, U.N., Kelly, L., Skaf, J.S., Drogowski, L.M., Kirkwood, J.M. and Panelli, M.C., 2010. Microrna profiling analysis of differences between the melanoma of young adults and older adults. *J. Transl. Med.* 8: 27.

Kadekaro, A.L., Kavanagh, R.J., Wakamatsu, K., Ito, S., Pipitone, M.A. and Abdel-Malek, Z.A., 2003. Cutaneous photobiology. The melanocyte vs. the sun: who will win the final round? *Pigment Cell Res.* 16(5): 434-447.

Kamb, A., Shattuck-Eidens, D., Eeles, R., Liu, Q., Gruis, N.A., Ding, W., Hussey, C., Tran, T., Miki, Y., Weaver-Feldhaus, J. and et al., 1994. Analysis of the p16 gene (CDKN2) as a candidate for the chromosome 9p melanoma susceptibility locus. *Nat. Genet.* 8(1): 23-26.

Kamijo, T., Weber, J.D., Zambetti, G., Zindy, F., Roussel, M.F. and Sherr, C.J., 1998. Functional and physical interactions of the ARF tumor suppressor with p53 and Mdm2. *Proc. Natl. Acad. Sci. U. S. A.* 95(14): 8292-8297.

Kamijo, T., Zindy, F., Roussel, M.F., Quelle, D.E., Downing, J.R., Ashmun, R.A., Grosveld, G. and Sherr, C.J., 1997. Tumor suppression at the mouse INK4a locus mediated by the alternative reading frame product p19ARF. *Cell* 91(5): 649-659.

Karlsson, E.K., Baranowska, I., Wade, C.M., Salmon Hillbertz, N.H., Zody, M.C., Anderson, N., Biagi, T.M., Patterson, N., Pielberg, G.R., Kulbokas, E.J., 3rd, Comstock, K.E., Keller, E.T., Mesirov, J.P., von Euler, H., Kampe, O., Hedhammar, A., Lander, E.S., Andersson, G., Andersson, L. and Lindblad-Toh, K., 2007. Efficient mapping of mendelian traits in dogs through genome-wide association. *Nat. Genet.* 39(11): 1321-1328.

Kasper, M., Regl, G., Frischauf, A.M. and Aberger, F., 2006. GLI transcription factors: mediators of oncogenic Hedgehog signalling. *Eur. J. Cancer.* 42(4): 437-445.

Katan-Khaykovich, Y. and Struhl, K., 2002. Dynamics of global histone acetylation and deacetylation in vivo: rapid restoration of normal histone acetylation status upon removal of activators and repressors. *Genes Dev.* 16(6): 743-752.

Kato, G.J., Lee, W.M., Chen, L.L. and Dang, C.V., 1992. Max: functional domains and interaction with c-Myc. *Genes Dev.* 6(1): 81-92.

King, R., Peterson, A.C., Peterson, K.C., Mihm, M.C., Jr., Fisher, D.E. and Googe, P.B., 2002. Microphthalmia transcription factor expression in cutaneous mast cell disease. *Am. J. Dermatopathol.* 24(3): 282-284.

Kishida, S., Yamamoto, H., Hino, S., Ikeda, S., Kishida, M. and Kikuchi, A., 1999. DIX domains of Dvl and axin are necessary for protein interactions and their ability to regulate beta-catenin stability. *Mol. Cell Biol.* 19(6): 4414-4422.

Kitayner, M., Rozenberg, H., Kessler, N., Rabinovich, D., Shaulov, L., Haran, T.E. and Shakked, Z., 2006. Structural basis of DNA recognition by p53 tetramers. *Mol. Cell* 22(6): 741-753.

Kozmik, Z., Ruzickova, J., Jonasova, K., Matsumoto, Y., Vopalensky, P., Kozmikova, I., Strnad, H., Kawamura, S., Piatigorsky, J., Paces, V. and Vlcek, C., 2008. Assembly of the cnidarian camera-type eye from vertebrate-like components. *Proc. Natl. Acad. Sci. U. S. A.* 105(26): 8989-8993.

Kreider, B.L., Benezra, R., Rovera, G. and Kadesch, T., 1992. Inhibition of myeloid differentiation by the helix-loop-helix protein Id. *Science* 255(5052): 1700-1702.

Kretzner, L., Blackwood, E.M. and Eisenman, R.N., 1992. Myc and Max proteins possess distinct transcriptional activities. *Nature* 359: 426-429.

Kuhlbrodt, K., Herbarth, B., Sock, E., Hermans-Borgmeyer, I. and Wegner, M., 1998a. Sox10, a novel transcriptional modulator in glial cells. *J. Neuroscience* 18: 237-250.

Kuhlbrodt, K., Schmidt, C., Sock, E., Pingault, V., Bondurand, N., Goossens, M. and Wegner, M., 1998b. Functional analysis of Sox10 mutations found in human Waardenburg- Hirschsprung patients. *J. Biol. Chem.* 273(36): 23033-23038.

Kumasaka, M., Sato, S., Yajima, I., Goding, C.R. and Yamamoto, H., 2005. Regulation of melanoblast and retinal pigment epithelium development by Xenopus laevis Mitf. *Dev. Dyn.* 243(3):523-534.

Kuzbicki, L., Gajo, B. and Chwirot, B.W., 2006. Different expression of lysosome-associated membrane protein-1 in human melanomas and benign melanocytic lesions. *Melanoma Res.* 16(3): 235-243.

Kvam, E. and Tyrrell, R.M., 1997. Induction of oxidative DNA base damage in human skin cells by UV and near visible radiation. *Carcinogenesis* 18(12): 2379-2384.

Lang, D., Lu, M.M., Huang, L., Engleka, K.A., Zhang, M., Chu, E.Y., Lipner, S., Skoultchi, A., Millar, S.E. and Epstein, J.A., 2005. Pax3 functions at a nodal point in melanocyte stem cell differentiation. *Nature* 433(7028): 884-887.

Langmead, B., Trapnell, C., Pop, M. and Salzberg, S.L., 2009. Ultrafast and memory-efficient alignment of short DNA sequences to the human genome. *Genome Biol.* 10(3): R25.

Larribere, L., Hilmi, C., Khaled, M., Gaggioli, C., Bille, K., Auberger, P., Ortonne, J.P., Ballotti, R. and Bertolotto, C., 2005. The cleavage of microphthalmia-associated transcription factor, MITF, by caspases plays an essential role in melanocyte and melanoma cell apoptosis. *Genes Dev.* 19(17): 1980-1985.

Lassar, A.B., Buskin, J.N., Lockshon, D., Davis, R.L., Apone, S., Hauschka, S.D. and Weintraub, H., 1989. MyoD is a sequence-specific DNA binding protein requiring a region of myc homology to bind to the muscle creatine kinase enhancer. *Cell* 58(5): 823-831.

Lassar, A.B., Paterson, B.M. and Weintraub, H., 1986. Transfection of a DNA locus that mediates the conversion of 10T1/2 fibroblasts to myoblasts. *Cell* 47(5): 649-656.

Lee, B.Y., Han, J.A., Im, J.S., Morrone, A., Johung, K., Goodwin, E.C., Kleijer, W.J., DiMaio, D. and Hwang, E.S., 2006. Senescence-associated beta-galactosidase is lysosomal beta-galactosidase. *Aging Cell* 5(2): 187-195.

Lee, M., Goodall, J., Verastegui, C., Ballotti, R. and Goding, C.R., 2000. Direct Regulation of the Microphthalmia Promoter by Sox10 Links Waardenburg-Shah Syndrome (WS4)-associated Hypopigmentation and Deafness to WS2. *J. Biol. Chem.* 275(48): 37978-37983.

Lerner, A.B., Shiohara, T., Boissy, R.E., Jacobson, K.A., Lamoreux, M.L. and Moellmann, G.E., 1986. A mouse model for vitiligo. *J. Invest. Dermatol.* 87(3): 299-304.

Levy, C., Khaled, M., Robinson, K.C., Veguilla, R.A., Chen, P.H., Yokoyama, S., Makino, E., Lu, J., Larue, L., Beermann, F., Chin, L., Bosenberg, M., Song, J.S. and Fisher, D.E., 2010a. Lineage-specific transcriptional regulation of DICER by MITF in melanocytes. *Cell* 141(6): 994-1005.

Levy, C., Khaled, M., Iliopoulos, D., Janas, M.M., Schubert, S., Pinner, S., Chen, P.H., Li, S., Fletcher, A.L., Yokoyama, S., Scott, K.L., Garraway, L.A., Song, J.S., Granter, S.R., Turley, S.J., Fisher, D.E. and Novina, C.D., 2010b. Intronic miR-211 assumes the tumor suppressive function of its host gene in melanoma. *Mol. Cell* 40(5): 841-849.

Levy, C., Khaled, M. and Fisher, D.E., 2006. MITF: master regulator of melanocyte development and melanoma oncogene. *Trends Mol. Med.* 12(9): 406-414.

Levy, C., Sonnenblick, A. and Razin, E., 2003. Role played by microphthalmia transcription factor phosphorylation and its Zip domain in its transcriptional inhibition by PIAS3. *Mol. Cell Biol.* 23(24): 9073-9080.

Levy, C., Nechushtan, H. and Razin, E., 2002. A new role for the STAT3 inhibitor, PIAS3: a repressor of microphthalmia transcription factor. *J. Biol. Chem.* 277(3): 1962-1966.

Li, D.M. and Sun, H., 1997. TEP1, encoded by a candidate tumor suppressor locus, is a novel protein tyrosine phosphatase regulated by transforming growth factor beta. *Cancer Res.* 57(11): 2124-2129.

Li, G., Satyamoorthy, K. and Herlyn, M., 2001. N-cadherin-mediated intercellular interactions promote survival and migration of melanoma cells. *Cancer Res.* 61(9): 3819-3825.

Li, J., Yen, C., Liaw, D., Podsypanina, K., Bose, S., Wang, S.I., Puc, J., Miliaresis, C., Rodgers, L., McCombie, R., Bigner, S.H., Giovanella, B.C., Ittmann, M., Tycko, B., Hibshoosh, H., Wigler, M.H. and Parsons, R., 1997. PTEN, a

putative protein tyrosine phosphatase gene mutated in human brain, breast, and prostate cancer. *Science* 275(5308): 1943-1947.

Lickwar, C.R., Mueller, F., Hanlon, S.E., McNally, J.G. and Lieb, J.D., 2012. Genome-wide protein-DNA binding dynamics suggest a molecular clutch for transcription factor function. *Nature* 484(7393): 251-255.

Lister, J.A., Close, J. and Raible, D.W., 2001. Duplicate mitf genes in zebrafish: complementary expression and conservation of melanogenic potential. *Dev. Biol.* 237(2): 333-344.

Lister, J.A., Robertson, C.P., Lepage, T., Johnson, S.L. and Raible, D.W., 1999. *nacre* encodes a zebrafish microphthalmia-related protein that regulates neural-crest-derived pigment cell fate. *Development* 126(17): 3757-3767.

Littlewood, T.D., Amati, B., Land, H. and Evan, G.I., 1992. Max and c-Myc/Max DNA-binding activities in cell extracts. *Oncogene* 7(9): 1783-1792.

Liu, F., Fu, Y. and Meyskens, F.L., Jr., 2009. MiTF regulates cellular response to reactive oxygen species through transcriptional regulation of APE-1/Ref-1. *J. Invest. Dermatol.* 129(2): 422-431.

Liu, L., Scolnick, D.M., Trievel, R.C., Zhang, H.B., Marmorstein, R., Halazonetis, T.D. and Berger, S.L., 1999. p53 sites acetylated in vitro by PCAF and p300 are acetylated in vivo in response to DNA damage. *Mol. Cell Biol.* 19(2): 1202-1209.

Liu, T., Ortiz, J.A., Taing, L., Meyer, C.A., Lee, B., Zhang, Y., Shin, H., Wong, S.S., Ma, J., Lei, Y., Pape, U.J., Poidinger, M., Chen, Y., Yeung, K., Brown, M., Turpaz, Y. and Liu, X.S., 2011. Cistrome: an integrative platform for transcriptional regulation studies. *Genome Biol.* 12(8): R83.

Livak, K.J. and Schmittgen, T.D., 2001. Analysis of relative gene expression data using real-time quantitative PCR and the 2(-Delta Delta C(T)) Method. *Methods* 25(4): 402-408.

Loercher, A.E., Tank, E.M., Delston, R.B. and Harbour, J.W., 2005. MITF links differentiation with cell cycle arrest in melanocytes by transcriptional activation of INK4A. *J. Cell Biol.* 168(1): 35-40.

Lowings, P., Yavuzer, U. and Goding, C.R., 1992. Positive and negative elements regulate a melanocyte-specific promoter. *Mol. Cell Biol.* 12(8): 3653-3662.

Lu, M., Breyssens, H., Salter, V., Zhong, S., Hu, Y., Baer, C., Ratnayaka, I., Sullivan, A., Brown, N.R., Endicott, J., Knapp, S., Kessler, B.M., Middleton, M.R., Siebold, C., Jones, E.Y., Sviderskaya, E.V., Cebon, J., John, T., Caballero, O.L., Goding, C.R. and Lu, X., 2013. Restoring p53 function in human melanoma cells by inhibiting MDM2 and cyclin B1/CDK1-phosphorylated nuclear iASPP. *Cancer Cell* 23(5): 618-633.

Ludwig, A., Rehberg, S. and Wegner, M., 2004. Melanocyte-specific expression of dopachrome tautomerase is dependent on synergistic gene activation by the Sox10 and Mitf transcription factors. *FEBS Lett.* 556(1-3): 236-244.

Ma, P.C., Rould, M.A., Weintraub, H. and Pabo, C.O., 1994. Crystal structure of MyoD bHLH domain-DNA complex: perspectives on DNA recognition and implications for transcriptional activation. *Cell* 77(3): 451-459.

Machanick, P. and Bailey, T.L., 2011. MEME-ChIP: motif analysis of large DNA datasets. *Bioinformatics* 27(12): 1696-1697.

Mak, S.S., Moriyama, M., Nishioka, E., Osawa, M. and Nishikawa, S.I., 2006. Indispensable role of Bcl2 in the development of the melanocyte stem cell. *Dev. Biol.*

Mammoto, A., Huang, S., Moore, K., Oh, P. and Ingber, D.E., 2004. Role of RhoA, mDia, and ROCK in cell shape-dependent control of the Skp2-p27kip1 pathway and the G1/S transition. *J. Biol. Chem.* 279(25): 26323-26330.

Mansky, K.C., Sankar, U., Han, J. and Ostrowski, M.C., 2002. Microphthalmia Transcription Factor Is a Target of the p38 MAPK Pathway in Response to Receptor Activator of NF-kappa B Ligand Signaling. *J. Biol. Chem.* 277(13): 11077-11083.

Marshall, C.J., 1995. Specificity of receptor tyrosine kinase signaling: transient versus sustained extracellular signal-regulated kinase activation. *Cell* 80(2): 179-185.

Martin, A.M., Pouchnik, D.J., Walker, J.L. and Wyrick, J.J., 2004. Redundant roles for histone H3 N-terminal lysine residues in subtelomeric gene repression in Saccharomyces cerevisiae. *Genetics* 167(3): 1123-1132.

Mazar, J., DeYoung, K., Khaitan, D., Meister, E., Almodovar, A., Goydos, J., Ray, A. and Perera, R.J., 2010. The regulation of miRNA-211 expression and its role in melanoma cell invasiveness. *PLoS One* 5(11): e13779.

McGill, G.G., Haq, R., Nishimura, E.K. and Fisher, D.E., 2006. c-Met expression is regulated by Mitf in the melanocyte lineage. *J. Biol. Chem.* 281(15): 10365-10373.

McGill, G.G., Horstmann, M., Widlund, H.R., Du, J., Motyckova, G., Nishimura, E.K., Lin, Y.L., Ramaswamy, S., Avery, W., Ding, H.F., Jordan, S.A., Jackson, I.J., Korsmeyer, S.J., Golub, T.R. and Fisher, D.E., 2002. Bcl2 regulation by the melanocyte master regulator Mitf modulates lineage survival and melanoma cell viability. *Cell* 109(6): 707-718.

Menges, C.W. and McCance, D.J., 2008. Constitutive activation of the Raf-MAPK pathway causes negative feedback inhibition of Ras-PI3K-AKT and cellular arrest through the EphA2 receptor. *Oncogene* 27(20): 2934-2940.

Meyskens, F.L., Jr., Chau, H.V., Tohidian, N. and Buckmeier, J., 1997. Luminol-enhanced chemiluminescent response of human melanocytes and melanoma cells to hydrogen peroxide stress. *Pigment Cell Res.* 10(3): 184-189.

Michaloglou, C., Vredeveld, L.C., Soengas, M.S., Denoyelle, C., Kuilman, T., van der Horst, C.M., Majoor, D.M., Shay, J.W., Mooi, W.J. and Peeper, D.S., 2005. BRAFE600-associated senescence-like cell cycle arrest of human naevi. *Nature* 436(7051): 720-724.

Miller, A.J. and Mihm, M.C., Jr., 2006. Melanoma. *N. Engl. J. Med.* 355(1): 51-65.

Miller, A.J., Levy, C., Davis, I.J., Razin, E. and Fisher, D.E., 2005. Sumoylation of MITF and its related family members TFE3 and TFEB. *J. Biol. Chem.* 280(1): 146-155.

Miller, A.J., Du, J., Rowan, S., Hershey, C.L., Widlund, H.R. and Fisher, D.E., 2004. Transcriptional regulation of the melanoma prognostic marker melastatin (TRPM1) by MITF in melanocytes and melanoma. *Cancer Res.* 64(2): 509-516.

Minvielle, F., Bed'hom, B., Coville, J.L., Ito, S., Inoue-Murayama, M. and Gourichon, D., 2010. The "silver" Japanese quail and the MITF gene: causal mutation, associated traits and homology with the "blue" chicken plumage. *BMC Genet.* 11: 15.

Mochii, M., Mazaki, Y., Mizuno, N., Hayashi, H. and Eguchi, G., 1998. Role of Mitf in differentiation and transdifferentiation of chicken pigmented epithelial cell. *Dev. Biol.* 193(1): 47-62.

Montagut, C., Sharma, S.V., Shioda, T., McDermott, U., Ulman, M., Ulkus, L.E., Dias-Santagata, D., Stubbs, H., Lee, D.Y., Singh, A., Drew, L., Haber, D.A. and

Settleman, J., 2008. Elevated CRAF as a potential mechanism of acquired resistance to BRAF inhibition in melanoma. *Cancer Res.* 68(12): 4853-4861.

Moyal, L., Lerenthal, Y., Gana-Weisz, M., Mass, G., So, S., Wang, S.Y., Eppink, B., Chung, Y.M., Shalev, G., Shema, E., Shkedy, D., Smorodinsky, N.I., van Vliet, N., Kuster, B., Mann, M., Ciechanover, A., Dahm-Daphi, J., Kanaar, R., Hu, M.C., Chen, D.J., Oren, M. and Shiloh, Y., 2011. Requirement of ATM-dependent monoubiquitylation of histone H2B for timely repair of DNA double-strand breaks. *Mol. Cell* 41(5): 529-542.

Murakami, H. and Arnheiter, H., 2005. Sumoylation modulates transcriptional activity of MITF in a promoter-specific manner. *Pigment Cell Res.* 18(4): 265-277.

Murre, C., McCaw, P.S. and Baltimore, D., 1989. A new DNA binding and dimerization motif in immunoglobulin enhancer binding, daughterless, MyoD, and myc proteins. *Cell* 56(5): 777-783.

Nair, S.K. and Burley, S.K., 2003. X-ray structures of Myc-Max and Mad-Max recognizing DNA. Molecular bases of regulation by proto-oncogenic transcription factors. *Cell* 112(2): 193-205.

Nakayama, A., Nguyen, M.T., Chen, C.C., Opdecamp, K., Hodgkinson, C.A. and Arnheiter, H., 1998. Mutations in microphthalmia, the mouse homolog of the human deafness gene MITF, affect neuroepithelial and neural crest-derived melanocytes differently. *Mech. Dev.* 70(1-2): 155-166.

Nambu, J.R., Lewis, J.O., Wharton, K.J. and Crews, S.T., 1991. The Drosophila single-minded gene encodes a helix-loop-helix protein that acts as a master regulator of CNS midline development. *Cell* 67(6): 1157-1167.

Nazarian, R., Shi, H., Wang, Q., Kong, X., Koya, R.C., Lee, H., Chen, Z., Lee, M.K., Attar, N., Sazegar, H., Chodon, T., Nelson, S.F., McArthur, G., Sosman, J.A., Ribas, A. and Lo, R.S., 2010. Melanomas acquire resistance to B-RAF(V600E) inhibition by RTK or N-RAS upregulation. *Nature* 468(7326): 973-977.

Nguyen, M. and Arnheiter, H., 2000. Signaling and transcriptional regulation in early mammalian eye development: a link between FGF and MITF. *Development* 127(16): 3581-3591.

Nikolaev, S.I., Rimoldi, D., Iseli, C., Valsesia, A., Robyr, D., Gehrig, C., Harshman, K., Guipponi, M., Bukach, O., Zoete, V., Michielin, O., Muehlethaler, K., Speiser, D., Beckmann, J.S., Xenarios, I., Halazonetis, T.D., Jongeneel, C.V., Stevenson, B.J. and Antonarakis, S.E., 2012. Exome sequencing identifies recurrent somatic MAP2K1 and MAP2K2 mutations in melanoma. *Nat. Genet.* 44(2): 133-139.

Nishimura, E.K., Granter, S.R. and Fisher, D.E., 2005. Mechanisms of hair graying: incomplete melanocyte stem cell maintenance in the niche. *Science* 307(5710): 720-724.

Nishimura, E.K., Jordan, S.A., Oshima, H., Yoshida, H., Osawa, M., Moriyama, M., Jackson, I.J., Barrandon, Y., Miyachi, Y. and Nishikawa, S., 2002. Dominant role of the niche in melanocyte stem-cell fate determination. *Nature* 416(6883): 854-860.

Oboki, K., Morii, E., Kataoka, T.R., Jippo, T. and Kitamura, Y., 2002. Isoforms of mi transcription factor preferentially expressed in cultured mast cells of mice. *Biochem. Biophys. Res. Commun.* 290(4): 1250-1254.

Olbryt, M., Jarzab, M., Jazowiecka-Rakus, J., Simek, K., Szala, S. and Sochanik, A., 2006. Gene expression profile of B 16(F10) murine melanoma cells exposed to hypoxic conditions in vitro. *Gene Expr.* 13(3): 191-203.

Omholt, K., Platz, A., Kanter, L., Ringborg, U. and Hansson, J., 2003. NRAS and BRAF mutations arise early during melanoma pathogenesis and are preserved throughout tumor progression. *Clin. Cancer Res.* 9(17): 6483-6488.

Omholt, K., Karsberg, S., Platz, A., Kanter, L., Ringborg, U. and Hansson, J., 2002. Screening of N-ras codon 61 mutations in paired primary and metastatic cutaneous melanomas: mutations occur early and persist throughout tumor progression. *Clin. Cancer Res.* 8(11): 3468-3474.

Omholt, K., Platz, A., Ringborg, U. and Hansson, J., 2001. Cytoplasmic and nuclear accumulation of beta-catenin is rarely caused by CTNNB1 exon 3 mutations in cutaneous malignant melanoma. *Int. J. Cancer* 92(6): 839-842.

Opdecamp, K., Vanvooren, P., Riviere, M., Arnheiter, H., Motta, R., Szpirer, J. and Szpirer, C., 1998. The rat microphthalmia-associated transcription factor gene (Mitf) maps at 4q34-q41 and is mutated in the mib rats. *Mammalian Genome* 9(8): 617-621.

Opdecamp, K., Nakayama, A., Nguyen, M.T., Hodgkinson, C.A., Pavan, W.J. and Arnheiter, H., 1997. Melanocyte development in vivo and in neural crest cell cultures: crucial dependence on the Mitf basic-helix-loop-helix-zipper transcription factor. *Development* 124(12): 2377-2386.

Pan, M.R., Peng, G., Hung, W.C. and Lin, S.Y., 2011. Monoubiquitination of H2AX protein regulates DNA damage response signaling. *J. Biol. Chem.* 286(32): 28599-28607.

Patel, J.H., Du, Y., Ard, P.G., Phillips, C., Carella, B., Chen, C.J., Rakowski, C., Chatterjee, C., Lieberman, P.M., Lane, W.S., Blobel, G.A. and McMahon, S.B., 2004. The c-MYC oncoprotein is a substrate of the acetyltransferases hGCN5/PCAF and TIP60. *Mol. Cell Biol.* 24(24): 10826-10834.

Patton, E.E., Widlund, H.R., Kutok, J.L., Kopani, K.R., Amatruda, J.F., Murphey, R.D., Berghmans, S., Mayhall, E.A., Traver, D., Fletcher, C.D., Aster, J.C., Granter, S.R., Look, A.T., Lee, C., Fisher, D.E. and Zon, L.I., 2005. BRAF mutations are sufficient to promote nevi formation and cooperate with p53 in the genesis of melanoma. *Curr. Biol.* 15(3): 249-254.

Pingault, V., Bondurand, N., Kuhlbrodt, K., Goerich, D.E., Préhu, M.-O., Puliti, A., Herbarth, B., Hermans-Borgmeyer, I., Legius, E., Matthijs, G., Amiel, J., Lyonnet, S., Ceccherini, I., Romeo, G., Clayton-Smith, J., Read, A.P., Wegner, M. and Goossens, M., 1998. SOX10 mutations in patients with Waardenburgs-Hirschprung disease. *Nat. Genet.* 18: 171-173.

Pinner, S., Jordan, P., Sharrock, K., Bazley, L., Collinson, L., Marais, R., Bonvin, E., Goding, C. and Sahai, E., 2009. Intravital imaging reveals transient changes in pigment production and Brn2 expression during metastatic melanoma dissemination. *Cancer Res.* 69(20): 7969-7977.

Planque, N., Turque, N., Opdecamp, K., Bailly, M., Martin, P. and Saule, S., 1999. Expression of the microphthalmia-associated basic helix-loop-helix leucine zipper transcription factor Mi in avian neuroretina cells induces a pigmented phenotype. *Cell Growth Differ.* 10(7): 525-536.

Pogenberg, V., Ogmundsdottir, M.H., Bergsteinsdottir, K., Schepsky, A., Phung, B., Deineko, V., Milewski, M., Steingrimsson, E. and Wilmanns, M., 2012. Restricted leucine zipper dimerization and specificity of DNA recognition of the melanocyte master regulator MITF. *Genes Dev.* 26(23): 2647-2658.

Polesskaya, A., Duquet, A., Naguibneva, I., Weise, C., Vervisch, A., Bengal, E., Hucho, F., Robin, P. and Harel-Bellan, A., 2000. CREB-binding protein/p300 activates MyoD by acetylation. *J. Biol. Chem.* 275(44): 34359-34364.

Pollock, P.M., Harper, U.L., Hansen, K.S., Yudt, L.M., Stark, M., Robbins, C.M., Moses, T.Y., Hostetter, G., Wagner, U., Kakareka, J., Salem, G., Pohida, T., Heenan, P., Duray, P., Kallioniemi, O., Hayward, N.K., Trent, J.M. and Meltzer, P.S., 2003. High frequency of BRAF mutations in nevi. *Nat. Genet.* 33(1): 19-20.

Polo, S.E., Kaidi, A., Baskcomb, L., Galanty, Y. and Jackson, S.P., 2010. Regulation of DNA-damage responses and cell-cycle progression by the chromatin remodelling factor CHD4. *EMBO J.* 29(18): 3130-3139.

Pomerantz, J., Schreiber-Agus, N., Liegeois, N.J., Silverman, A., Alland, L., Chin, L., Potes, J., Chen, K., Orlow, I., Lee, H.W., Cordon-Cardo, C. and DePinho, R.A., 1998. The Ink4a tumor suppressor gene product, p19Arf, interacts with MDM2 and neutralizes MDM2's inhibition of p53. *Cell* 92(6): 713-723.

Potterf, S.B., Mollaaghababa, R., Hou, L., Southard-Smith, E.M., Hornyak, T.J., Arnheiter, H. and Pavan, W.J., 2001. Analysis of SOX10 function in neural crest-derived melanocyte development: SOX10-dependent transcriptional control of dopachrome tautomerase. *Dev. Biol.* 237(2): 245-257.

Potterf, S.B., Furumura, M., Dunn, K.J., Arnheiter, H. and Pavan, W.J., 2000. Transcription factor hierarchy in Waardenburg syndrome: regulation of MITF expression by SOX10 and PAX3. *Hum. Genet.* 107(1): 1-6.

Poulikakos, P.I., Zhang, C., Bollag, G., Shokat, K.M. and Rosen, N., 2010. RAF inhibitors transactivate RAF dimers and ERK signalling in cells with wild-type BRAF. *Nature* 464(7287): 427-430.

Prendergast, G.C., Hopewell, R., Gorham, B.J. and Ziff, E.B., 1992. Biphasic effect of Max on Myc cotransformation activity and dependence on amino- and carboxy-terminal Max functions. *Genes Dev.* 6(12): 2429-2439.

Prendergast, G.C., Lawe, D. and Ziff, E.B., 1991. Association of Myn, the murine homolog of max, with c-Myc stimulates methylation-sensitive DNA binding and ras cotransformation. *Cell* 65(3): 395-407.

Price, E.R., Ding, H.F., Badalian, T., Bhattacharya, S., Takemoto, C., Yao, T.P., Hemesath, T.J. and Fisher, D.E., 1998a. Lineage-specific signaling in melanocytes. C-kit stimulation recruits p300/CBP to microphthalmia. *J. Biol. Chem.* 273(29): 17983-17986.

Price, E.R., Horstmann, M.A., Wells, A.G., Weilbaecher, K.N., Takemoto, C.M., Landis, M.W. and Fisher, D.E., 1998b. alpha-Melanocyte-stimulating hormone signaling regulates expression of microphthalmia, a gene deficient in Waardenburg syndrome. *J. Biol. Chem.* 273(49): 33042-33047.

Primot, A., Mogha, A., Corre, S., Roberts, K., Debbache, J., Adamski, H., Dreno, B., Khammari, A., Lesimple, T., Mereau, A., Goding, C.R. and Galibert, M.D., 2010. ERK-regulated differential expression of the Mitf 6a/b splicing isoforms in melanoma. *Pigment Cell Melanoma Res.* 23(1): 93-102.

Prince, S., Carreira, S., Vance, K.W., Abrahams, A. and Goding, C.R., 2004. Tbx2 Directly Represses the Expression of the p21(WAF1) Cyclin-Dependent Kinase Inhibitor. *Cancer Res.* 64(5): 1669-1674.

Puffenberger, E.G., Hosoda, K., Washington, S.S., Nakao, K., deWit, D., Yanagisawa, M. and Chakravart, A., 1994. A missense mutation of the endothelin-B receptor gene in multigenic Hirschsprung's disease. *Cell* 79(7): 1257-1266.

Qi, J., Chen, N., Wang, J. and Siu, C.H., 2005. Transendothelial migration of melanoma cells involves N-cadherin-mediated adhesion and activation of the beta-catenin signaling pathway. *Mol. Biol. Cell* 16(9): 4386-4397.

Quelle, D.E., Zindy, F., Ashmun, R.A. and Sherr, C.J., 1995. Alternative reading frames of the INK4a tumor suppressor gene encode two unrelated proteins capable of inducing cell cycle arrest. *Cell* 83(6): 993-1000.

Quinlan, A.R. and Hall, I.M., 2010. BEDTools: a flexible suite of utilities for comparing genomic features. *Bioinformatics* 26(6): 841-842.

Rahuel, C., Vinit, M.A., Lemarchandel, V., Cartron, J.P. and Romeo, P.H., 1992. Erythroid-specific activity of the glycophorin B promoter requires GATA-1 mediated displacement of a repressor. *EMBO J.* 11(11): 4095-4102.

Raposo, G. and Marks, M.S., 2007. Melanosomes--dark organelles enlighten endosomal membrane transport. *Nat. Rev. Mol. Cell Biol.* 8(10): 786-797.

Razin, E., Zhang, Z.C., Nechushtan, H., Frenkel, S., Lee, Y.N., Arudchandran, R. and Rivera, J., 1999. Suppression of microphthalmia transcriptional activity by its association with protein kinase C-interacting protein 1 in mast cells. *J. Biol. Chem.* 274(48): 34272-34276.

Read, A.P. and Newton, V.E., 1997. Waardenburg syndrome. *J. Med. Genet.* 34(8): 656-665.

Rimm, D.L., Caca, K., Hu, G., Harrison, F.B. and Fearon, E.R., 1999. Frequent nuclear/cytoplasmic localization of beta-catenin without exon 3 mutations in malignant melanoma. *Am. J. Pathol.* 154(2): 325-329.

Rodriguez, M., Aladowicz, E., Lanfrancone, L. and Goding, C.R., 2008. Tbx3 represses E-cadherin expression and enhances melanoma invasiveness. *Cancer Res.* 68(19): 7872-7881.

Rogakou, E.P., Pilch, D.R., Orr, A.H., Ivanova, V.S. and Bonner, W.M., 1998. DNA double-stranded breaks induce histone H2AX phosphorylation on serine 139. *J. Biol. Chem.* 273(10): 5858-5868.

Rommel, C., Clarke, B.A., Zimmermann, S., Nuñez, L., Rossman, R., Reid, K., Moelling, K., Yancopoulos, G.D. and Glass, D.J., 1999. Differentiation Stage-Specific Inhibition of the Raf-MEK-ERK Pathway by Akt. *Science* 286(5445): 1738-1741.

Rothhammer, T., Poser, I., Soncin, F., Bataille, F., Moser, M. and Bosserhoff, A.K., 2005. Bone morphogenic proteins are overexpressed in malignant melanoma and promote cell invasion and migration. *Cancer Res.* 65(2): 448-456.

Rubinfeld, B., Robbins, P., El-Gamil, M., Albert, I., Porfiri, E. and Polakis, P., 1997. Stabilization of beta-catenin by genetic defects in melanoma cell lines. *Science* 275(5307): 1790-1792.

Sabo, A., Lusic, M., Cereseto, A. and Giacca, M., 2008. Acetylation of conserved lysines in the catalytic core of cyclin-dependent kinase 9 inhibits kinase activity and regulates transcription. *Mol. Cell Biol.* 28(7): 2201-2212.

Saito, H., Yasumoto, K.I., Takeda, K., Takahashi, K., Fukuzaki, A., Orikasa, S. and Shibahara, S., 2002. Melanocyte-specific MITF isoform activates its own gene promoter through physical interaction with LEF-1. *J. Biol. Chem.* 277: 28787-28794.

Sakaguchi, K., Herrera, J.E., Saito, S., Miki, T., Bustin, M., Vassilev, A., Anderson, C.W. and Appella, E., 1998. DNA damage activates p53 through a phosphorylation-acetylation cascade. *Genes Dev.* 12(18): 2831-2841.

Sanchez-Martin, M., Rodriguez-Garcia, A., Perez-Losada, J., Sagrera, A., Read, A.P. and Sanchez-Garcia, I., 2002. SLUG (SNAI2) deletions in patients with Waardenburg disease. *Hum. Mol. Genet.* 11(25): 3231-3236.

Sardiello, M., Palmieri, M., di Ronza, A., Medina, D.L., Valenza, M., Gennarino, V.A., Di Malta, C., Donaudy, F., Embrione, V., Polishchuk, R.S., Banfi, S.,

Parenti, G., Cattaneo, E. and Ballabio, A., 2009. A gene network regulating lysosomal biogenesis and function. *Science* 325(5939): 473-477.

Sartorelli, V., Puri, P.L., Hamamori, Y., Ogryzko, V., Chung, G., Nakatani, Y., Wang, J.Y. and Kedes, L., 1999. Acetylation of MyoD directed by PCAF is necessary for the execution of the muscle program. *Mol. Cell* 4(5): 725-734.

Sato, S., Roberts, K., Gambino, G., Cook, A., Kouzarides, T. and Goding, C.R., 1997. CBP/p300 as a co-factor for the Microphthalmia transcription factor. *Oncogene* 14: 3083-3092.

Schepsky, A., Bruser, K., Gunnarsson, G.J., Goodall, J., Hallsson, J.H., Goding, C.R., Steingrimsson, E. and Hecht, A., 2006. The microphthalmia-associated transcription factor Mitf interacts with beta-catenin to determine target gene expression. *Mol. Cell Biol.* 26(23): 8914-8927.

Schwarz, E., Freese, U.K., Gissmann, L., Mayer, W., Roggenbuck, B., Stremlau, A. and zur Hausen, H., 1985. Structure and transcription of human papillomavirus sequences in cervical carcinoma cells. *Nature* 314(6006): 111-114.

Scott, G., Leopardi, S., Printup, S. and Madden, B.C., 2002. Filopodia are conduits for melanosome transfer to keratinocytes. *J. Cell Sci.* 115(Pt 7): 1441-1451.

Seftor, E.A., Brown, K.M., Chin, L., Kirschmann, D.A., Wheaton, W.W., Protopopov, A., Feng, B., Balagurunathan, Y., Trent, J.M., Nickoloff, B.J., Seftor, R.E. and Hendrix, M.J., 2005. Epigenetic transdifferentiation of normal melanocytes by a metastatic melanoma microenvironment. *Cancer Res.* 65(22): 10164-10169.

Serbedzija, G.N., Fraser, S.E. and Bronner-Fraser, M., 1990. Pathways of trunk neural crest cell migration in the mouse embryo as revealed by vital dye labelling. *Development* 108(4): 605-612.

Serrano, M., Lin, A.W., McCurrach, M.E., Beach, D. and Lowe, S.W., 1997. Oncogenic ras provokes premature cell senescence associated with accumulation of p53 and p16INK4a. *Cell* 88(5): 593-602.

Serrano, M., Hannon, G.J. and Beach, D., 1993. A new regulatory motif in cell-cycle control causing specific inhibition of cyclin D/CDK4. *Nature* 366(6456): 704-707.

Servant, N., Gravier, E., Gestraud, P., Laurent, C., Paccard, C., Biton, A., Brito, I., Mandel, J., Asselain, B., Barillot, E. and Hupe, P., 2010. EMA - A R package for Easy Microarray data analysis. *BMC Res. Notes* 3: 277.

Sharpless, E. and Chin, L., 2003. The INK4a/ARF locus and melanoma. *Oncogene* 22(20): 3092-3098.

Sharpless, N.E., Ramsey, M.R., Balasubramanian, P., Castrillon, D.H. and DePinho, R.A., 2004. The differential impact of p16(INK4a) or p19(ARF) deficiency on cell growth and tumorigenesis. *Oncogene* 23(2): 379-385.

Shay, J.W. and Roninson, I.B., 2004. Hallmarks of senescence in carcinogenesis and cancer therapy. *Oncogene* 23(16): 2919-2933.

Shi, H., Moriceau, G., Kong, X., Lee, M.K., Lee, H., Koya, R.C., Ng, C., Chodon, T., Scolyer, R.A., Dahlman, K.B., Sosman, J.A., Kefford, R.F., Long, G.V., Nelson, S.F., Ribas, A. and Lo, R.S., 2012. Melanoma whole-exome sequencing identifies (V600E)B-RAF amplification-mediated acquired B-RAF inhibitor resistance. *Nat. Commun.* 3: 724.

Shi, W., Oshlack, A. and Smyth, G.K., 2010. Optimizing the noise versus bias trade-off for Illumina whole genome expression BeadChips. *Nucleic Acids Res* 38(22): e204.

Shimizu, T., Toumoto, A., Ihara, K., Shimizu, M., Kyogoku, Y., Ogawa, N., Oshima, Y. and Hakoshima, T., 1997. Crystal structure of PHO4 bHLH domain-DNA complex: flanking base recognition. *EMBO J.* 16(15): 4689-4697.

Shin, H., Liu, T., Manrai, A.K. and Liu, X.S., 2009. CEAS: cis-regulatory element annotation system. *Bioinformatics* 25(19): 2605-2606.

Shiohara, M., Shigemura, T., Suzuki, T., Tanaka, M., Morii, E., Ohtsu, H., Shibahara, S. and Koike, K., 2009. MITF-CM, a newly identified isoform of microphthalmia-associated transcription factor, is expressed in cultured mast cells. *Int. J. Lab. Hematol.* 31(2): 215-226.

Shoag, J., Haq, R., Zhang, M., Liu, L., Rowe, G.C., Jiang, A., Koulisis, N., Farrel, C., Amos, C.I., Wei, Q., Lee, J.E., Zhang, J., Kupper, T.S., Qureshi, A.A., Cui, R., Han, J., Fisher, D.E. and Arany, Z., 2013. PGC-1 coactivators regulate MITF and the tanning response. *Mol. Cell* 49(1): 145-157.

Shogren-Knaak, M., Ishii, H., Sun, J.M., Pazin, M.J., Davie, J.R. and Peterson, C.L., 2006. Histone H4-K16 acetylation controls chromatin structure and protein interactions. *Science* 311(5762): 844-847.

Siebert, P.D. and Fukuda, M., 1987. Molecular cloning of a human glycophorin B cDNA: nucleotide sequence and genomic relationship to glycophorin A. *Proc. Natl. Acad. Sci. U. S. A.* 84(19): 6735-6739.

Slominski, A., Tobin, D.J., Shibahara, S. and Wortsman, J., 2004. Melanin pigmentation in mammalian skin and its hormonal regulation. *Physiol. Rev* 84(4): 1155-1228.

Smalley, M.J., Sara, E., Paterson, H., Naylor, S., Cook, D., Jayatilake, H., Fryer, L.G., Hutchinson, L., Fry, M.J. and Dale, T.C., 1999. Interaction of axin and Dvl-2 proteins regulates Dvl-2-stimulated TCF-dependent transcription. *EMBO J.* 18(10): 2823-2835.

Smyth, G.K., 2004. Linear models and empirical bayes methods for assessing differential expression in microarray experiments. *Stat. Appl. Genet. Mol. Biol.* 3: Article3.

Soengas, M.S., Capodieci, P., Polsky, D., Mora, J., Esteller, M., Opitz-Araya, X., McCombie, R., Herman, J.G., Gerald, W.L., Lazebnik, Y.A., Cordon-Cardo, C. and Lowe, S.W., 2001. Inactivation of the apoptosis effector Apaf-1 in malignant melanoma. *Nature* 409(6817): 207-211.

Solit, D.B., Garraway, L.A., Pratilas, C.A., Sawai, A., Getz, G., Basso, A., Ye, Q., Lobo, J.M., She, Y., Osman, I., Golub, T.R., Sebolt-Leopold, J., Sellers, W.R. and Rosen, N., 2006. BRAF mutation predicts sensitivity to MEK inhibition. *Nature* 439(7074): 358-362.

Solomon, D.L., Amati, B. and Land, H., 1993. Distinct DNA binding preferences for the c-Myc/Max and Max/Max dimers. *Nucleic Acids Res.* 21(23): 5372-5376.

Sosman, J.A., Kim, K.B., Schuchter, L., Gonzalez, R., Pavlick, A.C., Weber, J.S., McArthur, G.A., Hutson, T.E., Moschos, S.J., Flaherty, K.T., Hersey, P., Kefford, R., Lawrence, D., Puzanov, I., Lewis, K.D., Amaravadi, R.K., Chmielowski, B., Lawrence, H.J., Shyr, Y., Ye, F., Li, J., Nolop, K.B., Lee, R.J., Joe, A.K. and Ribas, A., 2012. Survival in BRAF V600-mutant advanced melanoma treated with vemurafenib. *N. Engl. J. Med.* 366(8): 707-714.

Southard-Smith, E.M., Kos, L. and Pavan, W., 1998. *Sox10* mutation disrupts neural crest development in *Dom* Hirschprung mouse model. *Nat. Genet.* 18: 60-64.

Stark, M.S., Tyagi, S., Nancarrow, D.J., Boyle, G.M., Cook, A.L., Whiteman, D.C., Parsons, P.G., Schmidt, C., Sturm, R.A. and Hayward, N.K., 2010.

Characterization of the Melanoma miRNAome by Deep Sequencing. *PLoS One* 5(3): e9685.

Steck, P.A., Pershouse, M.A., Jasser, S.A., Yung, W.K., Lin, H., Ligon, A.H., Langford, L.A., Baumgard, M.L., Hattier, T., Davis, T., Frye, C., Hu, R., Swedlund, B., Teng, D.H. and Tavtigian, S.V., 1997. Identification of a candidate tumour suppressor gene, MMAC1, at chromosome 10q23.3 that is mutated in multiple advanced cancers. *Nat. Genet.* 15(4): 356-362.

Steel, K.P., Davidson, D.R. and Jackson, I.J., 1992. TRP-2/DT, a new early melanoblast marker, shows that steel growth factor (c-kit ligand) is a survival factor. *Development* 115(4): 1111-1119.

Steingrimsson, E., Copeland, N.G. and Jenkins, N.A., 2004. Melanocytes and the Microphthalmia Transcription Factor Network. *Annu. Rev. Genet.* 38: 365-411.

Steingrimsson, E., Tessarollo, L., Pathak, B., Hou, L., Arnheiter, H., Copeland, N.G. and Jenkins, N.A., 2002. Mitf and Tfe3, two members of the Mitf-Tfe family of bHLH-Zip transcription factors, have important but functionally redundant roles in osteoclast development. *Proc. Natl. Acad. Sci. U. S. A.* 99(7): 4477-4482.

Steingrimsson, E., Nii, A., Fisher, D.E., Ferre-D'Amare, A.R., McCormick, R.J., Russell, L.B., Burley, S.K., Ward, J.M., Jenkins, N.A. and Copeland, N.G., 1996. The semidominant Mi(b) mutation identifies a role for the HLH domain in DNA binding in addition to its role in protein dimerization. *EMBO J.* 15(22): 6280-6289.

Steingrímsson, E., Moore, K.J., Lamoreaux, M.L., Ferré-D'Amaré, A.R., Burley, S.K., Sanders Zimring, D.C., Skow, L.C., Hodgkinson, C.A., Arnheiter, H., Copeland, N.G. and Jenkins, N.A., 1994. Molecular basis of mouse *microphthalmia* (*mi*) mutations helps explain their developmental and phenotypic consequences. *Nat. Genet.* 8: 256-263.

Storey, J.D., 2002. A direct approach to false discovery rates. *Journal of the Royal Statistical Society: Series B (Statistical Methodology)* 64(3): 479-498.

Stott, F.J., Bates, S., James, M.C., McConnell, B.B., Starborg, M., Brookes, S., Palmero, I., Ryan, K., Hara, E., Vousden, K.H. and Peters, G., 1998. The alternative product from the human CDKN2A locus, p14(ARF), participates in a regulatory feedback loop with p53 and MDM2. *EMBO J.* 17(17): 5001-5014.

Strub, T., Giuliano, S., Ye, T., Bonet, C., Keime, C., Kobi, D., Le Gras, S., Cormont, M., Ballotti, R., Bertolotto, C. and Davidson, I., 2011. Essential role of microphthalmia transcription factor for DNA replication, mitosis and genomic stability in melanoma. *Oncogene* 30(20): 2319-2332.

Sun, H.B., Zhu, Y.X., Yin, T., Sledge, G. and Yang, Y.C., 1998. MRG1, the product of a melanocyte-specific gene related gene, is a cytokine-inducible transcription factor with transformation activity. *Proc. Natl. Acad. Sci. U. S. A.* 95(23): 13555-13560.

Sun, X.H., Copeland, N.G., Jenkins, N.A. and Baltimore, D., 1991. Id proteins Id1 and Id2 selectively inhibit DNA binding by one class of helix-loop-helix proteins. *Mol. Cell Biol.* 11(11): 5603-5611.

Sviderskaya, E.V., Gray-Schopfer, V.C., Hill, S.P., Smit, N.P., Evans-Whipp, T.J., Bond, J., Hill, L., Bataille, V., Peters, G., Kipling, D., Wynford-Thomas, D. and Bennett, D.C., 2003. p16/Cyclin-Dependent Kinase Inhibitor 2A Deficiency in Human Melanocyte Senescence, Apoptosis, and Immortalization: Possible Implications for Melanoma Progression. *J. Natl. Cancer Inst.* 95(10): 723-732.

Sykes, S.M., Mellert, H.S., Holbert, M.A., Li, K., Marmorstein, R., Lane, W.S. and McMahon, S.B., 2006. Acetylation of the p53 DNA-binding domain regulates apoptosis induction. *Mol. Cell* 24(6): 841-851.

Tachibana, M., Takeda, K., Nobukuni, Y., Urabe, K., Long, J.E., Meyers, K.A., Aaronson, S.A. and Miki, T., 1996. Ectopic expression of *MITF*, a gene for Waardenburgs syndrome type 2, converts fibroblasts to cells with melanocyte characteristics. *Nat. Genet.* 14: 50-54.

Tachibana, M., Perez-Jurado, L.A., Nakayama, A., Hodgkinson, C.A., Li, X., Schneider, M., Miki, T., Fex, J., Francke, U. and Arnheiter, H., 1994. Cloning of MITF, the human homolog of the mouse microphthalmia gene and assignment to chromosome 3p14.1-p12.3. *Hum. Mol. Genet.* 3(4): 553-557.

Tafvizi, A., Huang, F., Fersht, A.R., Mirny, L.A. and van Oijen, A.M., 2011. A single-molecule characterization of p53 search on DNA. *Proc. Natl. Acad. Sci. U. S. A.* 108(2): 563-568.

Taipale, J. and Beachy, P.A., 2001. The Hedgehog and Wnt signalling pathways in cancer. *Nature* 411(6835): 349-354.

Takada, S., Stark, K.L., Shea, M.J., Vassileva, G., McMahon, J.A. and McMahon, A.P., 1994. Wnt-3a regulates somite and tailbud formation in the mouse embryo. *Genes Dev.* 8(2): 174-189.

Takeda, K., Yasumoto, K., Kawaguchi, N., Udono, T., Watanabe, K., Saito, H., Takahashi, K., Noda, M. and Shibahara, S., 2002. Mitf-D, a newly identified isoform, expressed in the retinal pigment epithelium and monocyte-lineage cells affected by Mitf mutations. *Biochim. Biophys. Acta* 1574(1): 15-23.

Takeda, K., Takemoto, C., Kobayashi, I., Watanabe, A., Nobukuni, Y., Fisher, D.E. and Tachibana, M., 2000a. Ser298 of MITF, a mutation site in Waardenburg syndrome type 2, is a phosphorylation site with functional significance. *Hum. Mol. Genet.* 9(1): 125-132.

Takeda, K., Yasumoto, K., Takada, R., Takada, S., Watanabe, K., Udono, T., Saito, H., Takahashi, K. and Shibahara, S., 2000b. Induction of melanocyte-specific microphthalmia-associated transcription factor by Wnt-3a. *J. Biol. Chem* 275(19): 14013-14016.

Takemoto, C.M., Yoon, Y.J. and Fisher, D.E., 2002. The identification and functional characterization of a novel mast cell isoform of the microphthalmia-associated transcription factor. *J. Biol. Chem.* 277(33): 30244-30252.

Tamkun, J.W., Deuring, R., Scott, M.P., Kissinger, M., Pattatucci, A.M., Kaufman, T.C. and Kennison, J.A., 1992. brahma: a regulator of Drosophila homeotic genes structurally related to the yeast transcriptional activator SNF2/SWI2. *Cell* 68(3): 561-572.

Tang, Y., Luo, J., Zhang, W. and Gu, W., 2006. Tip60-dependent acetylation of p53 modulates the decision between cell-cycle arrest and apoptosis. *Mol. Cell* 24(6): 827-839.

Tassabehji, M., Newton, V.E. and Read, A.P., 1994a. Waardenburg syndrome type 2 caused by mutations in the human *microphthalmia* (*MITF*) gene. *Nat. Genet.* 8: 251-255.

Tassabehji, M., Newton, V.E., Leverton, K., Turnbull, K., Seemanova, E., Kunze, J., Sperling, K., Strachan, T. and Read, A.P., 1994b. PAX3 gene structure and mutations: close analogies between Waardenburg syndrome and the Splotch mouse. *Hum. Mol. Genet.* 3(7): 1069-1074.

Tassabehji, M., Read, A.P., Newton, V.E., Patton, M., Gruss, P., Harris, R. and Strachan, T., 1993. Mutations in the PAX3 gene causing Waardenburg syndrome type 1 and type 2. *Nat. Genet.* 3(1): 26-30.

Tassabehji, M., Read, A.P., Newton, V.E., Harris, R., Balling, R., Gruss, P. and Strachan, T., 1992. Waardenburg's syndrome patients have mutations in the human homologue of the Pax-3 paired box gene. *Nature* 355(6361): 635-636.

Tawbi, H.A. and Kirkwood, J.M., 2007. Management of metastatic melanoma. *Semin. Oncol.* 34(6): 532-545.

Thomas, A.J. and Erickson, C.A., 2009. FOXD3 regulates the lineage switch between neural crest-derived glial cells and pigment cells by repressing MITF through a non-canonical mechanism. *Development* 136(11): 1849-1858.

Thomas, A.J. and Erickson, C.A., 2008. The making of a melanocyte: the specification of melanoblasts from the neural crest. *Pigment Cell Melanoma Res.* 21(6): 598-610.

Thurber, A.E., Douglas, G., Sturm, E.C., Zabierowski, S.E., Smit, D.J., Ramakrishnan, S.N., Hacker, E., Leonard, J.H., Herlyn, M. and Sturm, R.A., 2011. Inverse expression states of the BRN2 and MITF transcription factors in melanoma spheres and tumour xenografts regulate the NOTCH pathway. *Oncogene* 30(27): 3036-3048.

Tsai, J., Lee, J.T., Wang, W., Zhang, J., Cho, H., Mamo, S., Bremer, R., Gillette, S., Kong, J., Haass, N.K., Sproesser, K., Li, L., Smalley, K.S., Fong, D., Zhu, Y.L., Marimuthu, A., Nguyen, H., Lam, B., Liu, J., Cheung, I., Rice, J., Suzuki, Y., Luu, C., Settachatgul, C., Shellooe, R., Cantwell, J., Kim, S.H., Schlessinger, J., Zhang, K.Y., West, B.L., Powell, B., Habets, G., Zhang, C., Ibrahim, P.N., Hirth, P., Artis, D.R., Herlyn, M. and Bollag, G., 2008. Discovery of a selective inhibitor of oncogenic B-Raf kinase with potent antimelanoma activity. *Proc. Natl. Acad. Sci. U. S. A.* 105(8): 3041-3046.

Tsvetkov, L.M., Yeh, K.H., Lee, S.J., Sun, H. and Zhang, H., 1999. p27(Kip1) ubiquitination and degradation is regulated by the SCF(Skp2) complex through phosphorylated Thr187 in p27. *Curr. Biol.* 9(12): 661-664.

Udono, T., Yasumoto, K., Takeda, K., Amae, S., Watanabe, K., Saito, H., Fuse, N., Tachibana, M., Takahashi, K., Tamai, M. and Shibahara, S., 2000. Structural organization of the human microphthalmia-associated transcription factor gene containing four alternative promoters. *Biochim. Biophys. Acta* 1491(1-3): 205-219.

Vachtenheim, J. and Novotna, H., 1999. Expression of genes for microphthalmia isoforms, Pax3 and MSG1, in human melanomas. *Cell. Mol. Biol. (Noisy-le-grand)* 45(7): 1075-1082.

Valsesia, A., Rimoldi, D., Martinet, D., Ibberson, M., Benaglio, P., Quadroni, M., Waridel, P., Gaillard, M., Pidoux, M., Rapin, B., Rivolta, C., Xenarios, I., Simpson, A.J., Antonarakis, S.E., Beckmann, J.S., Jongeneel, C.V., Iseli, C. and Stevenson, B.J., 2011. Network-guided analysis of genes with altered somatic copy number and gene expression reveals pathways commonly perturbed in metastatic melanoma. *PLoS One* 6(4): e18369.

Valyi-Nagy, I.T., Hirka, G., Jensen, P.J., Shih, I.M., Juhasz, I. and Herlyn, M., 1993. Undifferentiated keratinocytes control growth, morphology, and antigen expression of normal melanocytes through cell-cell contact. *Lab. Invest.* 69(2): 152-159.

Vance, K.W., Carreira, S., Brosch, G. and Goding, C.R., 2005. Tbx2 is overexpressed and plays an important role in maintaining proliferation and suppression of senescence in melanomas. *Cancer Res.* 65(6): 2260-2268.

Vempati, R.K., Jayani, R.S., Notani, D., Sengupta, A., Galande, S. and Haldar, D., 2010. p300-mediated acetylation of histone H3 lysine 56 functions in DNA damage response in mammals. *J. Biol. Chem.* 285(37): 28553-28564.

Venkatesh, S., Smolle, M., Li, H., Gogol, M.M., Saint, M., Kumar, S., Natarajan, K. and Workman, J.L., 2012. Set2 methylation of histone H3 lysine 36 suppresses histone exchange on transcribed genes. *Nature* 489(7416): 452-455.

Vervoorts, J., Luscher-Firzlaff, J.M., Rottmann, S., Lilischkis, R., Walsemann, G., Dohmann, K., Austen, M. and Luscher, B., 2003. Stimulation of c-MYC transcriptional activity and acetylation by recruitment of the cofactor CBP. *EMBO Rep.* 4(5): 484-490.

Voronova, A. and Baltimore, D., 1990. Mutations that disrupt DNA binding and dimer formation in the E47 helix-loop-helix protein map to distinct domains. *Proc. Natl. Acad. Sci. U. S. A.* 87(12): 4722-4726.

Waardenburg, P.J., 1951. A new syndrome combining developmental anomalies of the eyelids, eyebrows and nose root with pigmentary defects of the iris and head hair and with congenital deafness. *Am. J. Hum. Genet.* 3(3): 195-253.

Wan, P.T., Garnett, M.J., Roe, S.M., Lee, S., Niculescu-Duvaz, D., Good, V.M., Jones, C.M., Marshall, C.J., Springer, C.J., Barford, D. and Marais, R., 2004. Mechanism of activation of the RAF-ERK signaling pathway by oncogenic mutations of B-RAF. *Cell* 116(6): 855-867.

Wang, Z., Zang, C., Cui, K., Schones, D.E., Barski, A., Peng, W. and Zhao, K., 2009. Genome-wide mapping of HATs and HDACs reveals distinct functions in active and inactive genes. *Cell* 138(5): 1019-1031.

Watanabe, A., Takeda, K., Ploplis, B. and Tachibana, M., 1998. Epistatic relationship between Waardenburg syndrome genes MITF and PAX3. *Nat. Genet.* 18(3): 283-286.

Watanabe, K.I., Takeda, K., Yasumoto, K.I., Udono, T., Saito, H., Ikeda, K., Takasaka, T., Takahashi, K., Kobayashi, T., Tachibana, M. and Shibahara, S., 2002. Identification of a Distal Enhancer for the Melanocyte-Specific Promoter of the MITF Gene. *Pigment Cell Res.* 15(3): 201-211.

Weilbaecher, K.N., Hershey, C.L., Takemoto, C.M., Horstmann, M.A., Hemesath, T.J., Tashjian, A.H. and Fisher, D.E., 1998. Age-resolving osteopetrosis: a rat model implicating microphthalmia and the related transcription factor TFE3. *J. Exp. Med.* 187(5): 775-785.

Wellbrock, C., Rana, S., Paterson, H., Pickersgill, H., Brummelkamp, T. and Marais, R., 2008. Oncogenic BRAF regulates melanoma proliferation through the lineage specific factor MITF. *PLoS ONE* 3(7): e2734.

Wellbrock, C., Ogilvie, L., Hedley, D., Karasarides, M., Martin, J., Niculescu-Duvaz, D., Springer, C.J. and Marais, R., 2004a. V599EB-RAF is an oncogene in melanocytes. *Cancer Res.* 64(7): 2338-2342.

Wellbrock, C., Karasarides, M. and Marais, R., 2004b. The RAF proteins take centre stage. *Nat. Rev. Mol. Cell Biol.* 5(11): 875-885.

Westbrook, T.F., Nguyen, D.X., Thrash, B.R. and McCance, D.J., 2002. E7 abolishes raf-induced arrest via mislocalization of p21(Cip1). *Mol. Cell Biol.* 22(20): 7041-7052.

Widlund, H.R., Horstmann, M.A., Price, E.R., Cui, J., Lessnick, S.L., Wu, M., He, X. and Fisher, D.E., 2002. {beta}-Catenin-induced melanoma growth requires the

downstream target Microphthalmia-associated transcription factor. *J. Cell Biol.* 158(6): 1079-1087.

Wu, J., Huen, M.S., Lu, L.Y., Ye, L., Dou, Y., Ljungman, M., Chen, J. and Yu, X., 2009. Histone ubiquitination associates with BRCA1-dependent DNA damage response. *Mol. Cell Biol.* 29(3): 849-860.

Wu, M., Hemesath, T.J., Takemoto, C.M., Horstmann, M.A., Wells, A.G., Price, E.R., Fisher, D.Z. and Fisher, D.E., 2000. c-Kit triggers dual phosphorylations, which couple activation and degradation of the essential melanocyte factor Mi. *Genes Dev.* 14(3): 301-312.

Xu, W., Gong, L., Haddad, M.M., Bischof, O., Campisi, J., Yeh, E.T. and Medrano, E.E., 2000. Regulation of microphthalmia-associated transcription factor MITF protein levels by association with the ubiquitin-conjugating enzyme hUBC9. *Exp. Cell. Res.* 255(2): 135-143.

Yajima, I., Endo, K., Sato, S., Toyoda, R., Wada, H., Shibahara, S., Numakunai, T., Ikeo, K., Gojobori, T., Goding, C.R. and Yamamoto, H., 2003. Cloning and functional analysis of ascidian Mitf in vivo: insights into the origin of vertebrate pigment cells. *Mech. Dev.* 120(12): 1489-1504.

Yang, X.J., Ogryzko, V.V., Nishikawa, J., Howard, B.H. and Nakatani, Y., 1996. A p300/CBP-associated factor that competes with the adenoviral oncoprotein E1A. *Nature* 382(6589): 319-324.

Yasumoto, K., Takeda, K., Saito, H., Watanabe, K., Takahashi, K. and Shibahara, S., 2002. Microphthalmia-associated transcription factor interacts with LEF-1, a mediator of Wnt signaling. *EMBO J.* 21: 2703-2714.

Yasumoto, K., Yokoyama, K., Shibata, K., Tomita, Y. and Shibahara, S., 1994. Microphthalmia-associated transcription factor as a regulator for melanocyte-specific transcription of the human tyrosinase gene. *Mol. Cell Biol.* 14(12): 8058-8070.

Yavuzer, U., Keenan, E., Lowings, P., Vachtenheim, J., Currie, G. and Goding, C.R., 1995. The Microphthalmia gene product interacts with the retinoblastoma protein in vitro and is a target for deregulation of melanocyte- specific transcription. *Oncogene* 10(1): 123-134.

Yokoyama, S., Woods, S.L., Boyle, G.M., Aoude, L.G., MacGregor, S., Zismann, V., Gartside, M., Cust, A.E., Haq, R., Harland, M., Taylor, J.C., Duffy, D.L., Holohan, K., Dutton-Regester, K., Palmer, J.M., Bonazzi, V., Stark, M.S., Symmons, J., Law, M.H., Schmidt, C., Lanagan, C., O'Connor, L., Holland, E.A., Schmid, H., Maskiell, J.A., Jetann, J., Ferguson, M., Jenkins, M.A., Kefford, R.F., Giles, G.G., Armstrong, B.K., Aitken, J.F., Hopper, J.L., Whiteman, D.C., Pharoah, P.D., Easton, D.F., Dunning, A.M., Newton-Bishop, J.A., Montgomery, G.W., Martin, N.G., Mann, G.J., Bishop, D.T., Tsao, H., Trent, J.M., Fisher, D.E., Hayward, N.K. and Brown, K.M., 2011. A novel recurrent mutation in MITF predisposes to familial and sporadic melanoma. *Nature* 480(7375): 99-103.

Yuan, W., Condorelli, G., Caruso, M., Felsani, A. and Giordano, A., 1996. Human p300 protein is a co-activator for the transcription factor MyoD. *J. Biol. Chem.* 271: 9009-9013.

Zelzer, E., Wappner, P. and Shilo, B.Z., 1997. The PAS domain confers target gene specificity of Drosophila bHLH/PAS proteins. *Genes Dev.* 11(16): 2079-2089.

Zhang, Y., Liu, T., Meyer, C.A., Eeckhoute, J., Johnson, D.S., Bernstein, B.E., Nusbaum, C., Myers, R.M., Brown, M., Li, W. and Liu, X.S., 2008. Model-based analysis of ChIP-Seq (MACS). *Genome Biol.* 9(9): R137.

Zhang, Y., Xiong, Y. and Yarbrough, W.G., 1998. ARF promotes MDM2 degradation and stabilizes p53: ARF-INK4a locus deletion impairs both the Rb and p53 tumor suppression pathways. *Cell* 92(6): 725-734.

Zhao, X., Fiske, B., Kawakami, A., Li, J. and Fisher, D.E., 2011. Regulation of MITF stability by the USP13 deubiquitinase. *Nat. Commun.* 2: 414.

Zhu, S., Wurdak, H., Wang, Y., Galkin, A., Tao, H., Li, J., Lyssiotis, C.A., Yan, F., Tu, B.P., Miraglia, L., Walker, J., Sun, F., Orth, A., Schultz, P.G. and Wu, X., 2009. A genomic screen identifies TYRO3 as a MITF regulator in melanoma. *Proc. Natl. Acad. Sci. U. S. A.* 106(40): 17025-17030.

Zimmermann, S. and Moelling, K., 1999. Phosphorylation and Regulation of Raf by Akt (Protein Kinase B). *Science* 286(5445): 1741-1744.

Zlotogora, J., Lerer, I., Bar-David, S., Ergaz, Z. and Abeliovich, D., 1995. Homozygosity for Waardenburg syndrome. *Am. J. Hum. Genet.* 56(5): 1173-1178.